BNL 20415
CONF-740673--

BNL WORKSHOP on PHYSICS with POLARIZED TARGETS

BROOKHAVEN NATIONAL LABORATORY
ASSOCIATED UNIVERSITIES, INC.
UNDER CONTRACT NO. E(30-1)-16 WITH THE
UNITED STATES ENERGY RESEARCH AND DEVELOPMENT ADMINISTRATION

PROCEEDINGS OF THE

BNL WORKSHOP ON PHYSICS WITH POLARIZED TARGETS*

June 3-8, 1974

Editor

James S. Russ

Carnegie-Mellon University

Pittsburgh, Pennsylvania 15213

* The Energy Research and Development Administration (ERDA) is the successor to the U.S. Atomic Energy Commission (AEC) and all references to the AEC herein shall be deemed to refer to ERDA.

NOTICE

Printed in the United States of America
Available from
National Technical Information Service
U.S. Department of Commerce
5285 Port Royal Road
Springfield, VA 22161
Price: Domestic $12.00; Foreign $14.50;
Microfiche $2.25

December 1975 631 copies

TABLE OF CONTENTS

TABLE OF CONTENTS (continued)

Forward:

The Brookhaven Workshop on Physics with Polarized Targets was intended to focus attention on the maturation of the physics utilization of polarized target technology and to invite interaction between theorists, polarized target experts, and other experimentalists interested in applying polarization measurements to new areas in high energy interactions. The utility of polarization measurements in limiting ambiguities in phase shift or amplitude analyses of elastic and charge exchange scattering is well known. Previous conferences on polarized targets such as the IInd International Conference on Polarized Targets, Berkeley, 1971, have extensively discussed this area. In the mid-1970's higher intensity beams, sophisticated particle detectors, and new developments in polarized target technology combine to extend greatly the scope of conceivable experiments with polarized targets. The excitement over the physics potential of adding an entire new dimension - spin structure - to the data base for analysis of elastic and inelastic reactions was clear to us at the workshop. I hope that this report conveys some of this physics challenge to the reader and inspires extension of some of the ideas discussed here.

The need for new kinds of data on inelastic reactions if one is to make progress in systematizing elementary particle dynamics was stressed repeatedly. Total and differential cross section measurements, however precise, cannot by themselves be used to unfold the amplitudes which govern particle interactions within some symmetry group, e.g., SU(3) multiplets. If we are to test symmetries and understand symmetry - breaking schemes, then we must isolate amplitudes, rather than measuring reactions.

As Chris Michael has put it, "If an experimenter proposes to study exchange mechanisms these days, the question should be why not measure P, R and A in the experiment, rather than whether they should be done."

In this general spirit, the workshop participants reviewed what work had already been done, attempted to isolate gaps in existing work, and projected new measurements that might be made, using new technologies. We also heard reports on polarized target research going on at ANL, BNL, CERN, LAMPF, and SLAC, pressing toward radiation-resistant targets for high intensity beams, frozen-spin targets to permit large solid angle access to the target without excessive cryogenic hardware to interfere, and new work by the CERN group in polarizing neutrons in deuterated hydrocarbons.

It is my pleasure to thank all participants for their active involvement in the workshop. The organization of it benefited greatly from the interest and involvement of Ronnie Rau, Bob Phillips and Satoshi Ozaki. The operation of the whole enterprise and the publication of the proceedings would have been impossible without the good work and good cheer of the Conference Secretary, Sharon Smith.

The objective of the workshop was a consideration of whether investment in new types of polarized target activity, extending the kinds of measurements made, extending the reaction types studied in polarized target experiments to include multibody systems and inclusive polarization studies, and exploiting higher sensitivities to extend t and s ranges of existing data, was worthwhile. The consensus of the participants was a resounding "yes". The reports in these proceedings stand in powerful support of that position.

James S. Russ

PARTICIPANTS

Ash, William	Stanford Linear Accelerator Center
Bar-Yam, Zvi	Southeastern Massachusetts University
Berley, David	Brookhaven National Laboratory
Borghini, Michel	CERN
Cool, Rodney	Rockefeller University
Cutkosky, Richard	Carnegie-Mellon University
Etkin, Asher	Yale University
Field, Richard	California Institute of Technology
Foley, Kenneth	Brookhaven National Laboratory
Fox, Geoffrey	California Institute of Technology
Gordon, Howard	Brookhaven National Laboratory
Graf, Erlend	SUNY at Stony Brook
Hughes, Vernon	Yale University
Hwang, Chester	Los Alamos Scientific Laboratory
Kern, Wolfhard	Southeastern Massachusetts University
Kimel, J. Daniel	Florida State University
Lai, Kwan-Wu	Brookhaven National Laboratory
Lindenbaum, Seymour	Brookhaven National Laboratory
Ozaki, Satoshi	Brookhaven National Laboratory
Phillips, Robert	Brookhaven National Laboratory
Rau, R. Ronald	Brookhaven National Laboratory
Russ, James	Carnegie-Mellon University
Sakitt, Mark	Brookhaven National Laboratory
Shafer, Janice	University of Massachusetts
Shapiro, Gilbert	Lawrence Berkeley Laboratory
Shutt, Ralph	Brookhaven National Laboratory
Sidhu, Deepinder	Rutgers University
Steinberg, Phillip	University of Maryland
Surko, Pamela	Princeton University
Trueman, Lawrence	Brookhaven National Laboratory
Willen, Erich	Brookhaven National Laboratory
Yokosawa, Akihiko	Argonne National Laboratory
Zeller, Michael	Yale University

SECTION I

PHYSICS APPLICATIONS OF POLARIZED TARGETS

Invariance Principles and Spin*

T. L. Trueman

Brookhaven National Laboratory, Upton, New York 11973

This talk is an elementary discussion of the description of scattering from polarized targets. It is intended to be basis for the more specific talks given during this workshop. It is not intended to be a review talk.

1. Total Cross Sections

Is there anything to be learned from total cross section measurements on polarized targets? We will consider p and d targets.

a) Polarized proton target.

Consider an unpolarized proton beam incident on a polarized proton target. Conservation of angular momentum and the identity of particles allows only five non-zero helicity amplitudes:

$$f_{++,++} \quad , \qquad f_{+-,+-} = f_{-+,-+} \quad , \qquad f_{++,--}$$

$$f_{--,--} \quad , \qquad f_{--,++}$$

If parity is conserved there are only three independent amplitudes and $f_{++,++} = f_{--,--}$, $f_{++,--} = f_{--,++}$. The corresponding invariant amplitude expansion is

---

* Work performed under the auspices of the U.S. Atomic Energy Commission.

$$M = A + B\,\vec{\sigma}_1\cdot\sigma_2 + C\,\vec{\sigma}_1\cdot\hat{\vec{p}}\;\vec{\sigma}_2\cdot\hat{\vec{p}}$$

where $\vec{p}$ is a incident momentum in the center-of-mass. The total cross section is

$$\sigma_T = \frac{4\pi}{p}\,\mathrm{Im}(\mathrm{Tr}\rho M)$$

and the density matrix ρ is given by

$$\rho = \tfrac{1}{4}(\mathbb{1}_1 + \vec{\sigma}_1\cdot\vec{P}_1)\mathbb{1}_2$$

where the matrix with subscript 1 is in the spin space of the target and the matrix with subscript 2 in the spin space of the projectile. $\vec{P}_1$ is the polarization vector of the target. Then

$$\sigma_T = \frac{4\pi}{p}\,\mathrm{Im}A$$

independent of $\vec{P}_1$.

Should parity not be conserved, but time reversal is good, there can be another term in M proportional to $(\vec{\sigma}_1-\vec{\sigma}_2)\cdot\vec{p}$ leading to a term in σ_T proportional to $\vec{p}\cdot\vec{P}_1$. Thus to detect parity violation a component of polarization in the longitudinal direction is needed.

If time reversal is violated, too, there can be another term in M proportional to $(\vec{\sigma}_1\times\vec{\sigma}_2)\cdot\vec{p}$ (i.e., $f_{++,--}\neq f_{--,++}$). This term can be detected only if both target and beam are polarized.

The discussion of $\frac{d\sigma}{d\Omega}$ for pp scattering is a special case of later discussion. We mention here only that for parity violation one looks for terms in $\vec{P}_1\cdot(\vec{p}+\vec{p}')$ and for time reversal one looks for terms in

$\vec{P}_1 \cdot (\vec{p}-\vec{p}')$ in the angular distribution. ($\vec{p}'$ denotes the scattered proton momentum in the c.m.).

b) Consider the scattering of a π on a polarized d target. (Scattering of unpolarized p's is essentially the same.) One way of writing the density matrix ρ of the deuteron is

$$\rho = \frac{1}{3}(1 + \frac{3}{2}\vec{J}\cdot\vec{P} + \frac{3}{4}Q_{ij}(J_iJ_j + J_jJ_i - \frac{4}{3}\delta_{ij}))$$

J_i denotes the usual 3 x 3 spin 1 angular momentum matrices. Q_{ij} is a real, traceless, symmetric tensor so the polarization state of d is specified by eight real parameters. Explicitly

$$\rho = \begin{pmatrix} \frac{1}{3} + \frac{1}{2}P_z + \frac{1}{4}Q_{zz} & \frac{1}{2}\frac{P_x - iP_y}{(2)^{\frac{1}{2}}} + \frac{1}{4}\frac{Q_{xz} - iQ_{yz}}{(2)^{\frac{1}{2}}} & \frac{1}{4}(Q_{xx} - Q_{yy} - iQ_{xy}) \\ \frac{1}{2}\frac{P_x + iP_y}{(2)^{\frac{1}{2}}} + \frac{1}{4}\frac{Q_{xz} + iQ_{yz}}{(2)^{\frac{1}{2}}} & \frac{1}{3} - \frac{1}{2}Q_{zz} & \frac{1}{2}\frac{P_x - iP_y}{(2)^{\frac{1}{2}}} - \frac{1}{4}\frac{Q_{yz} - iQ_{zz}}{(2)^{\frac{1}{2}}} \\ \frac{1}{4}(Q_{xx} - Q_{yy} + iQ_{xy}) & \frac{1}{2}\frac{P_x + iP_y}{(2)^{\frac{1}{2}}} - \frac{1}{4}\frac{Q_{xz} + iQ_{yz}}{(2)^{\frac{1}{2}}} & \frac{1}{3} - \frac{1}{2}P_z + \frac{1}{4}Q_{zz} \end{pmatrix}$$

In terms of helicity amplitudes

$$\sigma_T = \frac{4\pi}{p}\,\mathrm{Im}\left\{\frac{1}{3}(f_{++} + f_{00} + f_{--}) + \frac{1}{2}P_z(f_{++} - f_{--}) + \frac{1}{4}Q_{zz}(f_{++} + f_{--} - 2f_{00})\right\}$$

where the z-axis is along the beam momentum.

If parity is good $f_{++} = f_{--}$ and here, too, σ_T is independent of $\vec{P}$. However, if $Q_{zz} \neq 0$

$$\sigma_T(Q)-\sigma_T(0) = \frac{4\pi}{p} \mathrm{Im}\left(\frac{f_{++}-f_{00}}{2}\right) Q_{zz} \quad .$$

Note that positivity of the matrix ρ requires

$$-\frac{4}{3} \leq Q_{zz} \leq \frac{2}{3}$$

and

$$|P_z| \leq \frac{2}{3}\left(1+\frac{3}{4} Q_{zz}\right)$$

so a d completely polarized in the z direction must have $Q_{zz} = 2/3$. For pure transverse polarization, say $\langle J_x \rangle = 1$, we have

$$\rho = \begin{pmatrix} \frac{1}{4} & \frac{1}{2(2)^{\frac{1}{2}}} & \frac{1}{4} \\ \frac{1}{2(2)^{\frac{1}{2}}} & \frac{1}{2} & \frac{1}{2(2)^{\frac{1}{2}}} \\ \frac{1}{4} & \frac{1}{2(2)^{\frac{1}{2}}} & \frac{1}{4} \end{pmatrix}$$

or $P_z = 0$ but $Q_{zz} = -1/3$. So, in general, there is some information to be gained from total cross sections on polarized d's even when parity and time reversal invariance are good.

2. Polarization in Various Reference Frames

The density matrix ρ_1 of a polarized proton target is most simply given in its rest system, the lab system. There it has the familiar form

$$\rho_1 = \frac{1}{2}(1 + \vec{\sigma}\cdot\vec{P}) \qquad (2.1)$$

where the polarization vector $\vec{P}$ has its components defined with respect to axes defined in the lab. For definiteness we take the incident beam

in the negative z-direction and the y-axis can be chosen in any convenient way: the direction of the magnetic field or the normal to the reaction plane defined by the apparatus are typical choices. A state completely polarized in the y-direction has the form

$$|i> = \frac{1}{(2)^{\frac{1}{2}}} (|\tfrac{1}{2}> + i|-\tfrac{1}{2}>) \qquad (2.2)$$

corresponding to a density matrix

$$\rho_i = \frac{1}{2}\begin{pmatrix} 1 & -i \\ i & 1 \end{pmatrix} \quad . \qquad (2.3)$$

A Lorentz transformation to the center-of-mass system, i.e., s channel c.m., leaves the spin components along the z-direction unchanged:

$$L_z(p)|\mu> = |p,\mu> \quad . \qquad (2.4)$$

μ is then the helicity of the initial proton in the s c.m. Consequently,

$$L_z(p)|i> = \frac{1}{(2)^{\frac{1}{2}}} (|p,\tfrac{1}{2}> + i|p,-\tfrac{1}{2}>) \qquad (2.5)$$

and the helicity density matrix of the proton in the overall c.m. $\rho_i^{(s)}$ is simply

$$\rho_i^{(s)} = \rho_i = \frac{1}{2}(1+\vec{\sigma}\cdot\vec{P}) \quad . \qquad (2.6)$$

This is perfectly general and does not depend on the proton being in a pure state, because of (2.4) which defines helicity.

Now consider the process $\pi+p \to R+X$ (inclusive or exclusive.) It is for exactly this same reason that the helicity convention for the density matrix of the outgoing state R, denoted by $\rho_f^{(h)}$ satisfies

$$\rho^{(h)}_{f_{\lambda\lambda'}} = \rho^{(s)}_{f_{\lambda\lambda'}} \quad , \tag{2.7}$$

where $\rho_f^{(s)}$ is the helicity density matrix of R in the s c.m.

$$\rho^{(s)}_{f_{\lambda\lambda'}} = \sum_{\mu,\mu',\nu} f^{(s)}_{\lambda\nu,\mu}\, \rho^{(s)}_{i_{\mu\mu'}}\, f^{(s)*}_{\lambda'\nu,\mu'} \tag{2.8}$$

$f^{(s)}_{\lambda\nu,\mu}$ denotes the production amplitude with helicity indices λ,μ defined in the s-channel c.m. ν denotes all unobserved variables which are summed over. Recall that $\rho_f^{(h)}$ is defined in the rest frame of R reached by a pure Lorentz transformation from s c.m. along the direction opposite to its motion; i.e., its z-axis is opposite to the direction of the recoiling system X in R's rest frame. See Fig. 1.

We emphasize that using ρ_i and $\rho_f^{(h)}$ in this way is directly a measure of the s-channel helicity amplitudes $f^{(s)}_{\lambda\nu,\mu}$. We could express $\rho_f^{(h)}$ in terms of amplitudes $f^{(R)}_{\lambda\nu,\mu}$ defined in the R rest frame, should this be desirable for any reason. Then

$$\rho_f^{(h)} = \sum f^{(s)}_{\lambda\nu,\mu}\ \tfrac{1}{2}(1+\vec{\sigma}\cdot\vec{P})_{\mu\mu'}\ f^{(s)*}_{\lambda'\nu,\mu'}$$

$$= \sum f^{(R)}_{\lambda\nu,\sigma}\ d^{(1/2)}_{\sigma\mu}(\alpha)\ \tfrac{1}{2}(1+\vec{\sigma}\cdot\vec{P})_{\mu\mu'}\ d^{(1/2)}_{\sigma'\mu'}(\alpha)\ f^{(R)*}_{\lambda'\nu,\sigma'}$$

$$= \sum f^{(R)}_{\lambda\nu,\sigma}\ \tfrac{1}{2}(1+\vec{\sigma}\cdot\vec{P}')_{\sigma\sigma'}\ f^{(R)*}_{\lambda'\nu,\sigma'}$$

where $\vec{P}'$ is referred to axes rotated through α about the normal. See Fig. 2.

A more pertinent example is perhaps the t-channel helicity density matrix $\rho_f^{(t)}$. It is given by

$$\rho^{(t)}_{f_{\lambda\lambda'}} = \sum f^{(t)}_{\lambda\nu,\mu} \; \frac{1}{2}(1 + \vec{\sigma}\cdot\vec{P}'')_{\mu\mu'} \; f^{(t)*}_{\lambda'\nu,\mu}$$

where $f^{(t)}_{\lambda\nu,\mu}$ are the t-channel helicity amplitudes. By the same argument as before $\vec{P}''$ must be defined in the proton rest system, so that the t-channel c.m. is moving in the negative z-direction. This is either the same as or the opposite direction to the outgoing baryon's direction in the lab, depending on whether

$$-(s+m_p^2-m_\pi^2)(t+m_p^2-m_B^2)-2m_p^2(m_B^2-m_p^2+m_\pi^2-m_M^2)$$

is positive or negative, respectively. m_p, m_π, m_B, m_M denote the mass of the proton, pion, outgoing baryon and outgoing meson, respectively. This is shown in Fig. 3 for the former case. θ_L denotes the direction of the outgoing baryon in the lab. (Remember the incident π is moving in the negative z-direction.) In this case $\vec{P}''$ is the vector $\vec{P}$ rotated through an angle $(\pi-\theta_L)$ about the normal:

$$P_x'' = P_x \cos(\pi-\theta_L) + P_z \sin(\pi-\theta_L)$$

$$P_y'' = P_y$$

$$P_z'' = -P_x \sin(\pi-\theta_L) + P_z \cos(\pi-\theta_L) \quad .$$

(Note that when R is the outging baryon $\vec{P}' = \vec{P}''$. See Fig. 4.)

In all that follows we will not specify which frame is being used. The formulas are general and need only be supplemented by the proper definition of $\vec{P}$ and the polarization state of R that go along with the desired amplitude $f^{(s)}_{\lambda\nu,\mu}$ or $f^{(t)}_{\lambda\nu,\mu}$.

3. R = Baryon of Spin J

Consider processes like $\pi N \to \pi N^*$, $K\Lambda$, etc. with K a recoiling spin zero particle. Then

$$\rho_{\lambda\lambda'} = f_{\lambda\mu}\, f^*_{\lambda'\mu'}\, \tfrac{1}{2}(1 + \vec{\sigma}\cdot\vec{P})_{\mu\mu'}$$

$$= a_{\lambda\lambda'} + b_{\lambda\lambda'}\, \vec{P}\cdot\hat{n} + c_{\lambda\lambda'}\, \vec{P}\cdot\hat{p} + d_{\lambda\lambda'}\, \vec{P}\cdot\hat{n}\times\hat{p} \qquad (3.1)$$

where $\hat{n}$ is a unit vector normal to the reaction plane and $\hat{p}$ is a unit vector in the initial proton direction. The various matrices a,...,d are given by

$$\begin{aligned} a_{\lambda\lambda'} &= \tfrac{1}{2}(f_{\lambda+} f^*_{\lambda'+} + f_{\lambda-} f^*_{\lambda'-}) \quad , \\ b_{\lambda\lambda'} &= -\tfrac{1}{2}(f_{\lambda+} f^*_{\lambda'-} - f_{\lambda'} f^*_{\lambda'+}) \quad , \\ c_{\lambda\lambda'} &= \tfrac{1}{2}(f_{\lambda+} f^*_{\lambda'+} - f_{\lambda-} f^*_{\lambda'-}) \quad , \\ d_{\lambda\lambda'} &= \tfrac{1}{2}(f_{\lambda+} f^*_{\lambda'-} + f_{\lambda'-} f^*_{\lambda'+}) \quad . \end{aligned} \qquad (3.2)$$

The matrices are all hermitian: $a_{\lambda\lambda'} = a^*_{\lambda'\lambda}$, etc., and if parity is conserved

$$a_{\lambda\lambda'} = (-1)^{\lambda-\lambda'} a_{-\lambda,-\lambda'}, \quad b_{\lambda\lambda'} = (-1)^{\lambda-\lambda'} b_{-\lambda,-\lambda'}$$

$$c_{\lambda\lambda'} = -(-1)^{\lambda-\lambda'} c_{-\lambda,-\lambda'}, \quad d_{\lambda\lambda'} = -(-1)^{\lambda-\lambda'} d_{-\lambda,-\lambda'} \; . \qquad (3.3)$$

Note that $\rho_{\lambda\lambda'} \neq (-1)^{\lambda-\lambda'}\rho_{-\lambda,-\lambda'}$ unless $P_x = P_z = 0$. Evidently

a is determined by unpolarized p

b is " " P normal to plane

c is " " P longitudinal

d is " " P transverse in plane

Note that normal polarization can give components in the plane by varying the azimuth of the reaction plane. Since f cannot depend on Φ, this gives information on a combination of c and d. But without a longitudinally polarized target P_x and P_z cannot be varied independently:

$$\rho^{(s)}: \quad P_x = P\sin\Phi\,, \quad P_y = P\cos\Phi\,, \quad P_z = 0$$

gives $d^{(s)}$ but not $c^{(s)}$

$$\rho^{(t)}: \quad P_x = -P\sin\Phi\cos\theta_L, \quad P_z = -P\sin\Phi\sin\theta_L$$

$$\text{gives}\left(d^{(t)}\cos\theta_L + c^{(t)}\sin\theta_L\right)$$

However $c^{(t)}$ and $d^{(t)}$ will depend on θ_L and cannot be separated by varying θ_L.

Note that in general

$$\mathrm{Tr}\, c = \mathrm{Tr}\, d = 0 \tag{3.4}$$

so

$$\frac{d\sigma}{d\Omega} = \mathrm{Tr}\,\rho = \mathrm{Tr}\, a + \vec{P}\cdot\hat{n}\,\mathrm{Tr}\, b \tag{3.5}$$

depends only on the normal polarization (with parity conservation.) To get information on c and d some final state polarization must be measured.

If only the angular distribution of the decay of the N*, Λ, etc. is measured, it is given by

$$\sum_{\lambda,\lambda'\mu} \mathcal{D}^{J}_{\lambda\mu}(\theta,\varphi)\mathcal{D}^{J}_{\lambda',\mu}(\theta,\varphi)^{*} F_{\mu}F_{\mu}^{*}\rho_{\lambda\lambda'}$$

where μ is the helicity of the decay product baryon and F_{μ} the decay amplitude. If parity in the decay is conserved $|F_{\mu}| = |F_{-\mu}|$. A typical term is

$$e^{-i(\lambda-\lambda')\varphi}\sum_{\mu}(d^{J}_{\lambda\mu}(\theta)d^{J}_{\lambda',\mu}(\theta)|F_{\mu}|^{2}\rho_{\lambda\lambda'} + d^{J}_{-\lambda\mu}(\theta)d^{J}_{-\lambda',\mu}(\theta)|F_{\mu}|^{2}\rho_{-\lambda',-\lambda})$$

$$= e^{-i(\lambda-\lambda')\varphi}\sum_{\mu}(\rho_{\lambda\lambda'}|F_{\mu}|^{2} + (-1)^{\lambda-\lambda'}\rho_{-\lambda',-\lambda}|F_{-\mu}|^{2})d^{J}_{\lambda',\mu}(\theta)d^{J}_{\lambda',\mu}(\theta)$$

so if parity is conserved only

$$\rho_{\lambda\lambda'} + \rho_{-\lambda',-\lambda}(-1)^{\lambda-\lambda'}$$

is measurable. That is, only

$$\text{Re } a_{\lambda\lambda'} \quad , \quad \text{Re } b_{\lambda\lambda'}$$

$$\text{Im } c_{\lambda\lambda'} \quad , \quad \text{Im } d_{\lambda\lambda'}$$

are measurable. This is the generalization of the usual statement that only $\text{Re}\rho_{\lambda\lambda'}$ is measurable for unpolarized initial states.

However, there are additional relations that are apparent from (3.2); namely from parity conservation

$$a_{-\lambda,\lambda'} = (-1)^{\lambda-\frac{1}{2}}\, ib_{\lambda\lambda'}\eta(-1)^{J-\frac{1}{2}} \qquad (3.6a)$$

$$c_{-\lambda,\lambda'} = (-1)^{\lambda+\frac{1}{2}}\,\eta(-1)^{J-\frac{1}{2}}\,d_{\lambda\lambda'}\,, \qquad (3.6b)$$

where η is the intrinsic parity of the outgoing baryon. We learn two things from this: (i) if we can measure all of the elements of a and d we don't learn anything new by measuring b and c; in particular longitudinal polarization is not needed. (ii) if we can measure only Re a and Re b we can calculate Im a and Im b; hence a target with normal polarization removes the need for observing parity violating decays. (This is the generalization of the familiar equivalence between measuring final state polarization with an unpolarized target and measuring the asymmetry with a polarized target in $\pi N \to \pi N$.)

There are also nonlinear relations, for fixed kinematics, which may be useful. These are like rank conditions and follow simply from (3.2):

$$i(bd-db) = c\,\mathrm{Tr}\,a \qquad (3.7a)$$

$$(d^2+b^2) = a\,\mathrm{Tr}\,a \qquad (3.7b)$$

4. R = Meson of Spin J

Consider processes like $\pi N \to A_2 N$, $K^*\Lambda$, etc. where X is a recoiling spin 1/2 particle. The density matrix again has the form (3.1) and the symmetry conditions (3.3) are the same. The matrices are given by

$$a_{\lambda\lambda'} = \tfrac{1}{2} \sum_{\nu=\pm\frac{1}{2}} (f_{\lambda\nu,+}\, f^*_{\lambda'\nu,+} + f_{\lambda\nu,-}\, f^*_{\lambda'\nu,-})\,,$$

$$b_{\lambda\lambda'} = -\tfrac{i}{2} \sum_{\nu=\pm\frac{1}{2}} (f_{\lambda\nu,+}\, f^*_{\lambda'\nu,-} - f_{\lambda\nu,-}\, f^*_{\lambda'\nu,+})\,,$$

$$c_{\lambda\lambda'} = \frac{1}{2} \sum_{\nu=\pm\frac{1}{2}} (f_{\lambda\nu,+} f^*_{\lambda'\nu,+} - f_{\lambda\nu,-} f^*_{\lambda'\nu,-}) ,$$

$$d_{\lambda\lambda'} = \frac{1}{2} \sum_{\nu=\pm\frac{1}{2}} (f_{\lambda\nu,+} f^*_{\lambda'\nu,-} + f_{\lambda\nu,-} f^*_{\lambda'\nu,+}) . \qquad (4.1)$$

The discussion of measurability goes through but (3.6) and (3.7) are no longer valid.

Some simplification can be achieved if we go over to amplitudes corresponding to eigenstates of reflection:

$$f^{(\epsilon)}_{\lambda\mu,\nu} = \xi_\lambda (f_{\lambda\mu,\nu} + \epsilon\eta(-1)^{J-\lambda} f_{-\lambda\mu,\nu}) \qquad (4.2)$$

where $\xi_\lambda = 1/(2)^{\frac{1}{2}}$, $\lambda \neq 0$, $\xi_\lambda = 1/2$, $\lambda = 0$. η denotes the parity of R. These amplitudes correspond asymptotically to the exchange of definite naturality σ,

$$\sigma = \mp \eta(-1)^J .$$

Then

$$a^{\epsilon\epsilon'}_{\lambda\lambda'} = \xi_\lambda\xi_{\lambda'}(1+\epsilon\epsilon') (a_{\lambda\lambda'} + \eta(-1)^{J-\lambda}\epsilon a_{-\lambda\lambda'}) ,$$

$$b^{\epsilon\epsilon'}_{\lambda\lambda'} = \xi_\lambda\xi_{\lambda'}(1+\epsilon\epsilon') (b_{\lambda\lambda'} + \eta(-1)^{J-\lambda}\epsilon b_{-\lambda\lambda'}) ,$$

$$c^{\epsilon\epsilon'}_{\lambda\lambda'} = \xi_\lambda\xi_{\lambda'}(1-\epsilon\epsilon') (c_{\lambda\lambda'} + \eta(-1)^{J-\lambda}\epsilon c_{-\lambda\lambda'}) ,$$

$$d^{\epsilon\epsilon'}_{\lambda\lambda'} = \xi_\lambda\xi_{\lambda'}(1-\epsilon\epsilon') (d_{\lambda\lambda'} + \eta(-1)^{J-\lambda}\epsilon d_{-\lambda\lambda'}) . \qquad (4.3)$$

Evidently, $a^{\epsilon\epsilon'}$ and $b^{\epsilon\epsilon'}$ get contributions only from products of amplitudes of the same naturality while $c^{\epsilon\epsilon'}$ and $d^{\epsilon\epsilon'}$ get contributions only from interference between different naturality. This results from the sum on the unobserved final nucleon spin.

The advantage gained by going over to these matrices is that they are all of rank 2 while the original matrices were all of rank 4. This follows from the relation

$$f^{\epsilon}_{\lambda -\mu,\nu} = \epsilon(-1)^{\mu-\nu} f^{\epsilon}_{\lambda\mu,-\nu} \quad . \tag{4.4}$$

Hence

$$a^{\epsilon\epsilon'}_{\lambda\lambda'} = \xi_\lambda \xi_{\lambda'}(1+\epsilon\epsilon')\tfrac{1}{2} \sum_{\mu\nu} f^{\epsilon}_{\lambda\mu\nu}\, f^{\epsilon'*}_{\lambda'\mu\nu}$$

$$= \xi_\lambda \xi_{\lambda'}(1+\epsilon\epsilon') \sum_{\nu} f^{\epsilon}_{\lambda\frac{1}{2},\nu}\, f^{\epsilon'*}_{\lambda'\frac{1}{2}\nu} \quad ,$$

$$b^{\epsilon\epsilon'}_{\lambda\lambda'} = \xi_\lambda \xi_{\lambda'}(1+\epsilon\epsilon')(-\tfrac{1}{2}) \sum_{\mu,\nu} (-1)^{\frac{1}{2}-\nu} f^{\epsilon}_{\lambda\mu,\nu}\, f^{\epsilon'*}_{\lambda'\mu,-\nu}$$

$$= -i\xi_\lambda \xi_{\lambda'}(1+\epsilon\epsilon') \sum_{\nu} (-1)^{\frac{1}{2}-\nu} f^{\epsilon}_{\lambda\frac{1}{2},\nu}\, f^{\epsilon'*}_{\lambda'\frac{1}{2},-\nu} \quad ,$$

$$c^{\epsilon\epsilon'}_{\lambda\lambda'} = \xi_\lambda \xi_{\lambda'}(1-\epsilon\epsilon')\tfrac{1}{2} \sum_{\mu,\nu} (-1)^{\frac{1}{2}-\nu} f^{\epsilon}_{\lambda\mu,\nu}\, f^{\epsilon'*}_{\lambda\mu,\nu}$$

$$= \xi_\lambda \xi_{\lambda'}(1-\epsilon\epsilon') \sum_{\nu} (-1)^{\frac{1}{2}-\nu} f^{\epsilon}_{\lambda\frac{1}{2},\nu}\, f^{\epsilon'*}_{\lambda\frac{1}{2},\nu} \quad ,$$

$$d^{\epsilon\epsilon'}_{\lambda\lambda'} = \xi_\lambda \xi_{\lambda'}(1-\epsilon\epsilon')\tfrac{1}{2} \sum_{\mu,\nu} f^{\epsilon}_{\lambda\mu,\nu}\, f^{\epsilon'*}_{\lambda\mu,-\nu}$$

$$= \xi_\lambda \xi_{\lambda'}(1-\epsilon\epsilon')\tfrac{1}{2} \sum_{\nu} f^{\epsilon}_{\lambda\frac{1}{2},\nu}\, f^{\epsilon'*}_{\lambda\frac{1}{2},-\nu} \quad ,$$

where $\epsilon = \epsilon'$ has been used in the first pair and $\epsilon = -\epsilon'$ in the second. It is then easy to see that the matrices

$$a^{\epsilon\epsilon'} \pm b^{\epsilon\epsilon'} , \quad c^{\epsilon\epsilon'} \pm id^{\epsilon\epsilon'}$$

are all rank 1 and so are all subject to the usual rank conditions. This is probably most useful for $a \pm b$. As in the last section, if only Re a and Re b are measurable, then Im$(a \pm b)$ are both determined up to a sign. For additional discussion of these points, see the forthcoming publication of S.U. Chung and T.L. Trueman.[1]

It is also possible to derive expressions similar to (3.7a) which may be useful:

$$c^{\epsilon\epsilon} (\mathrm{Tr}\, a^{\epsilon'\epsilon'}\Delta_\epsilon - \mathrm{Tr}\, a^{\epsilon\epsilon}\Delta_{\epsilon'})$$

$$= i[d^{\epsilon\epsilon'}\Delta_\epsilon(2b^{\epsilon'\epsilon'} - \mathrm{Tr} b^{\epsilon'\epsilon'}) + (2b^{\epsilon\epsilon} - \mathrm{Tr} b^{\epsilon\epsilon})\Delta_{\epsilon'} d^{\epsilon\epsilon'}] ,$$

$$c^{\epsilon\epsilon'} (\mathrm{Tr}\, b^{\epsilon'\epsilon'}\Delta_\epsilon - \mathrm{Tr}\, b^{\epsilon\epsilon}\Delta_{\epsilon'})$$

$$= i[d^{\epsilon\epsilon'}\Delta_\epsilon(2a^{\epsilon'\epsilon'} - \mathrm{Tr} a^{\epsilon'\epsilon'}) + (2a^{\epsilon\epsilon} - \mathrm{Tr} a^{\epsilon\epsilon})\Delta_{\epsilon'} d^{\epsilon\epsilon'}] , \qquad (4.5)$$

where

$$\Delta_\epsilon = (\mathrm{Tr}(a^{\epsilon\epsilon})^2 - \mathrm{Tr}(b^{\epsilon\epsilon})^2)^{\frac{1}{2}} .$$

5. $\pi N \to \Lambda K$

This is a particularly nice case since the Λ decay allows the measurement of both $\rho_{\lambda\lambda'}$ and $\rho_{-\lambda'-\lambda}$. Now the matrices a,b,c, and d can be written out explicitly in terms of Pauli matrices and real scalar functions:

$$\rho = a_0 + a_1 \vec{\sigma}\cdot\hat{n} + (b_0 + b_1 \vec{\sigma}\cdot\hat{n})\vec{P}\cdot\hat{n}$$
$$+ (c_2 \vec{\sigma}\cdot\hat{p}_\Lambda + c_3 \sigma\cdot\hat{n}\times\hat{p}_\Lambda)\vec{P}\cdot\hat{p}$$
$$+ (d_2 \vec{\sigma}\cdot\hat{p}_\Lambda + d_3 \sigma\cdot\hat{n}\times\hat{p}_\Lambda)\vec{P}\cdot\hat{n}\times\hat{p} \quad . \qquad (5.1)$$

All unit vectors here are defined in the c.m. system.

In terms of the Mueller amplitudes $A_{\lambda'\mu',\lambda\mu}$ (see Fig. 5) we have

$$A_{++,++} = a_0+c_2 \qquad A_{++,+-} = -ib_0+d_2$$
$$A_{+-,+-} = a_0-c_2 \qquad A_{++,-+} = ia_1+c_3$$
$$A_{++,--} = b_1+d_3 \qquad A_{+-,-+} = -b_1+d_3$$
$$A_{+-,++} = ib_0+d_2 \qquad A_{+-,--} = ia_1-c_3 \; . \qquad (5.2)$$

The others are all related to these by parity and hermiticity:

$$A_{\lambda\mu,\lambda'\mu'} = A^*_{\lambda'\mu',\lambda\mu}$$
$$A_{-\lambda-\mu,-\lambda'-\mu'} = (-1)^{(\lambda-\mu)-(\lambda'-\mu')} A_{\lambda\mu,\lambda'\mu'} \qquad (5.3)$$

One could also parametrize the density matrix in terms of the Wolfenatein parameters which are referred to a mixed basis: the proton spin is quantized along the incident direction but the Λ spin is quantized along $\vec{p}_\Lambda$ in the lab. The former is appropriate for s-channel amplitudes, the latter for t-channel amplitudes so the crossing angle χ comes in. (see the discussion in Sec. II.) The angle is shown in Fig. 6. Our amplitudes have the Λ spin quantized along $\vec{p}_\Lambda$ in the s channel c.m. It is straightforward to work out the connection. It is given in the following table along with the required proton and Λ polarizations needed to measure them.

Wolfenstein parameters	Proton Polarization	Λ Polarization (P_Λ in lab)
$A = (-c_2 \sin X + c_3 \cos X)$	P_z	$\hat{p}_\Lambda \times \hat{n}$
$R = (-d_2 \sin X + d_3 \cos X)$	P_x	$\hat{p}_\Lambda \times \hat{n}$
$A' = (c_2 \cos X + c_3 \sin X)$	P_z	$\hat{p}_\Lambda$
$R' = (d_2 \cos X + d_3 \sin X)$	P_x	$\hat{p}_\Lambda$
$D = b_1$	P_y	$\hat{n}$
$P_2 = a_1$	none	$\hat{n}$
$P_1 = b_0$	P_y	none

1. S.U. Chung and T.L. Trueman, Phys. Rev. D11, 633 (1975).

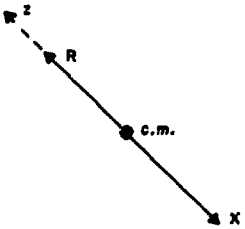

Figure 1

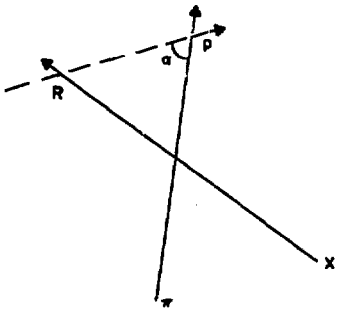

Figure 2

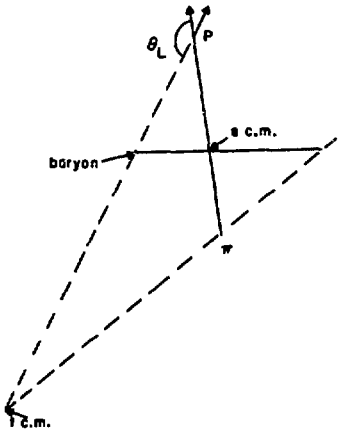

Figure 3.

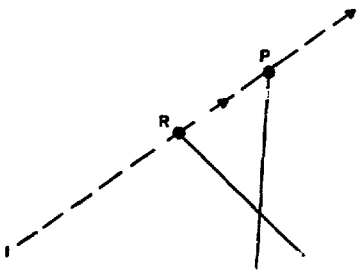

Figure 4.

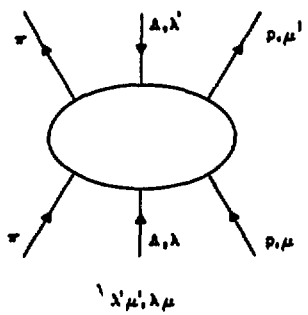

Figure 5.

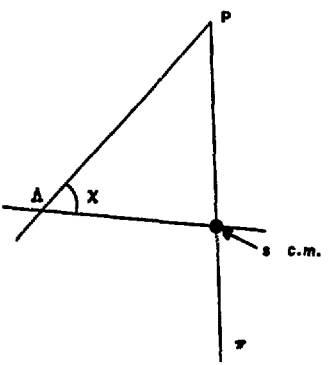

Figure 6.

NEW DIRECTIONS IN POLARIZATION PHYSICS*

A. Yokosawa

Argonne National Laboratory, Argonne, Illinois 60439

Presented at the

Brookhaven National Laboratory Workshop on Polarized Targets

June 1974

*Work performed under the auspices of the U.S. Atomic Energy Commission

NEW DIRECTIONS IN POLARIZATION PHYSICS

During the past 10 years, many experiments have been carried out with polarized targets. The results give new insights into hadronic physics and are extremely useful in answering many questions and checking theoretical predictions. So far, most of the experiments have been performed for two-body, final-state reactions for which many measurements are still to be taken. We are far from reaching our goal. New directions in polarization physics would involve decisive measurements to determine scattering amplitudes of two-body and multibody final-state reactions. We will start by discussing simple reactions and move on to more complicated reactions.

I. Elastic Scattering

A. πN Elastic Scattering and Charge-Exchange Reactions

1. πp Elastic Scattering

Polarization measurements in this reaction have been made far more than in other reactions. However, the existing data are limited to the following range:

Forward scattering:	up to 40 GeV/c
Large momentum-transfer region:	up to $\|t\| \approx 2.5$
Backward scattering:	up to 6 GeV/c
R and A parameters ($\|t\| < 0.5$):	only at 6 GeV/c (R parameter in π^-p also at 16 GeV/c)

Some of the typical polarization data in πp elastic scattering are presented here. Figure 1 shows a mirror symmetry between π^+p and π^-p

scattering. All-angle polarization data have good quality at intermediate energies. Figure 2 shows a simultaneous plot of $\pi^+ p$ and $\pi^- p$ data, and it is remarkable to see the t-channel exchange effect from the forward region all the way to the backward region.

One should pursue the study of the effect by covering the higher $|t|$ region at higher energies.

Limited data exist on A and R parameters in $\pi^\pm p$ scattering.[1] Forward data at 6 GeV/c are shown in Fig. 3. We still lack data with better accuracy covering wider $|t|$ range at various energies.

In backward scattering, we can study baryon-exchange processes. At present, this field is wide open and is definitely challenging. Figure 4 shows the remarkable energy dependence in $\pi^+ p$ polarization data. A similar study for $\pi^- p$ is in progress at ANL and CERN.

2. πp Charge-Exchange Reaction

The existing polarization data are limited to the following range:

Forward scattering: up to 11.2 GeV/c ($|t| < 0.3$)

up to 8 GeV/c ($|t| < 1.5$)

The result of the nonzero polarization in forward πp charge-exchange reaction made Regge-pole people think seriously about Regge cuts, absorption models, or extra poles besides the dominating ρ pole. The scope of all the existing charge-exchange polarization measurements is shown in Table I.

Figure 5 shows the results of measurements at 3.5 and 5.0 GeV/c in the range of $0.2 \leq |t| \leq 1.8$ $(\text{GeV/c})^2$. Experimentally, this is one of the most difficult channels, and we need data at higher energies as well as at intermediate energies.

The above data were used together with seven other measurements to determine the scattering amplitudes of πN scattering at 6 GeV/c. Some of the results[6] are shown in Fig. 6.

Table I Polarization Experiments in πp Charge Exchange

Experiments	$\|t\|$ Range Measured	π^0 Detector	Neutron Counters Used	Types of Polarized Proton Target	Target Polarization
CERN(old)[2], 5.9 and 11.2 GeV/c	< 0.2	Lead-sandwiched optical spark-chamber	Yes	LMN-24H_2O	60%
CERN(new)[3], 5 and 8 GeV/c	< 1.5	Same as above	No	Butanol	33%
ANL (old)[4], 2.07 GeV/c to 5.0 GeV/c	< 0.3	Lead-sandwiched Lucite Cerenkov counter (on-line)	Yes	LMN-24H_2O	60%
ANL(new)[5], 3.5 and 5.0 GeV/c	< 1.5	Lead-glass counter hodoscope (on-line)	No*	Ethylene glycol (frozen antifreeze)	60-80%

*Neutron counters were used to cover a limited angular region.

B. KN Elastic Scattering and Charge-Exchange Reaction

1. Kp Elastic Scattering

Polarization measurements at high energies have been made at CERN only in the forward regions. Some of the data are shown in Figs. 7 and 8. The results of polarization measurements in K^+p scattering at ANL are

available at all angles from 1.60 to 2.31 GeV/c as shown in Fig. 9.

2. Kp Charge Exchange

The $K^- p \to \bar{K}^0 n$ polarization has been measured at 8 GeV/c and for $|t|$ values from 0 to 1.2 $(GeV/c)^2$. The experiment was performed by using the unique CERN-ETH magnet for a polarized-proton target and, at the same time, for detecting the trajectories of the $\bar{K}^0$ produced in the forward direction. The experimental result is shown in Fig. 10. The polarization P(t) is definitely non-zero, in contradiction with the requirements of exchange degeneracy.

A Saclay group will be measuring the polarization in K^+ -neutron charge exchange at CERN by using a polarized-neutron target.

C. Nucleon-Nucleon Elastic Scattering

1. pp Elastic Scattering

Polarization in pp elastic scattering has been measured up to 17.5 GeV/c at CERN and up to 12 GeV/c at ANL. Some of the data[7,8] are shown in Figs. 11 and 12. There is a dip in the region $0.8 < |t| < 1.0$, and the polarization becomes large for $|t| > 1.0$. Data at large $|t|$ might provide valuable extra constraints on parton models.

A new direction in a study of the reaction would be to do p-p amplitude measurements, especially when both the polarized beam and polarized target are available. A minimum of nine measurements are needed to determine five complex amplitudes. Details of such an experimental program have been written elsewhere.[9]

2. $\bar{p}p$ Elastic Scattering

Polarization measurements in the forward region were made at 2.74, 6.0, and 10.0 GeV/c at CERN. More accurate data are badly needed from 0.5 GeV/c to higher energies for a search of possible resonant states.

3. $\bar{p}p$ Charge-Exchange Reaction

The $\bar{p}p \to \bar{n}n$ polarization[10] has been measured at 8 GeV/c for a momentum transfer $|t|$ from 0 to 0.8 $(GeV/c)^2$. The result is shown in Fig. 13. The polarization is small and negative.

4. np Elastic and np Charge Exchange

Polarization measurements in np elastic scattering were made up to 1.5 GeV/c. We can perform np amplitude measurements by using a polarized-neutron target and a polarized beam.

The polarization parameter in neutron-proton charge-exchange scattering[11] has been measured for incident neutron momentum up to 12 GeV/c in the region $0.01 \leq |t| \leq 1.0$ $(GeV/c)^2$. As shown in Fig. 14, results show a negative polarization whose magnitude increases with $|t|$; for fixed momentum transfer the polarization has little energy dependence.

II. Inelastic Scattering

A. $\pi^- p \to \eta^0 n$

This reaction is expected to proceed by the exchange of only the A_2 trajectory in the t channel. As shown in Fig. 15, the polarization data are

very limited. Measurements are scheduled at ANL by using both the lead-glass hodoscope and the neutron-counter hodoscope.

B. Hypercharge Exchange

1. π induced

The reaction $\pi p \to K$ hyperons is suited for amplitude measurements. By observing the decay distributions of hyperons, one can analyze their spin states. When a polarized target is used, a complete set of observables will be measured. Experiments planned or scheduled at CERN and RHEL are

$$\pi^- p \to K^o \Lambda^o / \Sigma^o,$$
$$\pi^+ p \to K^+ \Sigma^+, \text{ and}$$
$$\pi^+ p \to \Sigma^+ K^+.$$

The amplitude measurement of a baryon-exchange process, $\pi^- p \to \Lambda K^o$, has been performed at CERN. (CERN-ETH Zurich-Helsinki-L C. Collaboration) The polarization in $\pi^{\pm} p \to \Sigma K$ has been measured at 3.5 GeV/c by a CERN-Trieste group. Results of backward $\pi^+ p \to \Sigma^+ \Lambda$ scattering[12] are shown in Fig. 16 together with the $\pi^- p \to K^o \Lambda$ data at 4 GeV/c.[13] The striking difference of the two sets of data must be associated with the possibility of Λ exchanges in the $K\Sigma$ reaction.

2. K induced

Line-reversal pairs of reactions to be investigated are:

$\bar{K} N \to \pi \Lambda$	$\pi N \to K N$
$\bar{K} N \to \pi \Sigma^+$	$\pi N \to K \Sigma^+$
$\bar{K} N \to \pi Y_1^*(1385)$	$\pi N \to K Y_1^*(1385)$

In a study of the reactions $\bar{K}p \rightarrow \Lambda(\Sigma^0)$ + vector mesons, one observes the angular correlation of the hyperon and vector meson decays. One observes natural, as well as unnatural, parity exchange. Some of the measurements were carried out with the CERN 2-m bubble chamber.[14] Predictions of SU(3) symmetry and the quark model are that the following amplitudes are equal:

$$A(\pi^- p \rightarrow K^{*}\Lambda) = -A(K^- p \rightarrow \phi\Lambda),$$

$$A(\pi^- p \rightarrow K^{*}\Sigma) = -A(K^- p \rightarrow \phi\Sigma), \text{ and}$$

$$A(K^- p \rightarrow \rho\Lambda) = A(K^- p \rightarrow \omega\Lambda).$$

The agreement of the experimental data with the theoretical predictions is remarkable.

C. $\pi p \rightarrow \rho N$ and $\pi p \rightarrow \pi\pi N$

A Yale group (M. Zeller et al.) has recently measured the polarization in $\pi^- p \rightarrow \rho^0 n$ reaction at 2.7 GeV/c in the range $0.05 < |t| < 0.3$. The measurement in $\pi^- p \rightarrow \pi^+\pi^- n$ at higher energies will soon be done by a CERN-Munich group with wire-chamber magnetic spectrometer, Pb sandwich scintillation counter, and Cerenkov hodoscope.

Very limited data (by P. Sonderegger et al.) -- only a few points with large error -- of the polarization in $\pi^- p \rightarrow \pi^0\pi^0$ are available at 6 and 11 GeV/c. Accurate measurements of this reaction are badly needed.

D. $\bar{p}p \rightarrow \pi^+\pi^-$

The polarization in $\bar{p}p \rightarrow \pi^+\pi^-$ at a low energy was measured at the BNL AGS.[15] A DNPL-QMC-RHEL group has completed similar measurements in the momentum range 1.2 to 2.4 GeV/c with better statistics.

III. Inclusive Polarization Measurements

Spin dependence of pion-induced inclusive reactions, $\pi^{\pm}p \to \pi^{\pm} X$, has recently been investigated at CERN. (CERN-Orsay-Oxford Collaboration)

References

1. A. deLesquin et al., Phys. Lett. 40B, 277 (1972)
2. P. Bonamy et al., Nucl. Phys. B16, 335 (1970)
3. G. Cozzika et al., Phys. Lett. 40B, 281 (1972); M. Giffon, Nuovo Cimento 7A, 705 (1972)
4. D. Drobnis et al., Phys. Rev. Lett. 20, 274 (1968)
5. D. Hill et al., Phys. Rev. Lett. 30, 239 (1973)
6. P. Johnson et al., Phys. Rev. Lett. 30, 242 (1973)
7. J. H. Parry et al., Phys. Rev. 8D, 45 (1973)
8. G. W. Abshire et al., Phys. Rev. Lett. 32, 1261 (1974)
9. A. Yokosawa, Proceedings of the Symposium on High Energy Physics with Polarized Beams, XIII-1, (February, 1974)
10. P. LeDu et al., Phys. Lett. 44B, 390 (1973)
11. M. A. Abolins et al., Phys. Rev. Lett. 30, 1183 (1973)
12. F. Bradamante et al., Phys. Lett. 44B, 202 (1973)
13. W. Beusch et al., Nucl. Phys. B19, 546 (1974)
14. A. Rouge et al., Nucl. Phys. B44, 365 (1972)
15. R. D. Erlich et al., Phys. Rev. Lett. 28, 1147 (1972)

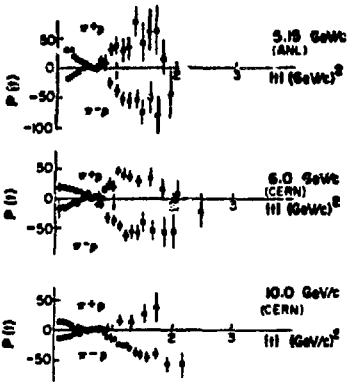

Figure 1. Forward polarization in $\pi^+ p$ and $\pi^- p$ elastic scattering.

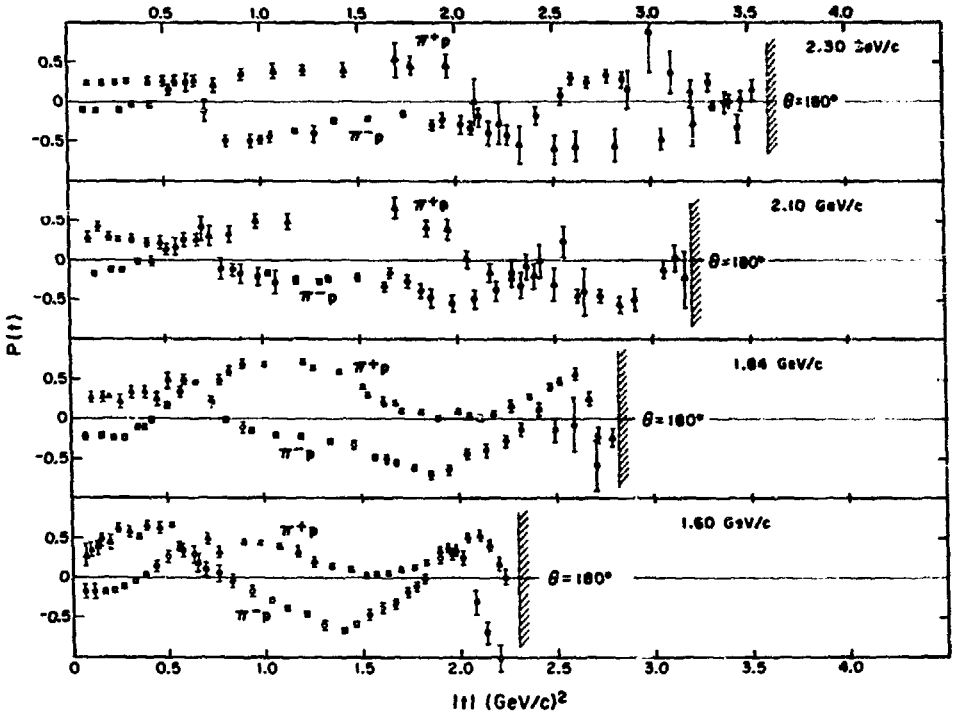

Figure 2. Polarization in $\pi^{\pm}p$ elastic scattering at all angles. Note that 1.80 GeV/c $\pi^{+}p$ and 1.88 GeV/c $\pi^{-}p$ data are shown as 1.84 GeV/c.

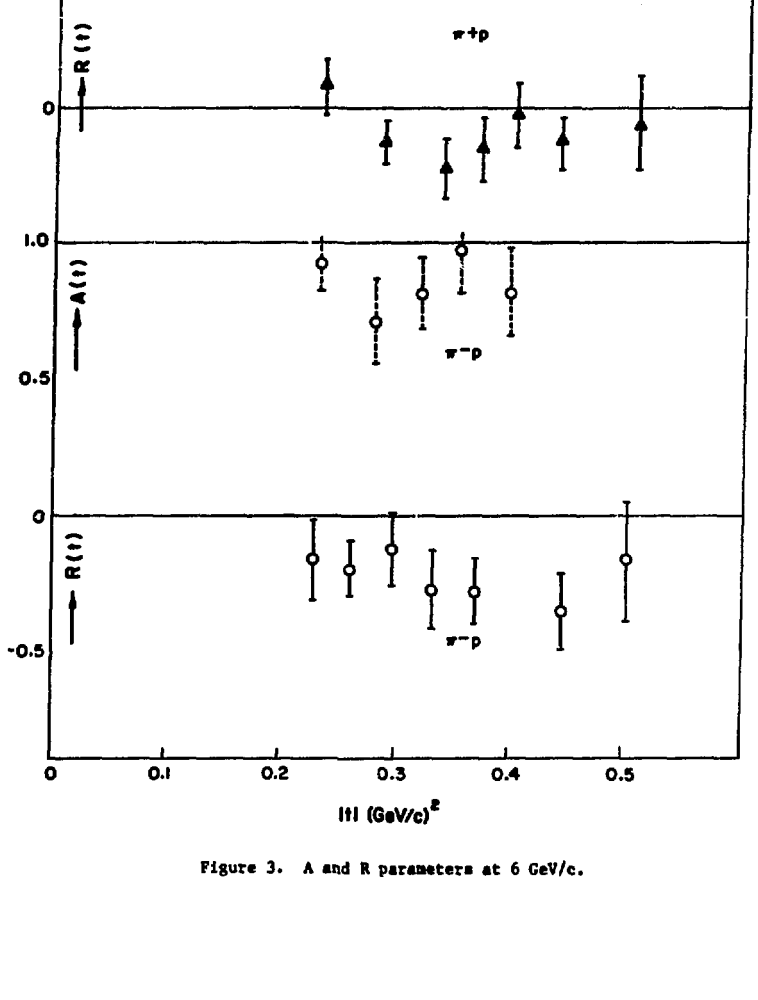

Figure 3. A and R parameters at 6 GeV/c.

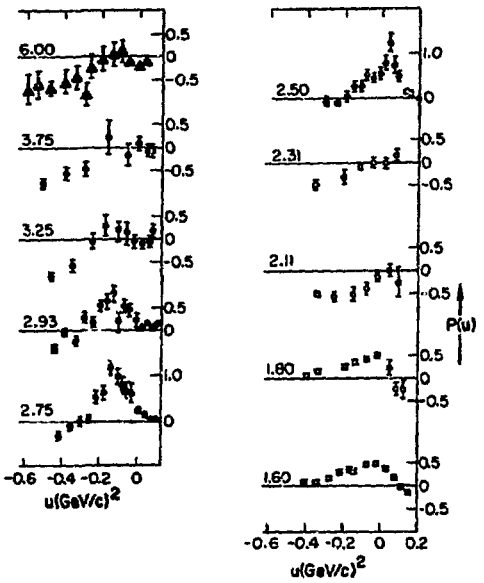

Figure 4. Backward polarization in $\pi^+ p$ from 1.6 to 6.0 GeV/c.

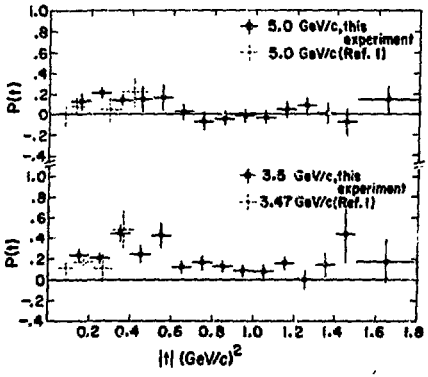

Figure 5. πp charge-exchange polarization P(t) at 5.0 and 3.5 GeV/c. The errors shown do not include the calibration uncertainty in P_T.

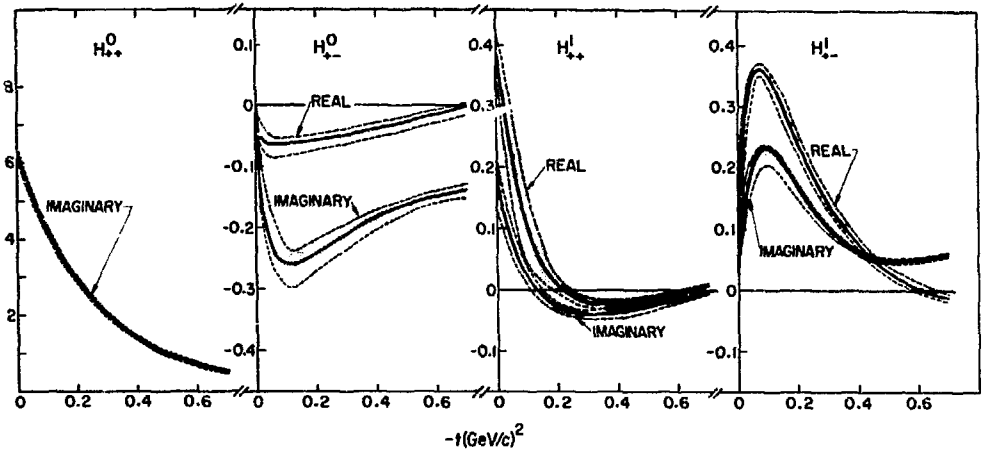

Figure 6. π N amplitudes at 6.0 GeV/c as determined from t-dependent fit shown by dark central lines. The error bands (determined by the envelope of fits to randomized data) are represented by shaded regions.

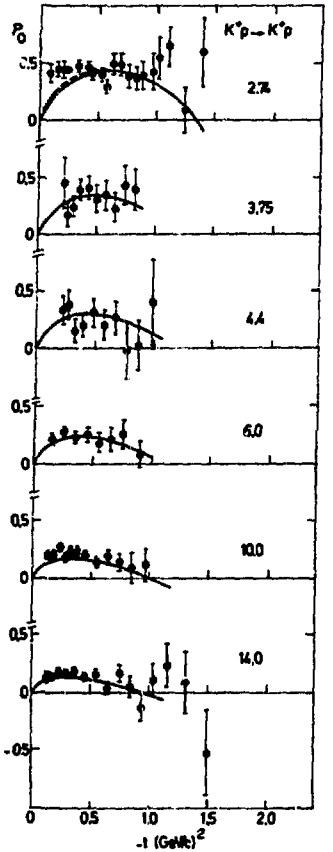

Figure 7. K^+p polarization data from 2.74 to 14.0 GeV/c.

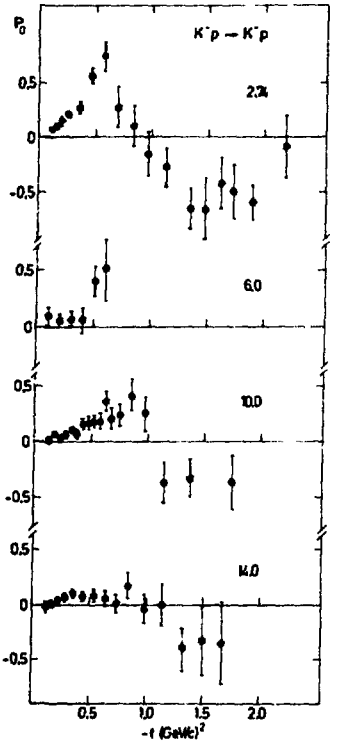

Figure 8. K^-p polarization data from 2.74 to 14.0 GeV/c.

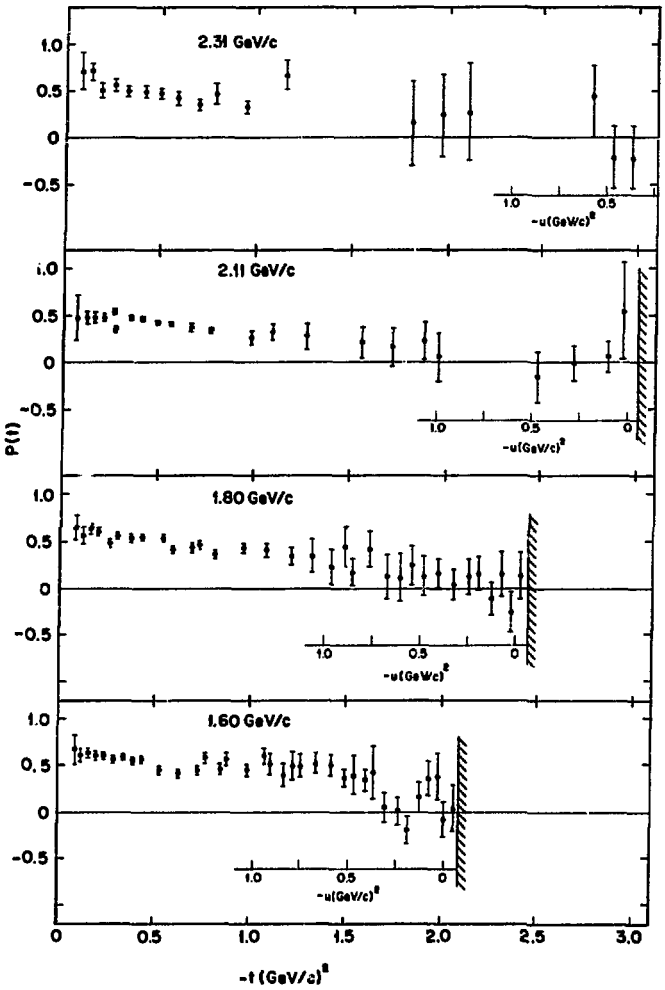

Figure 9. K⁻p polarization from 1.60 to 2.31 GeV/c.

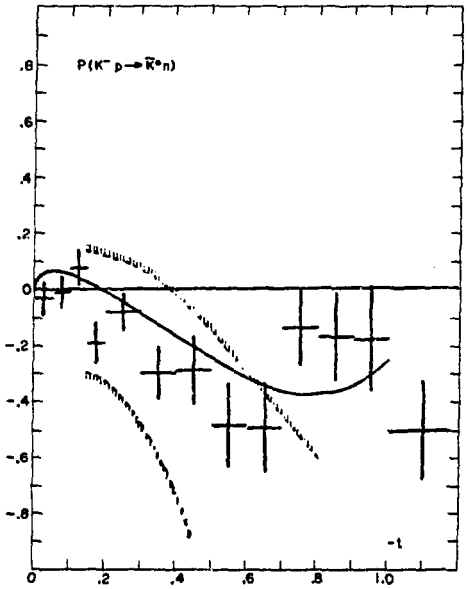

Figure 10. P(t) for $K^- p \to \overline{K}^0 n$ at 8 GeV/c.

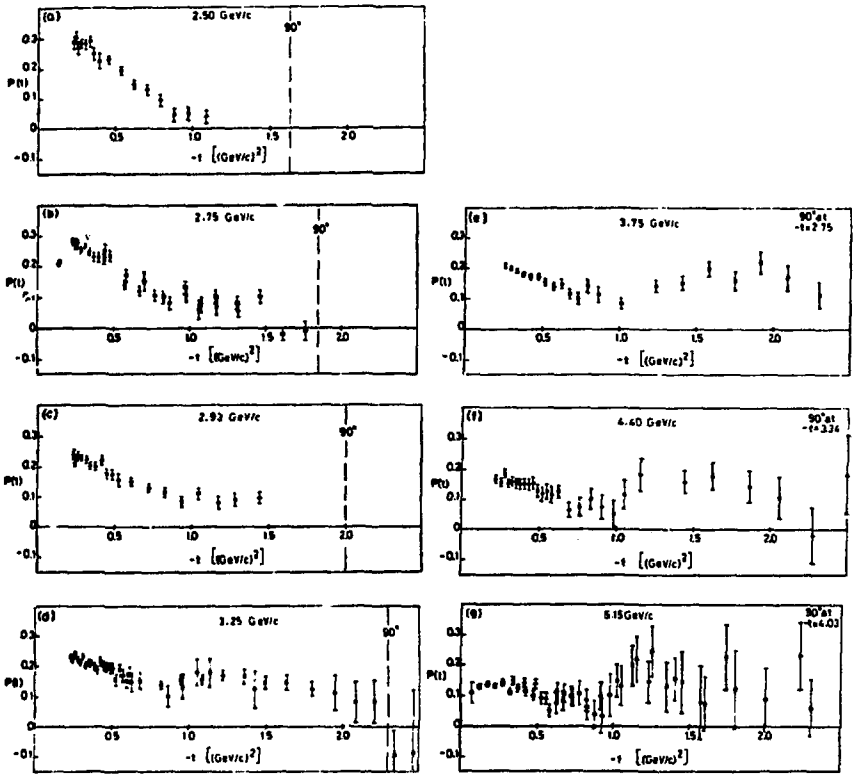

Figure 11. Polarization results in p p scattering for 2.50 to 5.15 GeV/c.

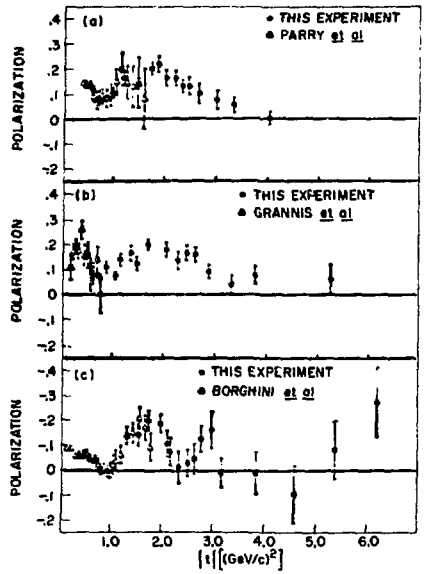

Figure 12. Polarization results in p p scattering for 5.15 to 12.33 GeV/c.

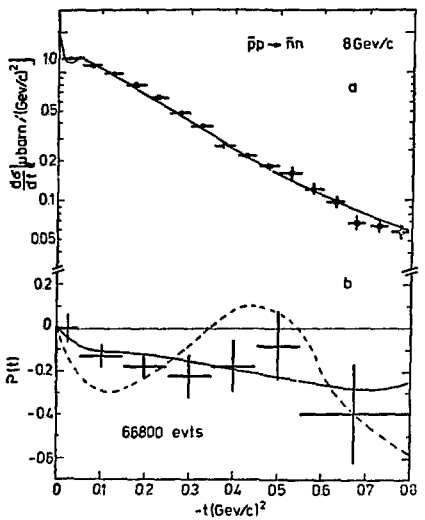

Figure 13. Polarization parameter for the reaction $\bar{p}\ p \to \bar{n}\ n$ at 8 GeV/c.

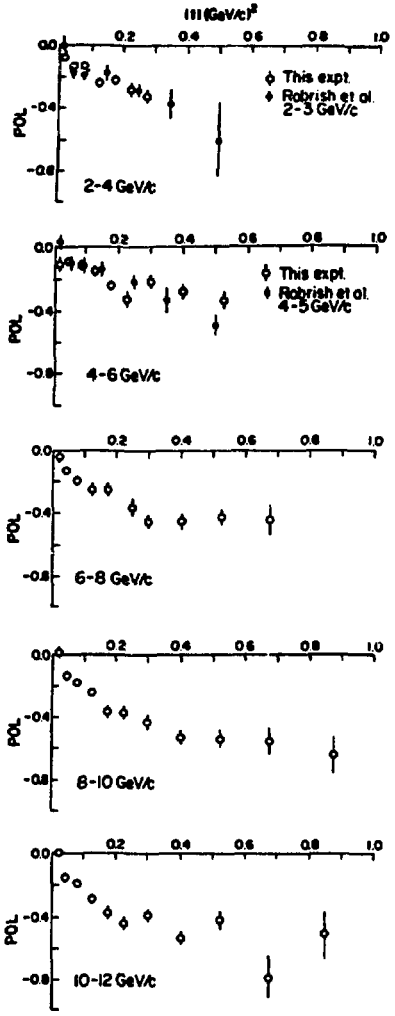

Figure 14. Polarization parameters in np charge-exchange scattering from 2 to 12 GeV/c.

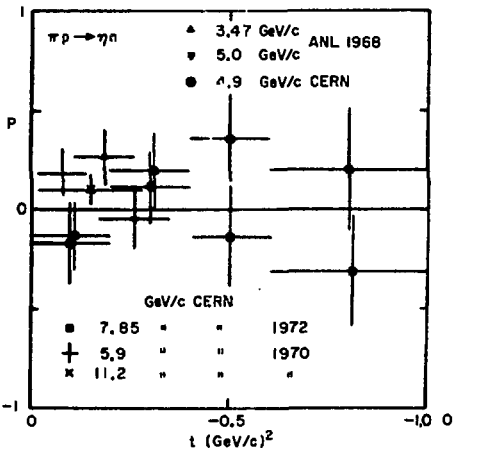

Figure 15. $\pi p \to \eta n$ reaction.

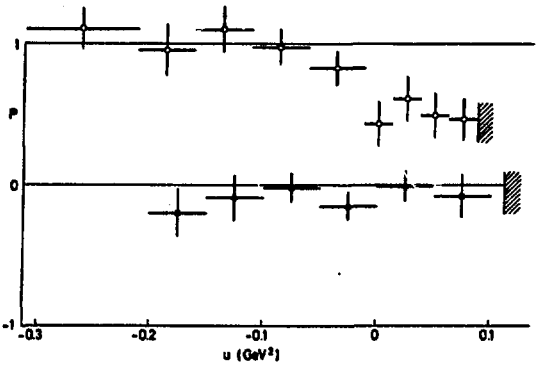

Figure 16. Polarization data at 3.5 GeV/c for $\pi^+ p \to \Sigma^+ K^+$ (dark circle) and at 4 GeV/c for $\pi^- p \to \Lambda K^0$ (white circle).

DIRECT CHANNEL PROBLEMS AND PHENOMENA

R. E. Cutkosky
Carnegie-Mellon University, Physics Department
Pittsburgh, Pennsylvania 15213

In this talk I shall cover briefly four loosely connected topics.

I. I shall attempt to describe the goals of precision hadron spectroscopy.

II. I shall discuss some of the requirements on the data base for precision hadron spectroscopy and suggest some experiments, using π-N scattering as an example.

III. I will comment on some relations between direct-channel and cross-channel effects, in the light of a simple model constructed by Alcock, Chao, and myself.

IV. Since this workshop deals with polarized targets, I shall review some considerations on spin-rotation phenomena as initially discussed by Wolfenstein and reexamined recently by Kelly, Sandusky, and myself.[1]

I. Need for Precision Hadron Spectroscopy

The central problems of hadron physics are: What are they made of? What is the origin of the observed regularities? How are the hadronic interactions ultimately related to electromagnetic and weak interactions? We

are not even able to say what information will eventually turn out to be most important for answering these questions, but it is clear that it is essential to have a very good empirical knowledge of the hadron spectrum and of couplings between hadron states. In particular, we wish to have improved knowledge in the following areas:

A) The extent of the spectrum

B) Questions regarding SU(3) classifications

C) Evidence regarding SU(3) symmetry of coupling constants

D) SU(6) or quark model relations, including questions related to the Melosh transformation

E) SU(3) symmetry breaking, both for masses and coupling constants

F) Isospin breaking (e.g. electromagnetic mass differences of resonant states)

G) Electromagnetic couplings.

Regarding the extent of the spectrum, there are two distinct questions. First, how high in energy can we follow the leading trajectories, recognizing particles on the trajectories and determining the shape of the trajectory, etc. Taking the N,Δ trajectories as examples, I think we should aim for going up to $E_{cm} \leq 3.5$ GeV, or $P_{Lab} \leq 6$ GeV/c, with the next generation of experiments and analyses. The second question concerns the degeneracy of the multiplet structure. To discuss this it is useful to refer to various quark models. In the simplest version, for a given

"principal quantum number" N we consider rotational states with L=N and combine SU(6) spin and charge-hypercharge states with the orbital angular states with the orbital angular momentum L. This gives the states $(56^+)(L=0)$, $(70^+)(L=1)$, $(56^+)(L=2)$, etc. The second model is the harmonic oscillator quark model; here the N=2 level contains an extra $(56^+)(L=0)$ set of states. Finally, in various dual (or "string") models, there is a further degeneracy which can be visualized as corresponding to excited vibrational modes of "rubber bands" holding the quarks together. It should be our goal to understand whether such extra states show up at the lowest energies where they might occur; for π-N scattering the range $1.5 \lesssim E_{cm} \lesssim 2.5$ GeV, or $0.6 \lesssim P_{Lab} \lesssim 3.2$ GeV is especially interesting.

At present we have a great deal of confidence in SU(3) but would like to see if other representations besides 1, 8, or 10 occur. Looking for and testing other symmetry properties is also extremely important. The breaking of SU(3) is very important because we can get especially important clues about the dynamics by studying the pattern of symmetry breaking. Mass-splitting effects (Gell-Mann-Okubo) are well studied empirically, but essentially nothing is known about breaking of coupling constant relations. Isospin breaking, to the extent that it involves coupling to the electromagnetic field, provides an especially valuable probe of hadron structure. I hope that mass splittings for the first N-Δ recurrences, i.e. for $E_{cm} \lesssim 2.0$ GeV/c, can be obtained with good precision.

Pole positions and residues may not turn out to be the most useful or fundamental quantities for discussing symmetry breaking, but they are

important because they are invariant in going from one experimental process to another, and also for discussing the degree and precision obtained from the experimental observations. Factorization of these poles is the best test for existence of a resonance.

II. Data Base for Precision Hadron Spectroscopy

Rather than attempt to survey all systems, I shall consider πN scattering as an illustration. It is useful to distinguish between "copious experiments" and "sparse experiments". Differential cross sections and polarization for $\pi^{\pm}p$ elastic scattering are examples of copious experiments. The $\pi^{+}p$ data is presently in reasonable shape, at least below 2 GeV/c. Some general needed improvements for this class of experiments are, first, a better (and better documented) treatment of correlated errors, and second, correction for bremsstrahlung, especially for $\pi^{-}p$. The documentation of normalization errors, especially regarding the correlation of possible normalization shifts at nearby energies, is sometimes overlooked. The same is true of momentum errors, where careful distinction should be made between the momentum bite, (R.M.S. beam spread), the overall momentum uncertainty for a set of data taken at nearby energies, and the energy-to-energy fluctuation OR uncertainty in the central momenta. Similar information regarding angular bins will be helpful for making full use of high precision data.

Recently, Sogard pointed out that radiative corrections are significant for precision data, especially for backward $\pi^{-}p$ scattering, for momenta as low as 1 GeV/c.[2] There are two effects to be distinguished: 1) smearing of the "effective energy" for the scattering, as a result of the energy carried

by the undetected photon. 2) reduction of the measured cross section below the "proper" value by kinematical cuts which exclude photons above some minimum energy. Effect 1) can best be accounted for by making the kinematical cuts stringent, especially with use of spectrometers. Effect 2) is best taken into account by the experimental group applying the corrections appropriate to their geometry. Unfortunately, formulas for the relevant geometries have not yet been provided by the theorists.

By sparse experiments, I mean those for which data does not exist at close enough momentum intervals to allow interpolation in momentum. For these, it is important to synchronize the momenta at which experiments are done so that interpolation is unnecessary.

Charge exchange data is invaluable for helping to pin down the amplitudes for $\pi^{\pm}p$ scattering. This data is unfortunately sparser than it should be. Significant additional information about amplitudes could also be obtained from spin rotation experiments, which I shall return to later.

Data on $\pi^{\pm}n$ scattering (in deuterium) would be valuable for analyses which did not make use of Isotopic spin symmetry. The deuteron corrections could be large for differential cross sections, but comparison with the proton cross sections could remove some effects. Also, polarization is believed to be less affected, which suggests the importance of polarized deuteron targets.

Systematic studies of the following two body reactions (with and without polarized targets) would help greatly to determine the low angular momentum states which are crucial to a better understanding of hadron

spectroscopy:

$$\pi^- p \to n\eta$$
$$K^0 \Lambda$$
$$K \Sigma$$
$$\pi^+ p \to K^+ \Sigma^+$$

The region up to P_{Lab} ~ 2-3 GeV/c would be especially important to cover well.

Lack of space, time, and knowledge about the many tricky theoretical questions encountered in dealing with quasi-two body reactions forces me to omit discussion of this important subject.

III. Some Relations Between Direct-Channel and Cross-Channel Effects

The question of the relation between a cross channel description of scattering and a direct channel description has been in the foreground of hadron physics for the last 15 years. I subscribe to the view that the cross channel (e.g. Regge pole) descriptions of high energy scattering are interesting and important insofar as we are able to understand, through the use of crossing symmetry and other analyticity arguments, how these processes are related to the spectrum of hadrons as found in the direct channel. Various versions of duality have, in the last half decade, provided a new way to think about these relations, even though there is, as yet, no dual model for baryons which is even approximately satisfactory.

Since a reasonably accurate "Born approximation" is a useful part of the ACE partial wave analysis method, Alcock, Chao, and I recently looked into the problem of how to abstract from beta-function formulas a new Regge pole formula which would be more accurate in the resonance region, and proposed the following for a t-channel Regge pole:

$$A(s,t) = \gamma(t)\Gamma(-\alpha(t))\left(\frac{s}{s_0}\right)^{\alpha(t)}\xi(t,s)$$

where $\gamma(t)$ is a residue function and where ξ is the signature factor; for the usual Regge pole,

$$\xi = 1 + \eta_t e^{-i\pi\alpha_t}$$

where $\eta_t = \pm 1$ is the signature. We add the term (to ξ)

$$-i\eta_t\eta_s \sin\alpha_t \pi \frac{e^{i\pi\alpha_R} - \eta_s e^{-\pi\alpha_I}}{\cosh\pi\alpha_I - \eta_s \cos\pi\alpha_R}$$

where η_s is the signature of an s-channel Regge pole with a complex trajectory function:

$$\alpha_s = \alpha_R + i\alpha_I$$

The correction term can be approximated by

$$2i\eta_t\eta_s \sin\pi\alpha_t \, e^{+i\pi\alpha_s}$$

at higher energies where Im α_s is larger. A similar formula is used for u-channel poles.

We made a fit to the amplitudes at low energies using the f, ρ, N_α and Δ trajectories and a simple fixed-pole pomeron which did not have a correction. The fit to higher energy data was about as good as such a simple Regge pole fit usually is. In the resonance region only about 30% of the structure of the amplitudes is given by the ordinary Regge poles, but with the "dual correction term" one gets about 60% of the structure. Much of the remaining discrepancy comes from absence of the N_γ trajectory as well as from the naive treatment of the Pomeron.

I think the main significance of our fit is negative - it tells what you cannot do in the resonance region with the usual Regge formula. The resonance terms have to be added on explicitly. The partial wave projection of our fit shows that the resonance loops come from the added term, not as "Schmid loops" from the ordinary signature factor. However, we also find interesting structure which is not explicitly associated with the input N_α and Δ s-channel trajectories, and these agree with the data nearly as well as quark model states do. The model may also be helpful for predicting the qualitative nature of direct channel resonance effects in quasi-two body production channels.

Even though the success of our fit is extremely limited, we are encouraged to believe that analyticity considerations, if eventually carried out more thoroughly, will be of great value for understanding the baryon spectrum.

Perhaps models such as this one can be useful in helping people to remember that the dichotomy between direct channel and cross channel descriptions is somewhat artificial, and also to realize the importance of

the transition energy region in which resonances slowly fade away and exchange effects become simpler.

IV. Spin Rotation Phenomena

Spin rotation experiments were first suggested by Wolfenstein, and Kelly, Sandusky, and I have recently called attention to some of his original ideas and discussed the problem of how to arrange such experiments to get the most information from them. We rewrite the conventional meson-baryon scattering amplitude

$$M = f + ig \sin\theta \sigma_n$$

in the form

$$M = M_0 \sqrt{1+P\sigma_n}\; e^{-1/2i\beta\sigma_n}$$

where

$$|M_0|^2 \equiv I_0 = |f^2| + |g^2| \sin^2\theta$$

$$I_0 P = 2 \operatorname{Im} fg^* \sin\theta$$

and

$$\beta = \arg \frac{f - ig \sin\theta}{f + ig \sin\theta}$$

is the "Wolfenstein angle" giving the relative phase of the two eigenstates of M. We write the target density matrix in the form

$$\rho_T = 1/2(1 + P_T \sigma_n + \underline{Q}_T \cdot \underline{\sigma})$$

$$\underline{Q}_T \cdot \underline{\hat{n}} = 0$$

The scattering intensity from an unpolarized target is

$$I_o = \mathrm{Tr}\, MM^+$$

and with a polarized target it is

$$I = \mathrm{Tr}\, M \rho_T M^+ = I_o(1 + PP_T) \equiv KI_o$$

where P is the polarization parameter. Let $Q = \sqrt{1-P^2}$. The recoil particle density matrix is

$$\rho_R = 1/2[1 + K(P+P_T)\sigma_n + KQ\underline{Q}_\beta \cdot \underline{\sigma}]$$

where

$$\underline{\sigma} \cdot \underline{Q}_\beta = e^{-1/2i\beta\sigma_n}\, \underline{\sigma} \cdot \underline{Q}_T e^{1/2i\beta\sigma_n}$$

showing that the component of polarization in the scattering plane is rotated through the Wolfenstein angle β (and multiplied by the factor KQ).

On going to body-fixed laboratory coordinates there is an additional kinematical rotation through an angle γ, giving for the Wolfenstein parameters

$$R = Q \cos(\beta+\gamma)$$

$$A = Q \sin(\beta+\gamma)$$

or, more generally, for an arbitrary component of the final polarization vector, $W = A \cos\alpha + R \sin\alpha$, we have

$$W = Q \cos(\alpha+\beta+\gamma).$$

Thus, use of the Wolfenstein angle β allows simpler formulas connecting the significant parameters for description of the amplitude to measured quantities.

If data on P and I_o are all that is available, the phase angle β is completely undetermined, although unitarity and analyticity restrict somewhat its dependence on θ. In a measurement of W, the propagated error in β is the appropriate measure of the amount of new information gained about the amplitude. For a given ΔW, the error $\Delta\beta$ is smallest when W is small, which in many cases can be achieved by careful selection of the angle α before the experiment is set up. (See Fig. [1]). A twofold ambiguity remains if there is a measurement at only one value of α, but usually this could be resolved by continuity. It is also clear from the figure that a second measurement at $\alpha+90^{o}$ could most easily distinguish the two values if W=0 in the first measurement.

Although spin rotation experiments are very hard, I urge that they be given serious consideration, because they provide invaluable tests of amplitude analyses and also provide information which is probably required if we are to push these analyses, and hence our knowledge of the baryon spectrum, to higher energies.

References

1. L. Wolfenstein, Annual Review of Nuclear Science, Vol. 6, p. 43 (1956); R. Cutkosky, R. Kelly, and J. Sandusky, Phys. Rev. D10, 2309 (1974).
2. M. Sogard, Phys. Rev. D9, 1486 (1974).

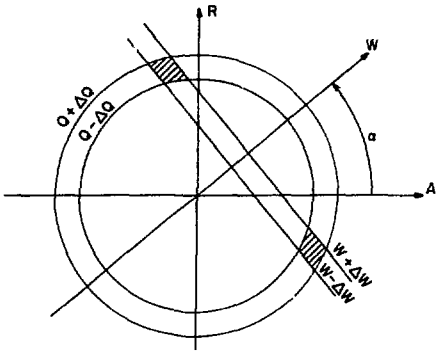

Figure 1

LOW ENERGY S-CHANNEL PROCESSES WITH POLARIZED TARGETS*

Mark Sakitt

Brookhaven National Laboratory

Upton, New York 11973

* Work performed under the auspices of the U.S. Atomic Energy Commission.

When I was asked to review the experimental situation in low energy s-channel processes with a view toward applications of polarized targets, both the organizer of the workshop and I agreed that such a task would be impossible to accomplish in one hour (or a short review article). The understanding was that a few topics would be selected using subjective criteria, i.e. personal interest. I will, therefore, mainly describe the situation in both the I=1 and I=0 K^+N system and make a few remarks about the $\bar{K}N$ system and ignore the πN system. The approach will be to show the highlights of what has been happening in that field rather than a detailed review, as can be found in standard conference proceedings. It will be aimed at the bulk of the conference attendees who are not working in this field rather than at the few experts present. I will show what "typical" results now seem to be coming from current experiments and phase shift analyses and then show what improvement could result from some polarized target experiments. In doing this task, I will borrow heavily on past conference reviews and articles.

In both the low energy K^+N and $\bar{K}N$ system the game is to extract complete amplitudes that describe the scattering system using either large conventional phase shift analysis programs or K matrix analysis programs. For the K^+N system the main interest right now is seeing if there is any resonant amplitude since that "exotic" resonance could not be accommodated in a simple quark model in which all baryons are composed of only three quarks. In the $\bar{K}N$ system the main interest is in a further understanding of the successful SU(3) classification scheme by finding missing states in various multiplets and by testing the predicted relationship among the many decay rates. We shall see that in many of the amplitude analyses ambiguities exist which could be resolved by polarization information.

Before going into more details about the current experimental situation, I would like to qualitatively describe what sort of polarization measurements are in principle possible in two-body meson-baryon scattering. Using the standard f and g for non-flip and flip amplitudes we can write:

$$\frac{d\sigma}{d\Omega} = I_o(1 + P_o \bar{P}_i \cdot \hat{n}_\perp)$$

and

$$\frac{d\sigma}{d\Omega}\bar{P} = 2\mathrm{Re}(f^* g)\hat{n}_\perp - 2\mathrm{Im}(f^* g)\hat{n}_\perp \times \bar{P}_i + (|f|^2 - |g|^2)\bar{P}_i + 2|g|^2(\hat{n}_\perp \cdot \bar{P}_i)\hat{n}_\perp$$

where

$$P_o = \frac{2\ \mathrm{Re}\ f^* g}{|f|^2 + |g^2|} \ ,$$

$$I_o = |f|^2 + |g|^2 \ .$$

$\bar{P}$ is the polarization of the outgoing nucleon, $\bar{P}_i$ is the initial polarization of the nucleon and $\hat{n}_\perp$ is the standard unit vertex perpendicular to the scattering plane. We can examine the four standard simple examples for the P_i direction.

(a) $\bar{P}_i = 0$

then $\frac{d\sigma}{d\Omega} = I_o$ and $\bar{P} = P_o \hat{n}_\perp$

In order to measure $\bar{P}$ we either have to do a double scattering experiment or observe a decay of the baryon where the decay can be used as an analyzer, i.e. $\Lambda \to p\pi^-$.

(b) $\bar{P}_i = P_i \hat{n}_\perp$

then $$\frac{d\sigma}{d\Omega} = I_o(1+P_o P_i) \text{ and } \bar{P} = \frac{P_o+P_i}{1+P_o P_i}\ \hat{n}_\perp$$

Here we can measure P_o by simply measuring the differential cross section and flipping the sign of P_i. In principle we learn nothing more than in case (a), as long as the polarization is perpendicular to the scattering plane. The particular final state will determine which experimental method for measuring P_o is to be preferred.

(c). $\bar{P}_i = P_i\ \hat{k}_{in} \times \hat{n}_\perp$ ($\hat{k}_{in}$ is incoming meson direction; see Fig. 1)

then $$\frac{d\sigma}{d\Omega} = I_o$$

and $$\bar{P} = P_o \hat{n}_\perp - A\, P_i\, \hat{n}_p + R\, P_i\, \hat{s}$$

where A and R (the spin rotation parameters) are independent functions of f and g. $\hat{n}_p$ is along the direction of the outgoing baryon and

$$\hat{s} = \hat{n}_\perp \times \hat{n}_p$$

We can then, by either a double scatter or decay and flipping the sign P_i, measure the polarization in the $\hat{s}$ direction and determine R.

(d) $\bar{P}_i = P_i \hat{n}_z$

we have

$$\frac{d\sigma}{d\Omega} = I_o$$

and

$$P = P_o \hat{n}_\perp + RP_i \hat{n}_p + AP_i \hat{s}.$$

We can measure A as described in the previous case.

Therefore in order to make four independent measurements of I_o, P, A and R to determine a complete set of variables, we need to do experiments where $\tilde{P}_i$ is not simply constrained to the perpendicular to the scattering plane. We shall see that many phase shift analysis ambiguities exist which could be resolved by A and R measurements. In fact there seem to be two "rules" governing these analyses.

Rule 1: If an amplitude analysis yields several solutions and the analysis is not based on a complete set of measurements, then the predictions of the solutions for the unmeasured parameters are in general significantly different.

This is the strong motivation for pushing for A and R measurements. Unfortunately there seems to be another rule.

Rule 2: When one measures the parameters, which were predicted to be different, it doesn't always resolve the solutions as clearly as one would have supposed.

While the new data is obviously an important constraint on the solutions, history has taught us that massive, opaque, phase shift programs have a partial ability to accommodate new data by readjusting the solutions.

KN (I=1) Interactions

The region that I'm going to discuss is only the region below 2 GeV/c. Below about 1 GeV/c the K^+p scattering is basically elastic and the amplitudes are roughly known. As the inelasticity rises between 1 and 2 GeV/c ambiguities arise and the main interest centers on whether or not an exotic Z_1^* resonance exists in the region around 1.5 GeV/c.

To get a general idea of the quality of the existing data that goes into these phase shift programs we can look at some "typical" experimental results. In showing these results there is no attempt being made to be complete but merely representative. Figure 2 shows the recent results[1] of Kycia's group at Brookhaven on the total cross section for K^+p scattering. These results, which have errors roughly at the 1% level, are relatively smooth and the earlier possible structure in the region around 600 MeV/c does not appear present in this newer data.

The differential cross sections are isotropic below about 600 MeV/c, and the ambiguity between S_{11} and P_{11} waves is clearly resolved in favor of S_{11} by examining the k dependence of the phase shift. These results from the Bologna-Glasgow-Rome-Trieste group[2] are shown in Figure 3. Newer results on the Coulomb interference term in this low energy region confirm the older results and show a definite constructive interference establishing the repulsive nature of the low energy s-wave K^+p interaction. While these have been measured at several momenta, Figure 4 shows the BGRT results[2] at two momenta. At higher momentum electronic experiments have accumulated extensive differential cross section data; some typical data from the Bristol-RHEL group[3] is shown in Figure 5 for the elastic channel. Some polarization data has existed in the region above 800 MeV/c for the elastic channel. An example of that data is a CERN experiment[4]; some of their results are shown in Figure 6. More polarization measurements with greater accuracy are in progress by the Yale group here at Brookhaven.

From these sorts of data many groups have performed phase shift analyses, each of which generally yields more than one solution. The interest has focussed on the P_{31} wave which might be resonant. The speed plots are either inconclusive or tend to look not quite like what one expects from a "normal" resonance.

Also in this momentum region the inelastic channel contributions are becoming important. At this conference P. Steinberg told us of some early results[4] of a K-matrix coupled channel analysis that he and his collaborators have done which favors a resonance interpretation for P_3. As can be seen from their Argand diagram shown in Fig. 7, the possible resonant P_3 wave is quite inelastic, which is a feature round in other people's phase shift analysis. Clearly when one is dealing with inelastic processes that are predominantly quasi-two-body channels, the K-matrix approach seems to be a powerful tool, as has been already demonstrated in the low energy $\bar{K}N$ system, since it is simple to build in the unitary constraints.

Since most people's solutions are derived from rather good total cross sections, differential cross sections and reasonably accurate polarization data, most people now believe one can only resolve the remaining ambiguities by A and R measurements. For example, in the phase shift analysis of Albrow, et al.[5] they predict the resulting R parameter distribution at 1.22 GeV/c which is shown in Fig. 8. While the solutions used are not the most current (they were done in 1970) the general idea holds that accurate A and R do resolve the different set of solutions. The point I'm trying to make is that if Brookhaven now embarks on a polarized target program we should build in the capability of having a sizeable component of the polarization not perpendicular to the scattering plane.

KN(I=0) Interactions

In this system most work has been done on the mixed isospin states

$$K^+n \to K^+n$$

and

$$K^+n \to K^0p,$$

both being done on deuterium targets. This system is also more complicated in that higher waves come into the picture a little earlier than in the

K^+p system. However, it is simpler in that the suspected resonance is at lower momentum, around 1 GeV/c, where the elastic channels still clearly dominate, while in the K^+p system the possible resonance region has appreciable inelastic channels present.

Total cross sections have been obtained for the I=0 state by unfolding techniques from both the K^+d and K^+p cross sections. The resulting cross sections from a recent experiment of the Kycia group[1] are shown in Fig. 9. The bump above 1 GeV/c is explained by the rapidly rising inelastic channels and is not believed to be a resonant structure. The elastic channel which causes the shoulder at around 800 MeV/c is the exciting candidate.

Most of the differential cross section data comes from bubble chamber experiments so the statistics are, of course, not as overwhelming as in the K^+p. Figures 10 and 11 show some of the results of the BGRT group.[6,7] For phase shift analyses the effects on the angular distributions due to the deuteron form factor are not small in some of the angular bins. For example, in the K^0p case the form factors go to zero in the forward direction due to the Pauli principle. One has either to do these corrections very carefully or exclude some of the angular region for the phase shift analysis. In the K^+n situation there are difficult experimental problems to overcome since the interactions with slow spectator momentum, less than 80 MeV/c, tend to be one-prong events in the chamber. The K-decay background and general scanning efficiency have to be very well understood.

The only polarization data that exists is one experiment by a Brookhaven-Carnegie-Mellon group[8] done several years with relatively poor statistics compared to the K^+p data. It used the double scatter technique to measure the polarization of the recoil proton in the reaction $K^+n \to K^0p$. These few data points are shown in Fig. 12. Some of the phase shift analyses have used

these points while others have only compared the resulting solutions, based on the other data, to these points. Since these points do not have high statistical weight in comparison to the large amount of the other data accumulated, the solutions by the different methods are not significantly different. One ends up trying to rule out a solution by examining the polarization prediction. Unfortunately since the phase shift programs always have a rather high χ^2 per degree of freedom a few extra badly fitting points do not convince one to rule out anything, but they are highly suggestive.

An example of the latest solutions obtained are the BGRT results[9] whose Argand plots for the three solutions obtained are shown in Fig. 13. The main candidate for a resonance is the $P_{1/2}$ wave in either the C or D solution as compared to the non-resonant solution A. The predictions of these solutions for the polarization in the charge exchange reaction are the curves drawn on Fig. 12. Clearly the few points favor the resonant solutions but more data is needed. The experiment which measured those points pushed the bubble chamber technique to the limit since it required about 10^6 pictures for those results. From the plots in Fig. 12 we can see that what is needed are reasonable accurate polarization measurements spread over the region from 0.6 to 1.3 GeV/c. The predicted results change slowly but significantly over that region. The slowness of the change corresponds to the fact that the possible resonance is quite broad and in one of the solutions there are predicted rapid changes of any amplitude. The most promising approach would seem to be to use a polarized neutron target, which has been built, as described by Borghini in his talk.

If we turn to the elastic channel $K^+n \to K^+n$, I have calculated the expected polarization for the outgoing neutron for each of the three solutions

at an incoming K^+ momentum of 800 MeV/c. These results are shown in Fig. 13. One notices that the separation between the non-resonance A solutions and the resonance $P_{1/2}$ solutions D and C are even greater than in the charge exchange reaction. A counter-spark chamber experiment is being set up by our group in collaboration with a Case-Western Reserve group to measure the K^+n polarization in the region from 0.7 to about 1 GeV/c using the double scattering technique. It utilizes the fact that in the region of interest the secondary np scattering has a large analyzing power.

In the KN(I=0) system, which has a promising candidate for an exotic resonance, a Z_0^*, the experiments that have to be pushed are the so-called first generation polarization experiments. But, with past experience as a guide, it will not be long after those experiments are done that the cry will be for A and R measurements to resolve whatever ambiguities are left.

Conclusions

There are many exciting experiments to be done in the low energy KN system, most of which require polarized targets. Brookhaven, having an extremely hot low energy beam, the C2, C4 beam, is in a position to make a major contribution to this program. One should keep in mind that at this date any project for a polarized target should build in the capability of being able to be an A and R type target and one should consider the possibility of polarized neutron targets.

References

(1) A.S. Carroll, T.F. Kycia, K.K. Li, D.N. Michael, P.M. Mockett, D.C. Rahm, and R. Rubinstein, Phys. Lett. 45B, 531 (1973).

(2) Bologna-Glasgow-Rome-Trieste contribution to Baryon Resonance Conference at Purdue University (1973), pp 159, 163.

(3) B.J. Charles, I.M. Cowan, T.R.M. Edwards, W.M. Gibson, A.R. Gillman, R.G. Gilmore, M.H. Gledhill, C.M. Hughes, J. Malos, V.J. Smith, R.J. Tapper, B. McCartney, G.C. Oades, D.L. Ward, P.D. Wroath, G.A. Beck, M. Coupland and S.G.F. Frank, Phys. Lett. 40B, 289 (1972).

(4) R.A. Arndt, R.H. Hackman, L.D. Roper and P.H. Steinberg, Phys. Rev. Lett. 33, 987 (1974).

(5) M.G. Albrow, S. Andersson/Almehed, B. Bosnjaković, C. Daum, F.C. Erné, Y. Kimura, J.P. Lagnaux, J.C. Sens, F. Udo and F. Wagner, Nucl. Phys. B30, 273 (1971).

(6) G. Giacomelli, P. Lugaresi-Serra, G. Mandriolli, A. Minguzzi-Ranzi, A.M. Rossi, F. Griffiths, A.A. Hirata, R. Jennings, B.C. Wilson, G. Ciapetti, P. Guidoni, G. Mastrantonio, A. Nappi, D. Zanello, G. Alberi, E. Castelli, P. Poropat and M. Sessa, Nucl. Phys. B56, 346 (1973).

(7) G. Giacomelli, P. Lugaresi-Serra, A. Minguzzi-Ranzi, A.M. Rossi, F. Griffiths, A.A. Hirata, I.S. Hughes, R. Jennings, B.C. Wilson, G. Ciapetti, P. Guidoni, G. Martellotti, A. Nappi, D. Zanello, E. Castelli, P. Poropat and M. Sessa, Nucl. Phys. B42, 437 (1972).

(8) A.K. Ray, R.W. Burris, H.E. Fisk, R.W. Kraemer, D.G. Hill and M. Sakitt, Phys. Rev. 183, 1183 (1969).

(9) G. Giacomelli, P. Lugaresi-Serra, G. Mandrielli, A. Minguzzi-Ranzi, A.M. Rossi, F. Griffiths, A.A. Hirata, I.S. Hughes, R. Jennings, B.C. Wilson, G. Ciapetti, G. Mastrantonio, A. Nappi, D. Zanello, G. Alberi, E. Castelli, P. Poropat and M. Sessa, Nucl. Phys. B71, 138 (1974).

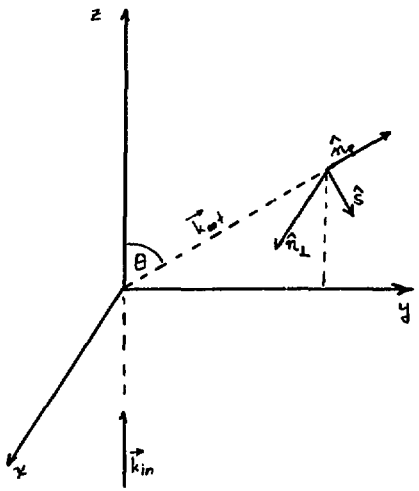

Figure 1. Diagram showing vectors used in polarization formalism.

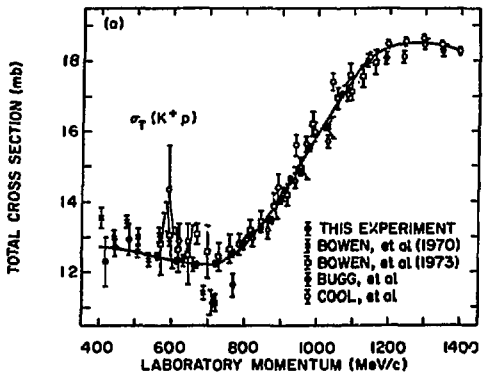

Figure 2. Total cross sections of K^+p scattering from A.S. Carroll, et al.(1)

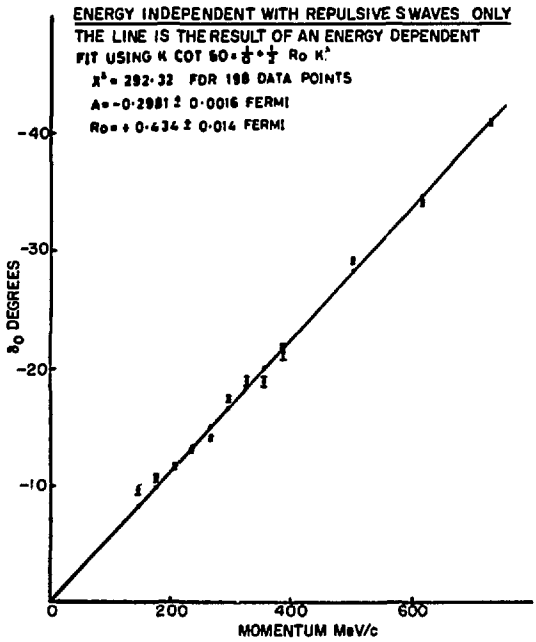

Figure 3. Fit to BGRT differential cross sections using s-wave scattering length and effective range.(2)

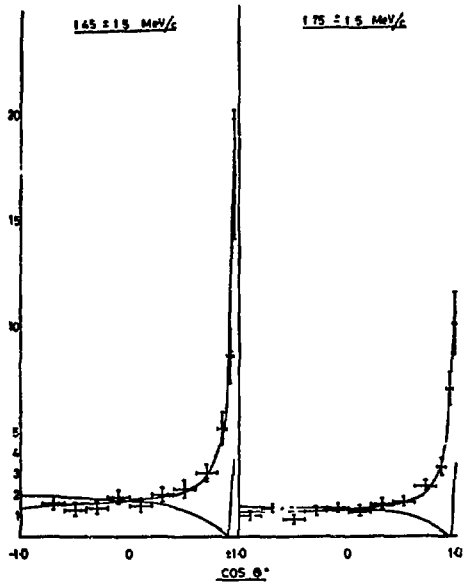

Figure 4. Differential cross section for K^+p elastic scattering.(2) The two curves correspond to constructive and destructive interferences.

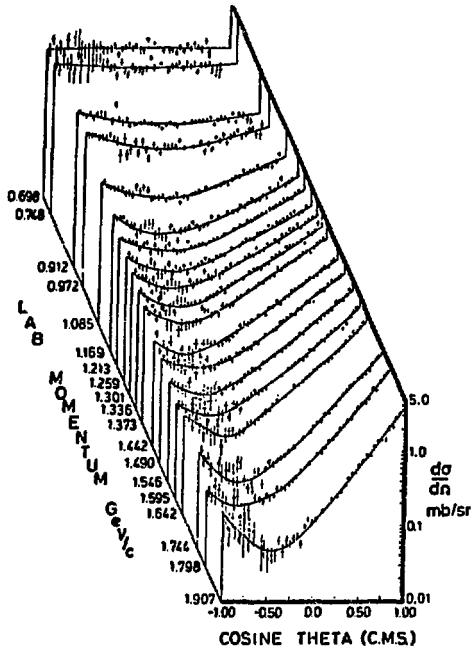

Figure 5. Elastic K^+p differential cross section data from B.J. Charles, et al.[3]

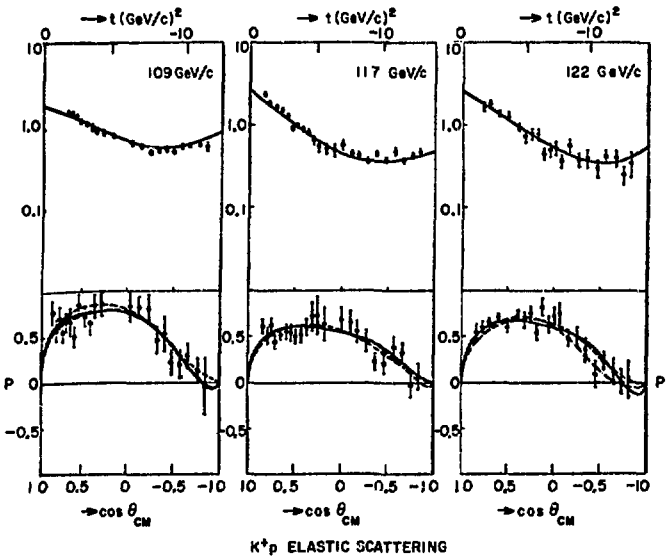

Figure 6. Polarization data from Albrow, et al.(5)

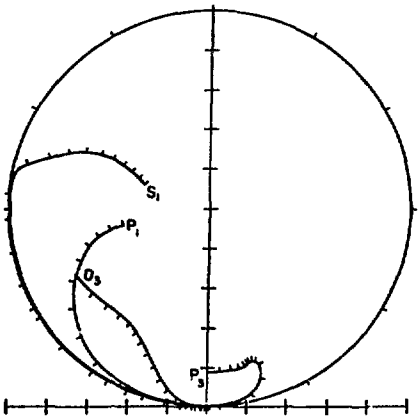

Figure 7. Argand plot of phase shift results for K^+p from R.A. Arndt, et al.(4)

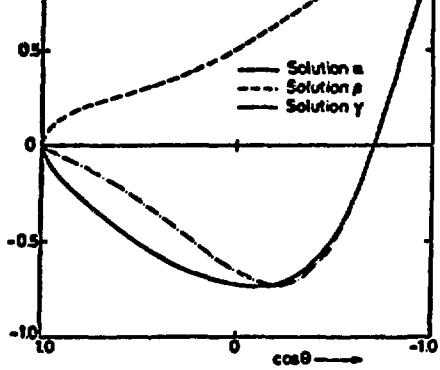

Figure 8. Predictions for the R parameter from the various phase shift solutions from Albrow, et al.(5)

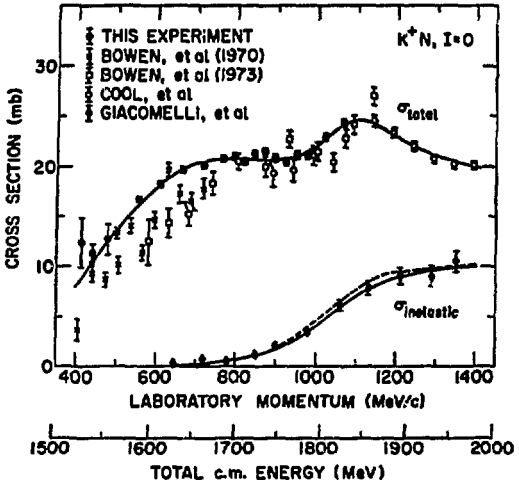

Figure 9. K^+-nucleon total cross section for I=0 from A.S. Carroll, et al.(1)

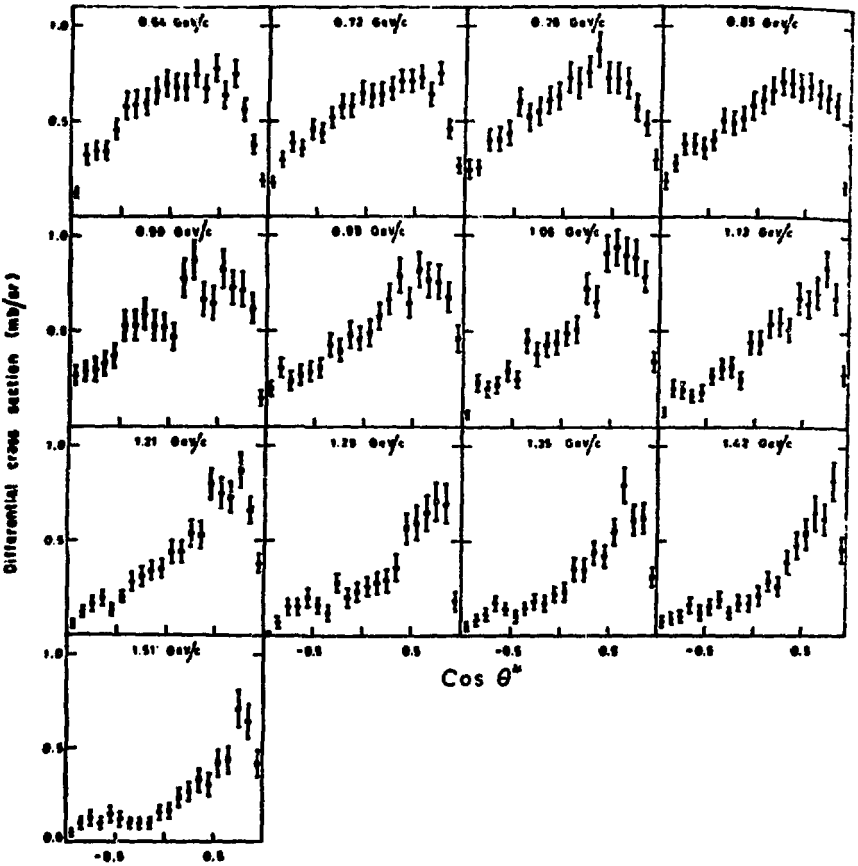

Figure 10. Charge exchange $K^+n \rightarrow K^0p$ differential cross section from C. Giacomelli.(7)

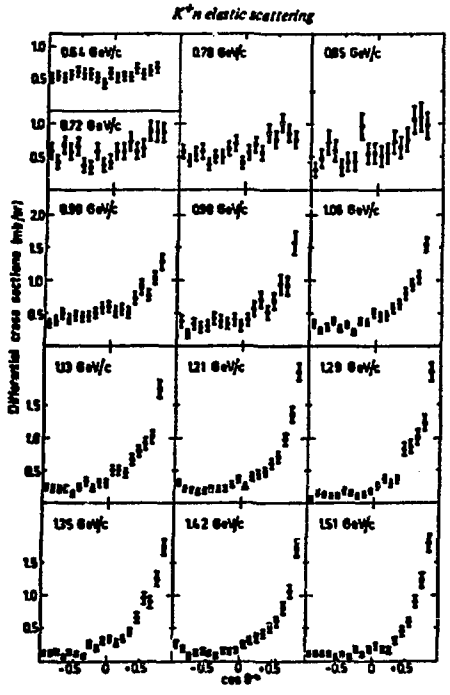

Figure 11. Elastic K^+n differential cross section data from G. Giacomelli, et al.(6)

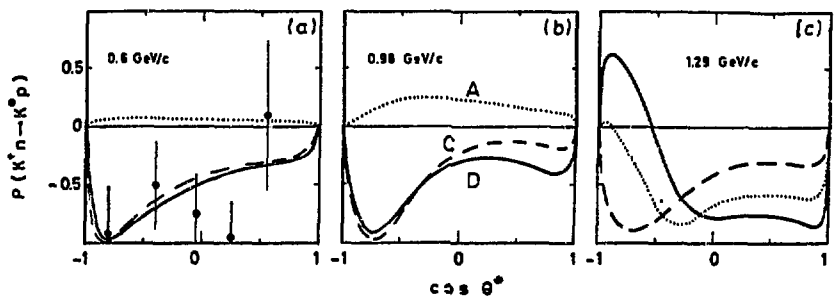

Figure 12. Predicted proton polarization for the three BGRT solutions from G. Giacomelli, et al.(9) The data at 0.6 GeV/c comes from Ray, et al.(8)

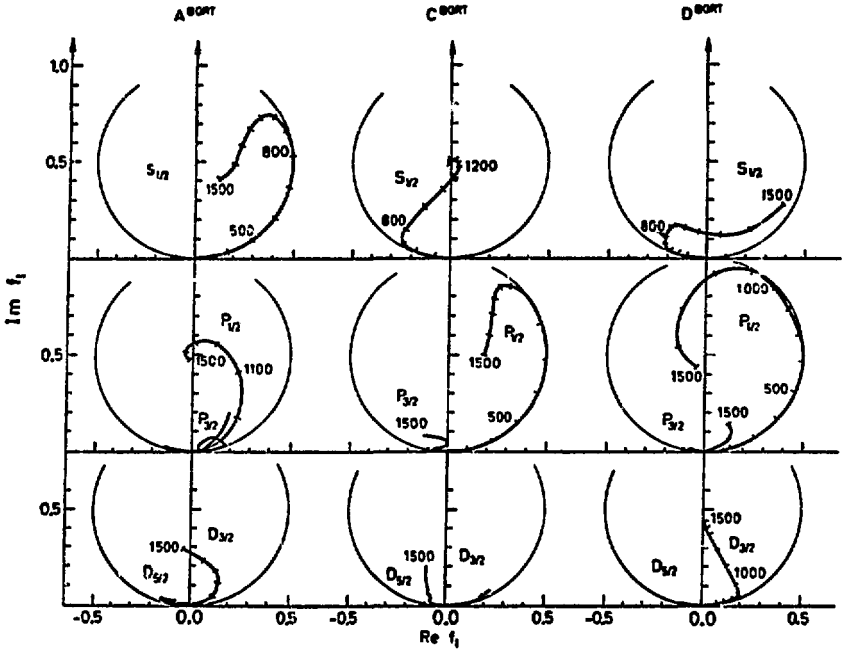

Figure 13. Argand plots showing the three solutions from the BGRT group.[9]

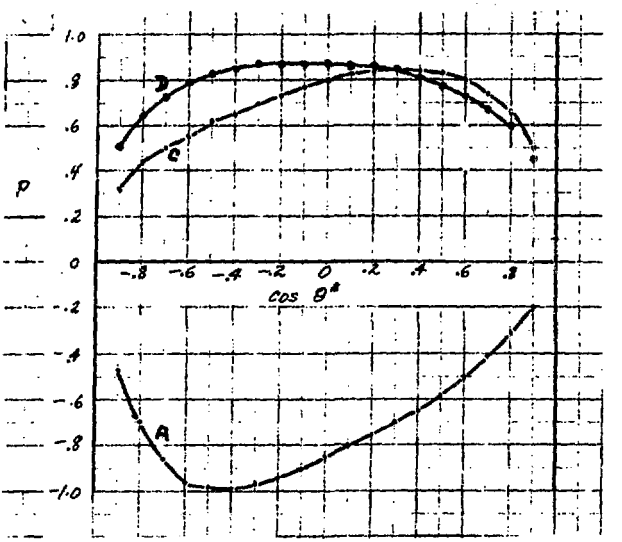

Figure 14. Polarization of the recoil neutron in K^+n elastic scattering at 800 MeV/c. The three curves are the phase shift solution predictions.

BNL 19416
NG-299

Presented at
BNL Workshop on Physics
with Polarized Targets
June 3-8, 1974

EXPERIMENTS STUDYING HADRON DYNAMICS MAINLY IN THE t-CHANNEL*

Howard A. Gordon

Brookhaven National Laboratory

Upton, New York 11973

* Work performed under the auspices of the U.S. Atomic Energy Commission.

Much about strong interactions has been learned by studying scattering processes in the t-channel.[1] The use of polarized targets in this class of reactions has often allowed the measurement of the phases and magnitudes of the amplitudes. The purpose here is not to give a systematic review but rather to select some data which involve the measurement of the polarization, show how that data has improved our knowledge of strong interactions and indicate what further experiments should be done. Most of the data involving polarized targets have come from studies of elastic scattering, which will be discussed first. Next will follow: two-body reactions, both nondiffractive and diffractive; a suggestion for producing exotic resonances using polarized targets; and inclusive processes.

Elastic Scattering

First consider $\pi^{\pm}p$ elastic scattering, which are dominated by the following amplitudes $P + f \mp \rho$. Historically as more and better measurements are made, more precise information on the properties of these amplitudes is obtained. A measurement of the polarization measures the interference between the s-channel helicity nonflip (F^I_{++}) amplitude and the s-channel helicity flip (F^I_{+-}) amplitudes. The amplitudes are, of course, complex and so even when we combine the I=0 P + f there are still eight numbers to determine as a function of s and t. The data in Fig. 1 show that the π^-p polarization is a mirror image of the π^+p polarization.[2] This is naturally explained by the change in sign of the ρ amplitude. That is, the polarization is the interference between the dominant F_{++} P-amplitude and the F_{+-} ρ-amplitude. In the simple Regge pole model the ρ-amplitude is supposed to have a zero at $t \sim -0.6$ GeV^2 where $\alpha(t) = 0$ and so both $\pi^{\pm}p$ polarization

would be expected to have the observed zero. So far so good, but to determine, for example, whether the real and imaginary parts of the F^1_{+-} ρ-amplitude display a Regge phase, and to find if there is any F^1_{++} amplitude present, more measurements are needed.

Next the polarization in $\pi^- p \to \pi^0 n$ (CEX)[3] was found to be about 40%. CEX involves only F^1_{++} and F^1_{+-} (ρ) and so since the polarization is not zero both amplitudes must be present. Then the A and R parameters in $\pi^\pm p$ elastic scattering were measured at 6 GeV/c for $-t < 0.5$ GeV^2.[4] (See Fig. 2) Actually the measurement determined that R was small and negative. This allowed a complete determination of the real and imaginary parts of the F_{++} and F_{+-} amplitudes for the I=0 and I=1 exchanges up to an overall phase. Without going into details of the amplitude analyses,[5-6] here are some of the conclusions of one of the analyses[5] to show the kind of information that may be obtained. F^0_{++}(P) dominates and has an exponential behavior. F^0_{+-} is small but significantly nonzero. The phase of F^0_{+-} relative to F^0_{++} is always close to 180°. Whether F^0_{+-} is due to P or f could perhaps be determined by measuring the s dependence of F^0_{+-}. $\mathrm{Im}F^1_{++}(\rho)$ has a zero in the region of the crossover of the differential cross section for πp elastic scattering ($t \sim -0.2$ GeV^2) whereas $\mathrm{Re}F^1_{++}$ vanishes at a larger value of t. A simple Regge-pole model would have predicted that the $\mathrm{Im}F^1_{++}$ was related to $\mathrm{Im}F^1_{+-}$ so this measurement clearly shows the need for absorption in the F^1_{++} amplitude.

Next a remeasurement of the CEX polarization[7], showing it to be $\sim$ 20% instead of $\sim$ 40% (see Fig. 3), allowed a redetermination of the amplitudes.[8] In particular this analysis found little difference between the location of the zero in $\mathrm{Re}F^1_{++}$ and $\mathrm{Im}F^1_{++}$. It is emphasized that not both the $\mathrm{Re}F^1_{+-}$ and $\mathrm{Im}F^1_{+-}$ amplitudes can vanish at $t \sim -0.6$ GeV^2.

As an aside, a precision remeasurement of the $\pi^{\pm}p$ elastic cross section differences $\Delta = (\sigma^- - \sigma^+)/\sqrt{8(\sigma^- + \sigma^+)}$, where $\sigma^{\pm} = \frac{d\sigma}{dt}(\pi^{\pm}p \to \pi^{\pm}p)$, shown in Fig. 4A allowed another amplitude analysis.[9] One of the conclusions here was that the phase of F^0_{++} with respect to F^1_{+-} was constant $\sim 60^o$. Since F^1_{+-} is thought to have a standard Regge phase, $\phi^1 = \frac{\pi}{2}[1 - \alpha(t)]$, this would imply that F^0_{++} would also have a rotating phase instead of the naive expectation of F^0_{++} being purely imaginary. In this case the slope of the P-trajectory would be similar to that of the ρ. Also the energy dependence of F^1_{+-} perpendicular to the F^0_{++} amplitudes is found in terms of an effective trajectory for the ρ as seen in Fig. 4C. This effective trajectory falls below that of the standard ρ effective trajectory which could imply a $\sim 30\%$ f^o contribution to the F^0_{++} amplitude. This matter would be elucidated by measuring the amplitudes as a function of s.

These πp elastic scattering experiments on polarized targets are some bread-and-butter measurements in strong interactions. Rather than being dependent on some theoretical model for interpretation, they determine the conditions any model must satisfy and so are quite fundamental. Measurement of the R and A parameters at larger values of t and at other values of s will refine these analyses. Also the CEX polarization should be measured at larger s.

Next consider $p\pi$ elastic scattering. Experimentally these measurements are not rate limited by the beam intensity so the measurements can cover a larger range of t than in πp polarization. However, since the projectile as well as the target have spin, there are even more amplitudes than in the πp case.

Figure 5A shows some of the work done at CERN on polarization in pp

elastic scattering.[10] The polarization at 10 GeV/c is small but positive at low t but then a peak appears at t ∿ -1.5 GeV. This peak seems to disappear as s increases. A recent measurement at ANL[11], shown in Fig. 5B, extends the polarization information to larger t values by using an extracted proton beam of ∿ 10^{11} protons/pulse. The data show the peak at t ∿ -1.5 GeV^2 still is present at 12.33 GeV/c and perhaps there are additional peaks at even larger t. The interpretation of this structure is difficult in a Regge model but may be more easily understood in terms of an optical model as indicated by the curve on Fig. 5C.

The next level of complexity is found b, using the ANL polarized proton beam elastically scattering off a polarized target. The results of the first experiment at 6 GeV/c are seen in Fig. 6 plotted versus $P_\perp^2$.[12] The conclusion is that the cross section for protons with spin up (with respect to the production normal) going to spin up ($\sigma_{\uparrow\uparrow}$) is up to 100% larger than the cross section for protons with spin down going to spin down $\sigma_{\downarrow\downarrow}$. The authors remark that spin is obviously quite important in strong interactions. More information from the polarized beam will be available soon.

Two-Body Scattering: Diffractive

Three years ago Fox and Berger[13] suggested a set of experiments which will be tested soon at ANL in the polarized beam. The suggestion was how to resolve resonances from "Deck effects" by using the knowledge of the polarization in elastic scattering. Consider the following three reactions:

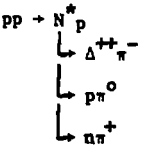

If the low mass enhancement in the N^* region were produced by a Deck effect the amplitude may include diagrams of the kind:

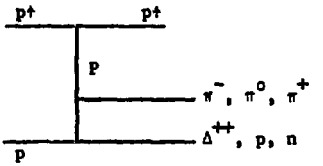

This diagram implies elastic πp scattering at the upper vertex. We saw earlier that the polarization in $\pi^{\pm}p$ elastic scattering have equal and opposite magnitudes so that one may expect there to be an observable difference in the proton polarization depending upon whether the $\pi^-\Delta^{++}$ or π^+n final state is observed. On the other hand, if the resonance is genuine:

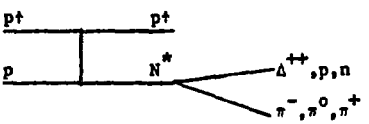

one may expect proton polarization to be independent of the final state.*

If in using the polarized beam one finds diffractively produced N^*'s, a determination of the spin-parity of these states would be required. Instead of doing this in pp scattering, the results might be simpler to interpret for a spinless projectile diffractively scattering off a polarized target: $\pi^{\pm} p\uparrow \to \pi^{\pm} N^*$. With the initial state polarization determined (and perhaps also measuring the final state polarization) one could do a partial wave analysis of the $\pi N, \pi\Delta$ final states to determine the N^* spin parities.

This argument has also been applied to the Q meson to test whether the Q is a genuine resonance or a kinematic effect:

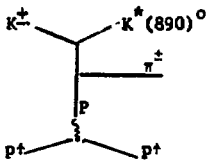

Again one can predict the proton polarization based on measured $\pi^{\pm} p$ elastic scattering polarization. In contrast, since the $K^+ p$ and $K^- p$ elastic polarization are of the same sign (see Fig. 7),[14] perhaps the proton polarization is the same sign independent of whether Q^+ or Q^- is produced.

Nondiffractive Two-Body Scattering

Quasi-two-body scattering has been studied for over ten years and still there is not a comprehensive understanding of the underlying dynamics. When there is a hyperon (Λ or Σ^+ typically) in the final state, the polarization can be measured, this being equivalent to studying the reaction on a polarized target but not observing the final polarization. Recently,

several amplitude analyses have been performed for reactions involving a final state hyperon (see for example R. Field's talk in this conference). In an additional example, the differential cross section and Λ polarization are shown in Fig. 8a[15] for the line-reversed (and isospin rotated) reactions

$$\pi^- p \to K^0 \Lambda$$

$$K^- n \to \pi^- \Lambda.$$

The polarizations are not zero nor a mirror image of one another as would be predicted by the simple notion of K^*, K^{**} exchange degeneracy. The polarization for $\pi^- p \to K^0 \Lambda$ goes through zero at $t \sim -0.4$ GeV^2 where the differential cross section shows a break. The results of an amplitude analysis of these reactions as well as the similar ones including Σ's are also shown in Fig. 8b.[16] This amplitude analysis shows that the nonflip amplitudes are strongly absorbed whereas the flip amplitudes behave like a simple Regge pole. The next step in the understanding of these reactions will come when the measurements are made using a polarized target so that the R and A parameters can be determined. This measurement is under way at CERN for $\pi^- p \to K^0 \Lambda$.

Once one has such a polarized target and a suitable spectrometer, a systematic list of experiments can be envisaged including a final state hyperon so that R and A parameters could be determined:

$$\underline{0^- \ 1/2^+}$$

$$\pi^+ p_\uparrow \to K^+ \Sigma^+_\uparrow$$

$$K^- p_\uparrow \to \pi^- \Sigma^+_\uparrow$$

$$\pi^- p_\uparrow \to K^0 \Lambda_\uparrow$$

$$K^- p_\uparrow \to \pi^0 \Lambda_\uparrow$$

$$\underline{0^- \ 3/2^+}$$

$$\pi^+ p_\uparrow \to K^+ \Sigma(1385)^+ \quad \Big\lfloor \to \Lambda_\uparrow \pi^+$$

$$K^- p_\uparrow \to \pi^- \Sigma(1385)^+$$

$$\underline{1^- \quad 1/2^+}$$

$$\pi^- p_\uparrow \to K^*(890)^0 \Lambda_\uparrow$$

$$K^- p_\uparrow \to \rho, \omega, \phi \; \Lambda_\uparrow$$

$$\underline{1^- \quad 3/2^+}$$

$$\pi \; p_\uparrow \to K^*(890) \; \Sigma(1385)$$

$$\underline{0^- \quad 1/2^-}$$

$$\pi^- p_\uparrow \to K^0 \; \Lambda(1520)$$

$$\hookrightarrow \Sigma^+_\uparrow \pi^-$$

Such experiments would determine the properties of the meson hypercharge exchanges. Also the same set of reactions could be studied in the u-channel expanding the knowledge of baryon exchange.

Another set of line-reversed reactions involving charge exchange, on which the polarization has been measured,[17] is

$$np \to pn$$

$$\bar{p}p \to n\bar{n} \; .$$

The amplitudes present are π, ρ, and A_2 exchange. In simple models, π exchange (unnatural parity) cannot interfere with ρ or A_2 exchange (natural parity) to produce polarization. In fact, if the ρ and A_2 are exchange degenerate, they do not contribute to the polarization. But as seen in Fig. 9, the polarization in both reactions is quite large. More information about A_2 exchange should come from the analysis of the recent BNL and CERN experiments $\pi^- p_\uparrow \to \rho^0 n$.

Exotic Production

Experiments have searched for the exotic Z^* in formation. A different approach would be to search in production:

Here there is vector and tensor exchange in the t-channel in contrast to pseudoscalar-induced formation experiments. If the Z^* has a stronger coupling to the vector meson than pseudoscalar, its production would be enhanced. Searches of this kind have been done using single arm spectrometers. In this case, only the missing mass is measured and so it is fairly hopeless to isolate an exotic resonance especially if the cross section is small. However, if one could trigger, say, the MPS on a fast forward K^- or π^+ and then measure all the associated particles, one could eliminate the allowed processes (e.g. $\pi^- p \to \Lambda K^- K_S^o p$) and search for the Z^*. The polarization of the target proton would help in the interpretation of any enhancement found.

Inclusive Processes

Inclusive processes are described in considerable detail in a separate contribution in this workshop by R. Field. Again the presence of the Λ or $\bar{\Lambda}$ in the final state of an inclusive reaction is an easy experimental way of maximizing the information. There are some preliminary results from the ANL polarized proton beam on $p_\uparrow p \to \Lambda_\uparrow + X$.[18] In this reaction there are 6 observables involving spin. One is D, which is +1 when there is no spin-flip going from $p \to \Lambda$ (natural-parity exchange) and

-1 when the spin flips (unnatural-parity exchange). The first measurement at 6 GeV/c was D = 0.27 ± 0.29 which precludes a simple explanation.

A systematic program with a polarized target would include t-channel inclusive Λ production:

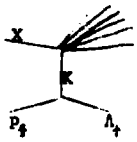

$X = \pi^{\pm}, K^{\pm}, p, \bar{p}$

The t channel exchange would be K and/or K^*, K^{**} exchange. In the Triple Regge picture tha polarization measures the difference between natural and unnatural exchanges.

One should also study u-channel Λ production:

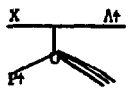

If $X = \pi^+$, for example, the Triple Regge diagram would look like

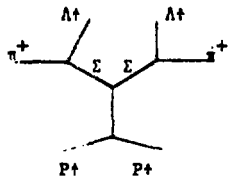

and so this would be a way of studying $\bar{\Sigma}\bar{\Sigma}p$ coupling.

Conclusions

There are certainly a multitude of reactions one can profitably study at the AGS energies with a polarized target. To be competitive, however, one must: (1) be able to study R and A parameters--this implies the design of the magnet must allow various orientations of the proton spin and (2) be able to study reactions other than elastic scattering--for this purpose a frozen spin target would be best, so background subtractions would be minimal.

Acknowledgements

I have greatly benefited by conversations with Dr. Kwan-Wu Lai.

References

1. See for example G.C. Fox and C. Quigg, Annual Review of Nuclear Science, Vol. 23, 1973.
2. R.J. Esterling, et al, Phys. Rev. Lett. 21, 1410 (1968).
3. P. Bonamy, et al., Nucl. Phys. B16, 335 (1970).
4. A. DeLesquen, et al. Phys. Lett., 40B, 277 (1972).
5. C. Cozzika, et al., Phys. Lett. 40B, 281 (1972).
6. F. Halzen and C. Michael, Phys. Lett. 36B, 367 (1971); R.L. Kelley, Phys. Lett. 39B, 635 (1972).
7. D. Hill, et al., Phys. Rev. Lett.30, 239 (1973).
8. P. Johnson, et al., Phys. Rev. Lett. 30, 242 (1973).
9. I. Ambats, et al. Phys. Rev. D9, 1179 (1974).
10. M. Borghini, et al. Phys. Lett. 36B, 501 (1971).
11. W. Abshire, et al., Phys. Rev. Lett. 32, 1261 (1974).
12. J.R. O'Fallon, et al., Phys. Rev. Lett. 32, 77 (1974).
13. E.L. Berger and G.C. Fox, Proceedings of the IIth International Conference on Polarized Targets, edited by G. Shapiro, (University of California Press, Berkeley, Calif. 1971), also G.C. Fox, Phys. Rev. D9, 3196 (1974).
14. M. Borghini, et al., Phys. Lett. 36B, 497 (1971).
15. D.J. Crennell, et al., Phys. Rev. D6, 1220 (1972).
16. V. Barger and A.D. Martin, Phys. Rev. Lett. 39B, 379 (1972).
17. M.A. Abolins, et al., Phys. Rev. Lett. 30, 1183 (1973); P. LeDu, et al., Phys. Lett. 44B, 390 (1973).
18. E.C. Swallow, ANL Symposium on High Energy Physics with Polarized Beams, February 8, 1974.

Measurements of the Polarization in $\pi^{\pm}p$ Elastic Scattering at 5.15 GeV/c

R.J. Esterling, et al.

Phys. Rev. Lett. 21, 1410 (1968)

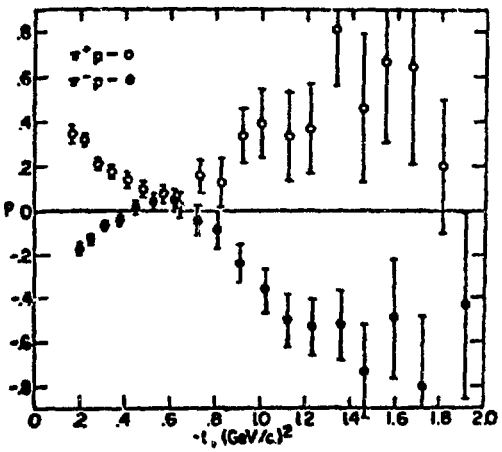

Figure 1. Polarization in $\pi^{\pm}p$ Elastic Scattering at 5.15 GeV/c

A. DeLesquen, et al.
Phys. Lett. 40B, 277 (1972)

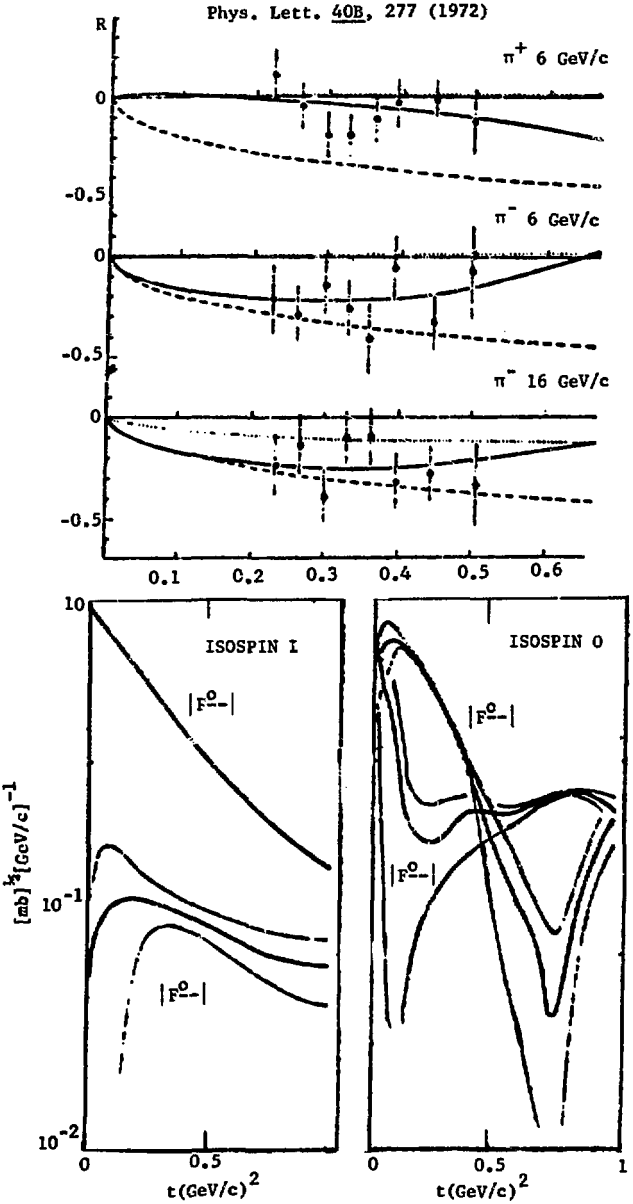

Figure 2.

Measurement of Polarization in $\pi^- p \to \pi^0 n$ at 3.5 and 5.0 GeV/c

D. Hill, et al.

Phys. Rev. Lett. 30, 239 (1973)

5.0 GeV/c, this experiment

3.5 GeV/c, this experiment

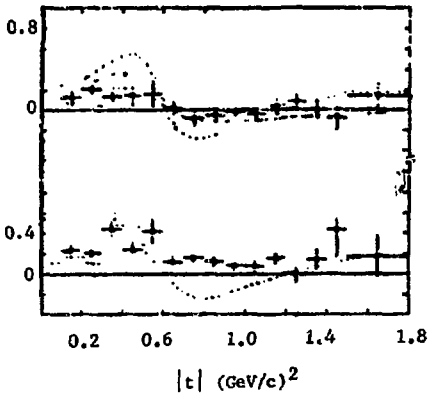

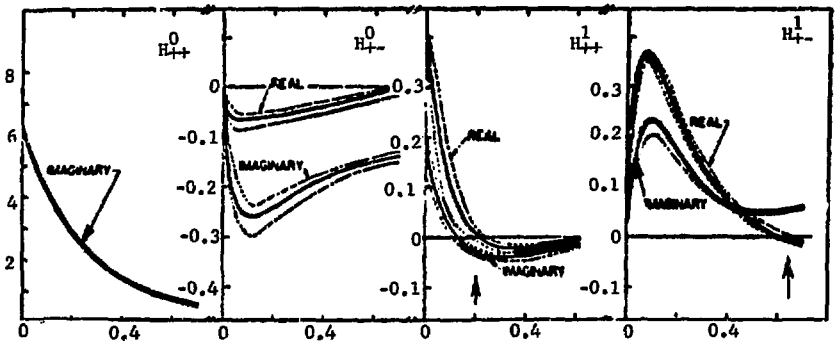

Figure 3. πN amplitudes at 6.0 GeV/c as determined from t-dependent fit shown by dark central lines. The error bands (determined by the envelope of fits to randomized data) are represented by shaded regions.

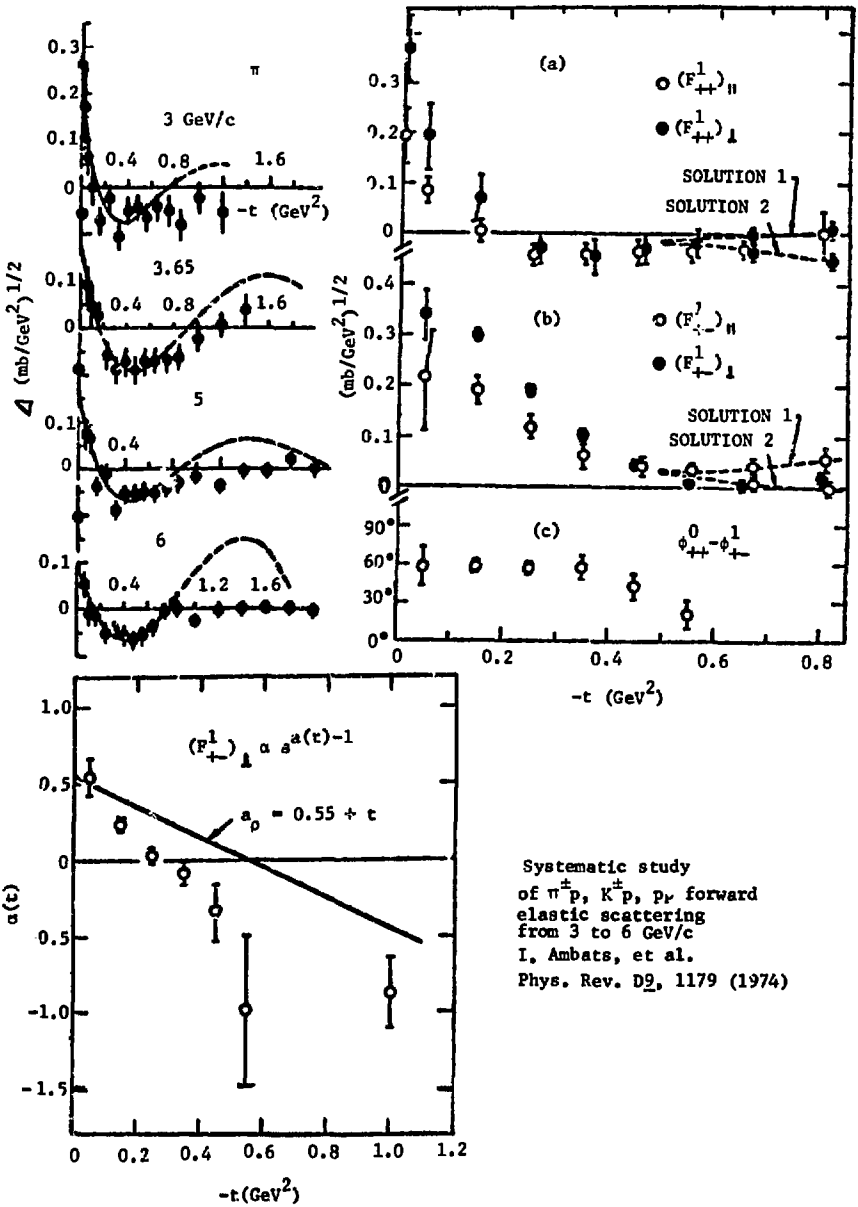

Systematic study of $\pi^{\pm}p$, $K^{\pm}p$, pp forward elastic scattering from 3 to 6 GeV/c
I. Ambats, et al.
Phys. Rev. D9, 1179 (1974)

Figure 4.

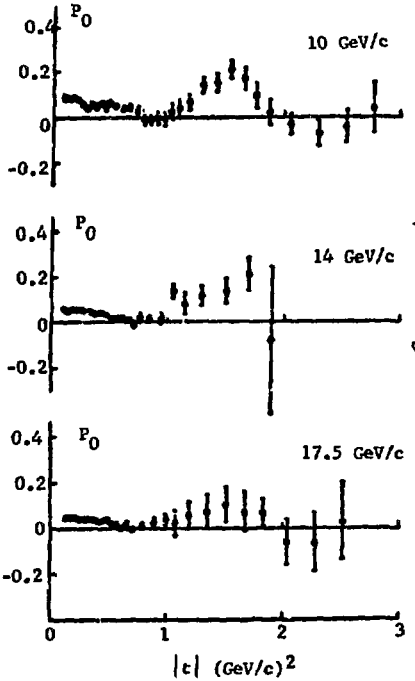

Polarization in Proton-Proton Elastic Scattering at 10, 14 and 17.5 GeV/c

M. Borghini, et al.

Phys. Lett. 36B, 501 (1971)

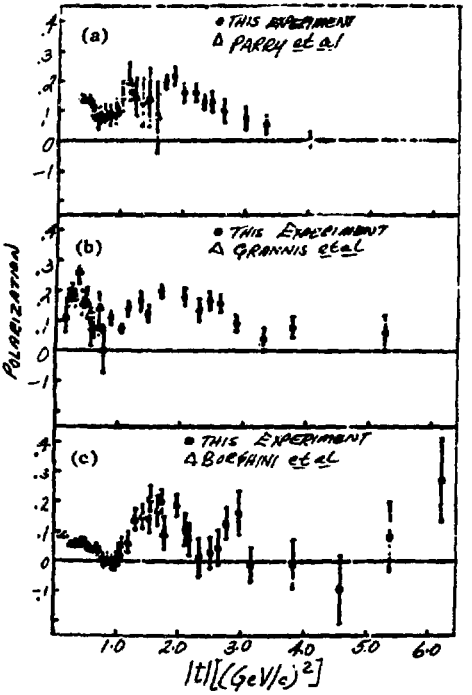

Polarization Structure in p-p Elastic Scattering

W. Abshire, et al.

Phys. Rev. Lett. 32, 1261 (1974)

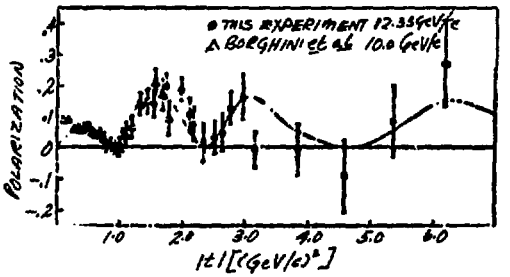

Figure 5.

J.R. O'Fallon, et al. Phys. Rev. Lett. 32, 77 (1974)

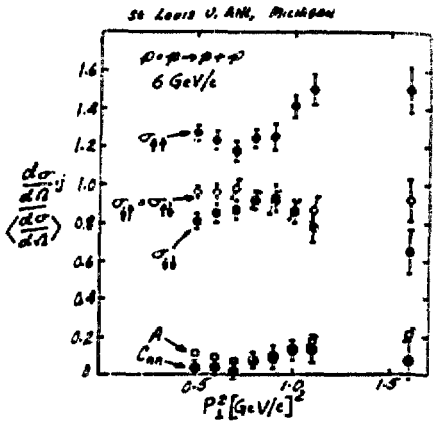

Figure 6.

Phys. Lett. 36B, 497 (1971)

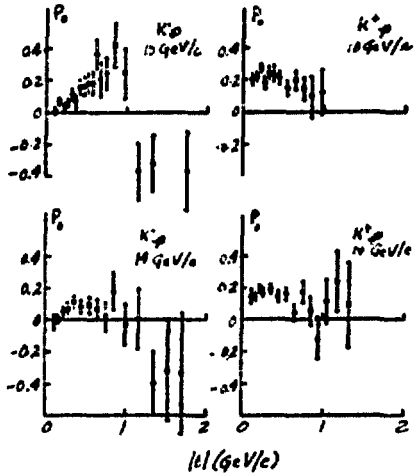

Figure 7.

Two-Body Strange-Particle Final State in $\pi^+ p$ Interactions at 4.5 and 6 GeV/c

H.A. Gordon, et al.

Phys. Rev. D6, 1220 (1972)

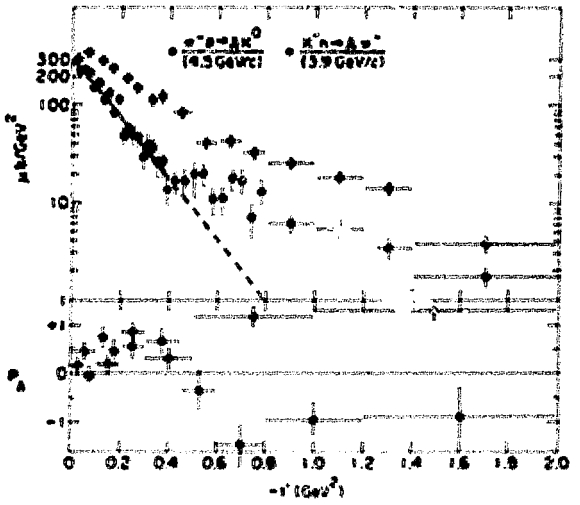

(A)

Amplitude Analysis for Hypercharge Exchange Reactions

V. Barger, et al. Phys. Lett. 39B, 379 (1972)

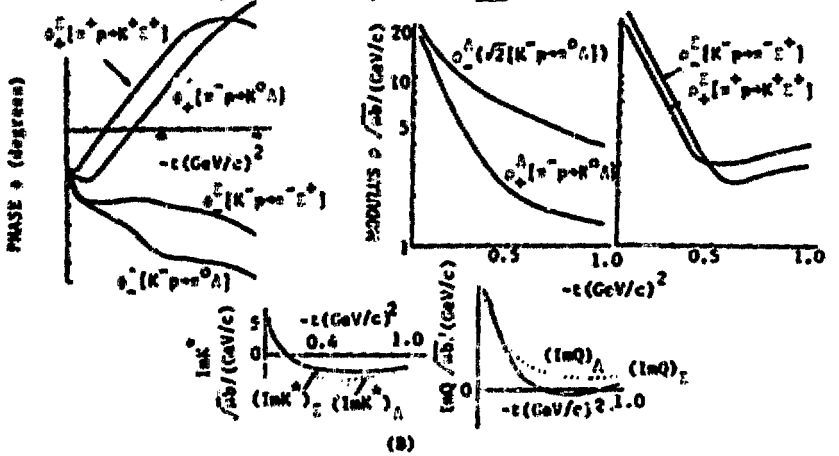

(B)

Figure 8.

Measurement of the Polarization Parameters in np Charge-Exchange Scattering from 2 to 12 GeV/c

Phys. Rev. Lett. 30, 1183 (1973)

P. LeDu, et al.

Phys. Rev. 44B, 390 (1973)

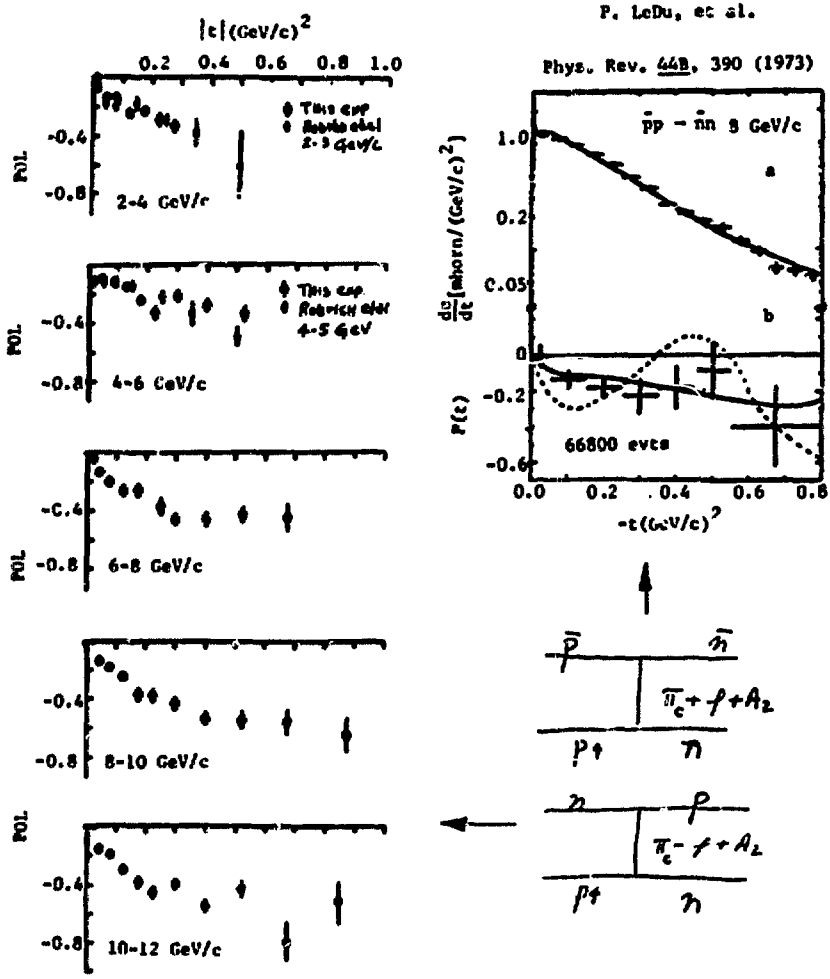

Figure 9.

CALT-68-466
AEC RESEARCH AND
DEVELOPMENT REPORT
September 9, 1974

I. Polarization Effects in Inelastic Exclusive Processes*†

by

R. D. Field

California Institute of Technology, Pasadena, California 91109

ABSTRACT

This paper deals with the phenomenology of polarization and spin effects in multiparticle exclusive processes. Vector-meson production with hypercharge exchange [$K^- p \to (\rho,\omega,\phi)(\Lambda,\Sigma^0)$, $\pi^- p \to K^{*0}(\Lambda,\Sigma^0)$]; $Y^*(1385)$ production; charge-exchange vector-meson production [$\pi^- p \to (\rho^0,\omega^0)n$, $K^{\pm}N \to K^{*0}N$] are examined in detail with emphasis on the importance of polarized target measurements. Existing amplitude analysis are discussed and predictions made for some polarized target observables. As an example of the usefulness of polarization information, the new polarized beam data on $p_{\uparrow}p \to n\Delta^{++}$ from Argonne are examined and a quark model comparison between this baryon-baryon scattering process and the meson-baryon reaction $K^+n \to K^{*0}p$ is made. The results are in remarkable agreement with the naive quark model.

*Work supported in part by the U.S. Atomic Energy Commission. Prepared under Contract AT(11-1)-68 for the San Francisco Operations Office, U.S. Atomic Energy Commission.

†Invited talk presented at the Workshop of Physics with Polarized Targets, Brookhaven National Laboratory, June 3-8, 1974.

I. Introduction.

This is the first of a two part paper concerned with the phenomenology of polarization and/or spin measurements in multiparticle production processes. In part I polarization effects in inelastic exclusive reactions are discussed, while part II deals with the phenomenology of polarization and spin effects in inclusive reactions. Those interested in the phenomenology of polarization should read the earlier reviews by Geoffrey Fox[1], R. J. N. Phillips and R. P. Worden[2] and R. D. Field[3].

The first and most important reason for measuring polarizations and spin correlations in two-body scattering $a + b \to c + d$ is to obtain a complete set of observables so that the underlying helicity amplitudes $H_{\lambda_c\lambda_d;\lambda_a\lambda_b}(s,t)$ can be determined. In my opinion amplitude determination should be the ultimate aim of experimenters since the complex helicity amplitudes contain <u>all</u> the information of a given two-body scattering process. The amplitudes are of course functions of both energy (s) and momentum transfer (t). Information is needed on both the t-dependence of each amplitude at fixed s and on the energy dependence at fixed t. Knowlege of the former is best obtained at BNL or ANL since many observables must be measured and large statistics are necessary. The energy dependences are best obtained by comparisons between BNL or ANL and Fermilab. An example of this can be seen in the reaction $\pi^- p \to \pi^0 n$, where amplitude analyses at 6.0 GeV/c[4] can be combined with recent data from Fermilab at 100 GeV/c.[5] Together these experiments provide much knowlege about the nature of the production mechanism (ρ-exchange),[6] whereas separately the experiments are much less profound. I have great hopes of seeing in the near future amplitude analyses preformed at BNL or ANL combined with energy dependences deduced from Fermilab for many elastic and inelastic processes.

Secondly, even if a complete set of observables is not available and hence an amplitude analysis not possible, measurement of polarizations and/or spin observables tells one a great deal about the production mechanism. In particular, in many cases one can form combinations of observables that project out amplitudes with definite t-channel quantum numbers. This is important in ascertaining what particle exchange forces are important in the production process (ie. A_1 exchange?). Particles have a dual role in high energy physics: They can be produced as a "particle" [either peripherally (Fig. 1a) or as a direct channel resonance (Fig. 1b)] or they can be exchanged and produce a "force" in the production process (see Fig. 1c). I view the experimental observation of the latter of equal importance as the former. Care must be taken, however, since observing a non-zero amplitude does not necessarily imply that a particle with those quantum numbers was exchanged (it might be a Regge cut). One must study the energy and t-dependence of the amplitude carefully to decide exactly what it was that was exchanged.

In this paper I will attempt to illustrate my above remarks with some specific examples. In Sec. II I will discuss vector-meson production with hypercharge exchange and in Sec. III $Y^*(1385)$ production. Sec. IV is concerned with charge-exchange vector-meson production. In each case I will describe what is already known about the process and indicate what additional information can be gained from polarization measurements. As an example of what can be learned from polarized beam experiments, in Sec. V the reaction $p_\uparrow p \to n\Delta^{++}$ is examined and new data from Argonne displayed. Sec. VI is reserved for summary and conclusions. Elastic polarization will be discussed by H. Gordon[7] and A. Yokosawa[7], while G. Fox[7] will examine among other things the reactions $K^-p \to \pi^-\Lambda$ and $\pi^-p \to K^0\Lambda$.

II. Vector-Meson Production with Y = 1 Exchange.[8]

A. $K^- p \to (\rho,\omega,\phi)\Lambda$, $\pi^- p \to K^{*0}\Lambda$.

In general there are twelve complex amplitudes for the process $PB \to VB'$, where P and V are pseudoscalar and vector mesons, respectively, and B and B' are spin $1/2^+$ baryons. Parity conservation reduces the number of independent complex amplitudes neccesary to describe the process to six (12 parameters at each s and t value). It is convenient to define transversity amplitudes $T^{\mu}_{\tau',\tau}(s,t)$, where τ, τ', and μ correspond to the components of spin of the target baryon B, baryon B', and vector-meson V, respectively, along the transversity z-axis (normal to production plane). In the absence of A and R type measurements these amplitudes are more closely connected to experiment than helicity amplitudes and are used at an intermediate point between the data and ultimately desired s-channel helicity amplitudes $H^{\lambda_V}_{\lambda_{B'},\lambda_B}(s,t)$ (see Fig. 2). The six transversity amplitudes are related to the helicity amplitudes as follows:

$$T_{++}^{\ 0} = -i\sqrt{2}\,A^+ \qquad T_{--}^{\ 0} = -i\sqrt{2}\,A^-$$

$$T_{-+}^{\ 1} = iB^+ + C^+ \qquad T_{+-}^{\ 1} = iB^- + C^-$$

$$T_{-+}^{-1} = -iB^+ + C^+ \qquad T_{+-}^{-1} = -iB^- + C^- \quad , \tag{2.1}$$

where

$$A^{\pm} = \frac{1}{2}\left[H_{++}^{\ 1} + H_{++}^{-1} \mp i(H_{-+}^{\ 1} + H_{-+}^{-1})\right]$$

$$B^{\pm} = \mp\frac{1}{2}\left[H_{++}^{\ 1} - H_{++}^{-1} \pm i(H_{-+}^{\ 1} - H_{-+}^{-1})\right]$$

$$C^{\pm} = \mp\frac{1}{\sqrt{2}}\left(H_{++}^{\ 0} \pm iH_{-+}^{\ 0}\right) \quad , \tag{2.2}$$

The $A^{\pm}$, $B^{\pm}$, and $C^{\pm}$ amplitudes are simply related to the amplitudes defined by Byers and Yang;[9] the superscripts $\pm$ refer to states with target baryon transversity $\tau = \pm 1/2$. It is interesting to note that amplitudes with definite natural (unnatural) parity in the t-channel maintain (change by one unit) the transversity between initial pseudoscalar P and final vector meson V. Thus transversity amplitudes with $\mu = 0$ ($\mu = \pm 1$) correspond to natural parity (unnatural parity) exchange in the t-channel.

Due to the self-analysing property of the Λ- hyperon, the reactions $K^-p \to (\rho,\omega,\phi)\Lambda$ and $\pi^-p \to K^{*0}\Lambda$ provide one the opportunity of learning much about the production amplitudes even in the absence of information as the polarization of the target baryon. Indeed observation of the joint density matrix elements between the vector meson V and Λ hyperon, in addition to the single density matrix elements of the vector meson, and the Λ polarization allows determination of the magnitudes of all six transversity amplitudes plus the determination of the relative phases between amplitudes with the same target baryon transversity (τ). The amplitudes can be divided into two sets of three amplitudes:

$$\begin{pmatrix} T_{++}^{0} \\ T_{-+}^{1} \\ T_{-+}^{-1} \end{pmatrix} \qquad \begin{pmatrix} T_{--}^{0} \\ T_{+-}^{1} \\ T_{+-}^{-1} \end{pmatrix} \tag{2.3a}$$

for the transversity amplitudes and

$$\begin{pmatrix} A^{+} \\ B^{+} \\ C^{+} \end{pmatrix} \qquad \begin{pmatrix} A^{-} \\ B^{-} \\ C^{-} \end{pmatrix} \tag{2.3b}$$

for the Byers and Yang type amplitudes. From the joint decay angular distributions of the vector meson V and Λ hyperon together with the differential cross section these amplitudes can be determined up to a relative phase ϕ_R between the target baryon transversity up ($\tau = 1/2$) and down ($\tau = -1/2$)

groups and an overall phase ϕ_o. Thus out of the 12 parameters at each s and t necessary to completely specify the amplitudes, 10 can be determined without polarized target information.

The magnitudes of the transversity amplitudes for $K^-p \to (\omega,\phi)\Lambda$ at 4.2 GeV/c[10,11] are shown in Fig. 3 as a function of momentum transfer, and where the normalization is as follows:

$$\sum_{\mu\tau'\tau} \left| T^{\mu}_{\tau',\tau} \right|^2 = 1 \quad . \tag{2.4}$$

Fig. 4 shows the relative phases

$$\theta^{\pm 1}_{\pm} = \text{Arg}\ (T^{\pm 1}_{\mp \pm}) - \text{Arg}(T^{o}_{\pm\pm}) \tag{2.5}$$

for $K^-p \to (\omega,\phi)\Lambda$ as a function of momentum transfer. As can be seen there are striking differences in the amplitude structure for the two reactions. In particular $K^-p \to \phi\Lambda$ has large values of the $|T^o_{--}|^2$ and small values of $|T^o_{++}|^2$, while $K^-p \to \omega\Lambda$ has large values of the latter and small values of the former.

The naive quark model[12] predicts that the amplitudes for $K^-p \to \phi\Lambda$ are identical to those for $\pi^-p \to K^{*o}\Lambda$. Fig.5 shows a comparison of the magnitudes of the amplitudes for these two reactions determined from various amplitude analyses[10,11,13,14]. These analyses are seen to give remarkably similar results in excellent agreement with the quark model predictions.

For processes such as $PB \to V\Lambda$ that allow both natural and unnatural parity exchange the recoil polarization of the Λ given by

$$P_{\Lambda}(s,t) = -4\ \text{Im} \sum_{\lambda_V} H^{\lambda_V}_{++}(s,t)\ H^{\lambda_V *}_{-+}(s,t) \ / \ \sigma_h \tag{2.6a}$$

is in general made up of two contributions as follows[15]

$$P_\Lambda(s,t) = P_N(s,t) + P_U(s,t) \quad , \tag{2.6b}$$

where P_N (P_U) arises from the interference between amplitudes with natural (unnatural) parity in the t-channel. The polarized target asymmetry (target polarized normal to production plane)

$$P_{asym}(s,t) = 4\mathrm{Im} \sum_{\lambda_V} H^{\lambda_V}_{++}(s,t)\, H^{\lambda_V *}_{+-}(s,t) \,/\, \sigma_h \tag{2.7a}$$

is given by

$$P_{asym}(s,t) = P_N(s,t) - P_U(s,t) \quad . \tag{2.7b}$$

If $P_U = 0$ then the recoil polarization P_B, and the polarized target asymmetry P_{asym} are equal. Having determined the magnitudes of the transversity amplitudes (Fig.3)one can determine $P_N(s,t)$ and $P_U(s,t)$ separately (they do not depend on ϕ_R or ϕ_o)[16]. Fig. 6 shows such a determination for the reactions $\bar{K}^- p \to (\omega,\phi)\Lambda$ at 4.2 GeV/c. It can be seen that the natural parity (K^{**} and K^*) amplitudes produce a sizable polarization P_N and that this polarization changes sign in going from ω to ϕ production.[17] In addition P_Λ does not equal P_{asym} (ie. P_U is not zero). In terms of t-channel unnatural parity exchanges P_U is made up of as follows

$$P_U \propto \mathrm{Im}\,[(K + K_B)(K_A)^*] \quad . \tag{2.8}$$

In the absence of an amplitude with the quantum numbers of the K_A the polarization P_U would vanish. The experimental data seem to indicate the presence

of $K - K_A$ interference, which was certainly not expected.

As we have seen, much can be learned about the processes $K^- p \to (\rho,\omega,\phi)\Lambda$ and $\pi^- p \to K^{*o}\Lambda$ without polarized target information [ie. without knowing $\phi_R(s,t)$]. However, we have learned little as to the structure of the s-channel helicity amplitudes $H^{\lambda_V}_{\lambda_{B'}\lambda_B}(s,t)$. From Eq. (2.1) and (2.2) it can be seen that both the magnitudes and phases of the s-channel helicity amplitudes depend on the relative transversity phase $\phi_R(s,t)$. To determine the behavior of the helecity amplitudes one must measure, in addition to the above 10 quantities, the phase $\phi_R(s,t)$. This is not an easy task since, as we have seen, target polarization observables with polarization normal to the production plane are independent of ϕ_R (ie. P_{asym} does not depend on ϕ_R). To determine ϕ_R one must measure either A or R type observables (see Fig. 7). It is convenient to define observables more directly connected to the helicity amplitudes as follows:

$$\hat{R}' = -4\ \mathrm{Re} \sum_{\lambda_V} H^{\lambda_V}_{++} H^{\lambda_V *}_{-+} \ / \ \sigma_h \qquad (2.9a)$$

$$\hat{R} = 4\ \mathrm{Re} \sum_{\lambda_V} H^{\lambda_V}_{++} H^{\lambda_V *}_{+-} \ / \ \sigma_h \qquad (2.9b)$$

$$\hat{A} = 2 \sum_{\lambda_V} \left\{ \left| H^{\lambda_V}_{++} \right|^2 - \left| H^{\lambda_V}_{-+} \right|^2 \right\} \ / \ \sigma_h \qquad (2.9c)$$

These quantities are simply related to the experimental A and R type parameters.[18]

Just as for the polarizations Eq. (2.6b) and Eq. (2.7b) these observables can be decomposed into natural and unnatural parity contributions as follows:

$$\hat{R}'(s,t) = \hat{R}_N(s,t) + \hat{R}_U(s,t) \qquad (2.10a)$$

$$\hat{R}(s,t) = \hat{R}_N(s,t) - \hat{R}_U(s,t) \qquad (2.10b)$$

$$\hat{A}(s,t) = \hat{A}_N(s,t) + \hat{A}_U(s,t) \ , \qquad (2.10c)$$

where in terms of transversity amplitudes

$$\hat{R}_N(s,t)\sigma_h = 2\mathrm{Im}\ T^0_{++}\ T^{0*}_{--} \tag{2.11a}$$

$$\hat{R}_U(s,t)\sigma_h = 2\mathrm{Im}\ T^1_{-+}\ T^{1*}_{+-} + 2\mathrm{Im}\ T^{-1}_{-+}\ T^{-1*}_{+-}$$

and

$$\hat{A}_N(s,t)\sigma_h = 2\mathrm{Re}\ T^0_{++}\ T^{0*}_{--} \tag{2.11c}$$

$$\hat{A}_U(s,t)\sigma_h = -2\mathrm{Re}\ T^1_{-+}\ T^{1*}_{+-} - 2\mathrm{Re}\ T^{-1}_{-+}\ T^{-1*}_{+-} \ . \tag{2.11d}$$

Clearly $\hat{R}$ and $\hat{A}$ measure the phase between the target baryon up ($T^U_{\tau',+}$) and target baryon down ($T^N_{\tau',-}$) transversity amplitudes. In particular if we define this phase by

$$\phi_R(s,t) \equiv \mathrm{Arg}(T^0_{--}) - \mathrm{Arg}(T^0_{++}) \tag{2.12}$$

then, for example,

$$\hat{R}_N(s,t)\sigma_h = 2|T^0_{++}||T^0_{--}| \sin\phi_R \tag{2.13a}$$

$$\hat{A}_N(s,t)\sigma_h = 2|T^0_{++}||T^0_{--}| \cos\phi_R \ . \tag{2.13b}$$

From our amplitude analysis without a polarized target we know everything except $\phi_R(s,t)$ and $\phi_0(s,t)$ (see Figs. 3 & 4), thus we can predict the above $\hat{A}$ and $\hat{R}$ type observables for various values of $\phi_R(s,t)$. This is important since, for example, if $|T^0_{--}|$ were exactly zero the $\hat{R}_N$ and $\hat{A}_N$ would be zero independent of ϕ_R. Fig. 8 shows the predicted values of $\hat{R}(s,t)$ and $\hat{A}(s,t)$ for $K^-p \to (\omega,\phi)\Lambda$ at 4.2 GeV/c as a function of ϕ_R for various values of t. The values never exceed 50% but they are not zero either. In Fig. 9 I have decomposed $\hat{A}$ into its various components ($\hat{A}_U = A^1_U + A^0_U$) at $t = -0.05(\mathrm{GeV/c})^2$ and

plotted them versus ϕ_R. It is clearly seen that $\hat{A}_N$ is proportional to cos ϕ_R.

Similarly the s-channel helicity amplitudes can be plotted as a function of ϕ_R. This is done for $K^-p \to (\omega,\phi)\Lambda$ at t = -0.05 GeV/c in Fig. 10[19]. pointed out earlier both the phases and magnitudes of the s-channel helicity amplitudes depend on ϕ_R. Having determined ϕ_R from a measurement of, for example, $\hat{R}_N$ one can simply read the corresponding values of the s-channel helicity amplitudes off Fig. 10.

A skeptic may ask whether it is worth performing a new and complicated polarized target counter experiment to determine essentially one quantity $\phi_R(s,t)$. The remaining 10 parameters at each s and t have been determined without the use of a polarized target. In my opinion the answer is yes for the following reasons:

(i) The new experiments will not be set up to measure just the one parameter ϕ_R. The magnitudes and phases (including ϕ_R) of the amplitudes will be determined simultaneously (11 independent numbers at each s and t) and they will be determined much more accurately than the previous bubble chamber analyses.

(ii) The hypercharge exchange reactions $K^-p \to (\omega,\phi)\Lambda$ and $\pi^-p \to K^{*o}\Lambda$ provide a nice "laboratory" to study production mechanisms. They allow both natural parity (K^{**},K^*) exchange and unnatural parity (K,K_A?,K_B?) exchange. In addition there are theoretical predictions from duality and/or EXD (ie. $K^-p \to \omega\Lambda$ should have purely real helicity amplitudes; $K^-p \to \phi\Lambda$ should have amplitudes with a rotating phase). These predictions are clearly broken (large polarizations), but it is crutial to learn how and why they are broken. Also these reactions allow for the study of the little known double-flip amplitude H^{-1}_{+-}.

B. $K^-p \to (\rho,\omega,\phi)\Sigma^o$, $\pi^-p \to K^{*o}\Sigma^o$.

These reactions are described by six complex transversity (or helicity) amplitudes just as the reactions $K^-p \to (\rho,\omega,\phi)\Lambda$ and $\pi^-p \to K^{*o}\Lambda$, however in this case one expects that the unnatural parity amplitudes $T^{\pm 1}_{\tau',\tau}(s,t)$ are less important.[20] This is because the K meson couples much more weakly to $\bar{p}\Sigma$ than to $\bar{p}\Lambda$ (ie. $g^2_{KN\Sigma} << g^2_{KN\Lambda}$). A recent transversity amplitude analysis of $\pi^-p \to K^{*o}\Sigma^o$ at 3.9 GeV/c by Yaffe et al.[21] show that this is indeed the case (see Fig.11). In fact, except for very small t, this reaction is described quite adequately by just one amplitude $T^o_{++}(s,t)$! The remaining amplitudes are roughly zero. This implies that the polarization of the Σ^o is positive and maximal (see Fig. 12) and that it arises totally from $P_N(s,t)$ in (2.6b) (ie. $P_U(s,t) \stackrel{\sim}{=} 0$).[16] This almost complete dominance of T^o_{++} means that essentially everything is already known about this reaction including the as yet unmeasured polarized target observables. For example, one expects

$$P_\Lambda(s,t) \stackrel{\sim}{=} P_{asym}(s,t) \stackrel{\sim}{=} 1.0 \qquad (2.14a)$$

$$\hat{R}(s,t) \stackrel{\sim}{=} \hat{R}_N(s,t) \stackrel{\sim}{=} \hat{R}_U(s,t) \stackrel{\sim}{=} 0 \qquad (2.14b)$$

$$\hat{A}(s,t) \stackrel{\sim}{=} \hat{A}_N(s,t) \stackrel{\sim}{=} \hat{A}_U(s,t) \stackrel{\sim}{=} 0 \qquad (2.14c)$$

Similarly all other observables can be determined. The quark model predicts the amplitudes for $K^-p \to \phi\Sigma^o$ to be identical to those for $\pi^-p \to K^{*o}\Sigma^o$. In addition SU(3) predicts that $K^-p \to \rho\Sigma^o$ is dominated by $T^o_{--}(s,t)$ in the same way that $\pi^-p \to K^{*o}\Sigma^o$ is dominated by $T^o_{++}(s,t)$. This implies that $P_{\Sigma^o} \stackrel{\sim}{=} -1$ for the reaction $K^-p \to \rho\Sigma^o$ and there is evidence that this is indeed the case.[20]

III. The Production of $Y^*(1385)$.

The reaction $K^-p \to \pi^-Y^{*+}(1385)$ is described by the transversity amplitudes $T_{2\lambda;2\lambda'}(s,t)$ where $\lambda(\lambda')$ corresponds to the component of spin of the Y^* (target

proton) along the transversity z-axis, which is normal to the production plane. Parity conservation implies $T_{31} = T_{1\,-1} = T_{-3\,-1} = 0$. The remaining four complex amplitudes are related to the eight transversity density matrix elements as follows:[22]

$$\rho_{33} = |T_{3\,-1}|^2 \tag{3.1a}$$

$$\rho_{11} = |T_{11}|^2 \tag{3.1b}$$

$$\rho_{-1\,-1} = |T_{-1\,-1}|^2 \tag{3.1c}$$

$$\rho_{-3\,-3} = |T_{-31}|^2 \tag{3.1d}$$

$$\mathrm{Re}\rho_{3\,-1} = \mathrm{Re}(T_{3\,-1}T^*_{-1\,-1}) = |T_{3\,-1}|\ |T_{-1\,-1}|\ \cos\delta_1 \tag{3.1e}$$

$$\mathrm{Im}\rho_{3\,-1} = \mathrm{Im}(T_{3\,-1}T^*_{-1\,-1}) = |T_{3\,-1}|\ |T_{-1\,-1}|\ \sin\delta_1 \tag{3.1f}$$

$$\mathrm{Re}\rho_{1\,-3} = \mathrm{Re}(T_{11}T^*_{-31}) = |T_{11}|\ |T_{-31}|\ \cos\delta_2 \tag{3.1g}$$

$$\mathrm{Im}\rho_{1\,-3} = \mathrm{Im}(T_{11}T^*_{-31}) = |T_{11}|\ |T_{-31}|\ \sin\delta_2 \quad , \tag{3.1h}$$

where δ_1 [δ_2] is defined as the relative phase between the amplitudes $T_{3\,-1}$ and $T_{-1\,-1}$ [T_{11} and T_{-31}].

By observing the two step decay of the $Y^*(1385)$ (ie., $Y^* \to \pi\Lambda$, $\Lambda \to \pi p$) in addition to the differential cross section for $K^-p \to \pi^- Y^{*+}$ one can determine all the transversity density matrix elements and thus the magnitudes of all four transversity amplitudes and the two relative phases δ_1 and δ_2. Without a polarized target one cannot determine the relative phase ϕ_R between the amplitudes with target proton transversity up ($\lambda' = 1/2$) and the amplitudes with target proton transversity down ($\lambda' = -1/2$). In addition, one of course cannot determine the overall phase of the amplitudes ϕ_o. One can thus determine 6 out of the 8 parameters needed at each s and t value to completely specify the production process $K^-p \to \pi^- Y^{*+}$. The transversity density matrix elements and the phases δ_1 and δ_2 resulting from an analysis[22] of $K^-p \to \pi^- Y^{*+}(1385)$ are displayed in Fig. 13, where the density matrix elements are normalized

according to

$$\rho_{33} + \rho_{11} + \rho_{-1\,-1} + \rho_{-3\,-3} = 1.$$

The simple non-relativistic additive quark model[12] assumes that the transversity amplitudes for production process $K^-p \to \pi^-Y^*$ can be represented by a sum of quark-quark scattering amplitudes (Fig. 14). Transversity amplitudes that require a flip of more than one of the baryon quarks, such as $T_{3\,-1}$ (Fig. 14), are not allowed and predicted to be zero. This model thus predicts

$$T_{3\,-1}(s,t) = T_{-31}(s,t) = 0 \quad . \tag{3.2a}$$

It also predicts

$$T_{11}(s,t) = T_{-1\,-1}(s,t) \ , \tag{3.2b}$$

since these amplitudes are given by the same sum over quark-quark amplitudes. The model thus predicts that $\rho_{11} = \rho_{-1\,-1} = 1/2$ and that the remaining transversity density matrix elements vanish. As can be seen from the data in Fig. 13 these predictions do explain the gross features of the amplitudes, however, they are not satisfied exactly. The data clearly show non-zero values of ρ_{33}, $\mathrm{Im}\rho_{3\,-1}$ in the small momentum transfer region $|t_o - t| \leq 0.3$ (GeV/c)^2 indicating a non-vanishing $T_{3\,-1}$ amplitude.

The as yet unmeasured polarized target asymmetries can be predicted from the transversity amplitudes already determined. In particular, we define the following asymmetries

$$2A_{33}(s,t) = 2[\rho_{33}(\uparrow) - \rho_{33}(\downarrow)] \ , \tag{3.3a}$$

$$2A_{11}(s,t) = 2[\rho_{11}(\uparrow) - \rho_{11}(\downarrow)] \ , \tag{3.3b}$$

where +(+) refer to target baryon polarization up (down) with respect to the normal to the production plane. In terms of the transversity amplitude one has

$$2A_{33}(s,t) = |T_{-3\ 1}(s,t)|^2 - |T_{3-1}(s,t)|^2 \qquad (3.4a)$$

$$2A_{11}(s,t) = |T_{11}(s,t)|^2 - |T_{-1-1}(s,t)|^2 \qquad (3.4b)$$

The Y^* polarization is defined by

$$P_{Y^*}(s,t) = 2A_{33}(s,t) + 2A_{11}(s,t) \quad . \qquad (3.5)$$

Clearly the quark model predicts zero for A_{33}, A_{11} and P and Fig.15 shows that the data are consistent with this prediction. Measurement of A and R type parameters are necessary to determine the unknown phase ϕ_R [ie. ϕ_R = Arg $T_{11}(s,t)$ = Arg $T_{-1-1}(s,t)$], which is predicted by the quark model to be zero.

Further, high statistics experimental studies of $K^-p \to \pi^-Y^*$ and $\pi^-p \to K^oY^*$ would be interesting in that one could examine the detail nature of the small quark model violations. Do they depend on energy? How does the quark model breaking differ from $K^-p \to \pi^-Y^*$ and $\pi^-p \to K^oY^*$? Can the breaking be attributed to absorption effects?

IV. Charge-Exchange Vector-Meson Production.

A. $\pi^-p \to \rho^on$.

The production mechanism for $\pi^-p \to \rho^on$ has been studied in great detail due to excellent data at 6.0 and 17.2 GeV/c[23], which includes ρ-ω mixing information[24]. Nevertheless there is still some confusion as to the precise nature of the unnatural parity exchanges. Some points that need further clarification are:

(1) There appears to be a change in slope of $\rho^H_{00}d\sigma/dt$ at $t \simeq -0.4$ $(GeV/c)^2$. Absorption models predict[25] an actual dip at about $|t| \simeq 0.4 - 0.5$ $(GeV/c)^2$

in this observable (see Fig. 16). What is the mechanism responsible for this structure in $\rho^H_{oo} d\sigma/dt$?

(iii) There appears to be very little Regge shrinkage in $\rho^H_{oo} d\sigma/dt$ between 6.0 and 17.2 GeV/c (see Fig. 17). The data imply a pion slope of $\alpha'_\pi \leq 0.5$ $(GeV/c)^{-2}$, while normal Regge poles (like the ρ) have a slope near one. Why is the π different?

(iii) How important are A_1 exchange contributions to ρ^o production?

The answer to this last question can be answered by polarized target experiments and once the answer is known perhaps it will help us to understand better questions (i) and (ii). In general the observable $\rho^H_{oo} d\sigma/dt$ is given in terms of the s-channel helicity amplitudes by

$$\rho^H_{oo} d\sigma/dt(s,t) = |H^{n=0}_{o+;+}(s,t)|^2 + |H^{n=1}_{o+;-}(s,t)|^2 \quad , \tag{4.1}$$

where to leading order in 1/s the amplitudes $H^{n=1}_{o+;-}$ ($H^{n=0}_{o+;+}$) receive contributions from π (A_1) exchange. The presence of an A_1 exchange contribution could have the following effects on $\rho^H_{oo} d\sigma/dt$:

(i) If A_1 exchange were important at small $|t|$ then $\rho_{oo} d\sigma/dt$ would not vanish like t as $t \to 0$ as is the case for π exchange.

(ii) If A_1 exchange became important at large $|t|$ the A_1 (or A_1 cut) could cause a change in slope of $\rho_{oo} d\sigma/dt$ as a function of t (see Fig. 18).

Actually, since the A_1 contribution has a zero at $\alpha_{A_1}(t) = 0$ (from signature and absence of $J^{PC} = 0^{-+}$ state, while the π contribution has a pole at $\alpha_\pi(t) = 0$, the ratio of A_1/π is expected to be quite small. These small A_1/π ratios will probably not affect the differential cross-section or density matrix observables much since they enter quadratically. On the other hand, polarization effects are linear in A_1/π and so could become significant particularly at $|t| > 0.3 (GeV/c)^2$. Experimentally one should check for the presence of A_1 exchange by studying

ρ^0 production off a polarized target.[1] In particular defining polarized target asymmetries as follows:

$$P_N \frac{d\sigma}{dt} = \rho_{+}\frac{d\sigma}{dt}(\uparrow) - \rho_{+}\frac{d\sigma}{dt}(\downarrow) \tag{4.2a}$$

$$A_U^1 \frac{d\sigma}{dt} = \rho_{-}\frac{d\sigma}{dt}(\uparrow) - \rho_{-}\frac{d\sigma}{dt}(\downarrow) \tag{4.2b}$$

$$A_U^0 \frac{d\sigma}{dt} = \rho_{oo}\frac{d\sigma}{dt}(\uparrow) - \rho_{oo}\frac{d\sigma}{dt}(\downarrow) \ , \tag{4.2c}$$

where $\uparrow(\downarrow)$ refers to target polarization up(down) with respect to the normal to the production plane and where $\rho_{\pm} = \rho_{11} \pm \rho_{1\,-1}$, one has a total polarized target asymmetry given by

$$P_{asym}(s,t) = P_N(s,t) - P_U(s,t) \ , \tag{4.3}$$

where $P_U = -A_U^1 - A_U^0$. The recoil nucleon polarization is given by

$$P_{recoil}(s,t) = P_N(s,t) + P_U(s,t) \ , \tag{4.4}$$

where in terms of t-channel unnatural parity exchanges P_U is made up of as follows

$$P_U(s,t) \propto \mathrm{Im}(\pi A_1^*) \ . \tag{4.5}$$

It is the interference between π and A_1 exchange. [This is completly analogous to the hypercharge case in Sec. II A, where P_U measured the interference between K and K_A exchange. In that case, due to the self analyzing property of the Λ hyperon, we did not have to have a polarized target to measure P_U.] In the absence of A_1 exchange $P_U(s,t)$ in Eq. (4.5) will vanish and $P_{recoil}(s,t) = P_{asym}(s,t) = P_N(s,t)$. Fig.19 shows the quantities $P_N(s,t)$, $A_U^1(s,t)$, $A_U^0(s,t)$, and $P_{asym}(s,t)$ for ρ^0 production for models with and without A_1 exchange.[25] Clearly experimental determination of the unnatural parity polarization $P_U(s,t)$ will answer the question as to the importance of A_1 exchange in ρ^0 production.

B. $\pi^- p \to \omega^o n$: Where do helicity zero ω^o's come from?

The observable $\rho^H_{oo} d\sigma/dt$ for ω^o production is given by Eq. (4.1) where the amplitudes $H^{n=1}_{o-;+}$ ($H^{n=0}_{o+;+}$) receive contributions from $B(Z;J^P I^G = 2^- 1^+)$[26] exchange. In the absence of $Z(J^P I^G = 2^- 1^+)$ exchange $\rho^H_{oo} d\sigma/dt$ vanishes like t as $t \to 0$ and since the B does not have a pole near the physical region (like the π) one expects very few small $|t|$ ω^o's to be produced. It can be shown[25] that due to ρ–ω mixing the reaction $\pi^+ n \to \tilde{\omega}^o p$ ($\tilde{\omega}$ is electromagnetically mixed ω) has substantially more helicity zero ω^o's than the unmixed reaction $\pi^+ n \to \omega^o p$, but the reaction $\pi^- p \to \tilde{\omega}^o n$ has less helicity zero ω^o's than the unmixed case (see Fig. 20). As is clear from Fig. 20 if one compares the models with the sum of $\pi^+ n \to \tilde{\omega}^o p$ and $\pi^- p \to \tilde{\omega}^o n$, which cancels out mixing effects, one cannot explain the large small $|t|$ values of ρ^H_{oo} with B exchange alone. Perhaps, as suggested by Irving and Michael[27], the remaining helicity zero ω^o's are produced by Z exchange. In ω^o production the B exchange contribution has a single zero at $\alpha_B(t) = 0$, while the $Z(J^P I^G = 2^- 1^+)$ exchange contribution need not vanish at $\alpha_Z(t) = 0$ so that, in contrast to the ratio of A_1/π for ρ^o production, the ratio Z/B might be important.

Again the best way to test for the presence of a possible $Z(J^P I^G = 2^- 1^+)$ exchange contribution is to measure $P_{IJ}(s,t)$ in Eq. (4.3) by the use of a polarized target. In this case $P_{IJ}(s,t)$ measures B–Z interference and vanishes in the absence of a Z exchange contribution.

C. $K^- p \to \bar{K}^{*o} n$, $K^+ n \to K^{*o} p$.

Using SU(3) one can directly relate the amplitudes for K^{*o} and $\bar{K}^{*o}$ production to those for ω^o and ρ^o production as follows:[28]

$$A(K^- p \to \bar{K}^{*o} p) = -[A(\pi^- p \to \omega^o n) - A(\pi^- p \to \rho^o n)] \,/\, \sqrt{2} \quad , \tag{4.6a}$$

$$A(K^+ n \to K^{*o} p) = -[A(\pi^- p \to \omega^o n) + A(\pi^- p \to \rho^o n)] \,/\, \sqrt{2} \quad . \tag{4.6b}$$

From these relations one can construct the following SU(3) sum rules

$$\rho_{ij}\frac{d\sigma}{dt}(K^{*o}) + \rho_{ij}\frac{d\sigma}{dt}(\bar{K}^{*o}) = \rho_{ij}\frac{d\sigma}{dt}(\rho^{o}) + \rho_{ij}\frac{d\sigma}{dt}(\omega^{o}) \quad , \tag{4.7}$$

which are quite nicely satisfied (see Fig. 21). In addition using (4.6a) and (4.6b) one can relate the line reversal breaking seen in K^{*o} and $\bar{K}^{*o}$ production to ρ-ω mixing phases β determined by studying the $\pi^{+}\pi^{-}$ mass spectra in $\pi^{\pm}N \rightarrow \pi^{+}\pi^{-}N$ as follows:

$$\Delta \equiv |A(K^{*o})|^2 - |A(\bar{K}^{*o})|^2 = 2|A(\omega^{o})|\ |A(\rho^{o})|\cos\beta \quad , \tag{4.8}$$

where $\beta = \mathrm{Arg}[A(\omega^{o}) / A(\rho^{o})]$. A comparison of the data at 4.0 GeV/c (Fig. 22) from Argonne[29] show good agreement between the left and right hand sides of (4.8).

The amplitudes for K^{*o} and $\bar{K}^{*o}$ production are in excellent agreement with the SU(3) relations (4.6a) and (4.6b). This implies that any $A_1[Z;J^{P}I^{G}=2^{-}1^{+}]$ exchange contributions present in $\rho^{o}[\omega^{o}]$ production will via SU(3) be present in K^{*} and $\bar{K}^{*o}$ production. The polarized target observable $P_U(s,t)$ Eq. (4.2) and (4.3) for $\bar{K}^{*o}$ and K^{*o} production is given by:

$$P_U(\bar{K}^{*o}) \propto \mathrm{Im}[(\pi - B)(A_1 - Z)^{*}] \tag{4.9a}$$

$$P_U(K^{*o}) \propto \mathrm{Im}[(\pi + B)(A_1 + Z)^{*}] \quad . \tag{4.9b}$$

Measurement of these observables will help to further our knowlege as to the nature of unnatural parity exchange.

V. Polarized Beam Study of $p_{\uparrow}p \rightarrow n\Delta^{++}$.[30]

A. Observables.

The observables for $p_{\uparrow}p \rightarrow p\pi^{+}n$ in terms of angular correlation functions and the beam polarization vector $\vec{P}$, where this vector is defined in the beam proton rest frame with the s-channel components

$$P_x = \vec{P} \cdot (\hat{n} \times \hat{p}_{beam}) \tag{5.1a}$$

$$P_y = \vec{P} \cdot \hat{n} \tag{5.1b}$$

$$P_z = \vec{P} \cdot \hat{p}_{beam} \text{ (zero for transversely polarized beam)} \tag{5.1c}$$

and where $\hat{n}$ is the normal to the scattering plane, are defined as follows:[31]

$$d^3\sigma/(dtd\cos\theta d\phi) = (1/2\pi)\frac{d\sigma}{dt}\left\{2(\rho_{33} + A_{33}P_y)W_1 + 2(\rho_{11} + A_{11}P_y)W_2 + 4(\rho_{33} + A_{31}P_y)W_3 + 4(\rho_{3-1} + A_{3-1}P_y)W_4 + 4(I^X_{31}P_x + I^Z_{31}P_z)W_3 + 4(I^X_{3-1}P_x + I^Z_{3-1}P_z)W_4\right\}, \tag{5.2a}$$

where we have only considered P-waves[32] and where

$$W_1 = 3/4\ \sin^2\theta \tag{5.2b}$$

$$W_2 = 1/4(1 + 3\cos^2\theta) \tag{5.2c}$$

$$W_3 = -\sqrt{3}\ (\sin 2\theta\cos\phi)\ /4 \tag{5.2d}$$

$$W_4 = -\sqrt{3}\ (\sin^2\theta\cos^2\phi)\ /4 \tag{5.2e}$$

and the angles θ and ϕ are the polar and azimuthal decay angles of the Δ^{++}. Thus, by the use of a polarized beam one can determine eight new observables A_{33}, A_{11}, A_{31}, A_{3-1}, I^X_{31}, I^Z_{31}, I^X_{3-1}, I^Z_{3-1} in addition to the usual Δ^{++} density matrix elements and the differential cross-section. However, due to the large number (sixteen) of independent complex amplitudes necessary to describe $pp \to n\Delta^{++}$ one cannot perform a model independent amplitude analysis even with the additional observables provided by polarized beam studies. Nevertheless, one can learn much about the nature of the production mechanism by studying these new observables. In particular one can make an interesting quark model comparison between the observables for $p_\uparrow p \to n\Delta^{++}$ and $K^+n \to K^{*o}p$.

B. Quark Model Comparison between $p_{\uparrow}p \to n\Delta^{++}$ and $K^{+}n \to K^{*o}p$.

In general the reaction $pp \to n\Delta^{++}$ is described by 16 complex amplitudes; 8 natural parity and 8 unnatural parity. The quark model predicts that the four amplitudes with $|m| = 2$ vanish, where m is defined as the net t-channel helicity flip at the $\bar{p}\Delta^{++}$ vertex. In addition the model requires that the two natural parity amplitudes with $m = 0$ vanish and that the remaining $|m| = 1$ amplitudes are related in pairs by $\sqrt{3}$ factors. This leaves a total of two natural and four unnatural parity amplitudes necessary to describe the reaction. As shown in Table 1 this is precisely the number of independent amplitudes present in the vector-meson production $K^{+}n \to K^{*o}p$. Both reactions $K^{+}n \to K^{*o}p$ and $pp \to n\Delta^{++}$ are exotic in the s-channel and both allow exactly the same t-channel Regge exchanges (ρ and A_2 natural parity exchanges and π and B unnatural parity exchanges). It is therefore not surprising that the quark model predicts a direct relationship between the t-channel helicity amplitudes for the two processes as shown in Table 2. From this it is an easy matter to predict relations among the t-channel observables for $pp \to n\Delta^{++}$ ($d\sigma/dt$, Δ^{++} density matrix elements in the Jackson frame) and $K^{+}n \to K^{*o}n$ ($d\sigma/dt$ and vector-meson density matrix elements). These predictions are also listed in Table 2.

Fig. 23 shows the quark model comparison for the differential cross sections for $pp \to n\Delta^{++}$ and $K^{+}p \to K^{*o}n$ and Fig. 24 shows the comparison for the density matrix elements (observables 2-5 in Table 2). The quark model predictions, although not exact, are seen to be in excellent agreement with the data. (Remember we are predicting baryon-baryon scattering from meson-baryon scattering!)

One must use care when testing the predictions for the $p_{\uparrow}p \to n\Delta^{++}$ polarized beam asymmetry observables (observables 6-13 in Table 2) since these observables can in general receive contributions from the $J = 1/2$ P-wave background[33] under the Δ^{++} for which the quark model predictions do not hold. This contamination

is, however, expected to be small for the asymmetries A_{11} and A_{33} since the P waves enter in the form Re $[P(J = 1/2)\ P(J = 3/2)^*]$[34]. The prediction of non-vanishing A_{11} and vanishing A_{33} is seen from Fig. 25 to be in reasonable agreement with the data. The remaining polarized beam observables (observables 8-13 in Table 2) receive P-wave background contamination in the form Im $[P(J = 1/2)\ P(J = 3/2)^*]$ which cannot be neglected and which inhibits any simple tests of the quark model predictions for these observables.

The quark model predicts that the polarization of the Δ^{++} is related to $Im\rho_{10}$ for K^{*o} production as follows

$$P_\Delta(s,t) = -\sqrt{2}\ \text{Im}\ \rho_{10}^{K^*}(s,t) \quad , \tag{5.3}$$

where we have combined observable (6) and (7) in Table 2 (ie. $P_\Delta \equiv 2A_{33} + 2A_{11}$), which removes any possible J = 1/2 P-wave background contamination. Eq. (5.3) implies that the dynamical mechanism responsible for non-zero values of Im ρ_{10} in K^{*o} production is responsible for the observed non-zero Δ^{++} polarization shown in Fig. 26. The former observable is related to the t-channel helicity amplitudes for K^{*o} production shown in Table 1 by

$$\text{Im}\ \rho_{10} = \text{Im}\ \left\{U^1_{++}\ U^{o*}_{++} + U^1_{-+}\ U^{o*}_{-+}\right\}\ /\ \Sigma \quad , \tag{5.4}$$

where Σ is the sum of the squares of all 6 helicity amplitudes given in Table 1. Thus Im ρ_{10} (and hence P_Δ) arises from the interference between unnatural parity amplitudes (ie. π and B exchange). If the π and B were EXD all unnatural parity amplitudes would be real and Im ρ_{10} (and P_Δ) would vanish. In an absorption picture[25] Im ρ_{10} and P_Δ arise from the interference between a predominantly real structureless (π - B) Regge flip amplitude and the Regge cuts (π_c, B_c, ρ_c, A_2^c) contributing to the evasive non-flip amplitude.

Unfortunatley Im ρ_{10} cannot be measured directly, but one can estimate it from amplitude analyses. As discussed in Sec. IV C, by the use of SU(3)

one can relate the amplitudes for $K^+n \to K^{*o}p$ to the amplitudes for $\pi^-p \to \omega^o n$ and $\pi^-p \to \rho^o n$ as follows [See Eq. (4.6a) and (4.6b)].

$$U_i(K^{*o}) = \left[U_i(\omega^o) + U_i(\rho^o)\right] / \sqrt{2} \quad , \tag{5.5}$$

where i corresponds to any of the amplitudes in Table 1 and $U(\omega^o)$ [$U(\rho^o)$] receives contributions from B exchange [π-exchange]. From (5.4) and (5.5) one has

$$\text{Im } \rho_{10}^{K^{*o}} = \text{Im}\left[U^1_{++}(\omega^o)\ U^o_{++}(\rho^o)^* + U^1_{++}(\rho^o)\ U^o_{++}(\omega^o)^*\right] \quad , \tag{5.6}$$

where for simplicity we have neglected A_1 exchange amplitudes. Using amplitude analyses of the reactions $\pi^-p \to \omega^o n$ and $\pi^-p \to \rho^o n$ including ρ-ω interference data (which determines relative ρ^o and ω^o amplitude phases)[35] we have estimated $\text{Im } \rho_{10}^{K^*}$ from (5.6) and compared it with the experimental values of Δ^{++} polarization in Fig. 25. The agreement is quite satisfactory.

It has been suggested[36] that the mechanism responsible for Δ^{++} should be the same as that producing the observed non-zero (negative) polarization in np charge exchange scattering. Given that the quark model is approximately satisfied this connection is somewhat subtle. Table 1 shows important differences between the amplitudes for the two reactions. The differences are as follows:

(i) For np CHEX there are additional natural parity amplitudes (N^o_{++}, N^1_{++}) coupling to m = 0 states, whereas for $pp \to n\Delta^{++}$ only unnatural parity amplitudes (U^o_{++}, U^o_{+-}) couple to these states.

(ii) For np CHEX there are only two unnatural parity amplitudes (U^1_{-+}, U^o_{++}), whereas $pp \to n\Delta^{++}$ has four unnatural parity amplitudes (U^1_{++}, U^1_{-+}, U^o_{-+}, U^o_{++}).

The polarization in np CHEX is given by

$$P_{CHEX}(s,t) = \text{Im}\ \left[(N^o_{++} - N^1_{-+})\ N^{1\,*}_{++}\right] / \Sigma \tag{5.7}$$

and thus arises from the interference between two natural parity amplitudes (ie. ρ and A_2 exchange). If the ρ and A_2 were EXD all natural parity amplitudes would be real and P_{CHEX} would vanish. In an absorption picture P_{CHEX} arises from the interference between a predominantly real structureless $(A_2 - \rho)$ amplitude and the Regge cuts (π_c, B_c, ρ_c, A_2^c) contributing to the evasive non-flip amplitude.[37]

The mechanisms responsible for the polarizations in $p_\uparrow p \to n\Delta^{++}$ and pn CHEX are similar since each arises from the interference between a predominantly real structureless Regge flip amplitude and the Regge cuts contributing to the evasive non-flip amplitude. For $p_\uparrow p \to n\Delta^{++}$ [pn CHEX] the predominantly real Regge flip amplitude receives contributions from the approximately EXD π-B [ρ-A_2] exchange. Fig. 26 shows that the $p_\uparrow p \to n\Delta^{++}$ pn CHEX polarizations do resemble one another. Both are negative and structureless, however P_{CHEX} is somewhat larger in magnitude.

VI. Summary and Conclusions.

A. $K^- p \to (\rho,\omega,\phi)\Lambda$, $\pi^- p \to K^{*o}\Lambda$ (6 complex amplitudes).

By observing the joint correlations between the vector-meson and the Λ-hyperon in addition to the single density matrix elements, Λ polarization, and $d\sigma/dt$, one can determine 10 out of the 12 parameters necessary to completely specify the amplitudes at each s and t value. The existing data indicate that

1. The quark model [or SU(3)] predictions of equality of the amplitudes for $K^- p \to \phi\Lambda$ and $\pi^- p \to K^{*o}\Lambda$ works remarkably well (Fig. 5).
2. Using SU(3) one can sucessfully relate the amplitudes for $K^- p \to \phi\Lambda$ and $K^- p \to \omega\Lambda$.[3,10,20]
3. The amplitudes with quantum numbers of the K^{**} and K^* exchange do <u>not</u> exhibit EXD and the systematics of this EXD breaking is similar to that found in $K^- n \to \pi^-\Lambda$ and $\pi^- p \to K^o\Lambda$.[3]

4. The amplitudes with the quantum numbers of the K_A are not zero at 4.2 GeV/c. Whether this is due to an actual K_A pole or Regge-Regge cuts or 1/s effects remains to be seen. In any case, these reactions provide an excellent place to study the properties of unnatural parity exchange (K, K_A, K_B).

Because of lack of knowlege of the relative transversity phase ϕ_R, we know little as to the nature of the s-channel helicity amplitudes for these processes (Fig. 10). Determination of this phase requires A or R type measurements with a polarized target. With such measurements one will be able to do a complete amplitude analysis of these reactions and determine the s-channel helicity amplitudes up to an overall phase ϕ_o. Amplitude analyses at BNL or ANL energies together with energy dependences deduced from comparisons with Fermilab experiments will provide maximal information from which viable theoretical descriptions should arise.

Some experimenters have asked me to use current theoretical models to predict the behavior of the s-channel helicity amplitudes for these processes so that these predictions could be compared with future experimental results. In my opinion we are not at a stage in our theoretical understanding of high energy production mechanisms where it makes sense to do this. This can be done in quantum electrodynamics, but for strong interaction physics the models cannot sucessfully describe all the features of existing data. A new experiment is not needed to rule out existing models! The proper question for an experimenter to ask is, "How much can we learn about the nature of the production mechanism (ie. s-channel helicity amplitudes) from my experiment?" Because of the self-analysing property of the Λ-hyperon these reactions are particularly suited for amplitude analyses type experiments and these amplitudes contain all the information about a given process.

B. $K^-p \to (\pi,\omega,\eta)\Sigma^0$, $\pi^-p \to K^{*0}\Sigma^0$ (6 complex amplitudes)

Present data on these processes indicate the following:

1. These reactions are dominantly natural parity (K^{**}, K^*) exchange. This is because the K meson couples only weakly to $\bar{p}p$ (ie. $g^2_{KNN} \ll g^2_{KN\Sigma}$).

2. The K^{**} and K^* exchange amplitudes exhibit large SMD breaking. In fact the polarization for these processes is almost maximal (Fig. 12).

3. These reactions can be successfully related to $K^-p \to (\pi,\omega,\eta)\Lambda$, $\pi^-p \to K^{*0}\Lambda$ via SU(3) (and known F/D ratio).[30]

In terms of transversity amplitudes $\pi^-p \to K^{*0}\Sigma^0$ ($K^-p \to \rho^0\Sigma^0$) is given essentially by just one amplitude $T^0_{++}(s,t)$ ($T^0_{--}(s,t)$) (Fig. 11). The remaining transversity amplitudes are roughly zero. This means that no new information is gained by making polarized target or A and R type measurements for these processes. New and more accurate data on the differential cross sections, density matrix elements, Σ^0-polarization, and correlations is badly needed, however. The quark model predicts that the amplitudes for these processes are related according to $A(K^-p \to \rho^0\Sigma^0) = A(K^-p \to \omega\Sigma^0)$ and $A(K^-p \to \phi\Sigma^0) = A(\pi^-p \to K^{*0}\Sigma^0)$.

C. $K^-p \to \pi^-Y^{*+}(1385)$ (4 complex amplitudes)

By observing the two-step decay of the $Y^{*+}(1385)$ together with $d\sigma/dt$ one can determine 6 out of 8 parameters necessary to completely specify the amplitudes at each s and t. The data indicate that

1. The quark model gives a good description of the transversity amplitudes although the predictions do not hold exactly (Fig. 13).

2. The quark model prediction of zero for the polarized target asymmetry also appears to be satisfied (Fig. 15).

Better statistics for this process and its line reversed partner $\pi^-p \to K^0Y^{*+}(1385)$ are needed.

D. $\pi^- p \to \pi^0 n$ (6 complex amplitudes)

Much has been learned about this process from high statistics experiments at 6.0 and 17.2 GeV/c. However, we still know little as to the importance of A_1 exchange and the lack of shrinkage of π exchange is a bit disturbing (Fig 17). Polarized target experiments can tell us the importance of A_1 exchange.

E. $\pi^- p \to \omega^0 n$ (6 complex amplitudes)

Of all vector-meson production reactions data on $\pi^- p \to \omega^0 n$ and $\pi^+ n \to \omega^0 p$ is the poorest. New data is badly needed here. Present data does indicate that perhaps B exchange alone is not sufficient to explain the small $|t|$ behavior of the unnatural parity projection $\rho^H_{00}\, d\sigma/dt$ (Fig. 20). It has been suggested that $Z(J^{PG} = 2^-1^+)$ exchange may be important. Polarized target experiments can tell us the importance of possible Z exchange contributions.

F. $K^- p \to \bar{K}^{*o} n$, $K^+ n \to K^{*o} p$ (6 complex amplitudes)

SU(3) works beautifully in relating ω^0 and ρ^0 production to $\bar{K}^{*o}$ and K^{*o} production (Fig. 21). In particular the line reversal breaking seen in $\bar{K}^{*o}$ and K^{*o} production can be successfully related to the ρ-ω mixing phase determined from studies of the $\pi\pi$ spectra in $\pi N \to \pi\pi N$ scattering (Fig. 22).

G. $p p \to n\Delta^{++}$ (16 complex amplitudes)

The successes that the naive quark model enjoyed in Sec. II [predicting equality of $K^- p \to \phi\Lambda$ and $\pi^- p \to K^{*o}\Lambda$] and Sec. III [predicting spin structure for $K^- p \to \pi^- Y^*(1385)$] are difficult to interpret since the same predictions can be arrived at using SU(3) on the various exchanged Regge poles plus M_1 dominance of the ρ (and A_2) couplings. One cannot decide whether to attribute successes to the quark model or to Regge exchange plus SU(3). However, the quark model, unlike SU(3), predicts relationships between meson-baryon and baryon-baryon scattering. We have seen the recent data on $pp \to n\Delta^{++}$ and $K^+ n \to K^{*o} p$ are in excellent agreement with quark model predictions (Fig. 23-24). This is particularly impressive since only with a quark type model can one relate baryon-baryon scattering to meson-baryon scattering. In addition, the sign and magnitude

of Im ρ_{10} for K^{*o} production arrived at via SU(3) from the amplitudes for ρ^o and ω^o production is found to explain quite nicely (as predicted by the quark model) the observed non-zero Δ^{++} polarization (Fig. 25).

Acknowledgements

I gratefully acknowledge useful discussions with R. Diebold, R.L. Eisner, G.C. Fox, S. Kramer, and A.B. Wicklund.

References

1. Geoffrey Fox, "Past Lessons and Future Dreams from Polarization Data in High-Energy Physics," invited talk presented at the Second International Conference on Polarization and Polarized Targets, Berkeley, 1971.
2. R.J.N. Phillips and R.P. Worden, "Polarization in Strong Interactions at High Energies," proceeding of a meeting held at Rutherford Laboratory 17th and 18th March, 1973 (RL-73-088).
3. R.D. Field, "Amplitude Analyses of Hypercharge Exchange Reactions," invited talk presented at the 1973 Tallahassee Conference, AIP Proceedings No. 13, Particles and Fields subseries No. 5.
4. F. Halzen and C. Michael, Phys. Letters 36B, 367 (1971); R. Kelley, Phys. Letters 39B, 635 (1972).
5. A.V. Barnes, D.J. Mellema, A.V. Tollestrup, R.L. Walker, O.L. Dahl, R.A. Johnson, R.W. Kenney, M. Pripstein, papers #1045 and #1046 submitted to the XVII International Conference on High Energy Physics, London, 1974.
6. See, for example, V. Barger and R.J.N. Phillips, "Compatibility of Old and New πN Charge-Exchange Results," University of Wisconsin preprint (1974); R.D. Field, "Some Aspects of Two-body Phenemenology," invited talk presented at the XVII International Conference on High Energy Physics, London, 1974.
7. Proceedings of the Workshop of Physics with Polarized Targets, Brookhaven National Laboratory, June 3-8, 1974.
8. See also, Ref. 3 and A.D. Martin, Proceedings of the Seventh Rencontre de Moriond (1972) ed. J. Tran Thanh Van.
9. N. Byers and C.N. Yang, Phys. Rev. 135, B796 (1964).
10. R.D. Field, R.L. Eisner, S.U. Chung, and H. Aguilar-Benitez, Phys. Rev. D7, 2036 (1973).

11. R.D. Field, S.U. Chung, R. L. Eisner, A. Rouge, H. Videau, M. Aguilar-Benitez, F. Barreiro, J. Rubio, J.P. de Brion, L. Moscoso, presented at the 2nd Aix En Provence Conference (1973).

12. A. Bialas and K. Zalewski, Nucl. Phys. B6, 449 (1968); B6, 465 (1965); B6, 478 (1968).

13. D. Crennell, H. Gordon, K.-W. Lai, and J.M. Scarr, Phys. Rev. D6, 1220 (1972).

14. M. Abramovich, A.C. Irving, A.D. Martin, and C. Michael, Phys. Letters 39B, 353 (1972).

15. The quantity σ_h in Eq. (2.6a) is defined by $\sigma_h = \sum_{\lambda_v \lambda_B \lambda_{B'}} \left| H^{\lambda_v}_{\lambda_{B'} \lambda_B}(s,t) \right|^2$.

16. The natural (P_N) and unnatural (P_U) parity polarizations are related to the transversity amplitudes by $P_N = |T^0_{++}|^2 - |T^0_{--}|^2$, $P_U = |T^1_{+-}|^2 + |T^{-1}_{+-}|^2 - |T^1_{-+}|^2 - |T^{-1}_{-+}|^2$.

17. This is predicted by SU(3). See Ref. 3 and Ref. 20.

18. The relationship between the experimental A and R parameters and $\hat{A}$ and $\hat{R}$ is $R = \hat{R}\sin\omega - \hat{A}\cos\omega$, $A = \hat{R}\cos\omega + \hat{A}\sin\omega$, where ω is the scattering angle of the target in the (helicity) rest frame of the recoil particle. See Ref. 1.

19. In Fig. 10. the unknown overall phase ϕ_o is fixed by setting T^0_{++} to be real and positive.

20. R.D. Field, R.L. Eisner, and M. Aguilar-Benitez, Phys. Rev. D6, 1863 (1972).

21. D. Yaffe, M. Abramovich, V. Chaloupka, A. Ferrando, M. Korkea-Aho, M.J. Losty, L. Montanet, E. Paul, J. Zatz, and Z. Zieminski, Nucl. Physics B75, 365 (1974).

22. M. Aguilar-Benitez, S.U. Chung, R.L. Eisner, and R.D. Field, Phys. Rev. Letters 29, 749 (1972).

23. D.S. Ayers, R. Diebold, A.F. Greene, S.L. Kramer, A.J. Pawlicki, and A.B. Wicklund, invited paper presented by R. Diebold at the International Conference on π-π Scattering and Associated Topics, Florida State University, March 28-30, 1973.

24. The CERN-Munich 17.2 GeV/c $\pi^- p \to \rho^0 n$ data was arrived at by calculating the observables from the amplitude analysis of P. Estabrooks and A.D. Martin TH 1668-CERN preprint, May 4, 1973.

25. R.D. Field and Deepinder P. Sidhu, Phys. Rev. D10, 89 (1974).

26. The so-called Z meson with quantum numbers $J^P I^G = 2^- 1^+$ should not be confused with the possible exotic K^+-p baryon resonance called Z^*.

27. A.C. Irving and C. Michael, "High Energy Production and Decay of Vector and Tensor Mesons," CERN preprint TH 1825 (1974).

28. See, for example, R.D. Field, "Predicting K^{*0} and $\bar{K}^{*0}$ Production from ρ^0 and ω^0 Production," invited talk presented at the 1973 meeting of the Division of Particles and Fields of the APS, Berkeley, California, 1973.

29. R. Diebold, S. Kramer, and A.B. Wicklund, (private communication).

30. This section was done in collaboration with A.B. Wicklund, D.S. Ayers, R. Diebold, J. Jost, S.L. Kramer, and A.J. Pawlicki at Argonne.

31. A.B. Wicklund, D.S. Ayers, R. Diebold, J. Jost, S.L. Kramer, and A.J. Pawlicki, "Inelastic Polarized Proton Interactions at 6.0 GeV/c," submitted to the XVII International Conference on High Energy Physics, London, 1974.

32. The s-wave observables can be uniquely separated from the P-wave observables.

33. For a general discussion of the effects of the $J = 1/2$ P-wave background under the $J = 3/2$ P-wave Δ^{++}, see Ref. 31.

34. The J = 1/2 P-wave is predominantly real, whereas the J = 3/2 P-wave is predominantly imaginary.

35. R. Diebold, invited talk presented at the 2nd International Conference on Elementary Particles, Aix En Provence, 1973.

36. G.L. Kane and U.P. Sukhatme, "Interpreting Data from Polarized Beams," University of Michigan preprint HE 73-30,

37. See, for example, G.L. Kane, "Phenomenology of High Energy Processes," invited talk presented at the 1973 meeting of the Division of Particles and Fields of the APS, Berkeley, 1973.

38. S.L. Kramer, D.S. Ayres, R. Diebold, A.F. Greene, A. J. Pawlicki, A.B. Wicklund, "Interference between ρ and ω Production in $\pi^+ N \to \pi^+\pi^- N$ at 3.4, and 6 GeV/c," submitted to the XVII International Conference on High Energy Physics, London, 1974.

39. A.B. Wicklund, D.S. Ayres, R. Diebold, A.F. Greene, S.L. Kramer, A.J. Pawlicki, "$K^*(890)$ Production from 3 to 6 GeV/c," submitted to the XVII International Conference on High Energy Physics, London, 1974.

40. M.A. Abolins, M.T. Lin, R.C. Ruchti, J.G. Horowitz, R.C. Kammerud, N.W. Reay, K. Reibel, N.R. Stanton, K.W. Edwards, D.G. Crabb, and J.R. O'Fallon, Phys. Rev. Letters 30, 1183 (1973).

Table 1: The t-channel helicity amplitudes $f_{\lambda_c-\lambda_a;\lambda_d\lambda_{\bar{b}}}(s,t)$ for the process $a + b \to c + d$, where the quark model relations for $pp \to n\Delta^{++}$ have been used. The amplitudes $N^m_{\lambda_c-\lambda_a}(s,t)$ [$U^m_{\lambda_c-\lambda_a}(s,t)$] correspond to defin te natural [unnatural] parity in the t-channel, where m is the net helicity flip at the $d\bar{b}$ vertex ($m = |\lambda_d - \lambda_{\bar{b}}|$).

m	$nK^+ \to pK^{*o}$	$pp \to n\Delta^{++}$	$pn \to np$
1	$f_{++;1}=N^1_{++}+U^1_{++}$	$f_{++;3/2\ 1/2}=\sqrt{3}f_{++;1/2-1/2}=N^1_{++}+U^1_{++}$	$f_{++;1/2-1/2}=N^1_{++}$
1	$f_{--;1}=N^1_{++}-U^1_{++}$	$f_{--;3/2\ 1/2}=\sqrt{3}f_{--;1/2-1/2}=N^1_{++}-U^1_{++}$	$f_{--;1/2-1/2}=N^1_{++}$
1	$f_{-+;1}=N^1_{-+}+U^1_{-+}$	$f_{-+;3/2\ 1/2}=\sqrt{3}f_{-+;1/2-1/2}=N^1_{-+}+U^1_{-+}$	$f_{-+;1/2-1/2}=N^1_{-+}+U^1_{-+}$
1	$f_{+-;1}=-N^1_{-+}+U^1_{-+}$	$f_{+-;3/2\ 1/2}=\sqrt{3}f_{+-;1/2-1/2}=-N^1_{-+}+U^1_{-+}$	$f_{+-;1/2-1/2}=-N^1_{-+}+U^1_{-+}$
0	$f_{++;0}=U^0_{++}$	$f_{++;1/2\ 1/2}=f_{++;-1/2-1/2}=U^0_{++}$	$f_{++;1/2\ 1/2}=N^0_{++}+U^0_{++}$
0	$f_{-+;o}=U^0_{-+}$	$f_{-+;1/2\ 1/2}=f_{-+;-1/2-1/2}=U^0_{-+}$	$f_{-+;1/2\ 1/2}=-N^1_{++}$
0	-	-	$f_{--;1/2\ 1/2}=-N^0_{++}-U^0_{++}$
2		$f_{++;3/2-1/2}=0$	
2		$f_{--;3/2-1/2}=0$	
2		$f_{+-;3/2-1/2}=0$	
2		$f_{-+;3/2-1/2}=0$	

Table 2: Quark model prediction for the connection between $pp \to n\Delta^{++}$ and $K^+n \to K^{*o}p$.

	$K^+n \to K^{*o}p$	$pp \to n\Delta^{++}$	Regge Exchanges
t-channel amplitudes (see Table 1)			
(1)	N_{++}	$= (1/\sqrt{8})\ N^1_{++}$	ρ, A_2
(2)	U^1_{++}	$= (1/\sqrt{8})\ U^1_{++}$	π, B
(3)	N^1_{-+}	$= (1/\sqrt{6})\ N^1_{-+}$	ρ, A_2
(4)	U^1_{-+}	$= (1/\sqrt{8})\ U^1_{-+}$	A_1
(5)	U^o_{++}	$= (\sqrt{3}/4)\ U^o_{++}$	π, B
(6)	U^o_{-+}	$= (\sqrt{3}/4)\ U^o_{-+}$	A_1
observables (Jackson frame)			
(1)	$d\sigma/dt$	$= (3/8)\ d\sigma/dt$	
(2)	$\rho_{11} + \rho_{1-1}$	$= 4/3\rho_{33} + 4/\sqrt{3}\ \mathrm{Re}\ \rho_{3-1}$	
(3)	$\rho_{11} - \rho_{-1-}$	$= 4/3\rho_{33} - 4/\sqrt{3}\ \mathrm{Re}\ \rho_{3-1}$	
(4)	ρ_{oo}	$= 2\rho_{11} - 2/3\ \rho_{33}$	
(5)	$\mathrm{Re}\ \rho_{10}$	$= 4/\sqrt{6}\ \mathrm{Re}\ \rho_{31}$	
(6)	$-\sqrt{2}\ \mathrm{Im}\ \rho_{10}$	$= 2\ A_{11}$	
(7)		$2A_{33} = 0$	
(8)		$4A_{31} = 0$	
(9)		$4A_{3-1} = -\sqrt{3}\ (2A_{11})$	
(10)		$4\ I^X_{31} = 0$	
(11)		$4\ I^Z_{31} = \sqrt{3}\ (2A_{11})$	
(12)		$4\ I^X_{3-1} = -\sqrt{3}\ (2A_{11})$	
(13)		$4\ I^Z_{3-1} = 0$	

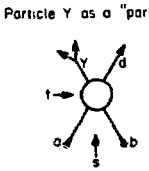

Figure 1. (a) "Particle" Y produced peripherally as a resonance.

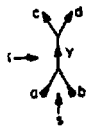

Figure 1. (b) "Particle" Y produced as a direct channel resonance.

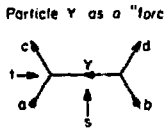

Figure 1. (c) Particle Y as an exchange "force".

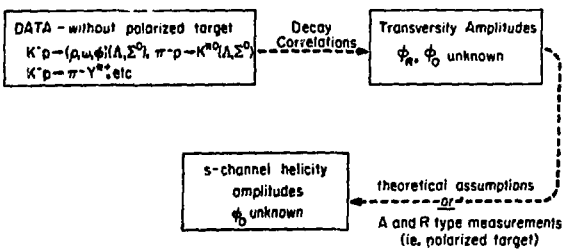

Figure 2. Self explanatory.

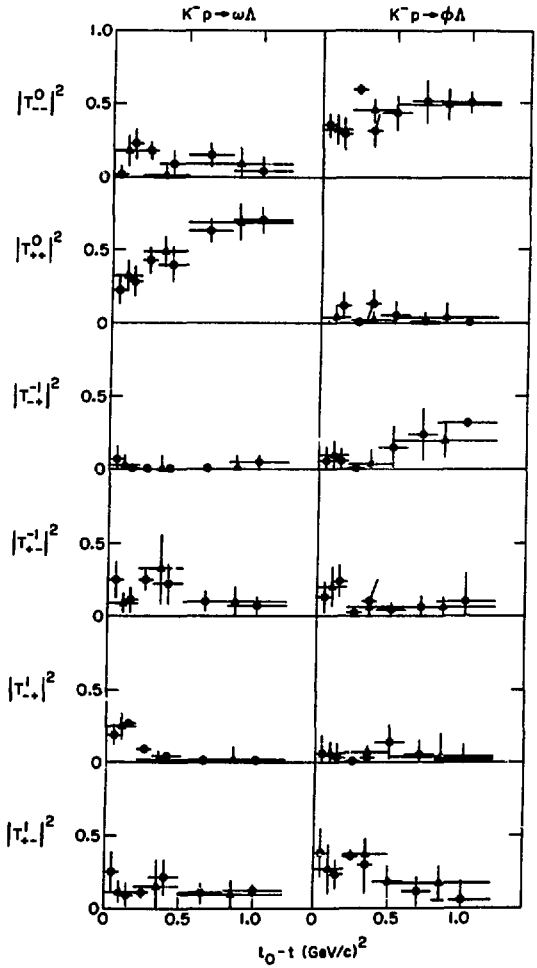

Figure 3. Magnitudes of the transversity amplitudes for the reactions $K^-p \to (\omega,\phi)\Lambda$. The triangles are the combined 3.9 and 4.6 GeV/c BNL data (Ref. 10) and the circles are combined BNL and Ecole Polytechnique data (Ref. 11).

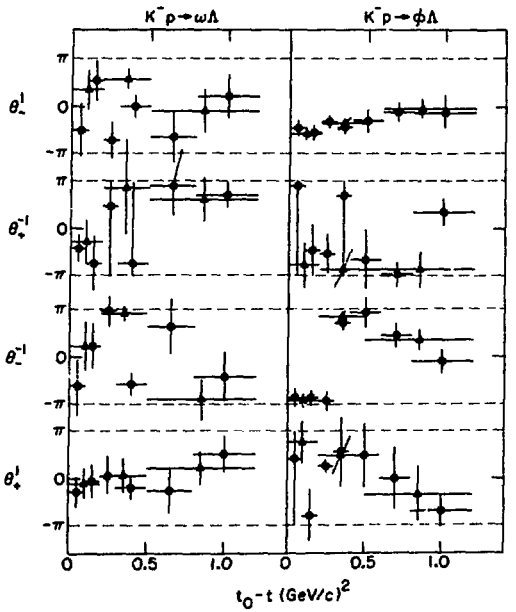

Figure 4. Relative phases of the transversity amplitudes, where

$$\theta^{+-1}_{\pm} = \mathrm{Arg}(T^{+-1}_{\pm\mp}) - \mathrm{Arg}(T^{00}_{\pm\pm}).$$

The data are the same as Figure 3.

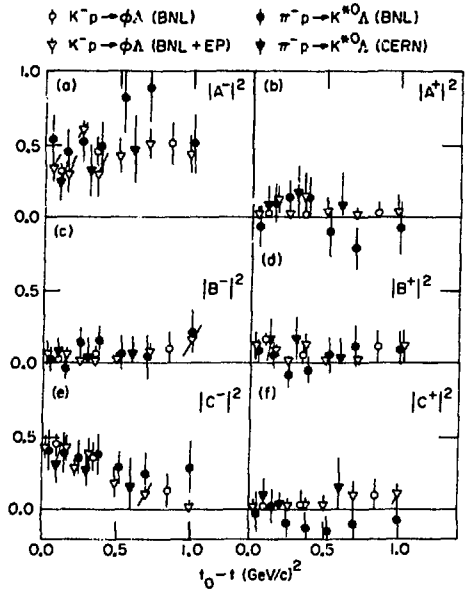

Figure 5. Comparison of the amplitudes for $K^-p \to \phi\Lambda$ using the BNL data (Ref. 10, open circles) and the BNL + EP data (Ref. 11, open triangles) with the amplitudes for $\pi^-p \to K^{*0}\Lambda$ at 3.9 GeV/c (Ref. 14, solid triangles) and at 4.5 GeV/c (Ref. 13, solid circles). The quark model predicts equality of the amplitudes for these two reactions.

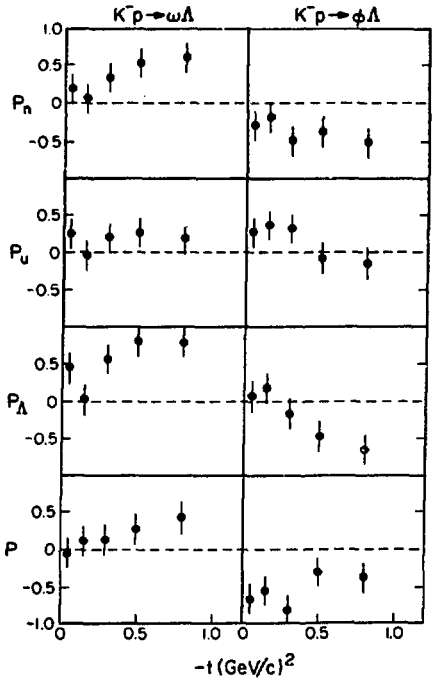

Figure 6. The natural parity polarization P_N; unnatural parity polarization P_U; Λ polarization P_Λ; and polarized target asymmetry P for $K^-p \to (\omega,\phi)\Lambda$ at 4.2 GeV/c predicted from the transversity amplitudes shown in Figure 3.

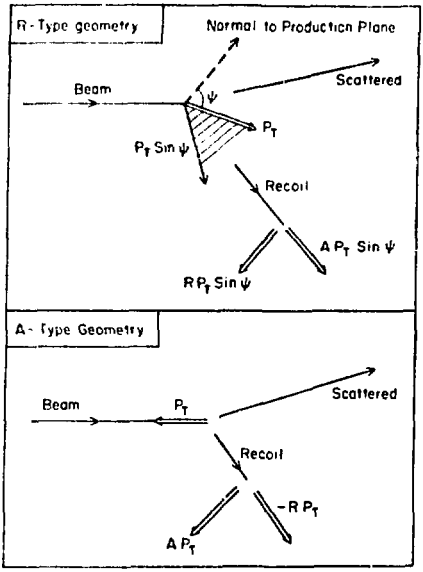

Figure 7. The geometry for R and A measurements in two body scattering. The quantities R and A are just the final components of the baryon polarization off a polarized target. Note that both configurations demand a sizeable component of target polarization in the production plane. (Figure taken from G. Fox Ref. 1).

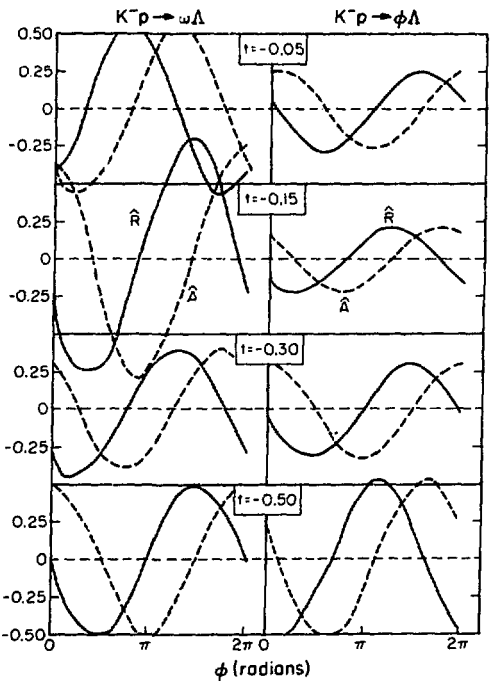

Figure 8. The $\hat{A}$ (Eq. 2.9c) and $\hat{R}$ (Eq. 2.9b) parameters plotted versus the relative transversity phase $\phi = \mathrm{Arg}(T^0_{--}) - \mathrm{Arg}(T^0_{++})$ for $K^-p \to (\omega,\phi)\Lambda$ at 4.2 GeV/c predicted from the transversity amplitudes shown in Figure 3.

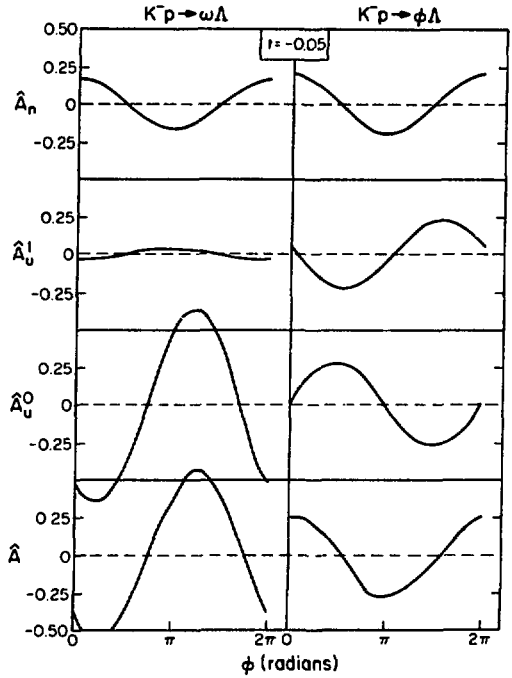

Figure 9. The natural (A_N) and unnatural (A_U^1, A_U^0) parity components of the A parameter (Eq. 3.9c), where

$$\hat{A} = \hat{A}_N + \hat{A}_U^1 + \hat{A}_U^0 ,$$

plotted versus the relative transversity phase $\phi = \mathrm{Arg}(T^0_{--}) - \mathrm{Arg}(T^0_{++})$ for $K^-p \to (\omega,\phi)\Lambda$ at 4.2 GeV/c predicted from the transversity amplitudes shown in Figure 3.

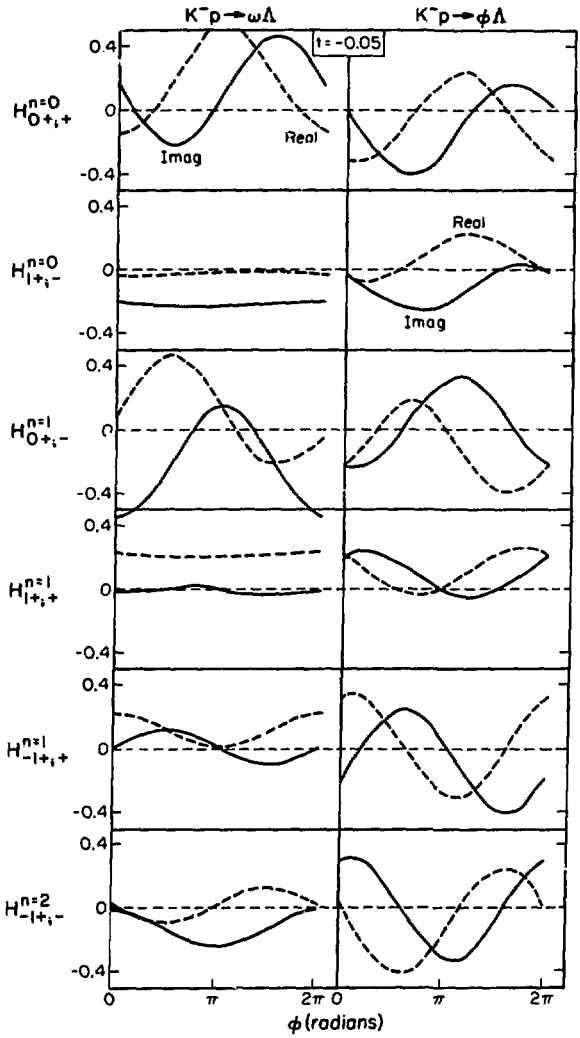

Figure 10. The s-channel helicity amplitudes at $t = -0.05$ $(GeV/c)^2$ for $K^-p \to (\omega,\phi)\Lambda$ at 4.2 GeV/c plotted versus the relative transversity phase $\phi = Arg(T^o_{--}) - Arg(T^o_{++})$ and predicted from the transversity amplitudes shown in Figure 3 and Figure 4. These amplitudes can of course be multiplied by the arbitrary phase factor $e^{in\phi_o}$. In this figure ϕ_o is fixed by setting T^o_{++} to be real and positive.

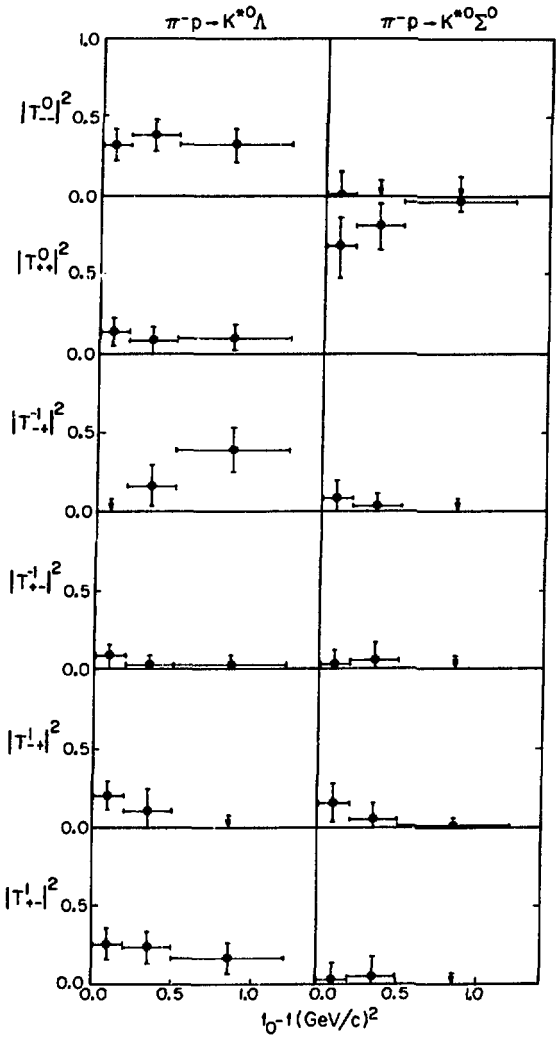

Figure 11. Magnitudes of the transversity amplitudes for $\pi^- p \to K^*(\Lambda,\Sigma^0)$ at 3.9 GeV/c from Ref. 21.

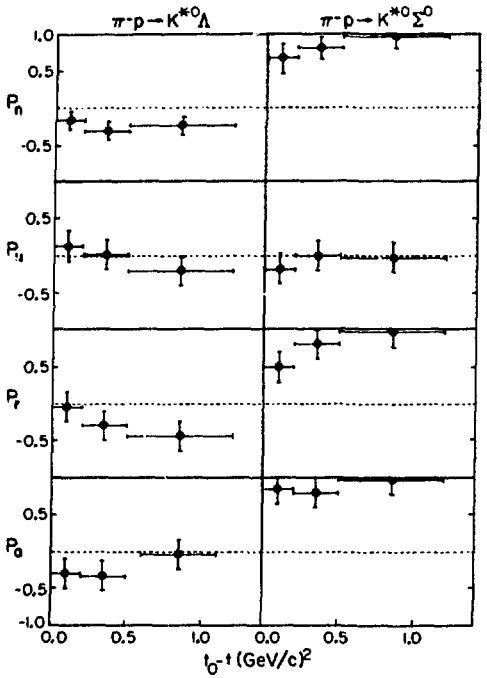

Figure 12. The natural parity polarization P_N; unnatural parity polarization P_U; recoil Λ polarization P_r; and polarized target asymmetry P_a for $\pi^- p \to K^{*0}(\Lambda,\Sigma^0)$ at 3.9 GeV/c determined from the transversity amplitudes of Figure 11.

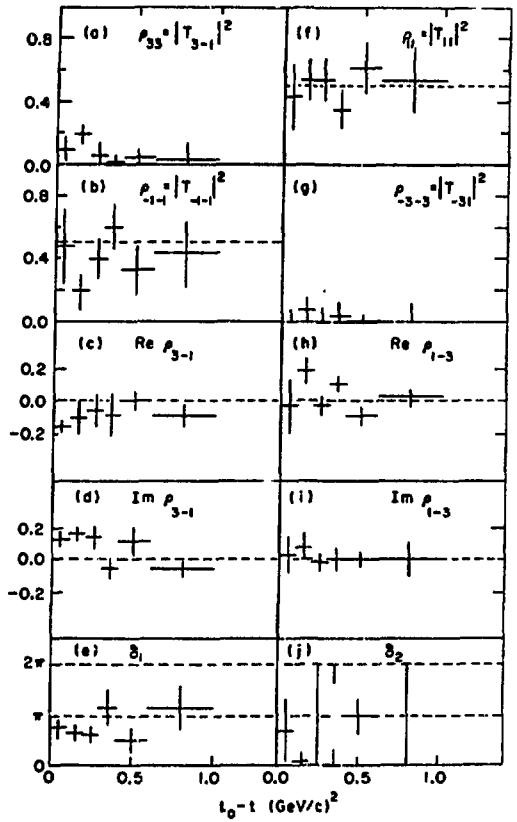

Figure 13. Transversity amplitudes and transversity density matrix elements for the reaction $K^-p \to \pi^-Y^{*+}(1385)$ from Ref. 22, where $\delta_1(\delta_2)$ is the relative phase between T_{3-1} and $T_{-1-1}(T_{11}$ and $T_{-31})$. The quark model predicts $T_{3-1} = T_{-31} = 0$ and $T_{11} = T_{-1-1} = 1/2$.

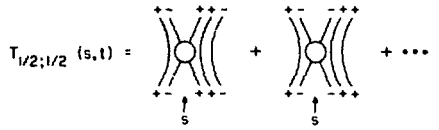

Figure 14. (a) Illustrates how T_{11} can be represented as a sum of quark-quark scattering amplitudes. The ± signs represent quark spin projections on the transversity z-axis (normal to production plane).

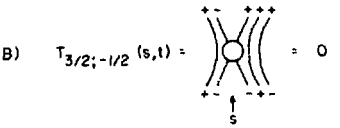

Figure 14. (b) Illustrates how T_{3-1} requires that more than one of the baryon quarks flip sign. The quark model thus predicts that this amplitude vanish.

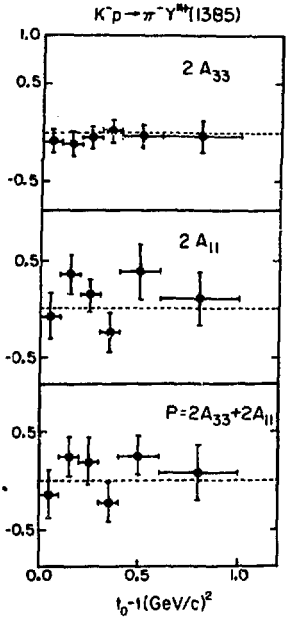

Figure 15. The polarized target asymmetries $2A_{33} = 2(\rho^{\uparrow}_{33} - \rho^{\downarrow}_{33})$, $2A_{11} = 2(\rho^{\uparrow}_{11} - \rho^{\downarrow}_{11})$, and the Y* polarization $P = 2A_{33} + 2A_{11}$ for the reaction $K^-p \to \pi^- Y^{*+}(1385)$ at 4.2 GeV/c determined from the transversity amplitudes of Figure 13.

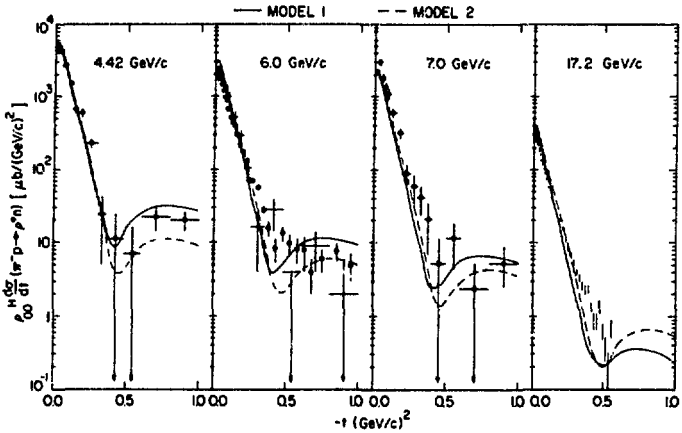

Figure 16. Comparison of several absorption model predictions with data for $\rho^H_{00} d\sigma/dt(\pi^- p \to \rho^0 n)$. (Figure taken from Ref. 25).

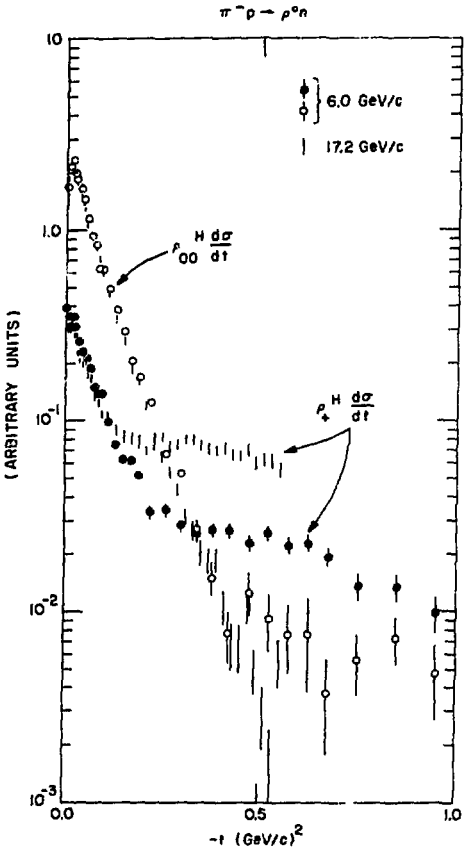

Figure 17. Comparison of the 6.0 (Ref. 23) and 17.2 GeV/c (Ref. 24) $\pi^- p \to \rho^0 n$ data. The data are normalized so that $\rho_{00}^H d\sigma/dt$ is equal in the forward direction at these two energies. The figure shows the lack of shrinkage of the unnatural parity projection $\rho_{00}^H d\sigma/dt$ and the relative increase of the natural parity projection $\rho_+^H d\sigma/dt$, where $\rho_+ = \rho_{11} + \rho_{1-1}$.

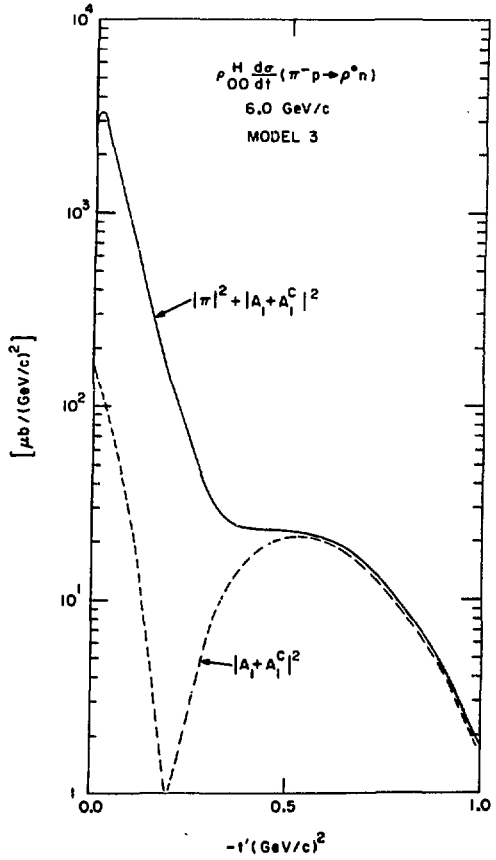

Figure 18. Contributions to $\rho_{00}^{H}d\sigma/dt(\pi^-p \to \rho^0n)$ at 6.0 GeV/c from a model that includes A_1 exchange. (Figure taken from Ref. 25).

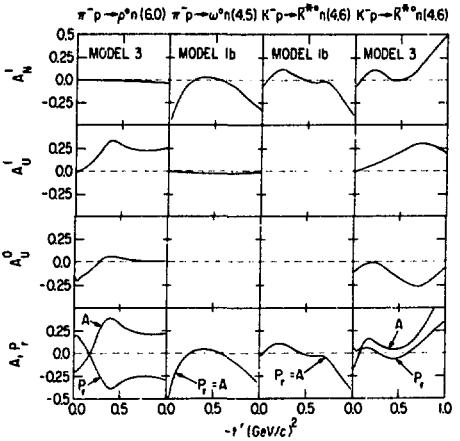

Figure 19. Predicted polarized target asymmetries A_N^1, A_U^1, A_U^0 (Eq. 4.2), where the total polarized target asymmetry is given by

$$A = A_N^1 + A_U^1 + A_U^0$$

and the recoil polarization is given by

$$P_r = A_N^1 - A_U^1 - A_U^0 .$$

Model 3 (1b) includes (excludes) A_1 exchange. No A_1 exchange contribution implies

$$A_U^1 = A_U^0 = 0$$

and $P_r = A$. (Figure taken from Ref. 25).

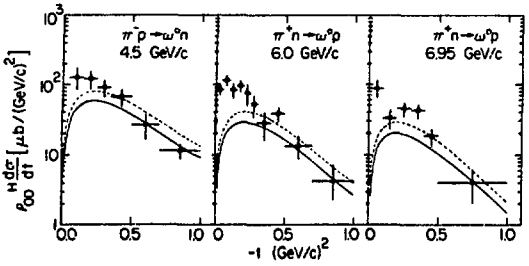

Figure 20. Comparison of various absorption models (solid and dashed curves) with data on $\rho_{00}^H d\sigma/dt$ for $\pi^-p \to \omega^0 n$ and $\pi^+p \to \omega^0 p$. The dotted curve shows the effect on the dashed curve model of including ρ-ω mixing. (Figure taken from Ref. 25.)

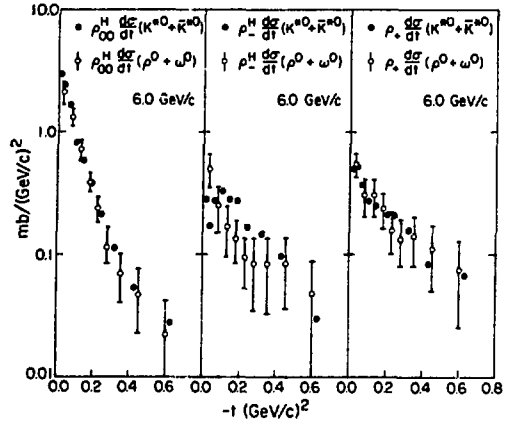

Figure 21. SU(3) comparison of data on $K^-p \to \bar{K}^{*0}n$, $K^+n \to K^{*0}p$, $\pi^-p \to \rho^0 n$, and $\pi^-p \to \omega^0 n$ at 6.0 GeV/c. SU(3) predicts the solid and open circles to be equal. The quantities $\rho_\pm^H$ are defined by

$$\rho_\pm^H = \rho_{11}^H \pm \rho_{1-1}^H.$$

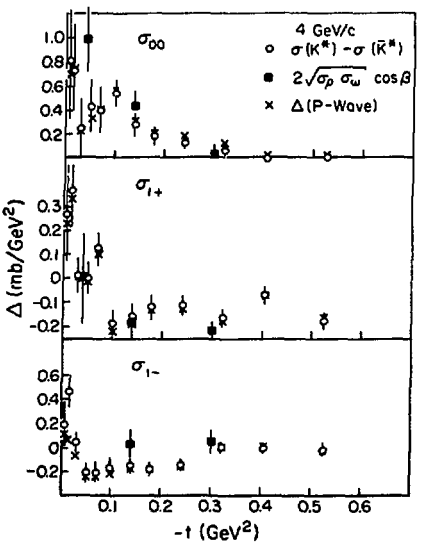

Figure 22. Compares the line-reversal differences $\Delta = \rho_{11}d\sigma/dt(K^+n \to K^{*o}p) - \rho_{11}d\sigma/dt(K^-p \to \bar{K}^{*o}n)$ [open circles] with the values predicted from SU(3) and the ρ-ω mixing phase β [solid squares]. The mixing phase is determined by observing the $\pi^+\pi^-$ mass spectra in $\pi^\pm N \to \pi^+\pi^- N$ scattering. The crosses are the same as the open circles but the s-wave under the K^{*o} and $\bar{K}^{*o}$ has been removed. (This figure is courtesy of S. Kramer and A.B. Wicklund and uses the Argonne data of Ref. 38.)

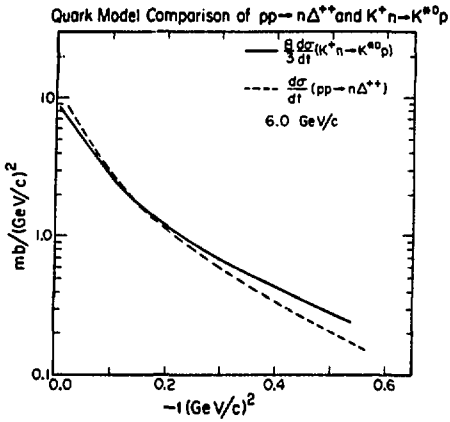

Figure 23. Quark model comparison of the differential cross sections for $pp \to n\Delta^{++}$ (Ref. 31) and $K^+n \to K^{*0}p$ (Ref. 39) at 6.0 GeV/c. The quark model predicts $(pp \to n\Delta^{++}) = 8/3(K^+n \to K^{*0}p)$.

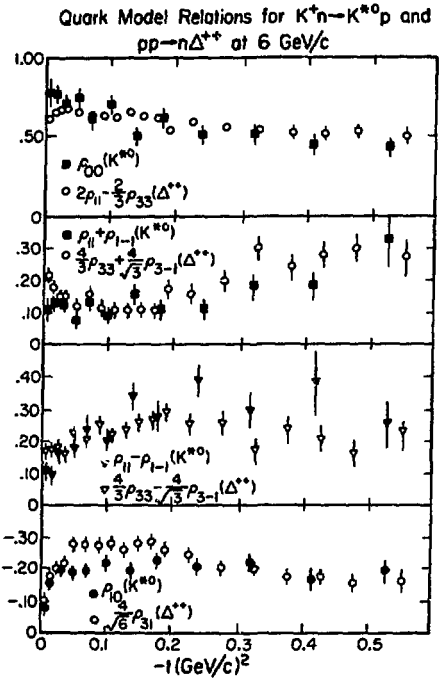

Figure 24. Quark model comparison of the K^{*0} vector-meson density matrix elements for $K^+n \to K^{*0}p$ and the Δ^{++} density matrix elements for $pp \to n\Delta^{++}$ at 6.0 GeV/c. The data is the same as in Figure 23.

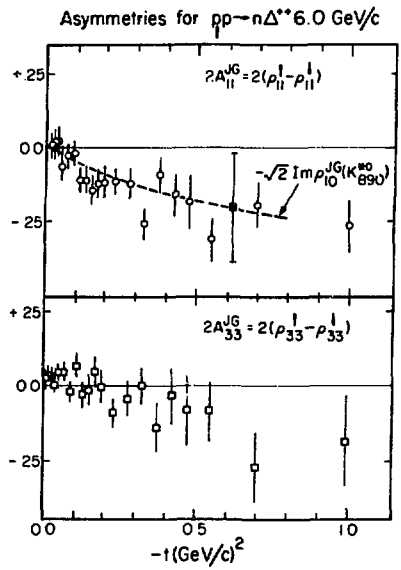

Figure 25. Polarized beam asymmetry observables (Jackson frame)

$$2A_{11} = 2(\rho^{\uparrow}_{11} - \rho^{\downarrow}_{11}),\ 2A_{33} = 2(\rho^{\uparrow}_{33} - \rho^{\downarrow}_{33})$$

for $p_{\uparrow}p \to n\Delta^{++}$ at 6.0 GeV/c (Ref. 31). The quark model predicts $2A_{33} = 0$ and $2A_{11} = -\sqrt{2}\ Im\ \rho_{10}(K^{*0})$, where $\rho_{ij}(K^{*0})$ is the vector-meson density matrix for $K^+n \to K^{*0}p$.

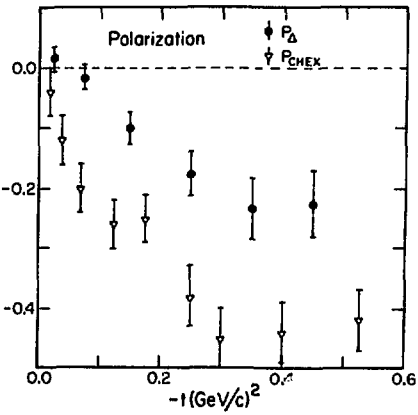

Figure 26. Comparison of the Δ^{++} polarization in $p_{\uparrow}p \to n\Delta^{++}$ ($P_{\Delta} = 2A_{33} + 2A_{11}$) at 6.0 GeV/c (Ref. 31) and the np CHEX polarization P_{CHEX} at 7.0 GeV/c (Ref. 40).

CALT-68-459
AEC RESEARCH AND
DEVELOPMENT REPORT
August 1, 1974

II. Polarization Effects in Inclusive Processes*†**

by

R. D. Field

California Institute of Technology, Pasadena, California 91109

ABSTRACT

This paper deals with the phenomenology of polarization and spin effects in inclusive processes. These effects are examined using the triple-Regge formalism valid at large s/M^2 and large M^2, however the connection between this region and the small M^2 region via finite-mass sum rules (FMSR) and M^2-duality is emphasized. The two distinct types of polarization effects [ie. type I = $(a_\uparrow \xrightarrow{b} c_\uparrow)$; type II = $(a \xrightarrow{b\uparrow} c)$] are discussed separately and in detail. Examples and predictions are given and existing data examined. Other observables in inclusive processes are also mentioned briefly.

*Work supported in part by the U.S. Atomic Energy Commission. Prepared under Contract AT(11-1)-68 for the San Francisco Operations Office, U.S. Atomic Energy Commission.

†Invited talk presented at the Workshop on Physics with Polarized Targets, Brookhaven National Laboratory, June 3-8, 1974.

**Submitted to the Summer Study on High Energy Physics with Polarized Beams, Argonne National Laboratory, July 22-26, 1974.

I. Introduction

This is the second part of a paper concerned with the phenomenology of polarization and/or spin measurements in multiparticle production processes. In part I polarization effects in exclusive multiparticle final state reactions like $K^- p_\uparrow \to \phi n$, $\pi^- p_\uparrow \to K^{*0}\Lambda$, $p_\uparrow p \to n\Delta^{++}$, etc. are discussed. This paper deals with the phenomenology of polarization and spin effects in inclusive reactions.

When A. Mueller[1] generalized the optical theorem from which one relates the total cross section in two-body scattering with the imaginary part of the forward elastic amplitude ($ab \to ab$) to one which relates the inclusive cross section ($ab \to cX$) to a particular discontinuity of the forward three-body amplitude ($ab\bar{c} \to ab\bar{c}$), he opened up the world of inclusive processes to Regge type analyses. Much of the knowledge gained from Regge type analyses of two-body scattering was immediately carried over into the inclusive domain with surprising success[2-4]. Just as in two-body scattering, however, the knowledge of just the unpolarized invariant inclusive cross section does not provide enough constraints to test all of our theoretical concepts. For example; the importance of triple-Regge interference terms[4,5] (i.e. terms of the form PRP and PRR); the EXD of triple-Regge couplings[4,6]; the importance of Regge cuts[7,8]; and the validity of factorization are questions that remain unanswered. In this paper we will examine how measurements of inclusive observables other than just the unpolarized invariant cross section shed light on these questions and more. We will concentrate on the large s/M^2, large M^2 region (triple-Regge region), but will indicate how predictions or observations made in this region can then be related to the small M^2 region via finite mass sum rules (FMSR) and M^2-duality.

In discussing the phenomenology of polarization in the inclusive process $a + b \to c + X$ it is necessary to distinguish between two distinct types of polarization effects. Type I are those polarization and/or spin correlation

effects resulting from particles a and c, where c is a fragment of a and which is written as $(a_\uparrow \xrightarrow{b} c_\uparrow)$. In the triple-Regge region the mechanisms producing type I polarization effects are analogous to those that produce polarization in two-body scattering and do not necessarily involve violations of factorization. Type II effects are those resulting from the polarization of particle b and are written as $(a \xrightarrow{b_\uparrow} c)$. In the triple-Regge region these type II effects vanish for factorizing poles. By studying these effects we learn about the importance of non-factorizing (Regge-cut) contributions to the Reggeon-particle forward scattering amplitude.

In Section II we review the triple-Regge formalism and show how it can be extended to include polarization and spin observables. The question of extending triple-Regge predictions to small M^2 via FMSR and M^2-duality is also discussed. Section III is devoted to the phenomenology of polarization and spin effects in inclusive reactions and existing data are examined. Section IV is reserved for summary and conclusions.

II. Triple Regge Formalism

A. Invariant cross section $ab \to cX$; $(a \xrightarrow{b} c)$.

We are interested in the inclusive process $a + b \to c + X$ (Fig. 1a), where a, b, and c are definite particles and X represents anything; and where λ_a, λ_b, and λ_c are the projections of their spins along some chosen axis (i.e. s-channel helicity, transversity, etc.). The generalized optical theorem relates the square of the amplitude $F^X_{\lambda_c;\lambda_a\lambda_b}(s,t,M^2)$ for $a + b \to c + X$ to a discontinuity (imaginary part) of the forward 3 to 3 amplitude $A_{ab\bar{c} \to ab\bar{c}}(s,t,M^2)$ as shown in Fig. 2. In particular if we define the invariant cross section

$$\sigma(s,t,M^2) \equiv s \frac{d\sigma}{dt dM^2}(s,t,M^2) \tag{2.1}$$

then

$$\sigma(s,t,M^2) = \frac{1}{16\pi s(2s_a+1)(2s_b+1)} \sum_{\text{all } X} \sum_{\lambda_a\lambda_b\lambda_c} \left| F^X_{\lambda_c;\lambda_a\lambda_b}(s,t,M^2) \right|^2 , \qquad (2.2)$$

which by the generalized optical theorem is given by

$$\sigma(s,t,M^2) = \frac{1}{16\pi s(2s_a+1)(2s_b+1)} \sum_{\lambda_a\lambda_b\lambda_{\bar{c}}} \text{DISC}_{M^2} \langle \lambda_a\lambda_b\lambda_{\bar{c}} \left| A(s,t,M^2) \right| \lambda_a\lambda_b\lambda_{\bar{c}} \rangle , \qquad (2.3)$$

where s_a and s_b are the spins of particles a and b, respectively. We now limit ourself to the kinematic region s/M^2 is large and t/s is small, which results in the near forward pseudo-two-body process shown in Fig. 1b. This diagram corresponds to the exchange of a leading Regge trajectory $\alpha(t)$ in the t-channel and upon squaring and summing over all states X leads to the diagram shown in Fig. 3a. The optical theorem applied to the Reggeon-particle total cross section gives an invariant cross section of the form

$$\sigma(s,t,M^2) = \frac{1}{16\pi s(2s_a+1)(2s_b+1)} \sum_{\lambda_a\lambda_b\lambda_{\bar{c}}} \sum_{i\ j} \beta^i_{\lambda_a\lambda_{\bar{c}}}(t)\ \beta^j_{\lambda_a\lambda_{\bar{c}}}(t)\ \xi_i(t)\ \xi^*_j(t) \cdot$$

$$\cdot\ s^{\alpha_i(t)+\alpha_j(t)}\ \text{Im}\, a_{ib\to jb}(\nu,t) , \qquad (2.4)$$

where $\nu = M^2 - t - M_b^2$, and the quantity $a(\nu,t)$ is referred to as the forward Reggeon particle scattering amplitude, and $\beta^i_{\lambda_a\lambda_{\bar{c}}}(t)$ is the coupling of Regge pole i to the particles $a\bar{c}$. The quantity $\xi_i(t)$ is the usual Regge signature factor:

$$\xi_i(t) = (\tau_i + e^{-i\pi\alpha_i(t)}) \,/\, [-\sin(\pi\,\alpha(t))] , \qquad (2.5)$$

where τ_i and $\alpha_i(t)$ are the signature and trajectory, respectively of the Regge pole i.

The large ν behavior of $a_{ib \to jb}(\nu,t)$ is controlled by the exchange of Regge poles $\alpha_k(o)$ which can couple to $b\bar{b}$ and $\alpha_i\bar{\alpha}_j$. Thus for large ν

$$\text{Im } a_{ib\to jb}(\nu,t) = \beta^k_{\lambda_b\lambda_b'}(o)\ \text{Im}\ \xi_k(o)\ g^k_{ij}(t)\ \nu^{\alpha_k(o)-\alpha_i(t)-\alpha_j(t)} \quad , \tag{2.6}$$

where $g^k_{ij}(t)$ is the triple-Regge coupling (see Fig. 3b). Combining (2.4) and (2.6) one arrives at the triple-Regge formula that describes the graph shown in Fig. 3c:

$$\sigma(s,t,M^2) = \frac{1}{s}\sum_{ijk} G_{ijk}(t)\ \left(\frac{s}{\nu}\right)^{\alpha_i(t)+\alpha_j(t)}\ \nu^{\alpha_k(o)} \quad , \tag{2.7a}$$

where

$$G_{ijk}(t) = \frac{1}{16\pi(2s_a+1)(2s_b+1)}\sum_{\lambda_a\lambda_b\lambda_c} \beta^i_{\lambda_a\lambda_c}(t)\beta^j_{\lambda_a\lambda_c}(t)\beta^k_{\lambda_b\lambda_b}(o)\cdot$$
$$\cdot\ g^k_{ij}(t)\xi_i(t)\xi^*_j(t)\text{Im}\xi_k(o) \quad . \tag{2.7b}$$

The term $G_{ijk}(t)$ denotes the triple-Regge coupling of the three Reggeons i, j, and k where Regge poles i and j with trajectories $\alpha_i(t)$, $\alpha_j(t)$, respectively, are exchanged and the Regge pole k with trajectory $\alpha_k(o)$ controls the Reggeon particle total cross section as shown in Fig. 3. Table 1 shows the corresponding coefficient of $G_{ijk}(t)$ for $d\sigma/dtdM^2$ and $d\sigma/dtdx$[10] with the forms $\alpha_p(t) = 1 + \gamma t$, $\alpha_R(t) = \alpha_o + \beta t$, and $\alpha_\pi(t) = 0.0 + \delta t$.

Consider the case where a and c are spin $1/2^+$ baryons. The invariant cross section (2.7) can be written

$$\sigma(s,t,M^2) = \sigma_N(s,t,M^2) + \sigma_U(s,t,M^2), \tag{2.8}$$

where $\sigma_N(\sigma_U)$ is the invariant cross section for the case where Regge poles i and j have natural (unnatural) parity. (Terms of the form i = natural, j = unnatural vanish in (2.7b) by parity.)[11] In particular

$$\sigma_N(s,t,M^2) = \frac{1}{s}\sum_{ijk} G^N_{ijk}(t)\,\left(\frac{s}{\nu}\right)^{\alpha_{N_i}(t)+\alpha_{N_j}(t)}\nu^{\alpha_k(o)}, \tag{2.9}$$

where

$$G^N_{ijk}(t) = \frac{1}{16\pi(2s_b+1)}\sum_{\lambda_b}\left\{\beta^{N_i}_{++}(t)\beta^{N_j}_{++}(t) + \beta^{N_i}_{+-}(t)\beta^{N_j}_{+-}(t)\right\}\xi_i(t)\xi^*_j(t)\cdot$$

$$\cdot\,\beta^k_{\lambda_b\lambda_b}(o)g^k_{ij}(t)\,\mathrm{Im}\,\xi_k(o)\quad. \tag{2.10}$$

A similar formula for $\sigma_U(s,t,M^2)$ can be written.

B. Type I Polarization and Spin Effects: $(a_\uparrow \xrightarrow{b} c_\uparrow)$.

Given that particle c is a fragment of particle a as shown in Fig. 1b, type I polarization effects involve the spins of particles a or c or both, but do not include polarization effects due to the spin of particle b. In what follows it is convenient to define the spin projections λ_a, λ_b, etc. along the transversity axis, which is normal to the production plane ($\hat{n} = \vec{p}_a \times \vec{p}_c \,/\, |\vec{p}_a \times \vec{p}_c|$). In this frame the asymmetry off a polarized particle a (spin $1/2^+$ baryon) is

$$P_a(s,t,M^2) = \sum_{\lambda_c}\left(\rho^{\lambda_c\lambda_c}_{\uparrow\uparrow}(s,t,M^2) - \rho^{\lambda_c\lambda_c}_{\downarrow\downarrow}(s,t,M^2)\right) \tag{2.11}$$

where we have defined

$$\rho^{\lambda_c\lambda_c'}_{\lambda_a\lambda_a'} = \sum_{\lambda_b} \sum_{\text{all } X} F^X_{\lambda_c;\lambda_a\lambda_b}(s,t,M^2)\, F^{X*}_{\lambda_c';\lambda_a'\lambda_b}(s,t,M^2)/\tilde{\sigma}(s,t,M^2) \qquad (2.12)$$

where $F^X_{\lambda_c;\lambda_a\lambda_b}(s,t,M^2)$ is the amplitude for $ab \to cX$ shown in Fig. 1b and $\uparrow(\downarrow)$ imply the spin of a is pointing up (down) relative to the transversity $\hat{z}$-axis (normal to the production plane). The total invariant cross-section (2.1) is given by

$$\sigma(s,t,M^2) = \frac{\tilde{\sigma}(s,t,M^2)}{16\pi s(2s_a+1)(2s_b+1)} \quad , \qquad (2.13a)$$

where

$$\tilde{\sigma}(s,t,M^2) \equiv \sum_{\lambda_a\lambda_b\lambda_c} \sum_{\text{all } X} \left| F^X_{\lambda_c;\lambda_a\lambda_b}(s,t,M^2) \right|^2 \quad . \qquad (2.13b)$$

Similarly for the recoil polarization of particle c (spin $1/2^+$ baryon) one has

$$P_c(s,t,M^2) = \sum_{\lambda_a} \left(\rho^{\uparrow\uparrow}_{\lambda_a\lambda_a}(s,t,M^2) - \rho^{\downarrow\downarrow}_{\lambda_a\lambda_a}(s,t,M^2) \right) \quad . \qquad (2.14)$$

The polarization formula (2.11) can, via the generalized optical theorem, be converted to a statement concerning the forward 3-3 amplitude as follows:

$$P_a(s,t,M^2)\tilde{\sigma}(s,t,M^2) = \sum_{\lambda_b\lambda_c} \text{DISC}_{M^2}\left\{ \left[\langle +\lambda_b\lambda_c \left| A(s,t,M^2) \right| +\lambda_b\lambda_c \rangle - \right.\right.$$

$$\left.\left. - \langle +\lambda_b\lambda_c \left| A(s,t,M^2) \right| +\lambda_b\lambda_c \rangle \right] \right\}, \qquad (2.15)$$

where $\tilde{\sigma}(s,t,M^2)$ is related to the unpolarized cross section by (2.13). Converting to the helicity frame using

$$|+\rangle = \frac{1}{\sqrt{2}}\,(-i|+1/2\rangle + |-1/2\rangle) \tag{2.16a}$$

$$|+\rangle = \frac{1}{\sqrt{2}}\,(-|+1/2\rangle + i|-1/2\rangle) \quad , \tag{2.16b}$$

where ±1/2 refers to s-channel helicity yields:

$$P_a\tilde{\sigma} = \sum_{\lambda_b\lambda_c} \mathrm{DISC}_{M^2}\left\{ i\langle +1/2\lambda_b\lambda_c|A(s,t,M^2)|-1/2\lambda_b\lambda_c\rangle - \right.$$

$$\left. -i\langle -1/2\lambda_b\lambda_c|A(s,t,M^2)|+1/2\lambda_b\lambda_c\rangle\right\} \quad . \tag{2.17}$$

Note that in contrast to the unpolarized cross section (2.3) and (2.4) the polarized cross section $P_a\tilde{\sigma}$ involves the forward 3-3 amplitude where the helicities $\lambda_a \neq \lambda_a'$ (see Fig. 3a.) In the triple-Regge region (2.17) can be converted into a statement about Regge couplings:

$$P_a\sigma(s,t,M^2) = \frac{1}{s}\sum_{ijk} \tilde{P}_{ijk}(t)\,\left(\frac{s}{\nu}\right)^{\alpha_i(t)+\alpha_j(t)}{}_{\nu}^{\alpha_k(o)} \tag{2.18a}$$

where for the case where particles a and c are spin $1/2^+$ baryons

$$\tilde{P}_{ijk}(t)+\hat{P}_{jik}(t) = \frac{1}{16\pi(2s_b+1)}\sum_{\lambda_b}\left\{\beta^i_{++}(t)\beta^j_{-+}(t)+\beta^i_{+-}(t)\beta^j_{--}(t)-\beta^j_{++}(t)\beta^i_{-+}(t)-\beta^j_{+-}(t)\beta^i_{--}(t)\right\}$$

$$\cdot\ \mathrm{Im}[\xi_i(t)\xi^*_j(t)]\,g^k_{ij}(t)\beta^k_{\lambda_b\lambda_b}(o)\mathrm{Im}\xi_k(o) \quad . \tag{2.18b}$$

This formula is anologous to the polarization formula for two-body scattering (except P_a is also a function of M^2), and has the following properties:

(i) $P_a(s,t,M^2) = 0$ if Regge pole i = j or if they have the same phase.

(ii) $P_a(s,t,M^2)$ arises from the interference between flip and non-flip amplitudes.

(iii) $P_a(s,t,M^2) = 0$ if i = unatural parity and j = unnatural parity, or vice versa[11].

Because of property (iii) the polarization can be written as the sum of two terms

$$P_a(s,t,M^2) = P_N(s,t,M^2) + P_U(s,t,M^2), \tag{2.19a}$$

where P_N arises from the interference between two natural parity Regge poles[12] ($i = N_1, j = N_2$) in (2.18b) and P_U arises from the interference between two unnatural parity Regge poles ($i = U_1, j = U_2$). From (2.14) one arrives at a similar type expression for the recoil polarization $P_c\sigma(s,t,M^2)$ except now

$$P_c(s,t,M^2) = P_N(s,t,M^2) - P_U(s,t,M^2). \tag{2.19b}$$

In general the two polarizations P_a and P_c will be different. However, if $P_U(s,t,M^2) = 0$, then $P_a(s,t,M^2) = P_c(s,t,M^2)$[13].

In general, assuming a and c are spin $1/2^+$ baryons and not measuring spin effects of particle b, there are a total of 8 observables one can measure[14]; the invariant cross section and 7 spin observables (P_a, P_c, R, R', A, A', and D). Table 2 defines these parameters in terms of the transversities of particles a and c. The observable $P_a\sigma$ and $P_c\sigma$ can be read off this table and are seen to agree with (2.11) and (2.14). The parameters R, R' and A, A' are anologous to the Wolfenstein R and A type parameters for elastic scattering. The $D(s,t,M^2)$ parameter is of particular interest since it is a measure of how well particle c "remembers" the spin of particle a. From Table 2 we have

$$D(s,t,M^2)\tilde{\sigma}(s,t,M^2) = \rho^{++}_{++} + \rho^{++}_{--} - \rho^{++}_{+-} - \rho^{++}_{-+} \quad , \tag{2.20a}$$

or using (2.16a) and (2.16b)

$$D\tilde{\sigma} = \text{DISC}_{M^2}\left\{\langle + +|A|- \rangle + \langle - -|A|+ +\rangle - \langle +-|A|-+\rangle - \langle -+|A|+-\rangle\right\}, \tag{2.20b}$$

where a sum over λ_b is assumed. In the triple Regge region we get

$$D\sigma(s,t,M^2) = \sigma_N(s,t,M^2) - \sigma_U(s,t,M^2) \quad , \tag{2.21}$$

where σ_N and σ_U are the natural and unnatural parity invariant cross sections defined in (2.8), (2.9), and (2.10). Thus $D\sigma$ measures the difference between the natural and unnatural parity exchange invariant cross sections and if $\sigma_N(s,t,M^2) \neq \sigma_U(s,t,M^2)$ particle c will "remember" something about the spin of particle a.

C. Type II Polarization Effects: $(a \xrightarrow{b^{\uparrow}} c)$.

Suppose particle c is a fragment of particle a as shown in Fig. 1b, then type II effects involve the spin of particle b. In terms of transversities the asymmetry of a polarized particle b (spin $1/2^+$ baryon) is

$$P_b(s,t,M^2)\tilde{\sigma}(s,t,M^2) = \sum_{\text{all } X}\sum_{\lambda_a\lambda_b}\left\{\left|F^X_{\lambda_c;\lambda_a+}(s,t,M^2)\right|^2 - \left|F^X_{\lambda_c;\lambda_a-}(s,t,M^2)\right|^2\right\} \quad , \tag{2.22}$$

where $F^X_{\lambda_c;\lambda_a\lambda_b}(s,t,M^2)$ is the amplitude for $ab \to cX$ shown in Fig. 1b and $\uparrow(\downarrow)$ imply the spin of b is pointing up (down) relative to the transaversity $\hat{z}$-axis which is normal to the scattering plane (i.e. $\hat{n} = \hat{p}_a \times \hat{p}_c$), and where $\tilde{\sigma}(s,t,M^2)$ is related to the unpolarized invariant cross section by (2.13a). Transforming

to helicities via (2.16a) and (2.16b) yields

$$P_b(s,t,M^2)\tilde{\sigma}(s,t,M^2) = 2\sum_{\text{all } X}\sum_{\lambda_a\lambda_c} \text{Im}\, F^X_{\lambda_c;\lambda_a+1/2} F^{X*}_{\lambda_c;\lambda_a-1/2} \quad , \qquad (2.23a)$$

Assuming s/M^2 large and t/s small so that F^X is given by Fig. 1b yields

$$P_b(s,t,M^2)\tilde{\sigma} = 2\text{Im}\sum_{ij}\sum_{\lambda_a\lambda_c} \beta^i_{\lambda_a\lambda_c}(t)\ \xi_i(t)\ \beta^j_{\lambda_a\lambda_c}(t)\ \xi^*_j(t)\cdot s^{\alpha_i(t)+\alpha_j(t)}$$

$$\cdot\sum_{\text{all } X} f(i+\to X)f^*(j-\to X), \qquad (2.23b)$$

where $f(k\lambda_b \to X)$ is the amplitude for Reggeon k scattering off particle b with helicity λ_b producing anything X. Unitarity states that

$$\text{DISC}_{M^2}\, a_{i+\to j-}(M^2,t) = \sum_{\text{all } X} f(i+\to X)\ f^*(j-\to X), \qquad (2.23c)$$

where $a_{i\lambda_b\to j\lambda_b'}(M^2,t)$ is the forward Reggeon particle scattering amplitude shown in Fig. 3b. Equation (2.23b) then becomes

$$P_b(s,t,M^2)\tilde{\sigma} = \sum_{ij}\sum_{\lambda_a\lambda_c} \beta^i_{\lambda_a\lambda_c}(t)\ \beta^j_{\lambda_a\lambda_c}(t)\cdot s^{\alpha_i(t)+\alpha_j(t)}$$

$$\text{Im}\left[\xi_i(t)\ \xi^*_j(t)\right]\text{Im}\left[a_{i+\to j-}(M^2,t)\right]. \qquad (2.23d)$$

which has the following properties:

(i) $P_b(s,t,M^2)$ vanishes if Regge pole i and Regge pole j have the same phase. (This is obvious since in this case $F^X_{\lambda_c;\lambda_a+1/2}$ and $F^X_{\lambda_c;\lambda_a-1/2}$ have the same phase and (2.23a) vanishes.)

(ii) The residues $\beta^i(t)$ and $\beta^j(t)$ enter diagonally (ie. $\beta^i_{++}(t)\beta^j_{++}(t) + \beta^i_{+-}(t)\beta^j_{+-}(t)$). Thus, for example, terms of the form i = P and j = ρ are suppressed since P(ρ) couples predominantly to helicity non-flip (flip).

(iii) $P_b(s,t,M^2)$ vanishes at large M^2 in a factorizing pole model[15]. This last property can be seen by assuming $a_{i+ \to j-}(\nu,t)$ is dominated at large ν by factorizing Regge poles so that

$$a_{i+ \to j-}(\nu,t) = \sum_k g^k_{ij}(t)\, \beta^k_{+-}(o)\, \xi_k(o)\, \nu^{\alpha_k(o)-\alpha_i(t)-\alpha_j(t)} , \qquad (2.24)$$

as shown in Fig. 4a. Since all fctorizing poles obey $\beta_{+-}(t) \alpha \sqrt{-t}$, the flip residues $\beta^k_{+-}(o)$ and $\beta^k_{-+}(o)$ vanish which implies $P_b(s,t,M^2)$ must vanish. This vanishing of type II polarization effects for factorizing pole models was first pointed out by Abarbanel[9]. However, as emphasized by Phillips, Ringland, and Worden[8], this vanishing is not a consequence of angular momentum conservation since the helicities of the incoming and outgoing $a\bar{c}$ system can compensate for the flip of b producing a forward $a\bar{c}b$ amplitude with no net helicity flip. A similar situation arises in the two-body process $\pi^- p \to \rho^o n$ (see Fig. 4b) where a factorizing pole model predicts that the evasive amplitude $H_{-1+;-}(s,t)$ vanish at t=0 even though this is not required by angular momentum[16]. This implies that the observable $\rho_{11}\, d\sigma/dt(\pi^- p \to \rho^o n)$ vanish in the forward direction where in fact the data show a spike (see Fig. 5). In two-body phenomenology this is "explained"by the presence of a large non-factorizing π cut contribution[17]. Numerous other examples from two-body scattering (i.e. $\gamma p \to \pi^+ n$, $pn \to np$) show the presence of Regge cuts which vitiate factorizing pole predictions[18]. We might thus anticipate the presence of non-factorizing cuts in the forward Reggeon-particle scattering amplitude, in which case type II polarization effects need not vanish. Studying type II effects in the triple-Regge region tells us the importance of Regge cuts in the forward Reggeon-particle scattering amplitude (see Fig. 4c).

D. Finite Mass Sum Rules and M^2-duality.

In two-body scattering the idea of duality began with the writing down of finite energy sum rules (FESR) which relate the integral over the low energy resonance region to the parameters of the high energy Regge exchange (Fig. 6a). It is a natural extension of the triple-Regge formalism to relate the low M^2 resonance production region to the high M^2 triple-Regge parameters by writing down similar sum rules for the Reggeon-particle scattering amplitude $a_{ib \to jb}(\nu,t)$ in (2.4)[19]. In this case the "dispersing variable" is ν or equivalently the missing mass M^2 rather than the incoming energy s; hence, the name finite mass sum rules. Also, in analogy to the two-body case, one can discuss the possibility of semi-local duality. In this case the large M^2 triple-Regge terms when extrapolated to small M^2 will be expected to reproduce on the average the low M^2 resonance region (see Fig. 6b). Thus M^2-duality and FMSR allow predictions to be made about the low M^2 region from the high M^2 triple- Regge formalism[20].

As in the two-body case, to derive the FMSR one needs to consider both the right and left hand cuts of $a(\nu,t)$. To do this it is convenient to use the antisymetric variable $\nu=M^2-t-M_b^2$ already introduced in (2.4). Given the large ν behavior of (2.6) and using (2.7) one can derive the following FMSR[20,21]:

$$I_n(s,t,\nu_o) = \frac{1}{2s}\sum_{ijk} G_{ijk}(t)(1+(-1)^{n+1}\tau_i\tau_j\tau_k) \cdot$$

$$\cdot (s/\nu_o)^{\alpha_i(t)+\alpha_j(t)}\nu_o^{\alpha_k(o)}/(\alpha_k(o) - \alpha_i(t) - \alpha_j(t) + n + 1) \ , \quad (2.25a)$$

where $I_n(s,t,\nu_o)$ is defined as the following integral over the low mass region

$$I_n(s,t,\nu_o) \equiv \frac{1}{2\nu_o^{n+1}}\int_o^{\nu_o} \nu^n \left\{\sigma_{ab \to cX}(s,t,\nu) + (-1)^{n+1}\sigma_{cb \to aX}(s,t,\nu)\right\} d\nu \ , \quad (2.25b)$$

where $G_{ijk}(t)$ is defined in (2.7) and where the invariant cross section $\sigma(s,t,\nu)$ is defined by (2.2). For the case where particle a equals particle c, the FMSR (2.25b) reduces to an integral over the single invariant cross section for $ab \to cX$ and is meaningful for odd n.

In addition to FMSR sum rules for the invariant cross section $\sigma(s,t,M^2)$ one can construct sum rules for other (type I) observables. For example, an FMSR for the polarized cross-section $P_a\sigma(s,t,\nu)$ looks like (assuming a=c):

$$I_n^P(s,t,\nu_o) = \frac{1}{s}\sum_{ijk} \tilde{P}_{ijk}(t)\ (s/\nu_o)^{\alpha_i(t)+\alpha_k(t)}\ \nu_o^{\alpha_k(o)}\ /$$

$$/\ (\alpha_k(o) - \alpha_i(t) - \alpha_j(t) + n + 1)\ , \qquad (2.26a)$$

where $I_n^P(s,t,\nu_o)$ is the following integral over the low mass polarized cross section

$$I_n^P(s,t,\nu_o) \equiv \frac{1}{\nu_o^{n+1}} \int_0^{\nu_o} \nu^n\ P_a(s,t,\nu)\ \tau\ (s,t,\nu)\ d\nu\ , \qquad (2.26b)$$

where n is odd and where $\tilde{P}_{ijk}(t)$ is given by (2.18) and the polarized invariant cross section $P_a\sigma$ is defined by (2.14).

Polarized FMSR sum rules provide a useful way of determining the importance of triple-Regge interference terms of the form PRR and R_1R_2R. These terms are very difficult to disentangle from the many diagonal terms when fitting only unpolarized invariant cross-section data[4,5].

E. Two Component Duality.

For two-body scattering the Harari-Freund two-component form of duality states that the resonance contributions to the FESR integral "build" the ordinary Regge trajectories, while background contributions "build" the Pomeron (Fig. 7a). For the case where the Reggeon i and j are ordinary Regge trajectories (not the Pomeron) the normal two-component form of duality can be carried over directly to the Reggeon particle scattering amplitude (Fig. 7b). For this case

resonances [background] in the M^2-channel are expected to "build" (via FMSR) ordinary [Pomeron] exchange in the crossed channel[20]. This implies that if the M^2 channel is exotic that the imaginary part of the Reggeon-particle scattering amplitude vanishes for i=R, j=R, and k=R (i.e. No RRR terms present in the invariant cross section Eq. 2.7). Due to the inequality[22]

$$G_{RPR}(t) + G_{PRR}(t) \leq 2\left(G_{PPR}(t) \cdot G_{RRR}(t)\right)^{1/2} \tag{2.27}$$

$G_{RRR}(t) = 0$ also implies $G_{RPR}(t) + G_{PRR}(t) = 0$, which means that if the Reggeon particle scattering amplitude is exotic only terms of the form PPP, RRP, PPR, PRP, and RPP are allowed.

The question of "what is dual to what" for Reggeon particle scattering becomes very complicated when i=j= pomeron. There are indications that PPP has an "abnormal" component of duality[5,23] (i.e. PPP dual to resonances in the M^2 channel), however, the situation is not completely clear[24].

III. Phenomenology and Predictions.

A. Type I Polarization Effects: $(a_\uparrow \xrightarrow{b} c_\uparrow)$.

1. $\pi^\pm p_\uparrow \to pX$ (Fig. 8a): $(p_\uparrow \xrightarrow{\pi^\pm} p)$.

Consider the reaction $\pi^\pm p \to pX$ off a polarized target. The leading triple-Regge terms responsible for the asymmetry $P_a(s,t,M^2)$ (see Eq. 2.18) are $P\rho\rho$ and $f\rho\rho$. It is easy to predict the following:

(i) Expect $P_a(s,t,M^2)$ to be similar to the elastic case which arises from $P\rho$ interference.

(ii) Expect $P_a(s,t,M^2)$ to be non-scaling and to decrease like $1/\sqrt{s}$ at fixed x[10].

(iii) Expect $P_a(s,t,M^2)$ to be mirror symmetric under the interchange of $\pi^\pm$.

(iv) Expect a dip in $P_a(s,t,M^2)$ at $t \simeq -0.6$ (GeV/c)^2 just as in the elastic case.

2. $K^{\pm} p_{\uparrow} \to pX$ (Fig. 8b): $(p_{\uparrow} \xrightarrow{K^{\pm}} p)$.

For this reaction off a polarized target the leading triple-Regge terms responsible for $P_a(s,t,M^2)$ are $P\rho\rho$ and PA_2A_2 (also $f\rho\rho$ and fA_2A_2). Here the polarization may differ from the elastic case. The elastic $K^{\pm}p$ polarizations are governed by the roughly EXD ρ and A_2 (i.e. P_{K^+p} is given by the interference between the predominantly imaginary Pomeron and the predominantly real $(A_2 - \rho)$). In the inclusive reaction there is no reason to expect the triple-Regge couplings $g_{PA_2A_2}(t)$ and $g_{P\rho\rho}(t)$ to be EXD and hence the inclusive polarization may not resemble the elastic.

3. $p_{\uparrow} p \to pX$ (Fig. 8c): $(p_{\uparrow} \xrightarrow{p} p)$.

There exists data from the Argonne group[25] on the reaction $p_{\uparrow}p \to pX$ with a polarized beam. The data are shown in Fig. 9. The triple-Regge predictions are similar to those for reaction (2) above. The terms responsible for $P_a(s,t,M^2)$ are $P\rho\rho$ and PA_2A_2 (and $f\rho\rho$, fA_2A_2). If the triple-Regge couplings $g_{PA_2A_2}(t)$ and $g_{P\rho\rho}(t)$ are (are not) EXD then we expect the polarization to be similar (not similar) to the elastic case. The data show an elastic polarization of about 10% for small $p_\perp$ values. As M^2 increases through the resonance region there is considerable structure in the polarization, however, it never greatly exceeds the elastic value. For the highest M^2 value ($M^2 \simeq 7$ GeV/c^2) the polarization is small (less than $\approx 4\%$). The polarization is expected to be largest for M^2 small and in the resonance region since $P\rho\rho$ and PA_2A_2 decrease like $1/M^2$ for fixed s and t (see Table 2). In order to make any quantitive statements concerning the sizes of $g_{P\rho\rho}(t)$ and $g_{PA_2A_2}(t)$, it is necessary to form a polarization FMSR by integrating the data over the low M^2 region and then compare with the triple-Regge formalism as discussed in Sec.II.D. Work on this is in progress[26].

By the use of isospin, one predicts that the asymmetry $P_a(s,t,M^2)$ should change sign in going from the inclusive reaction $(p_{\uparrow} \xrightarrow{p} p)$ to $(p_{\uparrow} \xrightarrow{n} p)$.

4. $K^-p \to \Lambda_\uparrow X$ (small t region - Fig. 10a): $(p \xrightarrow{K^-} \Lambda)$.

The triple-Regge terms responsible for the Λ-polarization in $K^-p \to \Lambda X$ are of the form $K^{**}K^{*}R$, where $R = f,\omega,\rho,A_2,\phi$, or f'. Note that the term $K^{**}K^{*}P$ vanishes by generalized C-parity (assuming P is an SU(3) singlet with C=+1). Thus at fixed x and t we expect $P_\Lambda(s,x,t)$ to decrease with increasing s[27]. This decrease can be seen in the data[28,29,30] (x near -1) shown in Fig. 11.

5. $K^-p \to \Lambda_\uparrow X$ (small u region - Fig. 10b): $(K^- \xrightarrow{p} \Lambda)$.

The near constant Λ polarization seen in $K^-p \to \Lambda X$ near $x = 1$[28,29] (Fig. 11) (fast forward Λ's) can be understood once one realizes that the RRP triple-Regge terms are small relative to RRR terms in the region 4.0 to 14.3 GeV/c. Thus both the Λ polarization $P_\Lambda\sigma(s,t,x)$ and the invariant cross section $\sigma(s,t,x)$ decrease approximately like $1/\sqrt{s}$ in this region, which results in $P_\Lambda = P_\Lambda\sigma/\sigma$ approximately constant for fixed x. The smallness of the RRP terms in the above region can be inferred from the smallness of the invariant cross section for $K^+p \to \bar{\Lambda}X$ (Fig. 10c) which by duality arguments has only RRP terms and which by crossing are equal in strength to the RRP terms in $K^-p \to \Lambda X$.

6. $p_\uparrow p \to \Lambda_\uparrow X$ (Fig. 10d): $(p_\uparrow \xrightarrow{p} \Lambda)$.

For this reaction the Reggeon-particle scattering is exotic which implies that contributions from Regge exchange should cancel (EXD) in such a way as to produce a purely real Reggeon-particle forward amplitude (see Sec.II.E.). Since it is the imaginary part of this amplitude that appears in the formula (2.4) for the observables we expect no contribution to any type I observable from terms of the the form RRR. The invariant cross section $\sigma(s,t,x)$ is thus expected to scale and the Λ-polarization $P_\Lambda(s,t,x)$ should be zero since it cannot be produced by terms of the form $K^{**}K^{*}P$ due to generalized C-parity (see (4.) above). The $D(s,t,x)$ parameter is expected to scale and can be seen from (2.21) and Table I to

have the form

$$D(t,x) = (r - 1 + x)/(r + 1 + x) \quad , \tag{3.1}$$

where we have used natural and unnatural invariant cross sections

$$\sigma_N(s,t,x) = C_N(t) \tag{3.2a}$$

$$\sigma_U(s,t,x) = C_U(t)(1 - x) \tag{3.2b}$$

and

$$r = r(t) = C_N(t) / C_U(t) \quad . \tag{3.2c}$$

The expected behavior of $D(t,x)$ for a particular value of $x_o(t) = 1 - r(t)$ is shown in Fig. 12. If for a particular value of t the natural parity invariant cross section dominated over the unnatural parity invariant cross section then $x_o(t)$ would be less than 0.75 and $D(t,x)$ would be positive over the whole triple-Regge region (dot-dashed curve)[31]. It could happen that $\sigma_N(t,x)$ and $\sigma_U(t,x)$ would be equal at some fixed value of t and $x = x_o(t)$ implying $D(t,x) = 0$ (solid curve), but since $\sigma_N(t,x)$ and $\sigma_U(t,x)$ have different x dependence (Table 1) they will not be equal for the same value of t and another value of x. Thus we expect $D(t,x) \neq 0$ except possibly at some isolated values of t and x. Since the parameter D measures how well the Λ "remembers" the polarization of the incoming proton this should be useful in constructing polarized Λ beams from polarized proton beams.

Recent data on $P_\Lambda(s,t,M^2)$ and $D(s,t,M^2)$ for $p_+p \to \Lambda X$ at 6.0 GeV/c from Argonne[32] are shown in Fig. 13. The data show zero Λ polarization (P_Λ) as expected[33] (see Table 3) but in addition show zero values of $D(s,t,M^2)$ contrary to expectations. Possible reasons for the unexpectedly small values of D are:

(i) The energy (6.0 GeV/c) is a bit low to use triple-Regge type arguments. Hopefully the experiment can be repeated at 12 GeV/c where the predictions are more applicable.

(ii) The observables have been averaged over large M^2 and t bins which could yield a net result of zero.

B. Type II Polarization Effects: $(a \xrightarrow{b_\uparrow} c)$.

1. $\pi^\pm p_\uparrow \to \pi^\pm X$ (Fig. 14a): $(\pi^\pm \xrightarrow{P_\uparrow} \pi^\pm)$.

Assuming that Regge-cuts are present in the Reggeon-particle scattering amplitude, one predicts contributions to the polarized target asymmetry $P_b(s,t,M^2)$ (2.23d) in the triple-Regge region from the terms $P\rho\rho_c$ and $f\rho\rho_c$ (ρ_c = ρ-cut). It is an easy matter to then predict[8]:

(i) Expect $P_b(s,t,M^2)$ to be mirror symmetric under the interchange of $\pi^\pm$.

(ii) Expect $P_b(s,t,x)\sigma(s,t,x)$ to be non-scaling and to decrease roughly like $1/\sqrt{s}$ at fixed x.

Recent data[34] on $\pi^\pm p_\uparrow \to \pi^\pm X$ off a polarized target at 8 GeV/c do show non-zero asymmetries for $x \gtrsim 0.7$ which are mirror symmetric under the interchange of $\pi^\pm$ (see Fig. 15). This data is very interesting but one must use caution before interpretating it as indicating the presence of a ρ-cut in the forward Reggeon particle scattering amplitude. The data is at a fairly low energy ($s \approx 16$ GeV^2) which means that for $x \simeq 0.85$ one is still at low M^2 ($M^2 \approx 2.4$ GeV^2). The triple-Regge factorization arguments discussed in Sec. II can only be applied at M^2 large ($M^2 \gtrsim 5$ GeV^2) which means one must apply M^2-duality to interpret the 8 GeV/c data. It could happen that $P_b(s,t,M^2)\sigma(s,t,M^2)$ would oscillate positive and negative over the low M^2 region implying a small Regge cut contribution or it could remain positive indicating a substantial cut contribution. In addition if one is going to use the triple-Regge formalism one is restricted to $x > 0.8$ so clearly more data is needed[35].

2. $pp_{\uparrow} \to pX$ (Fig. 14b): $(p \xrightarrow{p_t} p)$.

Asymmetries off a polarized target have also been observed for $pp \to pX$ at 8 GeV/c[34] (see Fig. 16). Because of the relatively low energy, interpretations in terms of triple-Regge contributions $P\rho\rho_c$ or $f\rho\rho_c$ are difficult for the same reasons as described above. These results are nonetheless very interesting and further experiments at higher energies should be encouraged.

C. Other Interesting Inclusive Observables.

Valuable knowledge as to the nature of inclusive production mechanisms can be gained by studying other observables in addition to the polarization observables discussed above. We briefly mention some of the most interesting examples.

1. $\rho_{11}\, d\sigma/dtdM^2$ $(\pi^- p \to \rho^o X)$: $(\pi^- \xrightarrow{p} \rho^o)$.

By observing the density matrix elements of outgoing vector mesons produced in inclusive reaction one will be able to further probe the nature of the production mechanism. Consider for example the inclusive reaction $\pi^- p \to \rho^o X$ and the observable:

$$\rho^H_{11} \frac{d\sigma}{dtdM^2}(s,t,M^2) = \frac{1}{32\pi s^2} \sum_{\text{all } X} \sum_{\lambda_b = \pm 1/2} F^X_{1;\lambda_b}(s,t,M^2) F^{X*}_{1;\lambda_b}(s,t,M^2). \qquad (3.3)$$

In the triple-Regge region using the generalized optical theorem this becomes

$$\rho^H_{11} \frac{d\sigma}{dtdM^2}(s,t,M^2) = \frac{1}{s^2} \sum_{ijk} G^{ijk}_{11}(t) \left(\frac{s}{\nu}\right)^{\alpha_i(t)+\alpha_j(t)} \nu^{\alpha_k(o)}, \qquad (3.4)$$

where

$$G^{ijk}_{11}(t) = \frac{1}{32\pi} \sum_{\lambda_b = \pm 1/2} \beta^i_j(t)\beta^j_1(t)\beta^k_{\lambda_b\lambda_b}(o) g^k_{ij}(t)\xi_i(t)\xi^*_j(t) \text{Im}\, \xi_k(o). \qquad (3.5)$$

As discussed in Sec.II.C in a factorizing pole model the residues behave like $\beta_1(t) \propto \sqrt{-t}$ which implies $G_{11}(t)$ vanish at $t = 0$. However, as pointed out earlier, this prediction is violated experimentally for $\pi^- p \to \rho^0 n$ (see Fig. 5) by the presence of non-factorizing Regge cuts[17]. It would be extremely interesting to study the behavior of these cuts as M^2 is increased from a nucleon mass to the high M^2 region. There is evidence that these cuts decrease in strength as one increases the mass (or spin) of the produced mesons [i.e. $\pi^- p \to (\rho,f,g)n$] which leads one to suppose that perhaps cuts decrease in general as M^2 increase[36]. The study of $\rho_{11} d\sigma/dt dM^2(\pi^- p \to \rho^0 X)$ would certainly shed light on this most interesting phenomenon.

Similar studies could be carried out on the reaction $K^- p \to \bar{K}^{*0} X$ or $K^+ n \to K^{*0} X$.

2. $pn \to pX(n \to p)$; $pp \to nX(p \to n)$

One can gain knowledge as to the M^2 dependence of evasive amplitude cuts similar to that discussed in example (1.) above without measuring density matrix elements by observing the small $|t|$ inclusive cross section for $pn \to pX$ (or equivalently $pp \to nX$). Factorization arguments lead one to expect a dip in the invariant cross section (and in the np CHEX differential cross section) as t goes to zero. The data on np CHEX[37], on the other hand, shows a sharp spike at $t = 0$ resulting from a large non-factorizable π-cut contribution[38]. It would be most interesting to study the M^2 dependence of this cut by observing the small $|t|$ behavior of the invariant cross section for the inclusive process $pn \to pX(n \to p)$.

IV. Summary and Conclusions

In two-body exclusive processes, polarization and density matrix data have been crucial in testing and refining our theoretical models. In inclusive processes measurements of observables other than just the invariant cross section may well be of equal importance. Type I polarization and/or spin effects in the inclusive reaction $ab \to cX$ arise from spin measurements on particles a and/or c,

where c is a fragment of a $(a_\uparrow \overset{b}{\to} c_\uparrow)$. These effects arise from mechanisms similar to the corresponding two-body analogue and need not vanish if factorization holds. In Table 3 we tabulate many predictions for type I polarization effects using the triple-Regge formalism. Triple-Regge predictions are valid for $x \gtrsim 0.8$, t/s small, and M^2 large; however, the last restriction can be relaxed and predictions made concerning the low M^2 region by the use of M^2-duality and FMSR.

The study of type I polarization effects should provide information as to the importance of triple-Regge interference terms and the status of EXD for triple-Regge couplings. The investigation of observables like $\rho_{11} d\sigma/dt dM^2$ $(\pi^- p \to \rho^0 X)$ will provide "insight" into the behavior of absorptive corrections. Furthermore, by studying the connection between the low and high M^2 region one will gain valuable knowledge as to the nature of M^2-duality.

Type II spin effects are those involving the spin of particle b $(a \overset{b_\uparrow}{\to} c)$. These effects vanish at large M^2 for factorizing pole models. The investigation of these effects will tell us the importance of non-factorizing Regge cuts in the Reggeon-particle forward scattering amplitude. This is a subject of great interest since Regge cuts do play a crucial role in understanding two-body scattering. (See table 4 for a summary of type II predictions.)

Finally we point out that the majority of both type I and II polarization effects are expected to decrease at fixed x like $1/\sqrt{s}$ (they are non-scaling effects). Therefore we are interested in the approach to scaling. Brookhaven and Argonne are, thus, ideally suited for this sort of study. In particular, the polarized beam at Argonne makes spin studies "easy." However, if one is to make full use of the triple-Regge formalism every effort should be made to do polarized beam experiments at 12 GeV/c rather than 6 GeV/c as is now the case.

Acknowledgements

I gratefully acknowledge helpful discussions with J. Dash, R. Eisner, G. Fox, A. B. Wicklund, and D. Wray. In addition I thank the theory group at Argonne National Laboratory for the hospitality shown me during a recent visit where the writing of this paper was carried out.

Table 1. Triple Regge Formulae, where

$\alpha_p(t) = 1.0 + \gamma t$, $\alpha_R(t) = \alpha_o + \beta t$, and

$\alpha_\pi(t) = 0.0 + \delta t$.

Triple Regge Term	$d\sigma/dtdM^2$		$d\sigma/dtdx$	
i j k	Cosmic[a]	Full	Cosmic[a]	Full
PPP	$1/M^2$	$\frac{s^{2\gamma t}}{(M^2)^{1+2\gamma t}}$	$1/(1-x)$	$\frac{1}{(1-x)^{1+2\gamma t}}$
PRP	$1/(M\sqrt{s})$	$\frac{s^{\alpha_o+(\beta+\gamma)t-1}}{(M^2)^{\alpha_o+(\beta+\gamma)t}}$	$1/(1-x)^{1/2}$	$\frac{1}{(1-x)^{\alpha_o+(\beta+\gamma)t}}$
RRP	$1/s$	$\frac{s^{2\alpha_o+2\beta t-2}}{(M^2)^{2\alpha_o+2\beta t-1}}$	1	$\frac{1}{(1-x)^{2\alpha_o+2\beta t-1}}$
PPR	$1/M^3$	$\frac{s^{2\gamma t}}{(M^2)^{2-\alpha_o+2\gamma t}}$	$1/\sqrt{s} \cdot 1/(1-x)^{3/2}$	$\frac{(M^2)^{\alpha_o-1/2}}{\sqrt{s}\ (1-x)^{3/2+2\gamma t}}$
PRR	$1/(M^2\sqrt{s})$	$\frac{s^{\alpha_o+(\beta+\gamma)t-1}}{(M^2)^{1+(\beta+\gamma)t}}$	$1/\sqrt{s} \cdot 1/(1-x)$	$\frac{1}{s^{1-\alpha_o}(1-x)^{1+(\beta+\gamma)t}}$
RRR	$1/(sM)$	$\frac{s^{2\alpha_o+2\beta t-2}}{(M^2)^{\alpha_o+2\beta t}}$	$1/\sqrt{s} \cdot 1/(1-x)^{1/2}$	$\frac{1}{s^{1-\alpha_o}(1-x)^{\alpha_o+2\beta t}}$
$\pi\pi$P	M^2/s^2	$\frac{s^{2\delta t-2}}{(M^2)^{2\delta t-1}}$	$(1-x)$	$\frac{1}{(1-x)^{2\delta t-1}}$
$\pi\pi$R	M/s^2	$\frac{s^{2\delta t-2}}{(M^2)^{2\delta t-\alpha_o}}$	$(1-x)^{1/2}/\sqrt{s}$	$\frac{1}{\sqrt{s}(1-x)^{2\delta t-\alpha_o}}$

[a]Cosmic is defined by $\gamma=\beta=\delta=0$, $\alpha_o=1/2$ (See Ref. 4)

Table 2.

Type I observables for the inclusive reaction $(a_\uparrow {}^{b}\!\to c_\uparrow)$ in terms of the transversities (spin projections normal to production plane) of particles a and c, where

$$\rho^{\lambda_c\lambda'_c}_{\lambda_a\lambda'_a} = \sum_{\text{all } X}\sum_{\lambda_b} F^{X}_{\lambda_c;\lambda_a\lambda_b} F^{X*}_{\lambda'_c;\lambda'_a\lambda_b} \Big/ \tilde{\sigma} \quad \text{and} \quad \tilde{\sigma} = \sum_{\text{all } X}\sum_{\lambda_a\lambda_b\lambda_c} \left|F^{X}_{\lambda_c;\lambda_a\lambda_b}\right|^2 .$$

The amplitude for the process $ab \to cX$ is given by $F^{X}_{\lambda_c;\lambda_a\lambda_b}(s,t,M^2)$ and the observables are in general a function of s, t, and M^2.

$\rho^{\lambda_c\lambda'_c}_{\lambda_a\lambda'_a}$	$\lambda_c\lambda'_c$ → ↑ ↑	↑ ↑	↓ ↓	↓ ↑
$\lambda_a\lambda'_a$ ↑ ↑	1/4(1+D+P_a+P_c)	0	0	1/2(R+iA)
↓ ↓	0	1/4(1-D-P_a+P_c)	1/2(R'-iA')	0
↓ ↑ ↑	0	1/2(R'+iA')	1/4(1-D+P_a-P_c)	0
↓ ↓	1/2(R-iA)	0	0	1/4(1+D-P_a-P_c)

Table 3.

Expected behavior of Type I polarized cross sections $P(s,t,M^2)d\sigma/dtdM^2$ for various inclusive processes.

Reaction	Triple-Regge Terms responsible for $P(s,t,M^2)$	Cosmic[a] Behavior of $P(s,t,M^2)d\sigma/dtdM^2$	Predictions for $P(s,t,M^2)\sigma(s,t,M^2)$
1. $\pi^{\pm}p_{\uparrow} \to pX$	$\bar{P}pp$, fpp	$1/(M^2\sqrt{s}), 1/(sM)$	Non-scaling
$(p_{\uparrow} \xrightarrow{\pi^{\pm}} p)$			Mirror symmetric under $\pi^+ \to \pi^-$
Fig. 8a			dip at $t \approx -0.6$ (GeV/c)^2 should resemble elastic pol
2. $K^{\pm}p_{\uparrow} \to pX$	$P(A_2,\bar{P})(A_2,\bar{P})$	$1/(M^2\sqrt{s})$	Non-scaling
$(p_{\uparrow} \xrightarrow{K^{\pm}} p)$	$f(A_2,\bar{P})(A_2,\bar{P})$	$1/(sM)$	May or may not resemble elastic
Fig. 8b			depending on EXD of $g_{PA_2A_2}(t)$ and $g_{Ppp}(t)$
3. $p_{\uparrow}p \to pX$	$P(A_2,\rho)(A_2,\rho)$	$1/(M^2\sqrt{s})$	Non-scaling
$(p_{\uparrow} \xrightarrow{p} p)$	$f(A_2,\rho)(A_2,\rho)$	$1/(sM)$	May or may not resemble elastic
Fig. 8c			depending on EXD of $g_{PA_2A_2}(t)$ and $g_{Ppp}(t)$
4. $p_{\uparrow}n \to pX$	$P(A_2,\rho)(A_2,\rho)$	$1/(M^2\sqrt{s})$	Opposite sign from (3) by isospin
$(p_{\uparrow} \xrightarrow[n]{} p)$	$f(A_2,\rho)(A_2,\rho)$	$1/(sM)$	
5. $K^-p \to \Lambda X$	$K^{*\pm}K^{*0}R$	$1/(sM)$	Non-scaling
$(p \xrightarrow{K^-}_{\uparrow} \Lambda)$	$R=f,\omega,\rho,A_2,f',\phi$		Expect $P_{\Lambda}(s,t,x)$ to decrease with increasing s and fixed x.
Fig. 10a			
6. $K^-p \to \Lambda X$	$\bar{N}_i\bar{N}_j P$	$1/s$	$\bar{N}_i\bar{N}_j P$ small for $4.0 \le p_{lab} < 14.0$ GeV/c
$(K^- \xrightarrow{p}_{\uparrow} \Lambda)$	$\bar{N}_i\bar{N}_j R$	$1/(sM)$	so $P_{\Lambda}(s,t,x) \approx$ const at fixed x.
7. $p_{\uparrow}p \to \Lambda X$	None	-	$P_{\Lambda}(s,t,x) \approx 0$
$(p_{\uparrow} \xrightarrow{p}_{\uparrow} \Lambda)$			$D(s,t,x) \neq 0$ (see Fig. 12)
			$D(s,t,x)$ scales

[a] For definition of Cosmic see Table 1 and Ref. 4

Table 4.

Expected behavior of Type II polarization asymmetries $P_\beta(s,t,M^2)d\sigma/dtdM^2$ for various inclusive processes.

Reaction	Triple-Regge Terms responsible $P(s,t,M^2)$	Cosmic[8] Behavior of $P(s,t,M^2)d\sigma/dtdM^2$	Predictions for $P(s,t,M^2)\sigma(s,t,M^2)$
1. $\pi^\pm p_\uparrow \to \pi^\pm X$	Ppp_c	$1/(M^2\sqrt{s})$	Non-scaling
$(\pi^\pm \xrightarrow{p_\uparrow} \pi^\pm)$	fpp_c	$1/(sM)$	Mirror symmetric under $\pi^+ \to \pi^-$
Fig. 14a			
2. $pp_\uparrow \to pX$	Ppp_c, fpp_c	$1/(M^2\sqrt{s}), 1/(sM)$	Non-scaling
$(p \xrightarrow{p_\uparrow} p)$	$PA_2A_2^c, fA_2A_2^c$	$1/(M^2\sqrt{s}), 1/(sM)$	Changes sign for $(p \xrightarrow{p_\uparrow} n)$
Fig. 14b			

Footnotes and References

1. A.H. Mueller, Phys. Rev. D2, 2963 (1970); A.H. Mueller, Phys. Rev. D4, 150 (1971).
2. Chan Hong-Mo, C.S. Haue, C. Quigg, and J.-M. Wang, Phys. Rev. Letters 26, 672 (1971).
3. R.C. Brower, R.N. Cahn, J. Ellis, Phys. Rev. D7, 2080 (1973).
4. For a review see, for example, G.C. Fox, "Inclusive Structure of Diffractive Scattering," invited talk presented at the Fifth International Conference on High Energy Collisions, Stony Brook, August, 1973.
5. R.D. Field and G.C. Fox, "Triple Regge and Finite Mass Sum Rule Analysis of the Inclusive Reaction pp → pX," Caltech preprint CALT-68-434 (Nuclear Physics, to be published).
6. R. Shankar, Lawrence Berkeley Laboratory preprint LBL-2678 (1974).
7. J. Softer and D. Wray, Nucl. Phys. B73, 231 (1974).
8. R.J.N. Phillips, G.A. Ringland, and R.F. Worden, Phys. Letters 40B, 239 (1972).
9. H.D.I. Abarbanel and D.J. Gross, Phys. Rev. Letters 26, 732 (1971).
10. We define x by $x = p_{11}^{cm} / p_{max}^{cm}$, which for large s is related to s and M^2 approximately by $M^2 \approx s(1 - x)$.
11. Parity implies that for natural [unnatural] parity Regge exchange $\beta^N_{++}(t) = \beta^N_{--}(t)$, $\beta^N_{+-}(t) = -\beta^N_{-+}(t)$ [$\beta^u_{++}(t) = -\beta^u_{--}(t)$, $\beta^u_{+-}(t) = \beta^u_{-+}(t)$].
12. These two natural parity poles must of course have different phases (ie. $P \neq \rho$).
13. This is completely analogous to two-body scattering.
14. See, for example, M.G. Doncel and A. Mendez, Phys. Letters 41B, 83 (1972).

15. In addition, Ph. Salin and J. Soffer [Nucl. Phys. B71, 125 (1974)] have shown that in order to have a non-zero type II polarization the naturality of the object exchanged in the cross channel of the Reggeon particle amplitude $a_{i+,j-}(\nu,t)$ must be mixed (like a Regge cut).

16. See, for example, Lorella Jones, Phys. Rev. 163, 1523 (1967).

17. R.D. Field and Deepinder Sidhu, Phys. Rev. D (to be published - July 1974 issue).

18. See the review by G.C. Fox and C. Quigg, Annual Review of Nuclear Science, Vol. 23, 1973.

19. M.B. Einhorn, J. Ellis, and J. Finkelstein, Phys. Rev. D5, 2063 (1972).

20. P. Hoyer, R.G. Roberts, and D.P. Roy, Nucl. Physics B56, 173 (1973).

21. See, for example, "Duality and Regge Analysis of Inclusive Reactions," R.G. Roberts, Rutherford Laboratory preprint 1973.

22. H.D.I. Abarbanel, S.D. Ellis, M.B. Green, and A. Zee, "Restrictions on Pomeron Couplings," NAL-THY-71 preprint (1972).

23. Chan Hong-Mo, H.I. Miettinen, R.G. Roberts, Nucl Physics B54, 411 (1973).

24. P. Hoyer, "Finite-Mass Sum Rules and Duality," invited talk presented at the XVII International Conference on High Energy Physics, London, 1974.

25. A.B. Wicklund, D.S. Ayres, R. Diebold, J. Jost, S.L. Kramer, A.J. Pawlicki, (private communication).

26. R.D. Field and A.B. Wicklund, work in progress.

27. This is because the inclusive invariant cross section $\sigma(s,x,t)$ for $(p \xrightarrow{K^-} \Lambda)$ has a component independent of s (ie. K^*K^*P, KKP, etc.), so that $P_\Lambda = P_\Lambda \sigma / \sigma$ decreases with increasing s. For a discussion of the various triple-Regge contributions to $(p \xrightarrow{K^-} \Lambda)$ see T. Inami and H.I. Miettinen, Phys. Letters 49B, 67 (1974).

28. S.U. Chung, R.L. Eisner, S.D. Protopoescu, and R.D. Field, "Polarization Study of Inclusive Lambda Production in K^-p Interactions," Brookhaven National Laboratory preprint (1974), (to be published).

29. A. Borg, M. Bardadin-Otwinowaka, R. Barloutaud, C. Louedec, L. Moscoso, F. Perrre, M. Spiro, B. Cahurand, B. Drevillon, G. Labrosse, R. Lestienne, A. Rouge, R. Salmeron, H. Videau, R. Miller, K. Saler, J.J. Phelan, T.P. Shaha, and S. Tovey, Saclay preprint DPH PE 74-03 (1974).

30. Amsterdam - CERN - Nijmegen Collaboration, "Study of the Fragmentation $p \xrightarrow{K^-} \Lambda$ and $K^- P \to \Lambda$ at 4.2 GeV/c," submitted to the XVII International Conference on High Energy Physics, London, 1974.

31. Using factorization one can estimate $\sigma_N(t,x)$ and $\sigma_U(t,x)$ for $pp \to \Lambda X$ from the triple-Regge couplings for $pp \to pX$ given in Ref. 5. Such an estimate yields $x_o \approx 0.65$ for $t = -0.1$ $(GeV/c)^2$. This implies that at this value of t $D(t,x)$ is positive through the entire triple-Regge region! See also a discussion by E.C. Swallow, Phys. Letters 49B, 91 (1974).

32. I. Ambats, E. Hayes, W.T. Meyer, C.E.W. Ward, T.M. Knasel, E.C. Swallow, R. Winston, A. Lesnik, D.M. Schwartz, T.A. Romanowski, Argonne preprint (private communication).

33. Zero Λ-polarization (P_Λ) has also been seen in $pp \to \Lambda X$ at 19 GeV/c by the Scandinavian Collaboration, R. Buran, internal report (1973). I thank D. Wray for pointing this out to me.

34. D. Aschaan, C. Caverzasio, L. Dick, A. Gonidec, K. Green, A. Gsponer, K. Kuroda, A. Michalowicz, P. Phizacklea, M. Poulet, G.L. Salmon, and M. Werlen, paper No. 471 submitted to the XVII International Conference on High Energy Physics, London, 1974.

35. J. Soffer and D. Wray (Ref. 7) have, using crude arguments, attempted to explain the asymmetry observed in $\pi^{\pm}p_{\uparrow} \to \pi^{\pm}X$ at 8.0 GeV/c in terms of triple-Regge term $f\rho\rho_c(\rho_c = \rho\text{-cut})$. Their results do agree qualitatively with the data shown in Fig. 15.

36. See, for example, C. Michael, "Vector and Tensor Meson Productions," invited talk presented at the XVII International Conference on High Energy Physics, London, 1974.

37. E.L. Miller, Mark Elfield, N.W. Reay, N.R. Stanton, M.A. Abolins, M.T. Lin, and K.W. Edwards, Phys. Rev. Letters 26, 984 (1971).

38. See, for example, G.L. Kane, "Phenomenology of High Energy Processes," invited talk presented at the 1973 Meeting of the Division of Particles and Fields of the APS, Berkeley, 1973.

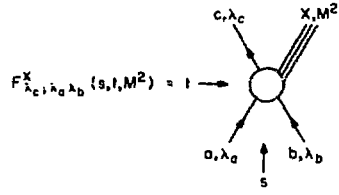

Figure 1. (a) Illustrates the amplitude
$$F^X_{\lambda_c;\lambda_a\lambda_b}(s,t,M^2)$$
for the inclusive process a + b → c + X, where particles a, b, and c have helicities λ_a, λ_b, and λ_c, respectively.

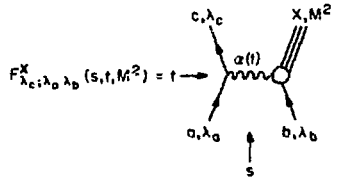

Figure 1. (b) Illustrates the diagram contributing to
$$F^X_{\lambda_c;\lambda_a\lambda_b}(s,t,M^2)$$
when s/M^2 is large and t/s is small so that the exchange of a leading Regge pole α(t) dominates.

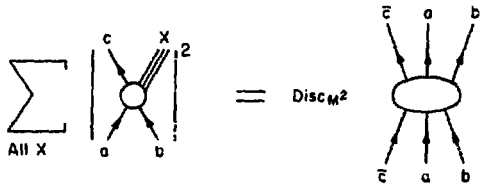

Figure 2. Illustration of the generalized optical theorem, which relates the square of the amplitudes for a + b → c + X summed over all X to the discontinuity of the forward 3 to 3 amplitude $ab\bar{c} \to ab\bar{c}$.

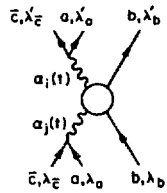

Figure 3. (a) Illustrates the resulting 3 to 3 forward amplitude when the Regge pole dominated amplitude for $a + b \to c + X$ in Figure 1b is squared and summed over all states X.

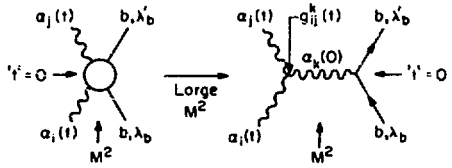

Figure 3. (b) Shows that at large M^2 the Reggeon particle forward scattering amplitude is given by the exchange of a Regge pole $\alpha_k(o)$ in the crossed channel. The coupling $g^k_{ij}(t)$ is the triple-Regge coupling.

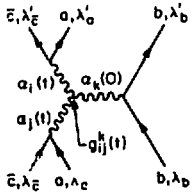

Figure 3. (c) This is the so-called triple-Regge diagram resulting from substituting the large M^2 behavior (b) and (a).

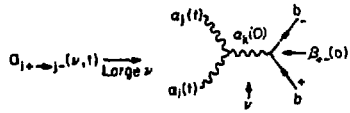

Figure 4. (a) Illustration of the forward Reggeon particle "flip" amplitude, which at large ν is given by the exchange of a Regge pole $\alpha_k(o)$ whose flip coupling $\beta_{+-}(o)$ vanishes by factorization arguments.

Figure 4. (b) Factorization arguments similar to those in (a) would predict a vanishing of

$$\rho_{11}^{H} \frac{d\sigma}{dt}(\pi^- p \to \rho^0 n)$$

in the forward direction.

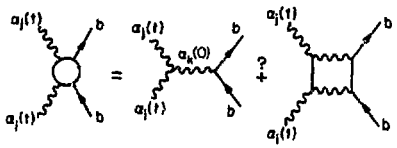

Figure 4. (c) Should one also consider Reggeon-cuts as well as Regge exchange when discussing the large ν behavior of the forward Reggeon particle scattering amplitude?

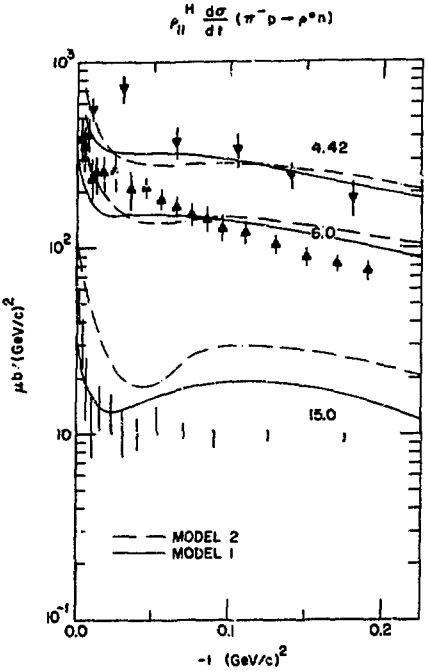

Figure 5. Experimental data on the small $|t|$ behavior of $\rho_{11}^H \frac{d\sigma}{dt}(\pi^- p \to \rho^0 n)$ (Figure from Ref. 17). The data show small $|t|$ spikes. The curves are from absorption model fits which have large π-cut (and A_2-cut) contributions at small $|t|$ producing the observed spike.

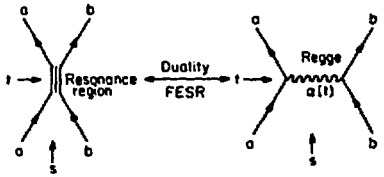

Figure 6. (a) Illustration of duality in particle-particle scattering. The small s resonacne region is related to the large s Regge region via Finite-Energy sum rules (FESR).

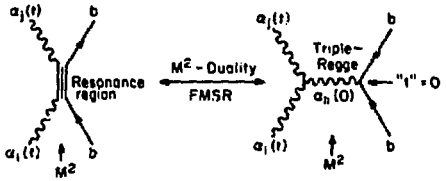

Figure 6. (b) Illustration of duality in Reggeon-particle scattering. The small M^2 resonance region is related to the large M^2 triple-Regge region via Finite-mass sum rules (FMSR).

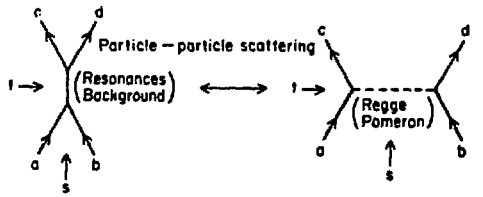

Figure 7. (a) Illustration of the two-component theory of duality for particle-particle scattering ab → cd. The s-channel resonances (background) are dual to t-channel Regge (Pomeron) exchange.

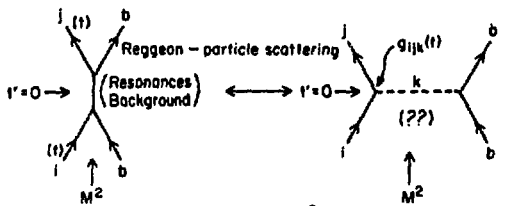

Figure 7. (b) Illustration of M^2-duality for Reggeon-particle scattering ib → jb. When $\alpha_i(t)$ and $\alpha_j(t)$ are ordinary Reggeons (not the Pomeron) than resonances (background) in the direct channel "build up" via FMSR the Regge (pomeron) exchange in the crossed channel. When $\alpha_i(t)$ or $\alpha_j(t)$ or both are pomerons the situation is more complicated (see text).

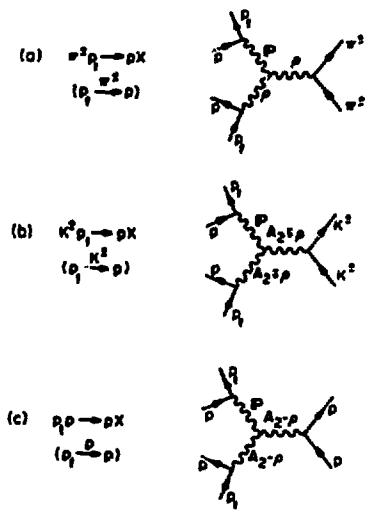

Figure 6. Leading triple-Regge terms responsible for type I polarization effects in the inclusive processes: (a) $\pi^\pm p_\uparrow \to pX$; (b) $K^\pm p_\uparrow \to pX$; (c) $p_\uparrow p \to pX$.

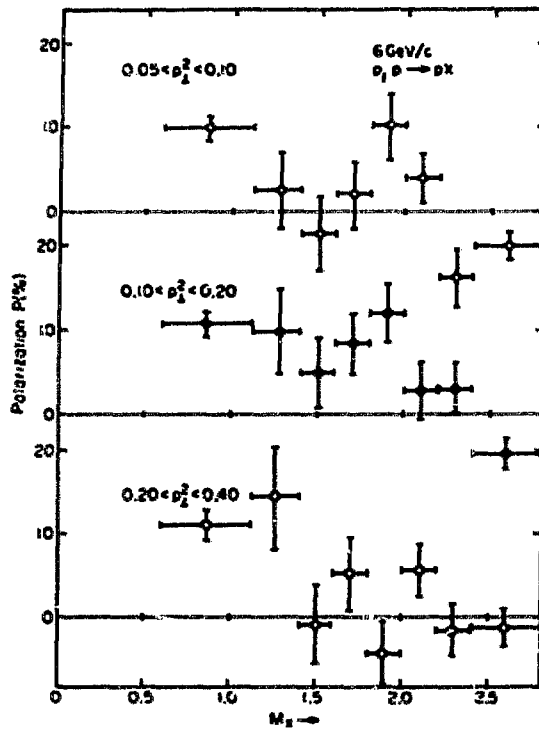

Figure 9. Experimental data on the type I polarization for the inclusive process $p_\uparrow p \to pX$ from a 6.0 GeV/c polarized beam experiment at Argonne (Ref. 25). The smallest mass (M_X) is the elastic polarization.

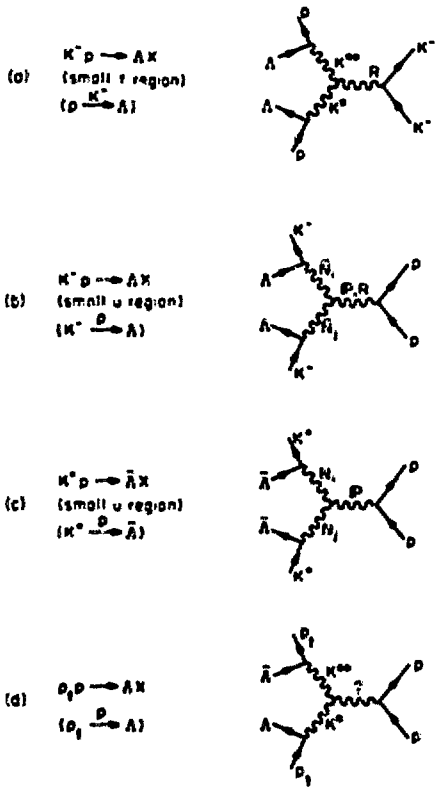

Figure 10. Leading triple-Regge terms responsible for type I polarization effects in the inclusive processes: (a) $K^-p \to \Lambda X$ (small t region); (b) $K^-p \to \Lambda X$ (small u region); (c) $K^+p \to \bar{\Lambda} X$ (small u region); (d) $p_\uparrow p \to \Lambda X$.

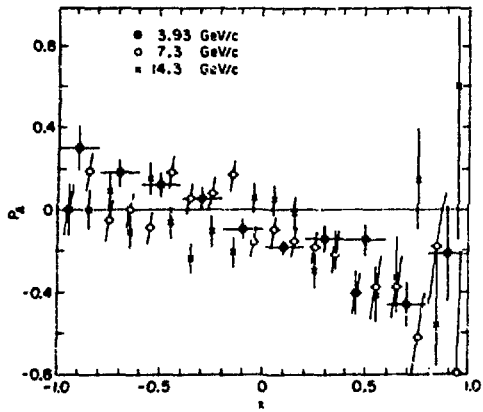

Figure 11. Experimental data on the Λ polarization for the inclusive process $K^-p \to \Lambda X$ at 3.93, 7.3, and 14.3 GeV/c. The region near x = -1.0(1.0) corresponds to the meson (baryon) exchange process shown in Figure 10a(b), (figure from Ref. 28).

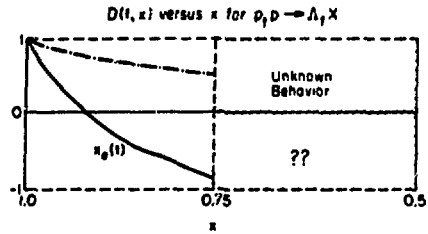

Figure 12. Expected behavior of the D(s,t,x) parameter for $p_\uparrow p \to \Lambda_\uparrow X$ versus x. The point $x_0(t)$ corresponds to the place where the unnatural and natural parity exchanges (see Figure 10d) are equal. The dot-dashed curve is expected if the natural parity dominates over the unnatural parity exchanges. The D(s,t,x) parameter is expected to scale (ie. be independent of s, D(s,t,x) = D(t,x)).

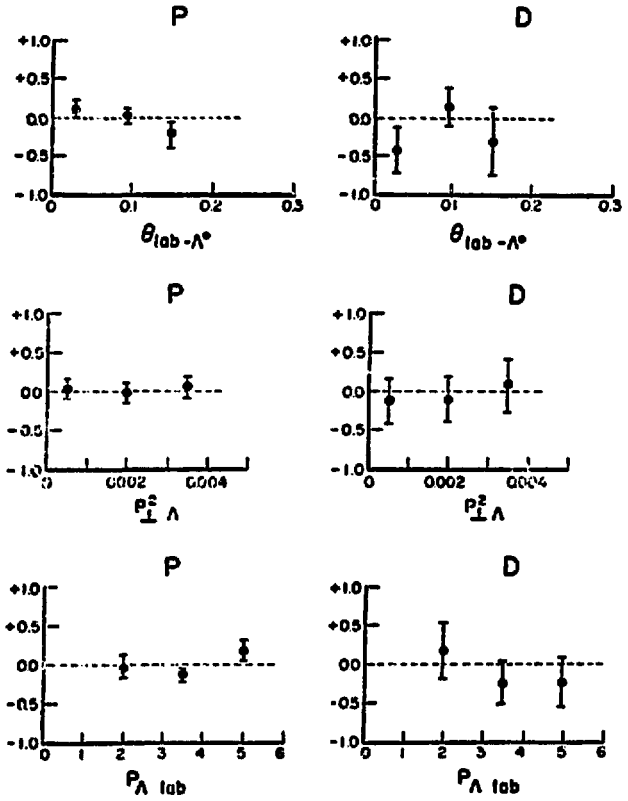

Figure 13. Experimental data on the type I Λ polarization P and the D parameter for the inclusive processes pp → ΛX from a 6.0 GeV/c polarized beam experiment at Argonne (Ref. 32).

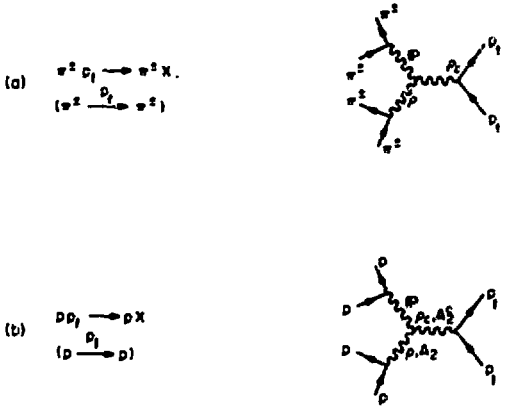

Figure 14. Leading triple-Regge terms responsible for type II polarization effects in the inclusive p_t processes: (a) $\pi^2 p_t \to \pi^2 X$; (b) $pp_t \to pX$, where σ_C (A_2^C) refers to the ρ (A_2) Regge cut contribution.

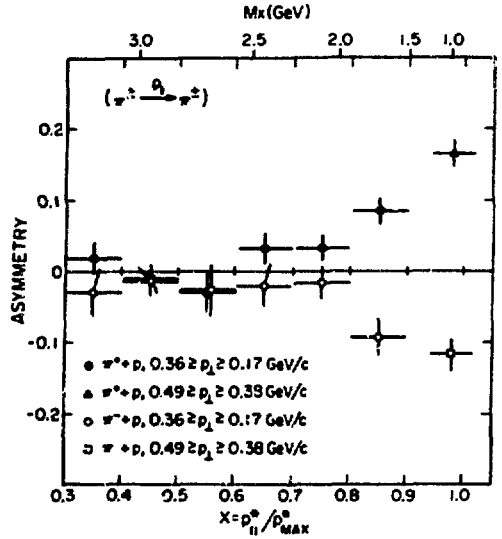

Figure 15. Experimental data on the type II polarized target asymmetry for the inclusive processes $\pi^{\pm} p_{\uparrow} \rightarrow \pi^{\pm} X$ at 8.0 GeV/c. (The data and figure are from Ref. 34).

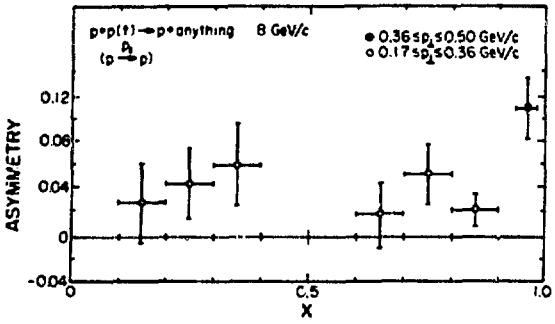

Figure 16. Experimental data on the type II polarized target asymmetry for the inclusive process $pp_{\uparrow} \rightarrow pX$ at 8.0 GeV/c versus x. (figure from Ref. 34).

Symmetries and Spin: Experimental Review

Michael Zeller
Physics Department
Yale University

Talk delivered at 1974 BNL Workshop on Polarized Targets.

Abstract

Experimental tests of time reversal and parity inversion invariance are reviewed with several proposals for future experiments included. Suggestions for possible experiments at BNL energies, and above, are made.

INTRODUCTION

In reviewing the experimental status of symmetries and spin, one is impressed by the small amount of data which presently exists testing invariance of the discrete symmetries of time reversal and parity inversion at BNL energies. In light of this, we will discuss a few salient experiments in order to obtain some perspective into the types of quanties that one might measure and the typical accuracies which have been obtained.[1] These experiments shall serve as a comparison and a point of departure for discussion of possible future experiments at BNL.

T TESTS - REVIEW

The first symmetry we shall consider will be that of time reversal invariance (T). In what follows, we will refer to Table I in which we briefly display various experimental results. The first column contains a description of the relevant measured variables, the second a result of the pertinent measurement, the third the laboratory kinetic energy of the incident particle, (in the case of a decay this is taken as zero), and the fourth the square of momentum transfer between relevant particles.

Since the observation of CP violation in K^0 decay,[2] there has been great interest in possible T violation in electromagnetic and/or weak interactions. This CP violation in K^0 decay is, of course, indirect evidence of T violation via the assumption of absolute CPT invariance. Certain measurements involving spin would be direct evidence of a T violating term in the interaction mechanism.

In the first order electromagnetic or weak decay of a particle into three or more particles one can look for a

dependence in the decay distribution of the type:

$$\langle\vec{\sigma}\rangle \cdot (\vec{P}_1 \times \vec{P}_2).$$

Such a term is odd under T reversal, and thus its presence would indicate a lack of T reversal invariance. A recent measurement of this type involves the β decay of free polarized neutrons.[3] For this experiment one measures the correlation between the neutron polarization vector, $\langle\vec{\sigma}_n\rangle$, and the normal to the plane formed by the momentum vectors of the decay electron and neutrino. In particular, one looks for a term in the decay rate of the type

$$D\,\langle\vec{\sigma}_n\rangle \cdot \frac{(\vec{P}_e \times \vec{P}_\nu)}{E_e \quad E_\nu}.$$

The parameter D is then a measure of T reversal violation. The most recent result is:

$$D = (1.1 \pm 1.7) \times 10^{-3}$$

which is consistent with T invariance.

Another experiment looking at weak decays, with larger q^2, is that of the correlation between the π and μ momentum vectors and the μ spin in the decay $K^0_L \to \pi^- \nu \mu^+$. An observation of a term of the type $\langle\vec{\sigma}_\mu\rangle \cdot \vec{P}_\pi \times \vec{P}_\mu$ would, of course, be a direct observation of T violation in K^0 decays, in which CP non-invariance has been seen. The most recent measurement employed precession of muon spin in a unique polarimeter, thus reducing possible systematic errors.[4] The results of this measurement are quoted in terms of Imξ where $\xi(q^2) = f^-(q^2)/f^+(q^2)$, the ratio of the form factors describing the hadron current involved in K decays. The measurement yielded Imξ= -0.060 ± 0.045, which is consistent with T reversal invariance.

The above experiments are effectively "static" measurements since the momentum transfers involved are so small. Moving to

scattering experiments at higher energies permits examination of a larger range of q^2. The simplest measureable interactions would involve spin 0- spin 1/2 scattering. However, examination of possible symmetry violating terms in the interaction show that those terms which violate T also violate P. Thus this class of experiments is not a good candidate to test T.

In spin 1/2 - spin 1/2 scattering, no such condition exists. Before discussing hadron-hadron interactions at BNL, we will examine inelastic electron scattering from polarized protons. Two measurements of this type have been made [5,6] and we shall concentrate on the most recent of these experiments.[6] These measurements are of interest to us because they demonstrate the attainable precision which one can expect in an experiment of this type employing a polarized target, and they are also concerned with radiation damage of a polarized target.

The measurements can be best described in Figure 1. In these diagrams the momentum vectors of the incoming and outgoing electrons, $\vec{k}_{in}$ and $\vec{k}_{out}$ respectively, are both in the plane of the paper. The proton, double line vector, has its spin vector out of this plane in Figure 1a and into the plane in Figure 1b; the cross sections for these figures are $\sigma_\uparrow$ and $\sigma_\downarrow$ respectively. An asymmetry which depends on $(\vec{\sigma}_p) \cdot \vec{k}_{in} \times \vec{k}_{out}$, $A = \frac{\sigma_\uparrow - \sigma_\downarrow}{\sigma_\uparrow + \sigma_\downarrow}$, would indicate a T violation. For elastic scattering A vanishes from CVC and hermiticity alone. Even with T invariance the asymmetry is non zero for two photon exchange diagrams, but comparison of e^- and e^+ scattering can remove this effect.

Since the recoil hadrons are not detected in this experiment, the effective polarization of the target is reduced to about

0.14 of that of the unbound protons. Furthermore, deterioration of target polarization due to radiation damage reduces the time averaged free proton polarization to less than its maximum; $\bar{P}_T \approx 0.22$. Hence, measured asymmetries were significantly smaller than "physics" asymmetries. Typical measured asymmetries were:

$$\epsilon = \frac{N_\uparrow - N_\downarrow}{N_\uparrow + N_\downarrow} \sim (0.06 \pm 0.03) \times 10^{-2}$$

where $N_\uparrow$ and $N_\downarrow$ are numbers of events detected in configurations a and b of Figure 1, respectively. Studies made of false asymmetries showed that systematic errors were less than the statistical uncertainties expressed above.[7] Thus, we see that one can make PPT measurements to an accuracy of a few parts in 10^4.

Figure 2 shows final results of the experiment, depicting A vs. missing mass, M_r, for different kinematic conditions. One can see no significant T violation in these data.

Since this experiment had an incident beam flux of 10^{11} electrons per second, radiation damage of the target became a concern. Quantative estimates of radiation damage are expressed in terms of the number of electrons per cm^2, φ_o, to cause target polarization to drop to 1/e of its initial, undamaged value. The target used was butanol cooled to 1^0 K in a 25kG field. For these conditions $\varphi_o = 4 \times 10^{14}$. Subsequent investigations of radiation damage [8] show that for He^3 (0.5^0K) cryostats or 1^0K at 50 kG, φ_o is significantly larger, i.e. $\varphi_o \approx 4 \times 10^{15}$ electrons/cm^2.

HADRON-HADRON TESTS

We now discuss hadron-hadron scattering experiments as they pertain to determination of T invariance. In particular, we

will concentrate on proton-proton elastic scattering using the notation as depicted in Figure 3. M is the scattering matrix and is shown in its most general form consistent with P and T invariance. Coefficients of the Pauli spin matrix operators are scalar functions of total cm energy and scattering angle. If one adds a term like

$$f\ (\sigma_P^1\ \sigma_K^2 + \sigma_K^1\ \sigma_P^2)$$

then T invariance is no longer valid.

The early experiments to test T involved comparison of left-right asymmetry, A (θ), at a particular angle θ resulting from elastic scattering of polarized protons from unpolarized protons, with the polarization induced, P (θ), on initially unpolarized protons by elastic scattering from the same target through the same angle. One can show that $\frac{d\sigma(\theta)}{d\Omega}\ (P(\theta) - A(\theta)) = 8 \cdot \mathrm{Im} f^* h$ where $\frac{d\sigma}{d\Omega}(\theta)$ is the unpolarized elastic scattering cross section into θ. Thus if the interaction is invariant under T, f=0 and this effect is zero. Unfortunately it would also be zero if both f and h had the same phase.

Predictions of non-zero (P-A) results have been published [9] and are shown in Figure 4 along with various experimental results. These predictions are based on a model introduced by Sudarshan [10] involving ρ and A_1 exchange as the mediators of neutron β decay: the ρ being responsible for the vector interaction, and the A_1 for the axial vector. The calculations are presumed correct only at the low energies shown, but we display the results to give an idea of what sort of effects one might expect. We note that in this model, the effects are significantly larger for n-p scattering than for p-p.

The above experiments are difficult because of systematic errors in comparing two distinct types of measurements. Another type of experiment, in which systematic errors would be greatly reduced can be made with a polarized proton beam or target and a measurement of recoil proton polarization in elastic p-p scattering. Figure 5 shows a schematic drawing of this experiment. One compares the final polarization of protons at an angle β to the final momentum vector, as shown, when the initial state is polarized at an angle α and the scattering angles are (θ^*, φ), with the polarization at angle α when the initial state is polarized at angle β and scattering angle $(\theta^*, \pi + \varphi)$. If P_A is the polarization as measured in Figure 5 a and P_B is that as measured in Figure 5b, one can show:

$$\frac{d\sigma}{d\Omega}(\theta^*)\,(P_A - P_B) = 8\mathrm{Re}\,f^* g \quad .$$

Predictions of $(P_A - P_B)$ using the above model are shown in Figure 6 along with experimental results [11] at 430 MeV. The measurement was made at $\theta^* = 65^0$ with results $P_A - P_B = 0.0019 \pm 0.0090$. Unfortunately the center of mass scattering angle was one where results are expected to be small. A similar experiment has been proposed for p-n elastic scattering at Nevis.[12]

A POSSIBLE BNL EXPERIMENT

One can consider doing an experiment of this type at the AGS with a polarized target, or at ANL with a polarized beam. We have designed an apparatus, to be used at the AGS, which would be applicable with a primary proton beam at small momentum transfer. We consider the region of small momentum transfer for two reasons:

1) since this is a double scattering experiment large cross sections are needed to obtain high statistical accuracy,

2) one can use the high analyzing power of carbon if the recoil proton momentum is kept small (<1.2 GeV/c).

For a polarized proton target magnet we have chosen a "Corrected Short Solenoid" design as suggested by Desportes.[13] This magnet, shown in Figure 7 consists of two superconducting short solenoid coils with currents in opposite relative directions. According to our calculations, this design permits the requisite homogeniety and has great flexibility for measurements in which the target is to be polarized in the scattering plane.

For our T measurement we chose a polarization angle such that $\alpha = \beta = 48^0$. This choice of angles permits simultaneous measurements at (θ^*, Φ) and $(\theta^*, \Phi + \pi)$. Transforming the spins from the center of mass to the lab and choosing appropriate magnetic fields to precess the recoil spins to permit analysis, we can specify the apparatus shown schematically in Figure 8.

The final analysis of the recoil proton spins can be accomplished with a carbon polarimeter employing proportional chambers. The analyzing power of such a device is approximately 0.3 and approximately 10^{-2} of the protons impinging on the the analyzer undergo an appropriate second scatter.

For the sake of discussion we have chosen an incident beam momentum of 20 GeV/c and a momentum transfer as shown of $-0.3(\text{GeV/c})^2$. Rate calculations from the factors shown in Table II then yield roughly 60 events per pulse detected after double scattering. This will yield 4.5×10^7 events in a 500

hour experiment. The statistical uncertainty on such an experiment would then be

$$\delta(P_A - P_B) = 0.8 \times 10^{-3}$$

Such a measurement would not be limited by systematic errors and would thus be comparable to the best present results for T tests.

P TESTS - REVIEW

We now turn to measurements of parity reversal invariance, (P). Tests of this sort are currently of great interest because of possible weak interaction, neutral current effects. We again have tabularized a set of experiments which are somewhat representative of the types of measurements that have been and can be, performed, (see Table 3).

The first class of experiments are observations of parity-forbidden decays of complex nuclear states. While these reactions do not explicitly involve spin, they are significant because of their sensitivity and because they demonstrate P violation in interactions strictly between hadrons. A recent example is the α particle decay from the 8.87 MeV ($J^P=2^-$) state in ^{16}O, $^{16}O(2^-,8.87) \rightarrow {}^{12}C + \alpha$.[14] If we characterize the fraction of parity violating interaction to parity conserving by a coefficient, p, then these forbidden transitions will measure $|p|^2$. The above mentioned experiment yielded a result $|p|^2 \simeq (0.26 \pm 0.11) \times 10^{-13}$, or $|p| \simeq (1.62 \pm 0.68) \times 10^{-7}$, i.e. the authors observed a statistically significant number of forbidden events. The complicated nuclear physics involved in these reactions makes specific model calculations difficult.

Gamma transitions in nuclei can also test parity violating effects. One looks for circularly polarized photons which are indicative of an interference between magnetic and electric transitions of the same multipole. In 1972 the world average for the polarization of γ's from ^{181}Ta was $-(4.9 \pm 0.6) \times 10^{-6}$.[15] This is, of course, a statistically significant observation of

parity violation, but relating these results to the parameter p is again made difficult because of the involvement of a complex nucleus.

An obvious experiment which would minimize the nuclear effects would be measurement of circular polarization in radiative capture of unpolarized neutrons on protons, $p(n,\gamma)d$, or radiative capture of unpolarized neutrons on deuterons, $d(n,\gamma)t$. The present published best value for the circular polarization in $p(n,\gamma)d$ is $P_\gamma = -(1.3 \pm 0.45) \times 10^{-6}$.[16] Further experiments have been proposed by a Glasgow, Sussex, Harvard, Darmstadt, Rutherford collaboration to be performed at the High Flux Reactor at Grenoble.[17] Their estimated accuracy of measurement on γ polarization is 1.5×10^{-7} and 2×10^{-6} for γd and γt final states, respectively.

An experiment relating to the circular polarization measurement is the measurement of the asymmetry of gamma rays produced in the capture of polarized neutrons on parahydrogen. This is effectively a search for a $\langle\vec{\sigma}_n\rangle \cdot \vec{p}_\gamma$ term in the reaction cross section for $n + p \rightarrow d + \gamma$: $\vec{p}_\gamma$ is the decay γ's momentum vector. This experiment has also been proposed for the Grenoble reactor.[18] It has been shown that the circular polarization would involve a $\Delta I=0$ parity violating force while the asymmetry involves the $\Delta I=1$ force.[19]

At a slightly higher energy, an experiment is presently under way to measure the asymmetry in the total proton-proton cross section due to reversal of incident proton helicity.[20] This experiment is being performed at the Los Alamos Van de Graff using longitudinally polarized protons of 15 MeV incident on a

3 atm. gas H_2 target. Both transmitted beam and outscattered particles are detected, and the systematic errors on the asymmetry are kept to $\sim 10^{-7}$, (a large factor in reducing systematic errors is that the incident proton polarization is reversed at a rate of 1 kHz). At present no asymmetry has been observed to the order of $\backsim 2$ parts in 10^6.[21] Calculations of the magnitude of this asymmetry due to the weak interaction yield $A \backsim \frac{P}{Mc} \times 10^{-6}$ [1], where P is the incident proton momentum and M is the proton mass. If these expectations are correct, the asymmetry in the above experiment would be on the order of $A \backsim 1.7 \times 10^{-7}$.

A similar experiment has been proposed employing the polarized proton beam at Argonne.[22] In this case, at 12.5 GeV, one might expect an asymmetry of $\backsim 10^{-5}$. The experiment is a measurement of total cross section via transmission. A sensitivity of $\sim 10^{-6}$ is expected since the full beam, $\sim 10^9$ protons per pulse, will be used.

The advent of a polarized electron source for SLAC [23] has prompted two proposals to investigate parity violation in inelastic electron-proton scattering. As with the above experiments these measurements look for an asymmetry in cross section as a function of electron helicity when scattering from unpolarized protons. Such an asymmetry implies a $\langle \vec{\sigma}_e \rangle \cdot \vec{p}_e$ force which would violate parity reversal invariance.

The first of these measurements involves the kinematic region of $q^2<(GeV/c)^2$ at incident electron energies $12<E<20$ GeV.[24] This is an attempt to observe an axial vector electromagnetic current of hadrons which might exist if there is formal connection between the weak and electromagnetic hadronic currents. Manifestations of such a current might have been seen in the circular polarization of photons discussed earlier. If the structure function involving the parity violating terms has a q^2 dependence similar to that of the weak interaction, one might observe significantly larger effects in the proposed momentum transfer range. The sensitivity of this experiment to an asymmetry is $\delta A \sim 0.2 \times 10^{-4}$ with some models predicting A as large as 0.18.

The other proposal involves the q^2 range of 10 $(GeV/c)^2$ and is an explicit attempt to observe effects due to a weak neutral current.[25] Since it presently appears that there are weak neutral currents of neutrinos, it is of significant interest to see if weak neutral currents of charged leptons exist also. Since a signature for the weak interaction is the lack of P invariance, this experiment becomes a sensitive test for the existence of such currents. If one uses a mass for the neutral vector boson propagator of 76 GeV then one might expect parity violating effects on the order of 4×10^{-3}. Thus the experiment is designed to have a sensitivity of $\delta A \sim 10^{-4}$.

POSSIBLE HIGH ENERGY EXPERIMENTS

We now turn to a possible experiment to investigate parity violation in hadron-hadron interactions at BNL energies and above. In particular we propose measuring the asymmetry in the differential cross section, $d\sigma/dt$, in elastic p-p scattering as a function of the helicity of the target proton. Adding a term of the sort $p\cdot(\sigma_p^1 + \sigma_p^2)$ to the operator in Figure 3 will yield such a parity violation. Any other parity violating term either is not T invariant or does not obey the exclusion principle. If σ_+ and σ_- represent $d\sigma/dt$ for target protons polarized parallel and antiparallel to the incident proton beam, respectively, then the desired asymmetry is:

$$A(t) = \frac{\sigma_+ - \sigma_-}{\sigma_+ + \sigma_-} = \frac{2\ \mathrm{Re}\ p^*\ (a + h)\ \cos\ \theta^*/2}{\sigma},$$

where θ^* is the center of mass scattering angle and σ is the unpolarized $d\sigma/dt$. As expected, we would measure the interference between a parity violating amplitude and parity conserving amplitudes.

If we assume that the odd parity amplitude, p, is proportional to the square root of the weak cross section and the other amplitudes are proportional to the square root of the strong cross section, and that these amplitudes have the same phase, the asymmetry becomes:

$$A(t) \sim \frac{\sqrt{\sigma_{wk}(t)}}{\sqrt{\sigma_{st}(t)}} \cos\ \theta^*/2$$

The cross section for elastic p-p scattering is shown in Figure 9.[26] The behavior of this cross section at high energies has been described using a Chou-Yang Model [27] employing electromagnetic form factors to describe internal proton structure.[28] If one assumes that the success of this model indicates the same parton structure for the strong interaction as observed for the electromagnetic, and one further assumes that the weak form factors are also the same as the electromagnetic, the asymmetry A(t) becomes independent of t except for the factor cos $\theta^*/2$. The magnitude of A would then be $\sim 10^{-5}$. Many assumptions have been made in the above conjecture, and it would be extremely interesting to investigate this asymmetry both at as large momentum transfer as possible and at a moderate momentum transfer.

We would thus propose two experiments to measure p-p elastic scattering from longitudinally polarized protons. The first of these is at large momentum transfer, $t \simeq -10(\text{GeV/c})^2$, and the experimental apparatus is shown in Figure 10. We propose an incident beam of $\sim 10^{11}$ protons per pulse on our target. The same compensated, short solenoid polarized target magnet will be used as described earlier. In order to reduce systematic errors and increase data rate, the experiment is performed for the projectile scattering to either side of the incident beam. For this apparatus, we use the following parameters:

$$d\sigma/dt = 10^{-34}\ \text{cm}^2/(\text{GeV/c})^2$$
$$\Delta t = 1\ (\text{GeV/c})^2$$
$$\Delta\varphi/2\pi = 0.093$$

With 500 hours of data acquisition, one could obtain $\sim 6 \times 10^5$ events. Assuming a target polarization of 0.80 we expect a statistical accuracy of $A = 1.5 \times 10^{-3}$. While this does not approach the expected weak value of 10^{-5}, it would be useful to verify P invariance at large momentum transfers to this accuracy.

Two, and possibly three, advantages are gained if the same experiment were to be performed at smaller momentum transfer, say $t \simeq -1.4 (\text{GeV/c})^2$.

1) The cross section is increased by four orders magnitude, a Δt bite of $0.2 (\text{GeV/c})^2$ then yields $\sim 10^9$ events, or $\delta A \simeq 6 \times 10^{-4}$, [29]
2) One could analyze the recoil proton to measure spin-spin correlations, i.e. the Wolfenstein A parameter, to an accuracy of 0.2.
3) If the weak interaction obeys a simple G_E^4 (t) dependence, dashed curve in Figure 9, parity violating effects might be increased by a factor of 3 over other t regions.

Again, we do not reach the desired accuracy of 10^{-5}, but this would be another interesting experiment.

SUMMARY

To summarize, we have seen T invariance is well validated by present experimental evidence, but can be tested at higher energies to a few parts in 10^3. Parity violation effects have been observed at a significantly higher level than one might expect via a simple weak interaction. We have shown that it is possible to test P invariance at BNL energies, and above, to an accuracy approaching this limit.

REFERENCES

1. An excellent review of low energy studies of P and T has been published by E.M. Henley, Ann. Rev. of Nuc. Sci. 19 367 (1969).

2. J.H. Christenson, J.W. Cronin, V.L. Fitch, R.Turlay, Phys. Rev. Letters 13, 138 (1964); A.Abashian et al., Phys. Rev. Letters 13, 243. (1964).

3. R.I. Steinberg, P. Liaud, B. Vignon, V.W. Hughes, Phys. Rev. Letters 33, 41 (1974).

4. J. Sandweiss, J. Sunderland, W. Turner, W. Willis, L. Keller, Phys. Rev. Letters 30, 1002 (1973).

5. J.R. Chen et al., Phys. Rev. Letters 21, 1279 (1968).

6. S. Rock et al., Phys. Rev. Letters 30, 748 (1970).

7. S. Rock, "Search for T-Violation in the Inelastic Scattering of Electrons from a Polarized Proton Target". PhD Thesis UCRL 20041 (197) (unpublished).

8. C.C. Morehouse, "Radiation Damage in Butanol Polarized Proton Targets at 50 Kilogauss and o.5°K". DESY Preprint (1971) (unpublished).

9. R. Bryan and A. Gersten, Phys. Rev. Letters 26, 1000 (1971). Sources of Data: 142 MeV (P-A), C.F. Hwang, T.R. Ophel, E.H. Thorndike, R. Wilson, Phys. Rev. 119, 352 (1960); 142 MeV A, G.F. Cox, G.H. Eaton, C.P. Van Zil, O.N. Jarvis, B. Rose, Nucl. Phys. B4, 353 (1968); 635 MeV, R. Zulkarneev, V. Nadezhdin, V. Satarov, in High Energy Physics and Nuclear Structure, Ed. S. Devons (Plenum, New York, 1970), p. 771.

10. E.C.G. Sudarshan, Proc. Roy. Soc. Ser. A 305, 319 (1968).

11. R. Handler et al., Phys. Rev. Letters 19, 933 (1967).

12. Nevis Proposal No. 12, "A Study of Time Reversal Invariance In Proton-Neutron Triple Scattering", P.J. Limon et al. (1970).

13. H. Desportes, in IInd International Conference on Polarized Targets ed. G. Shapiro, (LBL500,UC-34 Physics, National Technical Information Service, Springfield, Va.)p.57 (1971).

14. H. Hattig, K. Hunchen, H. Waffler, Phys. Rev. Letters 25, 941 (1970).

15. E.D. Lipson, F. Boehm and J.C. Vanderleeden. Phys. Rev. C4, 2218 (1971), and C5, 932 (1972).

16. V.M. Labashov, et al., Nucl. Phys. A197, 241 (1972).

17. Rutherford Proposal No. 132, "Search for Parity Violation in Radiative n-p and n-d Capture", G. Bishop and W.D. Hamilton (1973).

18. Rutherford Proposal, "Gamma Ray Asymmetry in Radiative n-p Capture of Polarized Neutrons" R. Wilson, P. Liaud, R. Steinberg, V. Bignon (1973).

19. G.S. Dinilov, Phys. Letters 18, 40 (1965).

20. L.A.S.L. Proposal 137, "Search for Parity Violating Contribution to the Scattering of Hadrons", H. Frauenfelder, D. Nagle, R. Mischke (1972).

21. C. Hwang, priviate communication.

22. Argonne Proposal No. P-354, "Parity Violation in Proton Scattering Processes", H.L. Anderson et al. (1973).

23. SLAC Proposal E80, "Measurement of Asymmetry in Deep Inelastic Scattering of Polarized Electrons by Polarized Protons", V.W. Hughes et al. (1971).

24. SLAC Expt. E95, "Experimental Tests for an Electromagnetic Axial Vector Current of Hadrons in Inelastic Scattering of Polarized Protons", C. Prescot et al. (1973).

25. SLAC Proposal, "Measurement of the Influence of Weak Neutral Currents in ep Scattering", R. Wilson et al. (1973).

26. R. Slansky, "High-Energy Hadron Production and Inclusive Reactions", Yale Report 3075-50 (1973) (unpublished).

27. T.T. Chou and C.N. Yang Phys. Rev. 170, 1591 (1968).

28. N. Byers, "High Energy pp Elastic Scattering and the Chou - Yang Formula", XIth International School of Subnuclear Physics, Erice, Sicily (1973) (to be published).

29. One would use a 1°K target to permit rapid polarization reversal necessary to keep systematic errors consistant with statistical uncertainties.

TABLE I

T Invariance Tests

MEASUREMENT	RESULT	E_{lab} (GeV)	q^2 $(GeV/c)^2$
$\langle\vec{\sigma}_n\rangle \cdot (\vec{P}_\nu \times \vec{P}_e)$ n β Decay	$D = -(1.1 \pm 1.7) \times 10^{-3}$ [3]	0	10^{-6}
$\langle\vec{\sigma}_\mu\rangle \cdot (\vec{P}_\pi \times \vec{P}_\mu)$ $K^0_{\mu_3}$ Decay	$\mathrm{Im}\,\xi = -(0.060 \pm 0.045)$ [4]	0	0.13
$\langle\vec{\sigma}_p\rangle \cdot (\vec{K}_{in} \times \vec{K}_{out})$ $ep_\uparrow \rightarrow e\Gamma$	$A \sim 0.02 \pm 0.02$ [6]	12-18	0.41
P (θ) - A (θ) pp → pp	< 0.01 [9]	0.145- 0.635	~ 0.1
Spin Check pp → pp	0.0019 ± 0.009 [11]	0.430	~0.1
Spin Check pn → pn	$\sim 10^{-3}$ (proposed) [12]	0.550	~0.1
Spin Check pp → pp	$\sim 3 \times 10^{-3}$ (suggested)	~20	~0.3

TABLE II

Calculations pertaining to T Test - pp elastic scattering.

Incident Energy: 20 GeV/c

Momentum Transfer: $-0.3\ (GeV/c)^2$

Cross Section: $d\sigma/dt \approx 5\ mb/(GeV/c)^2$

Solid Angle: $\Delta\phi/2\pi = 0.035$
$\Delta t = 0.1\ (GeV/c)^2$

Target: 10 cm length
0.08 g/cm^3 free proton density
0.8 polarization.

Beam: 10^{10} protons per pulse
1500 pulses per hour
500 hours of data acquisition

Analyzer: 4 cm thick carbon
.1[illegible] x 10^{-2} sr = solid angle for dectection of recoil proton

$\frac{d\sigma}{d\Omega} = 130\ \frac{mb}{sr}$

TABLE III

MEASUREMENT	RESULT	E_{lab}	q^2
Forbidden Transition $\|p\|$	$= (1.62 \pm 0.68) \times 10^{-7}$[24]	0	~0
$^{16}O\ (2^-) \rightarrow {}^{12}C + \alpha$			
Circular Polarization of γ:			
$^{3He}T_a$	$P_\gamma = -(4.9 \pm 0.6) \times 10^{-6}$[18]	0	~0
$d(n,\delta)t$	$P_\gamma = -(1.3 \pm 0.45) \times 10^{-6}$[16]	0	~0
$d(n,\gamma)t$	$\delta P_\gamma < 1.5 \times 10^{-7}$ (proposed)[17]		
Asymmetry of δ			
$n_\uparrow\ p \rightarrow d\delta$	$\delta A \sim 6 \times 10^{-8}$ (proposed)[18]	~0	~0
$\sigma_{tot} - \vec{p}_\uparrow p$	$A < 2 \times 10^{-6}$ [21]	0.015	---
$\sigma_{tot} - \vec{p}_\uparrow p$	$\delta A \leq 10^{-6}$ (proposed)[22]	12.5	---
$(\vec{\sigma}_e) \cdot \vec{p}_e$	$\delta A \sim 2 \times 10^{-5}$ (proposed)[24]	12.20	<5
$e_\uparrow p \rightarrow e\Gamma$	$\delta A \sim 10^{-4}$ (proposed)[25]	12.20	~10
$d\sigma/dt$ $\vec{p}_\uparrow p \rightarrow p\ p$	$\delta A \sim 1.5 \times 10^{-3}$ (suggested)	25	10
	$\delta A \sim 6 \times 10^{-4}$ (suggested)	25	1.4

T TEST IN $e p_\uparrow \to e \Gamma$

LOOK FOR AN ASYMMETRY IN

$$\langle \vec{\sigma}_p \rangle \cdot (\vec{k}_{IN} \times \vec{k}_{OUT})$$

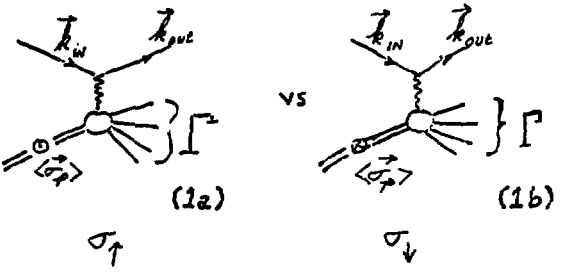

(1a) (1b)

$\sigma_\uparrow$ $\sigma_\downarrow$

ONE PHOTON EXCHANGE

$$A = \frac{\sigma_\uparrow - \sigma_\downarrow}{\sigma_\uparrow + \sigma_\downarrow}$$

$$\varepsilon = \text{MEASURED ASYMMETRY} = \frac{N_\uparrow - N_\downarrow}{N_\uparrow + N_\downarrow}$$

$$\varepsilon \approx (0.6 \pm 0.3) \times 10^{-3}$$

Figure 1. Schematic outline of T reversal test in $e_\uparrow p \to e\,\Gamma$.

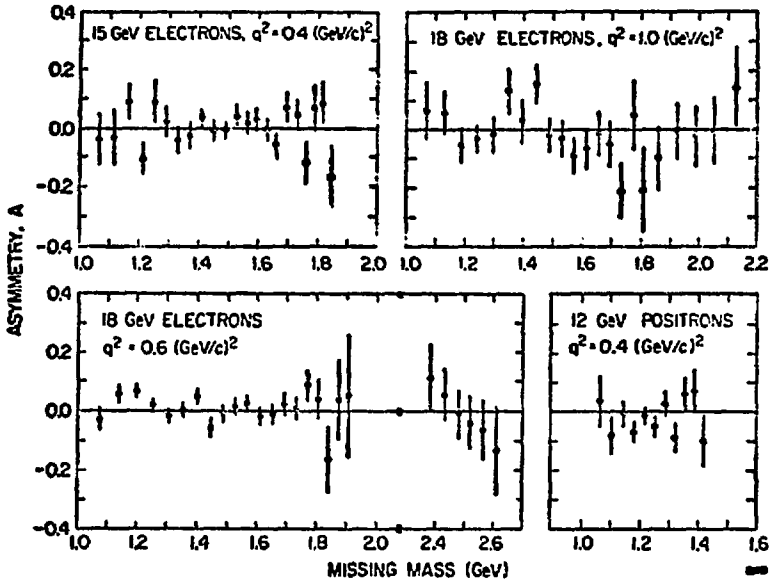

Figure 2. Asymmetry results from $e_{\uparrow}p \rightarrow e\,\Gamma$ experiment.[6]

P-P SCATTERING:

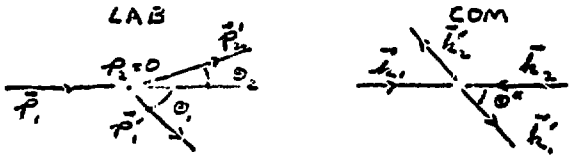

COORDINATES FOR M:

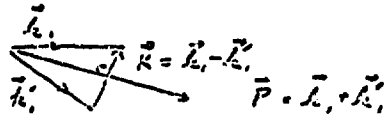

$$\vec{N} = \vec{P} \times \vec{K}$$

VECTORS TRANSFORM AS FOLLOWS:

	$\vec{k}_1$	$\vec{k}_1'$	$\vec{P}$	$\vec{K}$	$\vec{N}$	$\vec{\sigma}$
T	$-\vec{k}_1'$	$-\vec{k}_1$	$-\vec{P}$	$\vec{K}$	$-\vec{N}$	$-\vec{\sigma}$
P	$-\vec{k}_1$	$-\vec{k}_1'$	$-\vec{P}$	$-\vec{K}$	$-\vec{N}$	$\vec{\sigma}$

$$\sigma_N^i = \vec{\sigma}^i \cdot \hat{N} \quad \text{ON } i^{TH} \text{ PARTICLE}$$

$$M = a + ic(\sigma_N^1 + \sigma_N^2) + m(\sigma_N^1 \sigma_N^2) + g(\sigma_P^1 \sigma_P^2 + \sigma_K^1 \sigma_K^2) + h(\sigma_P^1 \sigma_P^2 - \sigma_K^1 \sigma_K^2)$$

INVARIANT UNDER T + P

ADDING $f(\sigma_P^1 \sigma_K^2 + \sigma_K^1 \sigma_P^2)$ VIOLATES T

Figure 3. Kinematic factors involved in pp elastic scattering.

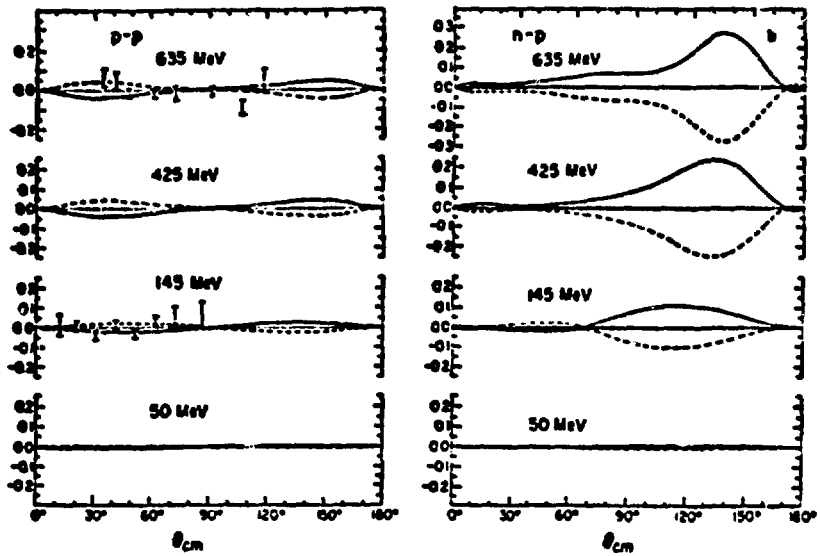

Figure 4. Predictions and results of P(θ) - A(θ) measurements in pp elastic scattering.

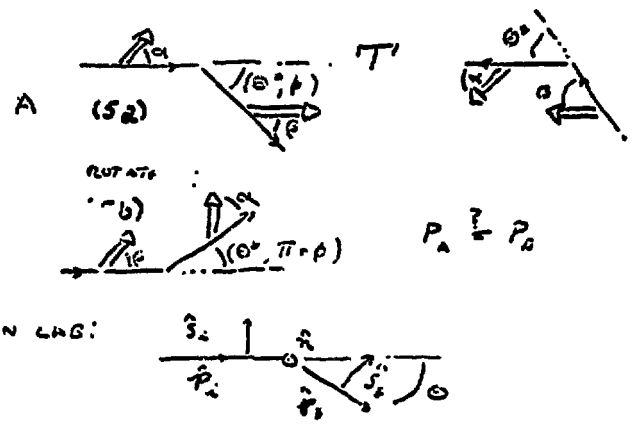

$$P_A \overset{?}{=} P_B$$

$$\langle \vec{\sigma}_3 \rangle = \frac{I_0}{I} \prod \left(P + D \langle \vec{\sigma} \rangle_i \cdot \hat{n} \right) \hat{n}$$
$$\cdot \left(A \langle \vec{\sigma}_i \rangle \cdot \hat{p}_i + R \langle \vec{\sigma}_i \rangle \cdot \hat{s}_i \right) \hat{s}_i$$
$$\cdot \left(A' \langle \vec{\sigma}_i \rangle \cdot \hat{p}_i + R' \langle \vec{\sigma}_i \rangle \cdot \hat{s}_i \right) \hat{p}_3 \Big]$$

$$P_A - P_B = \left[(A + R') \cos\Theta - (A' - R) \sin\Theta \right] \cdot \sin(\alpha + \beta)$$

IF T' GOOD $\quad \tan\Theta = \frac{A+R'}{A'-R}$

$\Rightarrow P_A = P_B$

IN GEN.: $P_A - P_B = 8\, R\, S^* g / I_0$

Figure 5. Schematic outline of T test via "spin check".

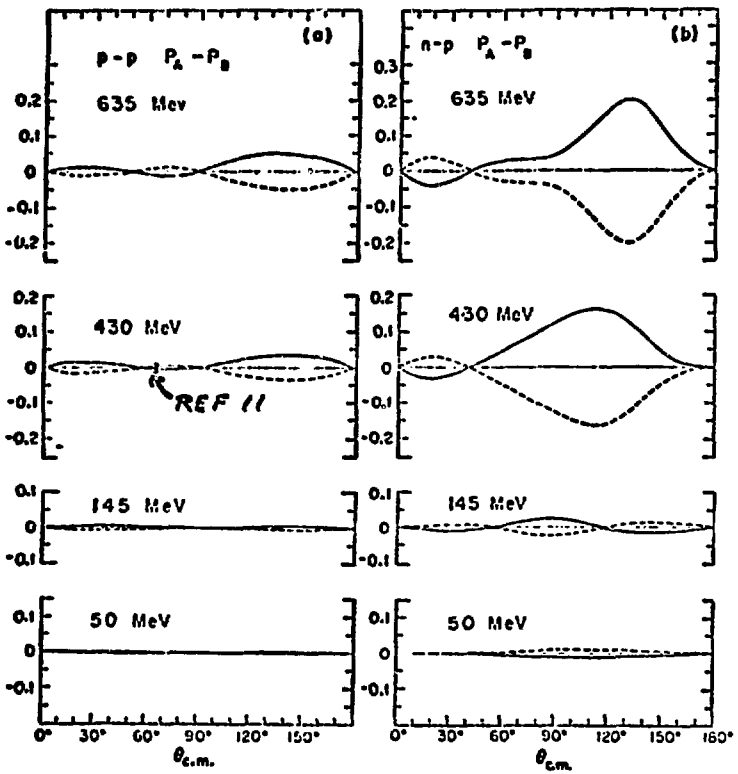

Figure 6. Predictions and results of "spin check" in pp and np elastic scattering.[9,11]

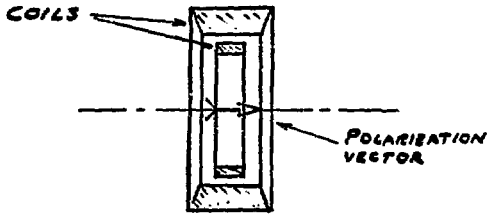

Figure 7. Compensated short solenoid magnet for a polarized proton target.[13]

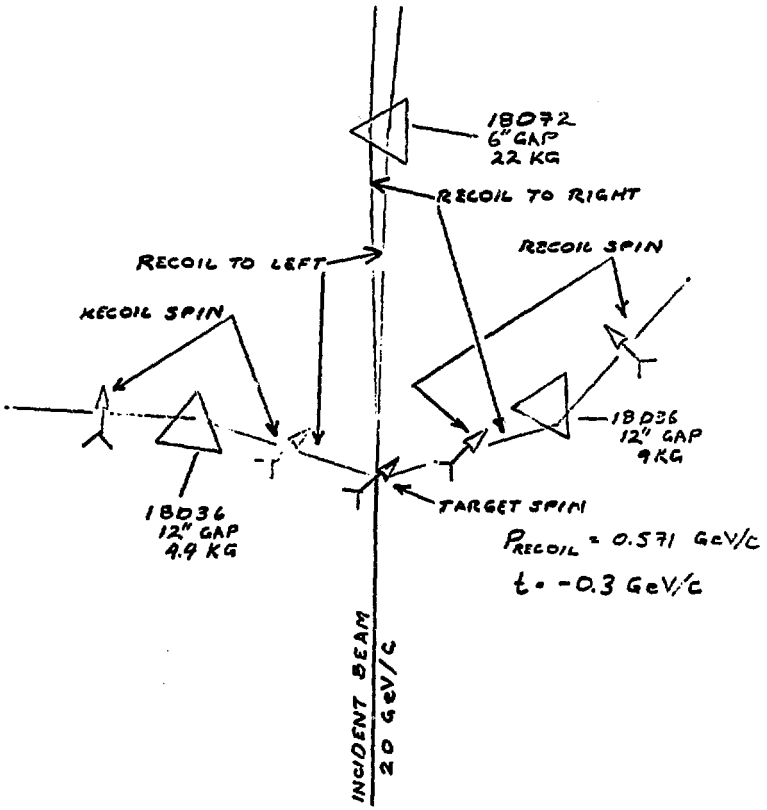

Figure 8. Experimental layout for "spin check" at BNL.

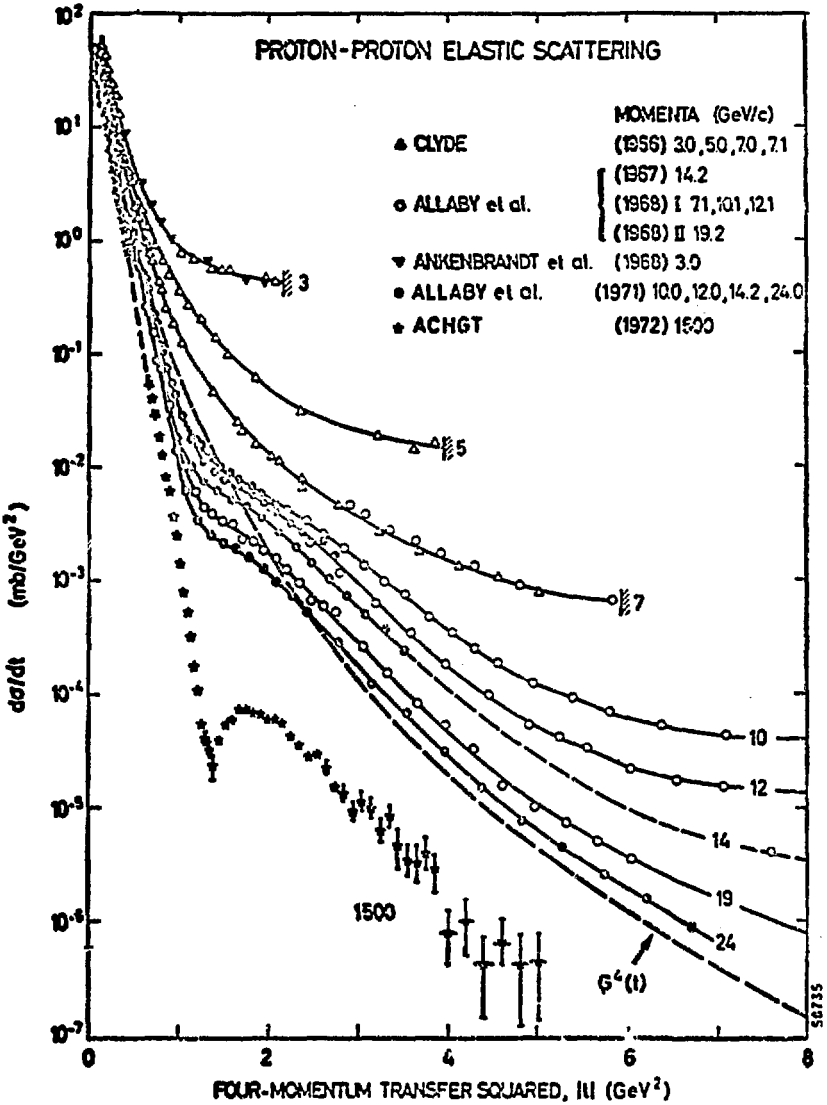

Figure 9. Differential cross sections for pp elastic scattering at various energies.

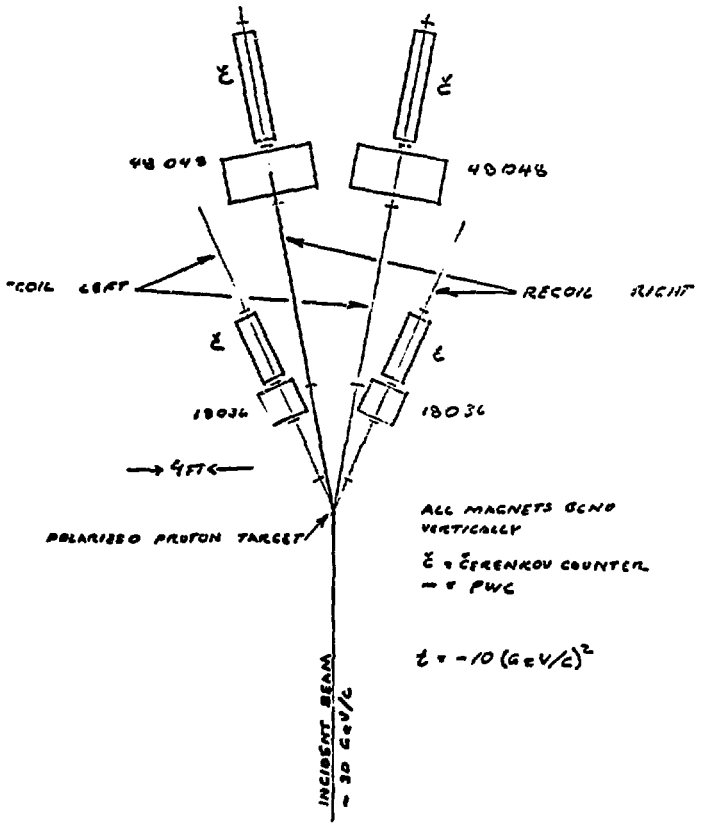

Figure 10. Experimental layout for P test at BNL.

CALT-68-461

A Spin for Everybody *†

G. C. FOX
California Institute of Technology, Pasadena, California 91109

ABSTRACT

We give a qualitative discussion of areas in which future polarization measurements will be useful. There are many rewarding experiments but most of them are rather hard.

---

*Work supported in part by the U. S. Atomic Energy Commission. Prepared under Contract AT(11-1)-68 for the Sa.. Franicsco Operations Office, U. S. Atomic Energy Commission.

†Invited talk for the Workshop on Polarization, Brookhaven National Laboratory, June 3-7, 1974.

I. INTRODUCTION

First I will apologize and indeed lament that I write as an elder statesman and not as an active analyzer of polarization data. I wrote a rather similar article three years ago but have since only been an educated observer. This may not matter too much as experimental and theoretical progress has been slow since then. Further, three years in the wings have not damped my ardour and I am confident that new vistas of polarization phenomena will be opened up in the next few years by such improved techniques as polarized electron and proton beams, "R and A" magnets and frozen spin targets in multiparticle spectrometers. The table below summarizes some major areas in high energy physics and indicates whether progress with the next round of experiments is likely to need polarization information.

The reader will notice my childhood training: a bias to strong interactions! In fact, I will treat weak and electromagnetic interactions only briefly and not mention symmetry tests at all. The latter were nicely covered in Zeller's talk at this conference.

I will discuss the four main strong interaction topics of this table in Secs. II - V. Section VI is reserved for the amplitude analysis of quark scattering processes possible in weak and electromagnetic reactions. Snappy conclusions will be found in Sec. VII.

Status	Field	Typical Reactions
	Strong Interactions	
*	Meson Spectroscopy: Field may be revolutionized by next round of spectrometer experiments.	$K^- n \to A_1^- \Lambda$
*, **	Baryon Spectroscopy: Well studied with and without polarization information information. Very successful: SU(3) quark model, etc.	$\pi^- p(\uparrow) \to \pi^0 n$ $K^+ p(\uparrow) \to K^0 \pi^+ p$
	t(u) channel Dynamics: two to (quasi) two scattering of well loved particles:	
*	Energy Dependence: NAL wins	$\pi^- p \to \pi^0 n$
**	Amplitude (t) Dependence: lower energy accelerators dominant.	$\pi^- p(\uparrow) \to K^0 \Lambda$ $K^- p(\uparrow) \to \omega \Lambda$ $pp\ (\uparrow) \to pp$
	t Channel Dynamics: Inclusive scattering.	$ab \to cX$
*	Generally no polarization effects expected except in	
*, **	Triple Regge } kinematic regions	
*, **	High p_T } where polarization could be sizeable.	$pp\ (\uparrow) \to \pi X$ $p(\uparrow) p(\uparrow) \to \pi X$

	Current (Weak and Electromagnetic Interactions)	
*	Scaling	$\ell p \to \ell X$, $\nu p \to \mu X$
**	Polarized Scaling Functions	$\ell(\uparrow)p(\uparrow) \to \ell X$
*	Neutral Currents	$\nu p \to \nu X$, $\ell p(\uparrow) \to \ell X$
	Symmetry Tests	
?	?	$\sigma_{tot}(p(\uparrow)p)$ $e\,p(\uparrow) \to eX$

Here * indicates that next round of experiments will be dominated by unpolarized and ** by polarized data.

II. SPECTROSCOPY IN FORMATION EXPERIMENTS

A. Continue the Good Work

The important role that polarization information in simple reactions such as $\pi^{\pm} p(\uparrow) \rightarrow \pi^{\pm} p$, plays in phase shift analyses is well documented.[1,2,3] The baryon spectrum as discovered by phase shift analysis of πN and $\bar{K}N$ scattering remains perhaps the most successful result in strong interaction phenomenology -- helping to spawn and nurture such far-reaching ideas as SU(3), SU(6), quark model and duality. However, one may well ask if further progress can be made. For instance although there is some useful work to be done at lower energies [4] -- filling in gaps and ambiguities in the phase shift analysis, with $d\sigma/dt$, polarization and R and A studies, there seems unlikely to be any major changes in the πN analyses below a lab momentum of 2 GeV/c. The main limitation is the difficulty of disentangling low spin broad resonances from nonresonant background. The region from 2 to 5 GeV/c is the next area to be tackled in πN scattering but it seems that the uncreasing density of overlapping resonances and just simply more spin states, renders the prospect for conventional phase shift analyses rather bleak. However, it appears still worthwhile to set up a systematic program of experimental study with both polarized and unpolarized targets in this region. One will still be able to identify the high spin resonances as conventional loops in the argand diagram

but interpretation may well concentrate on comparison of theoretical models with amplitude analyses of the data. The latter could be helped by theoretical dispersion relations[1] and experimental R and A measurements.

At low momentum transfer one would study the transition from resonances (s-channel) to Regge (t-channel) dominance. One should be able to finally understand the meaning of the mysterious dip in $\pi^{\pm}p$ elastic $d\sigma/dt$ at $t = -3(GeV/c)^2$.[2] More generally, the situation at high momentum transfers is really rather interesting. One should find there the low energy extrapolation of whatever mechanism (constituent interchange,[5] gluon exchange[6]) governs high p_T phenomena seen so dramatically at ISR and Fermilab. Such detailed low energy amplitudes could lead to new insights into the high energy mechanism. For instance the interchange model predicts that $\alpha_\rho(t)$ will asymptote to -1 as $t \to -\infty$: a finite energy sum rule analysis[7] finds evidence for the second wrong signature nonsense zero (WSNZ) of the ρ at $\alpha = -2$ ($t \approx -2.5$ $(GeV/c)^2$) and so contradicts this prediction. No doubt the analysis is not yet unambiguous but it is illustrative of the utility of low energy measurements in testing high energy models. Clearly accurate $\pi^{\pm}p$ polarization data for $t \approx -2.5$ $(GeV/c)^2$ is needed to clarify this -- just as the double zero in the polarizations at $t \approx -0.6$ $(GeV/c)^2$ indicated the first WSNZ $\alpha_\rho = 0$. In fact both πp[8] (see Fig. 1) and pp[9] (Fig. 2) show sizeable polarizations at large -t. It is interesting to note that the interchange

model predicts large energy independent mirror symmetric polarization for $-t > 6$ (GeV/c)^2 in πp scattering[10] whereas gluon exchange would not appear to naturally give any polarization effects.[11] We take up high p_T again in a later section. Here we remember that these studies are, of course, most direct at high energy: However, cross sections are bigger at low energy and so maybe a region around 5 GeV/c is the best compromise.

B. Ericson Fluctuations

Frautschi[12] has pointed out that this energy region, 2 to 5 GeV/c, is the best for looking for the cross section fluctuations expected in a statistical model for hadrons. The basic idea is that the amplitude is made up of a sum over a large number N of resonance contributions. Explicitly

$$\text{Im } A_{\text{resonance}}(s, t = 0) \propto \sum_{n=1}^{N} \gamma^2 (R_n \to \pi N) \quad . \tag{1}$$

This averages to the smooth Regge form in a manner made popular by duality.[3] However, the normal laws of statistics lead us to expect a fluctuations in this smooth average (1) of order $1/\sqrt{N}$. i.e.,

$$\frac{d\sigma/dt \text{ (fluctuating)}}{d\sigma/dt \text{ (smooth)}} \propto 1/N$$

which in the statistical bootstrap of Hagedorn and Frautschi[12] tends to zero rapidly as $s \to \infty$ for the number of resonances $N \propto$

exp $(\sqrt{s}/m_\pi)/s^{7/4}$ increases exponentially with energy. The range of 2 to 5 GeV/c is a compromise to make N large enough to allow statistical treatment and N small enough to give significant fluctuations. Experimental evidence for this effect has been reported recently: first,[14] Fig. 3 shows the asymmetry A

$$A = (N_+ - N_-)/(N_+ + N_-) \qquad (2)$$

where $N_\pm$ denote the number of events coming from dividing data at nominal momentum of 5 GeV/c into an upper and lower momentum slice differing by about 50 MeV/c. As expected A = 0 for small t but at large -t, A appears definitely nonzero for $\pi^+ p$ scattering. This observation of fluctuations in $\pi^+ p$ and not in $\pi^- p$ elastic can be explained by a larger number of resonances N in the second reaction. A similar effect is seen in an analysis[15] of the structure in $\pi^\pm p$ backward scattering (Fig. 4a) in terms of Ericson fluctuations (Fig. 4b). This interpretation corresponds to a resonance spacing of 20 KeV in $\pi^- p$ scattering at 5 GeV/c. Clearly we stand no chance of finding such resonances by conventional analysis. It is my feeling that the above work is not yet convincing as they have ignored the contribution of high-spin resonances on the leading trajectories (N_α, Δ_δ, etc.) which must be added to statistical fluctuations of low-spin resonances.

Nevertheless, the point of this and the previous discussion is to indicate that the region above 2 GeV/c is rich in good physics even if

phase shift analysis fails. So indeed one should continue the good work and both fill in those naughty gaps and move on to higher energy.

C. High Threshold Reactions

When discussing πN elastic scattering, we bemoaned the difficulty of extracting information on the low-spin resonances. This is conveniently solved by studying reactions with high thresholds so that the high spin states are suppressed. A nice example of this is the recent observation[17] (Fig. 5), in the production reaction $\pi N \to \pi N^*$, of a low spin ($J = 1/2$ or $3/2$) resonance near the ωp threshold with a mass of 1820 MeV and a width of 120 MeV. Undeniable evidence for this resonance would come from a phase shift analysis of the formation experiment $\pi^+ n \to \omega^0 p$ using polarization data to find the phase as well as the mass variation, characteristic of a resonance. For this particular example, the indicated formation experiment is probably impossible but there are many reactions, e.g.,

$$\pi^- p \to K^0 \Lambda$$
$$\pi^+ p \to K^+ \Sigma^+$$
$$\pi^- p \to \eta n,$$

whose systematic study with polarized and unpolarized targets would allow significant improvement in our knowledge of the baryon spectrum from conventional phase shift analysis. The hyperon reactions will even give you R and A information automatically. By choosing the

appropriate final states, one can vary the threshold and so study the low spin resonances over a wide range of mass. Figure 6 illustrates the threshold suppression rather effectively by comparing reactions which are equal (from exchange degeneracy) at high energy. The reaction with the higher threshold is suppressed by an order of magnitude at low energies.

Our poor knowledge of that grand-daddy high threshold reaction, $\bar{p}p$ annihilation, may be considered a worldwide catastrophe. A long series of experiments on many different processes have failed to reveal unambiguous evidence for meson resonances M^* formed in

$$\bar{p}p \rightarrow M^* \rightarrow \text{some annihilation channel}.$$

Direct methods having failed, it seems that the only hope is a systematic attempt to garner enough data on the theoretically tractable processes:

$$\bar{p}p \rightarrow \pi^+\pi^-,\ K^+K^-,\ \text{etc.}$$

to render an essentially unique phase shift analysis possible: current work allows too many ambiguities.[18] Clearly one needs both polarized and unpolarized target data with a concentration of data at the lowest practicable beam momenta[19] ($p_{lab} \lesssim 1.5$ GeV/c). This allows study of lowest possible $\bar{p}p$ mass region which has two advantages: first there are fewer spin states and hence fewer parameters; secondly, the

averaging of closely spaced resonances to Regge limit will be less perfect. The region with $p_{lab} < 0.8$ GeV/c is important, but difficult with a beam of $\bar{p}$'s: maybe one pion exchange is sufficiently reliable to allow use of the indirect process[20]

$$\pi^- p \to (\bar{p}p)n$$

in a $\bar{p}p \to \pi^-\pi^+$ phase shift analysis. Study of the extrapolation problems for high mass $\pi^+\pi^-$ systems[21] in

$$\pi^- p \to (\pi^+\pi^-)n$$

would be important in this regard.

Finally we remark that $\bar{p}p \to \pi^+\pi^-$, K^+K^- are good reactions to study possible Ericson fluctuations (as the effects are enhanced compared with πN elastic because the Regge exchange terms are smaller).

D. Quasi-Two-Body Final States

One of the most impressive results in formation reactions is the recent phase shift analysis of $\pi N \to \pi\pi N$.[22,23] The data is expressed, in the isobar model, as a sum of amplitudes for

$$\pi N \to \pi\Delta, \quad \pi N \to \rho N, \quad \pi N \to \epsilon N .$$

Typical argand plots for these reactions are shown in Fig. 7--clearly one is able to observe resonances by conventional phase shift analysis in quasi-two-body final states. There are two main reasons for such a study: first one is able to obtain the basic resonance parameters

(mass, width) of inelastic states that decay more strongly into ρN and $\pi\Delta$ than πN. For instance, four low spin (P_{11}, P_{13}, D_{13}, P_{33}) states around 1700 MeV were found, suggested, or confirmed in this work.[23] Secondly, one can test several new symmetry predictions: broken $SU(6)_W$ seems to relate $\pi\Delta$ and πN couplings very successfully while vector dominance relates ρN and γN couplings.[19, 22, 23, 24]

Clearly it would be good to continue this analysis using polarized target information--it will help the analysis in the same way that $\pi N \to \pi N$ polarization data helps elastic phase shift analyses. Note that polarization might be particularly valuable in $\pi N \to \rho N$ where we should be able to see the resonance contribution

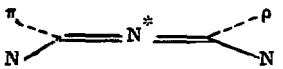

interfering with the purely real

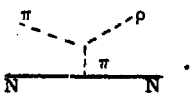

The importance of polarization information is even more obvious in the search for exotic resonances by phase shift analysis in KN and NN scattering. Here the whole background amplitude, e.g.,

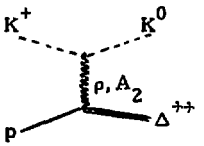

for the $K^+p \to K^0\Delta^{++}$ quasi two body component of $K^+p \to K^0p\pi^+$, is real from exchange degeneracy. One expects large polarization effects from the interference of (imaginary) inelastic Z^* resonance

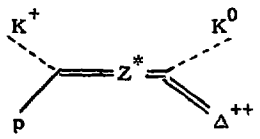

with this background amplitude. Figure 8 shows this expected polarization asymmetry[25] integrated over the Δ^{++} decay angles, and even more structure will be found on examining correlations between polarization of target and Δ^{++} decay. Actually more data on $K^+p \to K^0\pi^+p$, with an unpolarized target and $1 \leq p_{lab} \leq 1.5$ GeV/c, is urgently needed to allow a definitive study of this reaction analogous to the SLAC-LBL $\pi\pi N$ work.

In my Berkeley talk, I discussed the utility of polarized proton beam data on $p(\uparrow)p \to n\Delta^{++}$, $p_{lab} \sim 1.1$ GeV/c, to study a possible analogue of the Z^* in pp scattering. Figure 9 compares the very similar total cross section behavior in K^+p and pp scattering with the rapid rise at the first inelastic threshold. Classically this corresponds[25] to a strong force (e.g., π exchange in $pp \to n\Delta^{++}$) which could create the exotic resonance. Finally we note that the new P_{33} resonance (possibly) seen[23] at 1700 MeV in

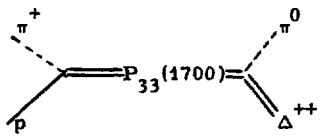

is a natural SU(3) analogue of

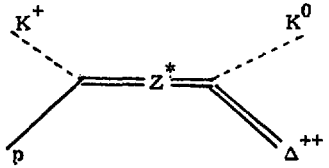

Classically the ρ exchange force creates the $P_{33}(1700)$ and ρ plus A_2 exchange the Z^* ($\approx$ 1900).

III. SPECTROSCOPY IN PRODUCTION EXPERIMENTS

The advent of multiparticle spectrometers is expected to herald a golden age of spectroscopy -- especially for meson resonances, e.g.,

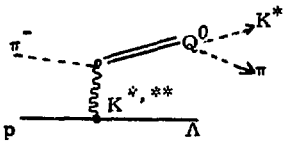

The role that polarization can play in this revival is somewhat limited. For instance, polarizing the proton in the above reachon and/or observing the polarization of recoil lambda, is not expected to help the $K^*\pi$ spectroscopy. Rather it will be a sensitive handle on the exchange dynamics of the process $\pi^- p \to Q^0 \Lambda$: This subject is, of course, interesting but I will treat it in the next section.

(i) For polarization to help the spectroscopy, it is clearly most useful if the polarized particle is at the same vertex as the resonance being studied. Examples with a polarized beam are

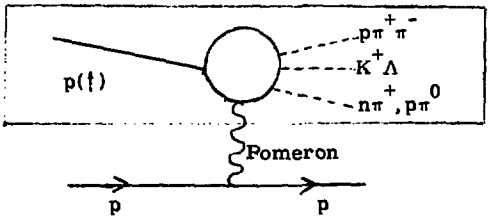

where we study Pomeron-polarized proton scattering to various final states. So this is "just" like formalism, of previous section with a Pomeron replacing incident π. As in the great Z^* search in $K^+p \to K^0\pi^+p$, we hope that polarization will be particularly sensitive to difference between

resonance

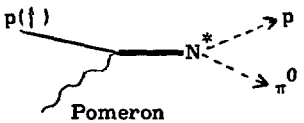

and Deck

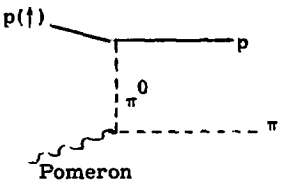

interpretation of low mass diffraction dissociation.

There are many other examples:

(ii)

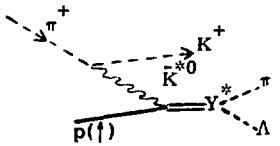

etc.

should be relatively easy to study (trigger is a fast K^+) with a polarized target in a multiparticle spectrometer. Note that as exchange is K^* and not K, this production process can advantageously (compared with K^-p formation experiment) study Y*'s that have a strong $\bar{K}^*p$ and weak $\bar{K}p$ coupling.

(iii) Again

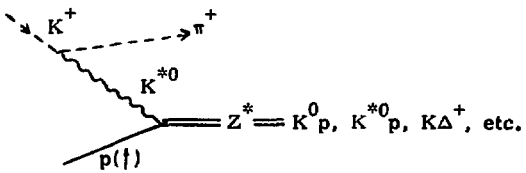

allows I = 0 and 1 Z^* study. Compared with the formation experiment discussed in last section, we have advantages of selecting inelastic $Z^{*'}$s with large $K^{*0}p$ coupling and getting polarization information in a perhaps somewhat easier fashion experimentally than the direct process $K^+p(\uparrow) \rightarrow K^0\pi^+p$.

(iv) A final series of reactions involves baryon exchange: namely

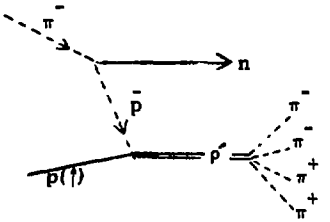

and again one hopes to use phase information given by polarization to distinguish broad resonant ρ' from a Deck-like nonresonant enhancement.

Such studies of meson spectroscopy with an unpolarized target in streamer chamber[26] or triggered bubble chamber[27] are only now being analyzed. It is clearly inappropriate to plan a detailed polarized target program at this time but it seems likely that this should be one of the early experiments when polarized targets are successfully operated inside a multiparticle spectrometer.

IV. t-CHANNEL DYNAMICS OF EXCLUSIVE REACTIONS

The study of well loved reactions (i.e., simple two to (quasi) two body processes e.g., $\pi^- p \to \pi^0 n$, $\pi^- p \to \rho^0 n$) has uncovered several striking ideas. However, even the most ardent fan of this field, must admit that it has stagnated in the last few years. We can understand the disease and perhaps also find a cure by discussing its successes. First there is the study of energy dependence which has revealed the importance of Regge trajectories. The detailed study of these and

their associated cuts has been hampered by the fact that only one trajectory (that of the ρ) has been reliably extracted as a function of t. Further progress demands the determination of other trajectories so that we can tell if the ρ results ("perfect" linear trajectory with slope $\approx 1\ (\mathrm{GeV/c})^{-2}$) are a fluke or the norm. We can hope that the wide energy range offered by Fermilab will lead to the desired progress.

A second successful area in two body dynamics is the study of symmetry relations: here we have SU(3), quark model, and less solidly EXD and duality. In general, these symmetry predictions have been well studied although more information on their violation, e.g., what is energy dependence of EXD breaking, would be helpful. A third area is the determination of the t dependence of amplitudes. This produced some surprises for although the energy dependence of our data indicates Regge effects, the t dependence of the imaginary part of the amplitude shows geometric or absorptive features. A great problem is to reconcile these conflicting ideas and in spite of the immerse amount of work on Reggeized absorption models,[28] there is as yet no convincing theory.[16,29] It is in this third area of t dependence of amplitudes that the pre-Fermilab accelerators can be of most value. Thus most evidence we have, suggests that the t dependence only varies slowly (i.e., logarithmically) with energy and so by studying details of t dependence at Fermilab, one loses more from smaller counting rates than one gains from proximity to asymptotia. Currently our detailed knowledge of nondiffractive

amplitudes is confined to two: the nonflip N and spinflip F ρ exchange amplitudes. These are most precisely found by an amplitude analysis of πN scattering and a reasonably upto date summary of this is contained in Figs. 10 and 11. The last figure shows the dramatic difference in the t dependence of N and F: the zero in Im N at $t \approx -0.15$ and in Im F at $t \approx -0.6$ $(GeV/c)^2$ corresponds to peripheral scattering centered at 1 fm. We do not want to discuss here the various theoretical deductions with their sunday caveats (you can find many of them in Ref. 16). Rather we emphasize that the basic task of the next series of two-body measurements must be to extend this type of phenomenology to different reactions. Questions one can ask are:

What happens in spinflip 2 amplitudes D? Speculation ranges from perfect Regge theory--with Im D $(-0.6) = 0$; to perfect peripheral scattering with Im D $(t \approx -1.2\ (GeV/c)^2) \approx 0$.

What happens in single flip amplitudes F for other exchanges? Thus for ρ exchange, the geometric and Regge WSNZ (wrong signature nonsense zero) predictions agree that Im $F(t \approx -0.6) = 0$. For other exchanges (π, B, K^*, ** etc.) this is no longer true, and the cults are divided as to whether zero will religiously follow geometric or Regge prediction.

What happens in "evasive" amplitudes, i.e., nonflip amplitudes N where factorization predicts that any simple pole will vanish at $t=0$. An example is the helicity amplitude

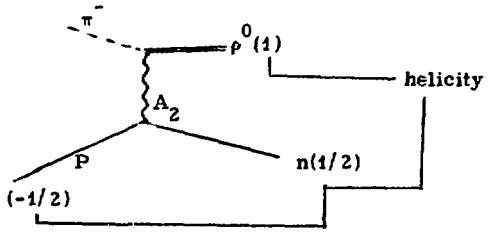

The current slightly depressing state of theory is such that persuasive arguments have been found for almost every possible extrapolation through our two ρ exchange amplitudes. As exemplified by our three questions above, we make further progress by establishing the amplitude structure in many different reactions. Things are not as bad as they look, because the symmetry schemes suggest that we do not need to measure all reactions: rather we must measure the dependence on exchange quantum numbers and spinflip in a few well chosen reactions and then we predict all remaining reactions by multiplying these by overall constants given by the symmetry theory.

Having defined the program, we now turn to its experimental execution. As we have mentioned above and is exhibited in Figs. 10 and 11, a striking feature of the known amplitudes is the very different behavior of both real and imaginary parts and flip and nonflip amplitudes. It follows that it is very difficult to disentangle the amplitudes from differential cross section measurements.

$$\frac{d\sigma}{dt} \propto |N|^2 + |F|^2 \qquad (3a)$$

Rather we need a complete set of observables, which for our simple example of $0^-1/2^+ \to 0^-1/2^+$ scattering, is

$$P = 2\,\mathrm{Im}\,(NF^*)/(|N|^2 + |F|^2) \tag{3b}$$

$$\hat{R} = 2\,\mathrm{Re}\,(NF^*)/(|N|^2 + |F|^2) \tag{3c}$$

$$\hat{A} = (|N|^2 - |F|^2)/(|N|^2 + |F|^2) \tag{3d}$$

The amplitudes in Fig. 10 and 11 come from solving Eqs. 3(a→d) for N and F using experimental values of the four observables. This gives the amplitudes upto a common phase which is determined (in πN scattering) by dispersion relations (FESR). This straightforward procedure is termed amplitude analysis.

One can try to find the amplitudes by supplementing a partial set of experimental observables with innocent theoretical assumptions to obtain unique amplitudes. This is often useful but its dangers are illustrated in Fig. 12 which shows innocent amplitude analyses of P and $d\sigma/dt$ for $\pi^- p \to K^0\Lambda$ and $K^- n \to \pi^-\Lambda$. The four different innocent assumptions give wildly different results: there have been more reasonable work since then[30, 31] but there are no truly innocent assumptions, and the only safe approach is to measure a complete set of observables. This automatically requires polarization information (P) and even (R and A) data with both a polarized target and measurement of recoil spin. The latter is only feasible to measure in elastic

scattering (where high cross-section allows you luxury of the inefficient measurement of final proton spin with a polarimeter) and reactions involving final state hyperons whose weak decay automatically gives their polarization .

We finish this section by discussing some specific reactions one would like to investigate with polarization information. The exact choice of reaction is not important for as indicated above, symmetry relations enable one to predict one reaction from another. For instance, the quark model predicts that the spinflip amplitude in $\pi^+ p \to \pi^0 \Delta^{++}$ is (up to an overall constants) identical to that in $\pi^- p \to \pi^0 n$ which has, as shown in Fig. 11, already been determined quite well. The main criterion should be to get enough statistics to, in fact, reliably determine the amplitudes from measured observables . Reference 25 shows how one can estimate in advance the necessary statistics by an elementary Monte Carlo calculation. The above discussion implies that the reactions mentioned below should be viewed as a typical and not a specific list.

The amplitude analysis of πN scattering will surely continue but as Figs. 10 and 11 show, it is hard to improve the current analyses for $|t| < 0.6\ (\mathrm{GeV/c})^2$: at larger t, we not only need an improvement in the basic data but also phenomenological study into ways of estimating the unknown overall phase present in any experimental amplitude analysis. The advent of a polarized proton beam at the ZGS has made an experimental program[32] of amplitude analysis in NN elastic

and maybe also charge exchange scattering possible. The current measurements[32, 33] are not yet complete enough to give new insight: hopefully these data could tell us

a) are there any amplitudes with A_1 or D ($I = 0$ partner of A_1) quantum numbers?

b) Structure of double flip and evasive nonflip (helicity transition $++ \rightarrow --$) amplitudes?

The latter may be easier to see in np CEX as current belief is that such spinflip amplitudes are only large for $I=1$ ρ and A_2 exchange. In any case the pp elastic measurements should be made over a range of energies so that we can tell apart asymptotic (diffractive), nonleading (ρ, A_2, f, ω exchange) and transient (low energy garbage effects). The rather nice polarization data[34, 35] on np CEX is shown in Fig. 13. This should be zero if EXD was exact (all amplitudes in np CEX should be real. The energy independent nonzero value has defied unambigous theoretical interpretation. We need to pin down which amplitudes have the sizeable imaginary parts responsible for polarization. As well as the point b) above, np CEX can also tell us about

c) Structure of unnatural parity (π and B) exchange.

The usefulness of R and A measurements and hence amplitude analysis in hypercharge exchange processes

$$\pi^- p \rightarrow K^0 \Lambda$$

$$K^- n \rightarrow \pi^- \Lambda \quad \text{etc.},$$

has been proclaimed for at least four years.[36] As reviewed in Ref. 16, there is much controversy as to t dependence of imaginary part of nonflip even signature (A_2, K^{**}) exchange (does it or does it not vanish at $t \approx -0.2$ $(GeV/c)^2$ like ρ-exchange). These data should both settle this and study EXD between K^* and K^{**} in greater detail. (Are violations more pronounced in nonflip than spinflip amplitudes?) As exemplified in Fig. 6, there is plenty of evidence that violations of EXD decrease with increasing energy. Correspondingly amplitude analysis of hypercharge exchange processes over a range of energies is indicated.

Figures 13 and 14 indicate excellent quality of the recent polarization data on np CEX and $\pi^- p \to K^0 \Lambda$[37] respectively. Unfortunately current theory is at a loss to interpret it until R and A measurement allow the amplitude analysis. This situation should be contrasted with that for the recent $pp \to \Delta^{++} n$ data[38] taken with the polarized beam at Argonne. The overall polarization shown in Fig. 15, is very similar to np CEX. This is by itself insufficient to allow a useful analysis, but the combination of p and Δ^{++} spin information gives nontrivial constraints. In his talk at this meeting, Field[39] describes some neat quark model tests: I believe one may be able to perform an innocent amplitude analysis by supplementing the data with some or all of the following assumptions:

a) Only amplitudes allowed by quark model are nonzero. (This leaves one with six out of possible sixteen amplitudes).

b) A_1 exchange is negligible.

c) Estimate the small nonflip amplitudes at $p\bar{n}$ vertex by quark model relation to $K^+n \to K^0\Delta^{++}$. This should be reliable--upto overall constants as they are net single spinflip amplitudes for which Regge theory is good.

d) Assume imaginary parts are peripheral.

Note that the theoretical lessons one learns from $pp \to n\Delta^{++}$ are similar to those in np CEX. If the former reaction is easier, it may be better to concentrate on it rather than spread one's polarization butter too thinly and try to measure both.

In the experiment $p(\uparrow)p \to (p\pi^+)n$, one gets polarization asymmetry effects not only from interference between production amplitudes for a given $p\pi^+$ spin-parity state: rather one also gets contributions from interference between different $p\pi^+ J^P$ states. (These were formally discussed in Sec. III). Figure 16 shows this second type of effect and the rough agreement with expectations from one pion exchange

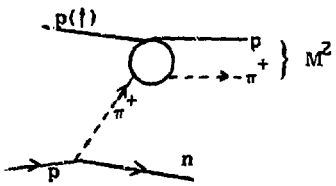

and low M^2, π^+p polarizations.

The two effects can be distinguished by (π^+p) mass and angular dependence: the original paper[38] has more details.

One can briefly mention a few more quasi-two-body reactions. Polarization data for $\pi^- p \to (\rho^0 \text{ or } \omega^0)n$ would be very valuable: even if a complete amplitude analysis is not feasible, we have learnt so much from unpolarized data that the polarization can be readily interpreted[25, 39] e.g., there is the well-known direct test for exchange of A_1 quantum numbers in $\pi^- p \to \rho^0 n$ or its EXD partner in $\pi^- p \to \omega^0 n$. A large contribution of the latter type was recently postulated[40] to explain violations of π-B exchange degeneracy.

We expect very little polarization in $\pi^+ p \to \pi^0 \Delta^{++}$ because the quark model (which agrees with unpolarized Δ^{++} density matrix elements Fig. 17) predicts purely spinflip amplitudes. Typical predictions are shown in Fig. 18: a nonzero polarization can come from either violations of the quark model[41] or absorption after crossing from s to t channel. The related reaction $K^- p \to \pi^- Y^*(1385)$ with decay Λ polarization observed has already been analyzed.[39,42] This work needs to be repeated with higher statistics and study of possible background under $Y^*(1385)$.

This last reaction is typical of many hypercharge exchange reactions producing resonances. Others are[39]

$$K^- p \to \rho \Lambda$$

$$\pi^+ p \to K^{*+} \Sigma^+$$

$$K^- p \to \omega Y^*(1385) \text{ etc.}$$

If the final hyperon polarization is observed, measurements off a polarized target will allow a complete amplitude analysis. This program is particularly attractive because, apart from restriction to K and K^* exchange, these reactions have sufficient spin complexity to answer the various theoretical questions posed throughout this section.

A wide open field is backward scattering: miserabile dictu the cross sections are small, the data is correspondingly poor and transient low energy effects are present upto ≈ 5 GeV/c where finally an asymptotic theory may be even qualitatively correct. There are no simple well-studied reactions like $\pi^- p \to \pi^0 n$ (data on single trajectory exchange $\pi^- p \to p\pi^-$ is quite poor) and the theories seen quite unconstrained and unpredictive. I fear therefore that any measurements short of a complete set of observables will be difficult to interpret. More optimistically one could hope that a systematic set of maybe incomplete measurements would establish an orderly phenomenology and so set the theories on the right track. Useful polarization and $d\sigma/dt$ measurements are discussed by Storrow and Winbow.[43]

V. Inclusive Processes

In the general inclusive process,

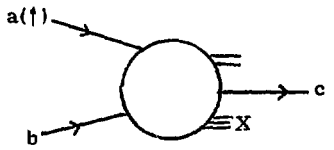

it is intuitively obvious that there can be little or no polarization effects. For instance, one is summing over many different exclusive reactions a(↑) b → c(X = given state) and polarizations will have random signs and average to zero. However there are specific kinematic regions where this will not be true and sizeable polarizations are expected. Refer to Fig. 19, which plots the allowed physical region for c in terms of

$$x_{\parallel} = 2p_{\parallel}/\sqrt{s}$$

$$x_{\perp} = 2p_T/\sqrt{s}$$

$$x_{\parallel}^2 + x_{\perp}^2 \leq 1$$

where $p_{\parallel}$ and p_T are longitudinal and transverse momenta of c in centre of mass system. As illustrated there, we expect polarizations in the large $x_r = \sqrt{x_{\parallel}^2 + x_{\perp}^2}$ region. This can be divided, artificially from some points of view,[5] into three regions.

Triple Regge region I: $x_{\parallel} > 0.8$: c fragment of a.

Triple Regge region II: $x_{\parallel} < -0.8$: c fragment of b.

and high p_T region: the large x_r region excluding the above two regions.

We have already briefly mentioned high p_T processes in Sec. II, while Field covered the first two regions at this conference. We will briefly summarize the three regions here. First refer to Fig. 20, which plots the angular distribution of the azimuthal angle between the π^- and polarization of the photon in the reaction[44]

$$\gamma(\uparrow)p \rightarrow \pi^- + \text{anything at 9.3 GeV.}$$

We find sizeable polarizations for positive $x_{\parallel}$ which disappears for small and negative values. This corresponds to polarization in triple Regge region I with none in central region or triple Regge region II. As we will see later, nonzero polarization in region II although possible is less natural than region I.

A. High p_T Region

My statement that sizeable polarizations are expected in this region is not based on hard calculations. Further the dividing line $x_r = 0.8$ in Fig. 19 has no quantitative basis.[45] Theories of low p_T, small $x_{\parallel}$ processes expect (and this is born out by experiment) inclusive production to be independent of beam and target quantum numbers. In particular it should not depend on their spin and there should be small polarization effects (cf., Fig. 20). On the other hand, theories of large p_T processes, definitely predict dramatic dependence on beam and target quantum numbers. For example, $\pi p \to \pi X$ is expected to be larger than $pp \to \pi X$ at large p_T because incident π has an antiquark to annihilate with quark in proton to produce final state π. Now unfortunately, we cannot immediately deduce that polarizations will be large as this requires not only spin dependence but also necessary relative phase between flip and nonflip amplitudes. However we have already commented that in at least one model[5] which is in fact a good description of the inclusive data, the elastic process does

appear to have sizeable polarization. Elastic scattering is the rim of the hemisphere $x_r = 1$ and based on the qualitative general argument plus existence in this special limit, we feel it would be worth investigating high p_T inclusive reactions for polarization effects. The easiest example is the polarized beam reaction:

$$p(\uparrow)p \to \pi + X$$

which might still be interesting at the low (for high p_T phenomena) ZGS energies. One may have enough cross section to allow studies with polarized target or final state polarimeter at higher energies.

One could consider investigating

$$p(\uparrow)\,p(\uparrow) \to \pi + X$$

with polarized beam and target. This may have larger effects as one does not need relative phase between amplitudes to get nonzero asymmetries.

B. Type 1 Triple Regge Region

First we give a qualitative derivation of the basic formula--a more precise treatment will be found in Field's talk. Taking the process $a(\uparrow)\,b \to cE$

where E is some fixed exclusive state, the polarization asymmetry for particle a aligned perpendicular to the scattering plane is

$$A\, d\sigma/dt \propto \sum_n \mathrm{Im}\,(H^{+\to+\ n}_{a\ \ c\,b,E}\ H^{*\ -\to+\ \ n}_{a\ \ \ c\ \ b,E})$$

where n runs over helicities of b and E and H is helicity amplitude for $a + b \to c + E$.

Putting in a Regge form for H, the above becomes pictorially

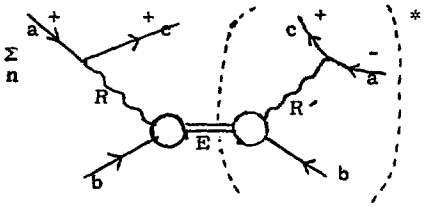

and summing over n and all exclusive states E, we can use the (generalized) optical theorem to find

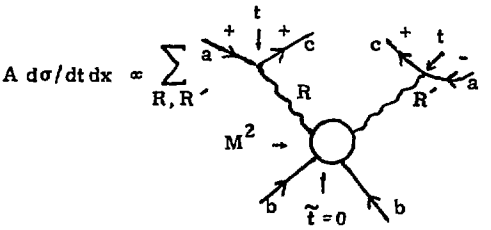

or putting in a Regge pole approximation for $Rb \to R'b$ forward amplitude

$$A\, d\sigma/dt\, dx \propto \sum_{R, R', R''}$$

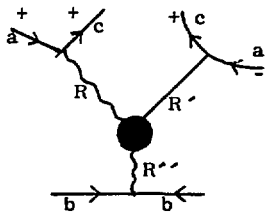

It follows that in this region I, the phenomenology of polarization is identical to that in two body scattering. The only change is that we choose R and R' not only so that they have a nonzero coupling to $a\bar{c}$ vertex but also so that triple Regge coupling $g_{RR' \to R''}$ is nonzero. The high energy fixed x limit is dominated by R'' = Pomeron and the latter restriction is relatively severe in this case. The essential features of the triple Regge formalism are as follows:

(a) The kinematic region for which the triple Regge expansion is valid is large s ($p_{lab} \gtrsim 100$ GeV/c) and $x_{\|}$ near 1 ($x_{\|} \gtrsim 0.8$).

(b) The detailed predictions are given by Field.[39] For example, if R'' is a Pomeron

$$(A)\quad d\sigma/dt\, dx \propto (1 - x)^{1 - \alpha_R(t) - \alpha_{R'}(t)}$$

Triple Regge theory predicts cross section to be both independent of s and have x shape, determined by trajectories $\alpha_R(t)$, $\alpha_{R'}(t)$, given above.

(c) A huge experimental advantage of inclusive triple Regge studies is that it studies same physics as (non)diffractive two body reactions but

triple Regge cross section and polarization is independent of energy whereas a specific two body cross section falls fast ($1/p_{lab} \rightarrow 1/p_{lab}^2$) with energy. For example, $\sigma(\pi^- p \rightarrow \pi^0 n)$ at 100 GeV/c is around 3 μb[46] whereas $\sigma(\pi^- p \rightarrow \pi^0 (x \geq 0.8) + \text{any})$ has about 100 μb of energy independent cross section.[47] It follows that triple Regge $d\sigma/dt$ and polarization measurements could replace conventional two body physics at Fermilab and SPS energies.

(d) Examples are easy: Field[39] has shown qualitative agreement between theory and experiment for $K^- p \rightarrow \Lambda X$; in general one needs only generalize any given two body reaction. For instance $\pi^- p \rightarrow p\pi^-$ is pure Δ_δ exchange and shows nonzero polarization at 6 GeV/c.[48] Its triple Regge form, $\pi^- p \rightarrow p + X$ would also exhibit energy independent cross section and polarization from the diagram

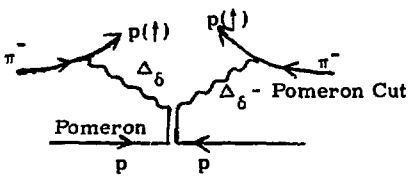

One can also use a polarized target and study

$$\text{any beam} + p(\uparrow) \rightarrow X + \pi^-$$

where π^- is fragment of proton.

A generalization of $\pi^- p \rightarrow (\pi^0 \text{ or } \rho^0)n$ is $\pi^- p(\uparrow) \rightarrow X + n$ with polarization from

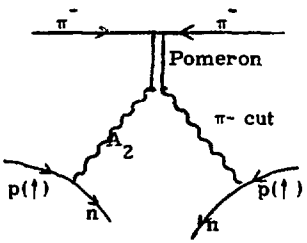

which is triple Regge generalization of mechanism used to get polarization in $\pi^- p \to \rho^0 n$ and $\gamma p \to \pi^+ n$.[25, 39]

The "opposite" generalization of $\pi^- p \to \pi^0 n$ i.e., $\pi^- p(\uparrow) \to \pi^0 + X$, is type II and is treated by formalism in next section.

(e) Now let us discuss diffractive processes i.e., reactions like $pp \to p + X$ where $\bar{a}c$ vertex allows a Pomeron coupling. Now for elastic processes, the polarization comes from pomeron interfering with ρ and A_2 exchange and so is not energy independent but rather falls like $1/\sqrt{s}$ at small t. Correspondingly in the triple Regge limit, the polarization also falls with energy in the same way. The dominant diagrams are

$A\, d\sigma/dt\, dx \sim$

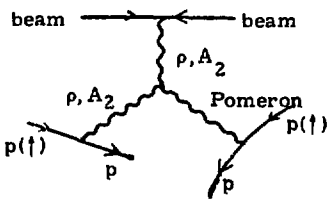

This gives asymmetry

$A \propto M/\sqrt{s}$ in region where cross section is dominated by PPR (small $M^2 = s(1-x)$).

$\propto 1/\sqrt{s}$ in larger M^2 region where PPP dominates.

As discussed by Field, these asymmetries have similar beautiful systematics to elastic scattering. For instance, $\pi^{\pm} p(\uparrow) \to X + p$ should have mirror symmetric asymmetries with a double zero at $t \approx -0.6$ $(GeV/c)^2$.

(f) In Fig. 21 we show experimental data on $p(\uparrow)p \to p + X$: the polarization is small and consistent with zero with present statistics. Clearly the triple Regge couplings $g_{\rho P \rho}$, $g_{A_2 P A_2}$ are quite small: more work is needed before we can test the formalism. However, the small polarization already allows some neat phenomenology.
Thus for low missing mass M, the inclusive reaction is made up of the two channels

$$p(\uparrow)\, p \to p\,(n\pi^+)$$

$$p(\uparrow)p \to p(p\pi^0)$$

and we can predict the polarizations in each of these two exclusive channels from the Deck model.[50] (This is so called "Berger-Fox" test.[51]) This model predicts large polarizations in the exclusive channel $pp \to pn\pi^+$ because in the Deck model,

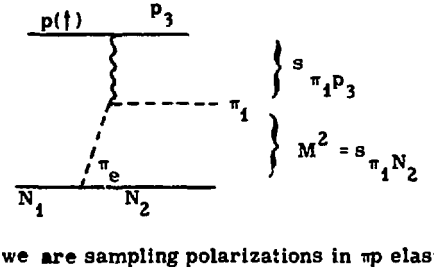

(D1)

we are sampling polarizations in πp elastic scattering at low subenergy $s_{\pi_1 p_3}$. The predictions in Fig. 22, are in clear disagreement with the inclusive data in Fig. 21. However, all is not lost and we let θ be Jackson angle of N_2 wrt N_1 in rest frame of $\pi_1 N_2$ system. Then the above diagram (D_1) is only expected to be valid for cos θ near 1, i.e., optimistically cos $\theta > 0$. For cos $\theta \lesssim 0$, we expect diagram with rapidity ordering of π, and N_2 reversed, to be dominant, i.e.,

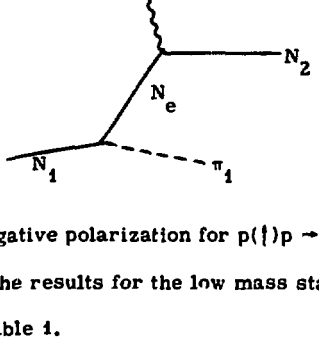

(D2)

and this gives negative polarization for $p(\uparrow)p \to pn\pi^+$ and positive for $p(\uparrow)p \to pp\pi^0$. The results for the low mass states are summarized in Fig. 23 and Table 1.

Returning to the inclusive reaction $p(\uparrow)p \to pX$, we see that low

mass X is made up of four diagrams--two give positive, one negative and the other zero polarization. We still expect net positive polarization but maybe it is not so surprising it is as small as Fig. 21 suggests.

We note that in a resonance model for the reaction

$$p(\uparrow)p \to p(X = N^{*}) ,$$

the polarization has to be independent of decay mode ($n\pi^{+}$ or $p\pi^{0}$) and decay angle θ of X. The essence of the Berger-Fox test[51] is that (generalized) Deck model gives polarizations that are dependent on both θ and decay mode and so is easily distinguished from resonance model. The experimental lesson is that it would be valuable to look at inclusive polarizations in a spectrometer where one can also examine the dependence on the make-up of the missing mass. Figure 22 indicates that polarizations could be large in certain kinematic regions.

C. Type II Triple Regge Region

This is kinematic region governed by diagram

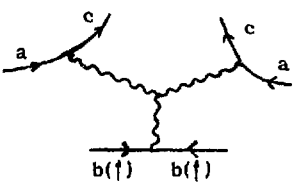

where now b, not a or c (as in type I), is polarized. Intuitively one would expect no polarization effects in this region -- mathematically this is

expressed by fact that it requires a conspiring cut or pole to get nonzero polarization effects. Such complexity has caused great theoretical delight[39, 52-54] and useful prediction that any nonzero asymptotic polarization implies a nonfactorizing pomeron in third leg. Figure 20 does show very small polarization in the type II region, and this is not surprising because of the large amount of data indicating approximate factorization of the Pomeron. On the contrary, the data[55], reviewed by Field,[39] on $\pi^{\pm}p(\uparrow) \to \pi^{\pm}X$ shows to my amazement large type II polarizations corresponding to nonasymptotic diagram

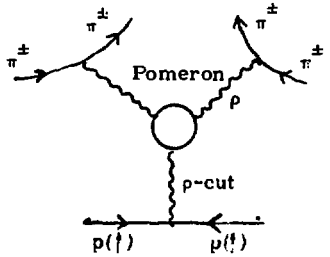

This interesting observation deserved to be explored more thoroughly.

D. Triple Regge Curiosities

In 5B, I made the authoritarian statement that the triple Regge formalism is only applicable for large s and $x_{\parallel} \gtrsim 0.8$. In this section, I note two relaxations of region of validity. Both are true for either polarization or simple differential cross section measurements.

(a) Staidly, we may note that the region of $x_{\parallel} > 0.8$ but medium s so that $M^2 = s(1 - x_r)$ runs upto around 4 $(GeV/c)^2$, is amenable to

analysis through finite mass sum rules (FMSR). These are quite uncontroversial theoretically[56] and experimentally successful.[57] They are described[39] by Field in this conference.

(b) Now life gets a little jollier as we describe a wrinkle in the triple Regge formalism which has so far escaped the elephants and is yet to be trampled flat by repeated use and abuse.

First we note[58] that it is well known that in the multiperipheral model (and hopefully also the real live world), we get power law behavior for all reactions like:

$$\pi^- p \to \text{all neutrals} \tag{4a}$$

$$\bar{p}p \to \text{any process not involving a baryon i.e., annihilation} \tag{4b}$$

$$K^- p \to \text{any process with no strange baryons.} \tag{4c}$$

The general class of reaction is

Beam + Target → all particles which do not satisfy a property P

or

$$\sigma_{tot}\,(b + t \to \text{all, P not true}). \tag{5}$$

So in examples

(4a): P is being charged

(4b): P is having nonzero baryon number

(4c): P is being a strange baryon.

The total cross section for any process of the type (5) can be described by a ladder, e.g.,

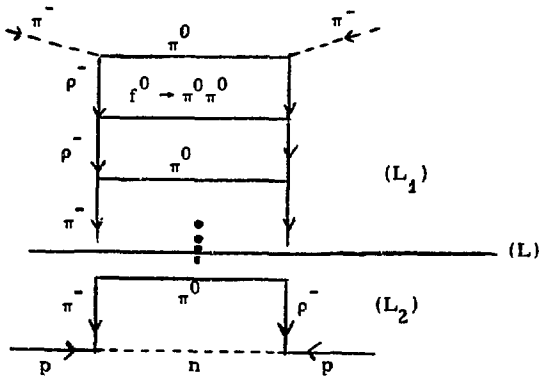

which satisfies a t-channel integral equation because if I break ladder at any point (e.g., solid line in (L) above), it breaks into two ladders (L_1) and (L_2) both of which are of type (5) with same property P. Solving integral equation, I will find Regge-like poles and power law behavior

$$\sigma_{tot}(b + t \to \text{all, not P}) = s^{\tilde{\alpha} - 1}$$

where $\tilde{\alpha}$ is position of pseudo-Regge pole gotten by solving integral equation, and we get same $\tilde{\alpha}$ for all reactions with a given property P, that are coupled in integral equation. Experimentally we discover:

(4a) $\tilde{\alpha} \approx 0$.

(4b), (4c) $\tilde{\alpha} \approx 1/2$.

The triple Regge generalization of the above formalism is trivial: take for example (4a) and reaction:

$$\pi^- p \to \pi^0 + \text{all neutrals.}$$

Triple Regge diagram is

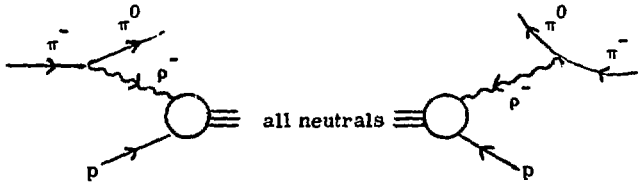

with $\rho^- p \to$ all neutral replacing $\rho^- p \to$ everything of true inclusive reaction. Clearly we can put in pseudo-Regge behavior of all neutral cross section to get pseudo-triple Regge graph

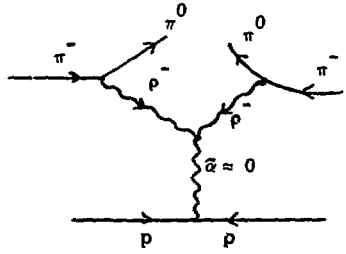

and triple Regge formalism is immediately applicable with intercept $\tilde{\alpha} \approx 0$ replacing Pomeron $\alpha = 1$ in basic formulae. The extension to general reaction (5) is obvious.

In the polarization example studied by Eisner and Field[39]

$$K^- p \to \Lambda(\uparrow) + X$$

there are many possible pseudo-analyses.

For limit,

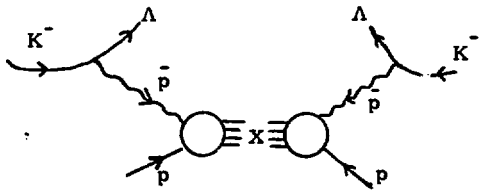

we could take

$$X = \text{no baryons:} \quad \tilde{\alpha} \approx 1/2,$$
$$= \text{all neutrals:} \quad \tilde{\alpha} \approx 0 .$$

For limit

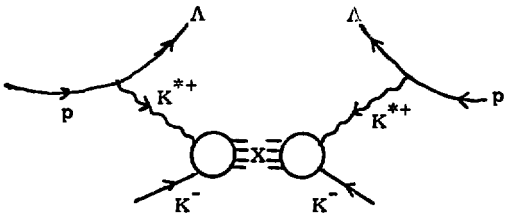

we could usefully take

X = no kaons: we don't know $\tilde{\alpha}$ here: by analogy to $\bar{p}p$

→ no baryons one might expect $\tilde{\alpha} \approx 1/2$.

and X = all neutrals again.

There is no point in listing all possibilities: the reader can see what is convenient for his trigger or bubble chamber scanning criterion.

We end by emphasizing that we have shown the interest in decomposing

the inclusive cross section into

a) exclusive channels cf. Berger-Fox tests.

b) general classes of inclusive channels cf., pseudo-Regge limit.

Both these types of study are well suited to bubble chambers and multiparticle spectrometers.

VI. PARTON SPIN STRUCTURE

A. Lepton and Target Polarized

There are several important experiments with polarized targets to study the electromagnetic and weak interaction.

The simplest is elastic scattering

$$\ell(\uparrow) N(\uparrow) \rightarrow \ell N$$

where the lepton (electron or muon) is polarized longitudinally and the target is polarized perpendicular to the beam but in the scattering plane. The polarization effect is proportional to product $G_E(q^2)G_M(q^2)$ of electric and magnetic form factors.[59] This allows one to extract $G_E(q^2)$ at large q^2, which is important because the usual unpolarized measurements $\ell N \rightarrow \ell N$ are only senstive to $G_M(q^2)$.

The inelastic scattering

$$\ell(\uparrow) N(\uparrow) \rightarrow \ell + \text{any}$$

has attracted a wealth of literature[60-70] with nice reviews in Refs. 60 and 66-68. The lepton is again polarized longitudinally and there are

two nucleon spin configurations[67]

a) nucleon spin parallel or antiparallel to beam

$$\frac{d^2\sigma^{\uparrow\uparrow}}{d\Omega' dk'} - \frac{d^2\sigma^{\uparrow\downarrow}}{d\Omega' dk'} = \frac{4k'\alpha^2}{kq^2}\{(k + k'\cos\theta)MG_1 + q^2G_2\} \qquad (6a)$$

b) nucleon spin in scattering plane but perpendicular to beam (as in elastic scattering above).

$$\frac{d^2\sigma^{\uparrow\rightarrow}}{d\Omega' dk'} - \frac{d^2\sigma^{\uparrow\leftarrow}}{d\Omega' dk'} = \frac{4k'\alpha^2}{kq^2} k'\sin\theta\,[MG_1 + 2kG_2] \qquad (6b)$$

The notation is conventional:

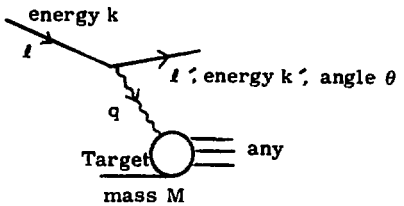

There are two new structure functions G_1 and G_2 in addition to W_1 and W_2 of the familiar unpolarized measurements. In the Bjorken limit, q^2, $\nu = k - k' \to \infty$ with $x = q^2/2M\nu$ fixed, one expects scaling of νG_1 and $\nu^2 G_2$ in the form

$$\begin{aligned} M^2\nu G_1(\nu, q^2) &\to g_1(x) \\ M\nu^2 G_2(\nu, q^2) &\to g_2(x) \end{aligned} \qquad (7)$$

These can be derived in quark[60,63,64] or light cone[62] approaches. In the former

$$g_1(x) = \frac{1}{2} \sum_i Q_i^2 \left(f_i^{\uparrow}(x) - f_i^{\downarrow}(x)\right)$$

where $f_i^{\uparrow}(x)$, $f_i^{\downarrow}(x)$ are respectively probability of parton of charge Q_i and momentum fraction x having same or opposite helicity as proton. g_2 involves proton polarized perpendicular to direction to motion rather along it as in $g_1(x)$.[60] There are many nice things to do experimentally

(a) check scaling (7).

(b) test sum rules[61,60,66-68]

$$\int_0^1 dx \left[g_1^{\text{proton}}(x) - g_1^{\text{neutron}}(x)\right] dx = \frac{1}{6} \frac{g_A}{g_V} \tag{8a}$$

$$\int_0^1 g_2(x)dx = 0 \tag{8b}$$

This clearly needs data with a polarized neutron target.

(c) Naive quark parton models[68] give

$$g_1^{\text{proton}} = \frac{5}{9} \times \text{unpolarized distribution function} \tag{9a}$$

$$g_1^{\text{neutron}} = 0 \tag{9b}$$

$$g_2 = 0 \tag{9c}$$

More sophisticated approaches[68,69] using Melosh transformation still give (9b), which again indicates utility of neutron targets.

(d) comparing Eqs. (6) and (7), we see that g_1 is best measured with configuration of parallel lepton and target spins, while g_2 is most sensitively determined by perpendicular spin arrangement. The latter unfortunately has asymmetries that are proportional to sin θ. However, it is an important measurement. For instance in a recent paper,[70] Colglazier and Rajaraman point out that one expects huge violations of scaling in this latter arrangement, from models in which partons have structure. These were proposed[71] to explain failure of e^+e^- annihilation to scale as expected.

There is also an interesting discussion of possible startling q^2 behavior in Refs. 66 and 68. This is based on purely phenomenological considerations -- namely $g_1(x \approx 1)$ is surely positive from parton model interpretation but for small q^2, it is experimentally established to be negative.

(e) The behavior in the Regge limit $\nu \to \infty$ (or $x \to 0$) is rather intriguing.[65,66] For instance $G_1(\nu, q^2)$ is controlled by mysterious A_1 exchange which is expected to be very small. Thus the spin dependent pp total cross section is formally similar (inelastic electron scattering is mathematically off shell photon proton total cross sections) and no evidence for this type of exchange was found.[72]

B. Theoretical Dreams, Experimental Nightmares

Other applications of polarized targets are not so easy. Most difficult is ν scattering off a polarized target[63,73]

$$\nu N(\uparrow) \rightarrow \begin{Bmatrix}\mu\\ \nu\end{Bmatrix} + \begin{Bmatrix}\text{any}\\ N\end{Bmatrix}$$

which has similar physics to processes discussed in previous subsection.

The scaling predictions for semi-inclusive process

$$\ell N(\uparrow) \rightarrow \ell + h + \text{any}$$

where h is some fixed hadron, have been discussed by Heimann[74] and Kingsley.[75] This would, for instance, be feasible experimentally when a polarized target is used in LASS spectrometer at SLAC. However, as we have yet to really test parton predictions for the corresponding unpolarized measurements, it is clearly premature to discuss polarization at this stage.

Finally the recent discovery of neutral currents, raises some interest in experiments to search for parity violating polarization effects in

$$\ell N(\uparrow) \rightarrow \ell N$$

$$\ell N(\uparrow) \rightarrow \ell + X$$

This would be expected from interference of electric and (neutral current) weak interaction. Their expected size is quite minute

$$A \sim 10^{-4} q^2$$

and probably can only be seen at Fermilab energies.[76] I have not been able to locate a comprehensive review -- only two articles[77,78] on the elastic

reaction. There appears, quite justifiably, more interest on the theoretically similar but experimentally easier reactions involving polarized leptons on unpolarized targets.[79,80]

VII. CONCLUSIONS

Conclusions in such an article are always liken unto asking the long distance runner to run a lap of honor as he lies collapsed on the ground, proud just to have breasted the finishing tape. Nevertheless, we will record some of the new areas in which we anticipate polarization will play an important role.

- → Low energy quasi-two-body reactions (Sec. IID),
- → Meson and baryon spectroscopy in production processes (Sec. III).
- → High p_T elastic and inclusive reactions (Secs. IIA and VA).
- → Amplitude analysis in hypercharge exchange processes (Sec. IV).
- → Triple regge polarization (Sec. V).
- → Inelastic electron and muon scattering (Sec. VI).

I hereby vow not to write another review article on polarization until both there is a significant amount of data in one of these areas and also I have really analyzed some of it.

ACKNOWLEDGMENTS

I would like to thank Jim Russ and Brookhaven for organizing an enjoyable conference. I am grateful to Fermilab for hospitality during preparation of this manuscript.

FOOTNOTES AND REFERENCES

[1]C. Lovelace, XVIth International Conference on High Energy Physics, Batavia, 1972.

[2]C. Lovelace, S. Almehed and Particle data group, LBL-63 (1973) summarizes the data.

[3]D. P. Hodgkinson, R. L. Kelly, R. E. Cutkosky and J. C. Sandusky, "πN data Compilation and Amalgamation," preprint LBL-3048 (1974).

[4]R. Cutkosky, this conference.

[5]A recent reference on the interchange model is R. Blankenbecler and S. J. Brodsky, "Unified Description of Inclusive and Exclusive Reactions at All Momentum Transfers," SLAC-Pub-1430 preprint (1974).

[6]A recent reference on gluon exchange is G. R. Farrar and C. C. Wu, "High Energy Fixed Angle Elastic Scattering," CALT-68-455, preprint 1974.

[7]F. Elvekjaer, T. Inami and G. Ringland, Phys. Lett. 44B, 91 (1973).

[8]M. Borghini et al., Phys. Lett. 31B, 405 (1970); ibid., 36B, 493 (1971).

[9]G. W. Abshire et al., Phys. Rev. Lett. 32, 1261 (1974).

[10]Interchange model predicts $\alpha_\rho(-\infty) = \alpha_{Pom}(-\infty) = \alpha_{P'}(-\infty) = -1$: which asymptotic trajectory is reached for $-t > 6$ (GeV/c)^2. The phase energy relation then gives real ρ and imaginary Pomeron-P′ amplitudes:

all we now need is a different ρ and Pomeron-P' spin structure to get mirror symmetric energy independent polarizations.

[11] In the gluon model, Ref. 6, all amplitudes appear to be real.

[12] S. Frautschi, Nuovo Cimento 12A, 133 (1972).

[13] In accordance with duality we identify (1) with the non-Pomeron part of the smooth amplitude, i.e., that associated with P' and ρ exchange -- see Refs. 12 and 15. This seems correct except as pointed out in Ref. 16, it runs into problems in K^+p backward scattering which shows an s-dependence identifiable with the fluctuating component just as in non-exotic processes like K^-p backward scattering.

[14] F. H. Schmidt, et al., Phys. Letters B45, 157 (1973).

[15] P. J. Carlson, Phys. Lett. B45, 161 (1973).

[16] G. C. Fox and C. Quigg, Ann. Rev. Nucl. Science, 23, 219 (1973).

[17] V. Davidson, et al., Phys. Rev. Lett. 32, 855 (1974).

[18] E. Eisenhandler et al., Phys. Letters B47, 536 (1973).

[19] J. L. Rosner, "The Classification and Decays of Resonant Particles," preprint SLAC-Pub-1391 (1974).

[20] G. Grayer et al., Phys. Lett. 39B, 563 (1972).

[21] W. Ochs and F. Wagner, Phys. Lett. 44B, 271 (1973).

[22] R. J. Cashmore, "Amplitude Analysis in Three-body Final States," SLAC-Pub-1316 preprint (1973). Invited talk at 1973 Scottish Summer School.

[23] R. S. Longacre et al., "N^* Resonance Parameters and K-Matrix fits to the Reactions $\pi N \rightarrow \Delta\pi + \rho N + \epsilon N$", SLAC-Pub-1390 preprint (1974). This references other publications on this work.

[24] A. J. G. Hey, P. J. Litchfield and R. J. Cashmore, "$SU(6)_W$ and Decays of Baryon Resonances," CERN/D. Ph. II/PHYS 74-19, preprint (1974).

[25] G. C. Fox, invited talk in Second International Conference on Polarized Targets, Berkeley (1971).

[26] T. O'Halloran, private communication.

[27] H. Ticho, private communication.

[28] G. Kane, "Phenomenology of High Energy Exchange Processes," preprint (1973).

[29] G. A. Ringland in 1973 Aix-en-Provence Conference.

[30] B. R. Desai and P. R. Stevens, Physics Lett. 45B, 497 (1973).

[31] C. E. W. Ward, W. T. Meyer and D. R. Rust, "Amplitudes for $\pi^- p \rightarrow K^0 \Lambda$ and $\pi^- p \rightarrow K^0 \Sigma^0$ at 5 GeV/c," preprint (1974).

[32] A. D. Krisch, A. Yokosawa, private communication (1974).

[33] J. R. O'Fallon et al., Phys. Rev. Letters 32, 77 (1974).

[34] P. R. Robrish et al., Physics Letters 31B, 617 (1970).

[35] M. A. Abolins et al., Phys. Rev. Lett. 30, 1183 (1973).

[36] E. L. Berger and G. C. Fox, Phys. Rev. Letters 25, 1783 (1970).

[37] C. E. W. Ward et al., Phys. Lett. 48B, 471 (1974).

[38] A. B. Wicklund, D. S. Ayres, R. E. Diebold, J. Jost, S. L. Kramer and A. J. Pawlicki, "Inelastic Polarized Proton Interactions at 6 GeV/c," preprint (1974).

[39] R. D. Field, this proceedings.

[40] A. C. Irving and C. Michael, "High Energy Production and Decay of Vector and Tensor Mesons," CERN-TH-1825 preprint (1974).

[41] This is exhibited, especially near $t = 0$, by nearly all Δ^{++} data and is exemplified in Fig. 17. It is also shown in analysis of Ref. 42.

[42] M. Aguilar-Benitez et al., Phys. Rev. Lett. 29, 749, 1201 (1972).

[43] J. K. Storrow and G. A. Winbrow, "Analysis of High Energy Backward πN Scattering, II," Daresbury preprint DL/P 205 (1974).

[44] K. C. Moffeit et al., Phys. Rev. D5, 1603 (1972).

[45] $x_r = 0.8$ is simply a trivial extension of triple Regge dividing line $|x_{\parallel}| = 0.8$.

[46]A. V. Barnes et al., preprint submitted to XVIIth International Conference on High Energy Physics, London (1974).

[47]R. D. Field, private communication (1974).

[48]L. Dick et al., Nucl. Phys. B64, 45 (1973).

[49]R. E. Diebold, A. B. Wicklund private communication (1974).

[50]G. C. Fox, Phys. Rev. D9, 3196 (1974).

[51]E. L. Berger and G. C. Fox, paper submitted to Second International Conference on polarized Targets, Berkeley (1971).

[52]H. Abarbanel and D. Gross, Phys. Rev. Lett. 26, 732 (1971).

[53]R. Phillips, G. Ringland and R. Worden, Phys. Lett. 40B, 239 (1972).

[54]Ph. Salin, J. Soffer, Nucl. Phys. B71, 125 (1974).

[55]D. Aschaan et al., preprint submitted to XVIIth International Conference on High Energy Physics, London (1974).

[56]M. B. Einhorn, J. Ellis and J. Finkelstein, Phys. Rev. D5, 2063 (1972).

[57]R. D. Field and G. C. Fox, "Triple Regge and Finite Mass Sum Rule Analysis of the Inclusive Reaction $pp \to pX$," CalTech preprint (1974).

[58]G. C. Fox, paper in preparation. This describes application to $\pi^- p \to \pi^0$ + all neutrals. I do not know a general reference but

pseudo-Regge poles pop up in many multiperipheral papers: for example, P. W. Coulter and D. R. Snider, Phys. Rev. D8, 4055 (1973). In particular there is no reference that has a comprehensive comparison of power law prediction with experiment for general reaction (5). It appears to work in the few cases I have glanced at it.

[59]N. Dombey, Rev. Mod. Phys. 41, 236 (1969).

[60]R. P. Feynman, "Photon-Hadron Interactions," pages 155-159, Benjamin (1972).

[61]J. D. Bjorken, Phys. Rev. 148, 1467 (1966).

[62]C. E. Carlson and W. K. Tung, Phys. Rev. D5, 721 (1972); A. J. G. Hey and J. E. Mandula, Phys. Rev. D5, 2160 (1972).

[63]C. Nash, Nucl. Phys. B31, 419 (1971).

[64]M. Gourdin, Nucl. Phys. B38, 418 (1972).

[65]R. L. Heimann, Nucl. Phys. B64, 429 (1973).

[66]F. Gilman, p. 71 of SLAC-167, Proceedings of Summer Institute on Particle Physics (1973).

[67]A. J. G. Hey, "What do We Learn from Deep Inelastic Scattering with Polarized Targets," CERN-TH-1841 (1974).

[68]F. E. Close, "Why Polarized Electroproduction is Interesting", CERN-TH-1843 (1974).

[69] F. E. Close, H. Osborn and A. M. Thomson, "Current and Constituent Quarks: Their Implications for Resonance Excitations, Polarized and Unpolarized Inelastic Structure Functions," CERN-TH-1818 (1974).

[70] E. W. Colglazier and R. Rajaraman, Phys. Rev. D10, 334 (1974).

[71] G. West, Phys. Rev. D10, 329 (1974).

[72] E. F. Parker et al., Phys. Rev. Lett. 31, 783 (1973).

[73] C. H. Llewellyn-Smith, Phys. Reports 3, 261 (1972).

[74] R. L. Heimann, "Polarized Coincidence Electroproduction," Cambridge preprint (1974).

[75] R. L. Kingsley, "On the Azimuthal Dependence of semi-inclusive Deep Inelastic Reactions in the Parton Model," Princeton preprint (1974).

[76] A similar time reversal experiment, (S. Rock, et al., Phys. Rev. Lett. 24, 748, 753 (1970)) reported no asymmetry at the 1 percent level for $q^2 \sim 0.5$ (GeV/c)^2. One need only repeat this for $q^2 \sim 100$ to almost have a viable chance of detecting the neutral current.

[77] P. Winternitz, in Second International Conference on Polarized Targets, Berkeley (1971).

[78] E. Reya and K. Schilcher, "Neutral Current Effects in Elastic Electron

Nucleon Scattering," Mainz preprint (1974).

[79]S. M. Berman and J. R. Primack, Phys. Rev. D9, 2171 (1974).

[80]W. J. Wilson, "Parity Violation in Deep Inelastic Lepton Hadron Scattering," Harvard Preprint (1973).

[81]G. C. Fox, in "Phenomenology in Particle Physics, 1971," edited by C. B. Chiu, G. C. Fox and A. J. G. Hey (Caltech, 1971).

TABLE 1

Polarizations in $pp(\uparrow) \to Xp$
(cf., Fig. 23)

Rapidity Ordering[a]			Polarization[b]
X		Observed Proton	
p	π^0	p	0
π^0	p	p	r/3
n	π^+	p	$r/2\,(1 - \cos \pi\alpha)$
π^+	n	p	-r/3
Δ^{++}	π^-	p	$-r/2\,(1 - \cos \pi\alpha)$
π^-	Δ^{++}	p	r
Δ^+	π^0	p	0
π^0	Δ^+	p	r/3
Δ^0	π^+	p	$r/2\,(1 - \cos \pi\alpha)$
π^+	Δ^0	p	-r/3

a) For instance, first row corresponds to diagram:

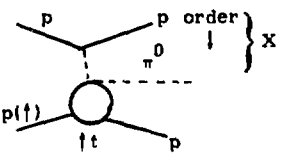

b) $r \propto \sqrt{-t}$ is a smooth function of t and M_X^2.

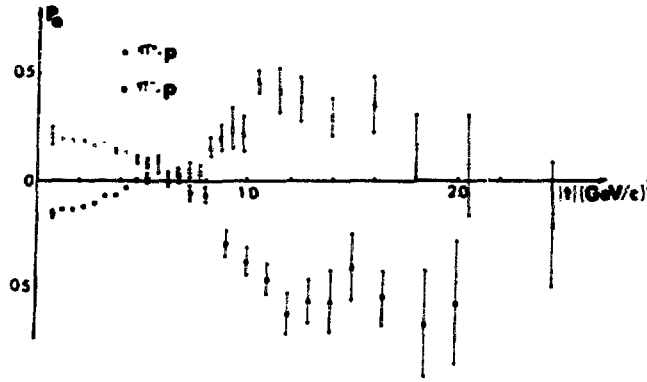

Figure 1. $\pi^{\pm}p$ elastic polarization data from Ref. 8 at lab momentum of 6 GeV/c.

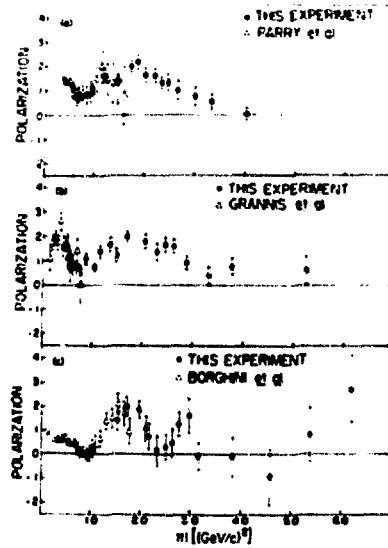

Figure 2. pp elastic polarization data from Ref. 9 at lab momenta of a) 5.15, b) 7 and c) 12.33 GeV/c.

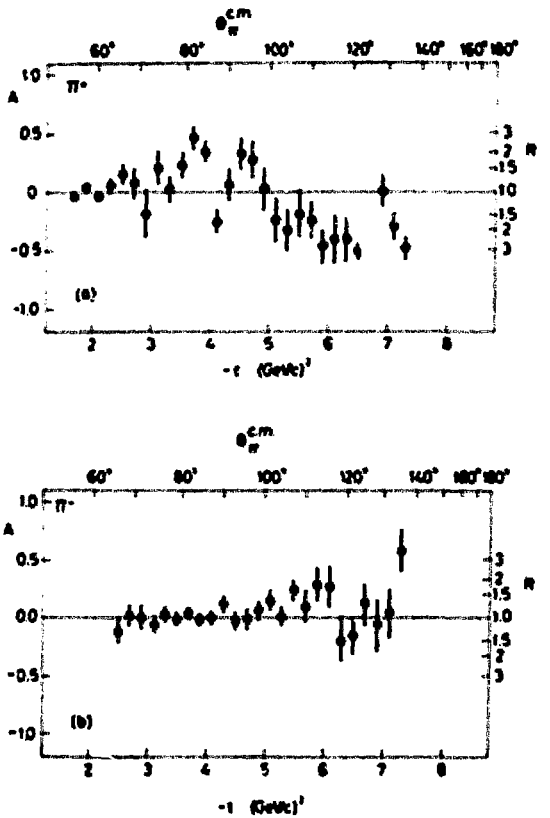

Figure 3. Plot taken from Ref. 14 of the normalized difference in a) $\pi^+ p$ and b) $\pi^- p$ elastic scattering between two momentum bins near 5 GeV/c. A is defined explicitly in Eq. (2) of the text.

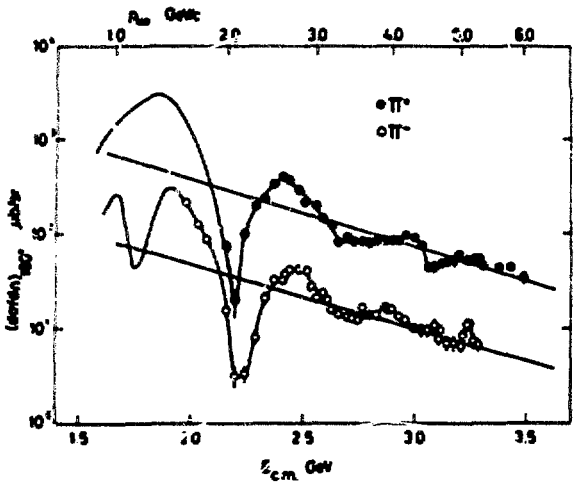

Figure 4. (a) Plot, taken from data compilation of the 180° cross section in $\pi^{\pm}p$ elastic scattering as a function of cm energy. The solid lines represent estimates of the "smooth" cross section discussed in the text.

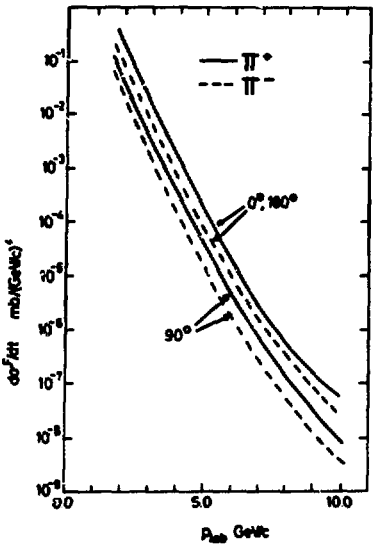

Figure 4. (b) Results from Ref. 15 of Ericson fluctuation analysis of 180° data in Figure 4a and 0° data (not shown). Plotted are the "fluctuating" cross sections discussed in text for $\pi^{\pm}p$ elastic at 0° (equal to 180°) and 90°. This analysis is claimed to be consistent with the data in Figure 3.

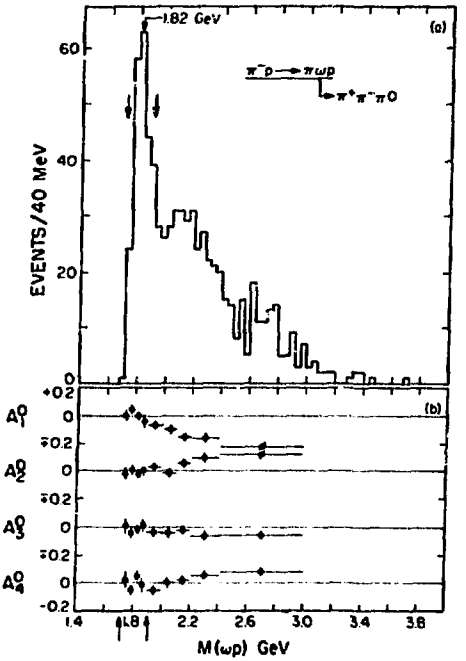

Figure 5. Evidence for ωp resonance at 1820 MeV seen in production process $\pi^- p \to \pi^-(\omega p)$ at 4.5, 6 and 14 GeV/c. (Ref. 17). Shown are the ωp mass spectrum and moments for $|t_{\pi\to\eta}| < 0.15$ $(GeV/c)^2$.

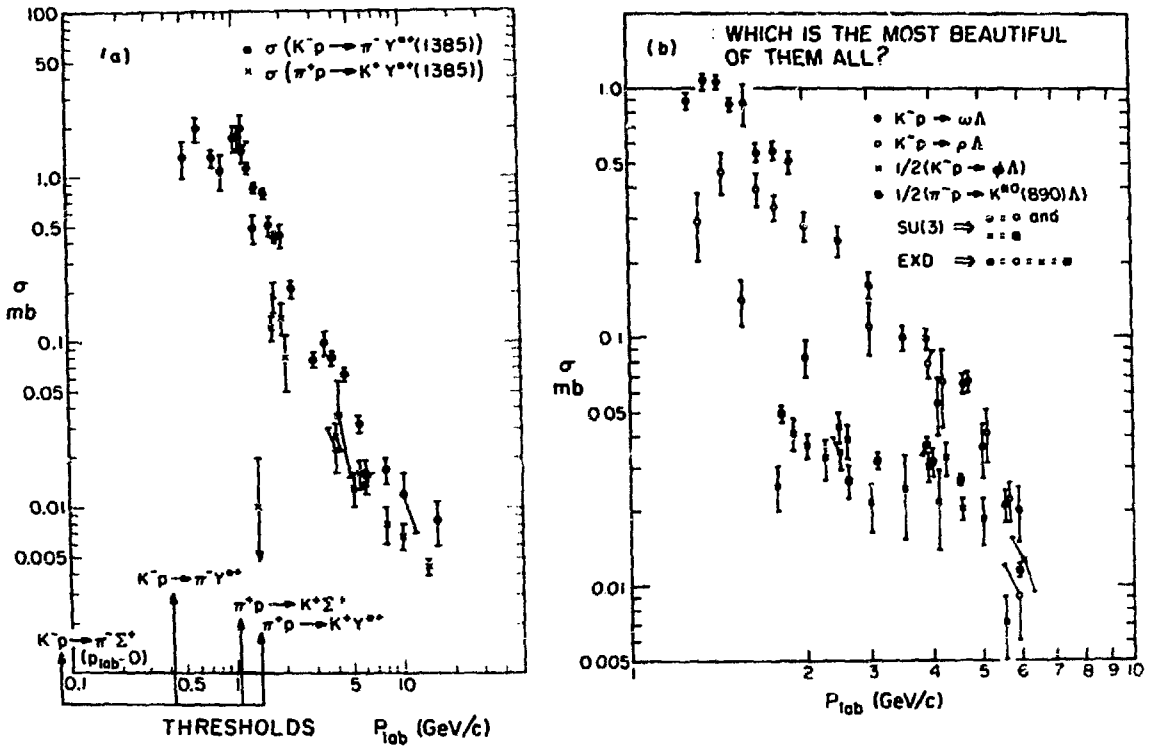

Figure 6. Comparison, taken from Ref. 16, of reactions expected to be equal at high energy indicating the importance of a high threshold in suppressing higher partial waves and so reducing cross section.

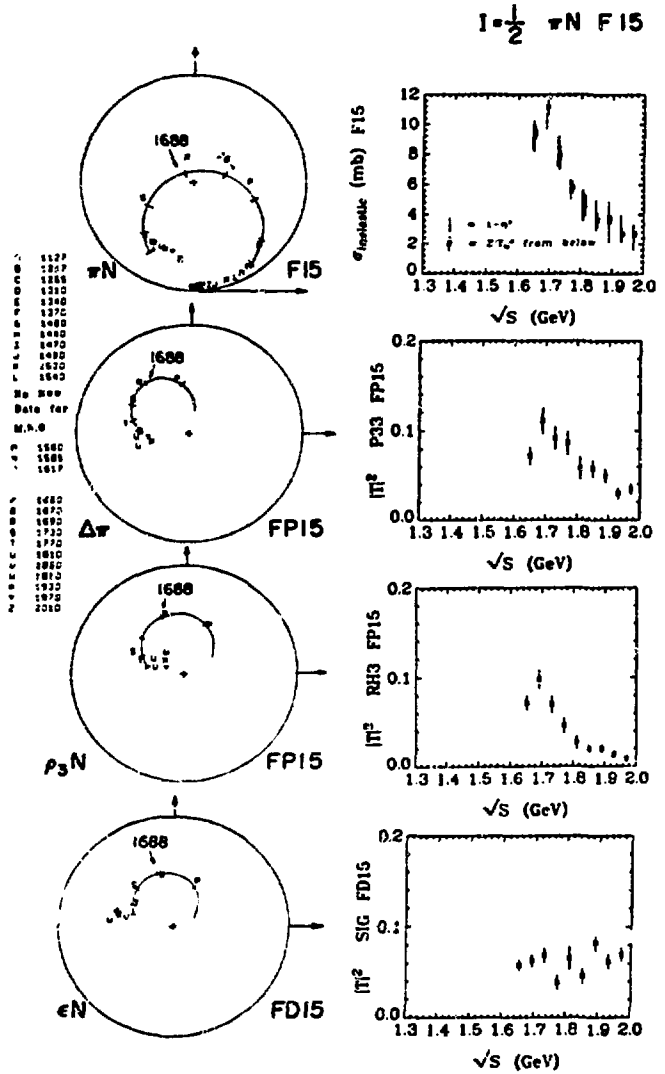

Figure 7. Argand diagrams from Ref. 22 for the F15 wave in the $\pi N \to \pi\pi N$ multiparticle phase shift analysis. The $\pi\Delta$, ρN and εN decays of the familar $5/2^+ N^*$ (1688) are clearly seen.

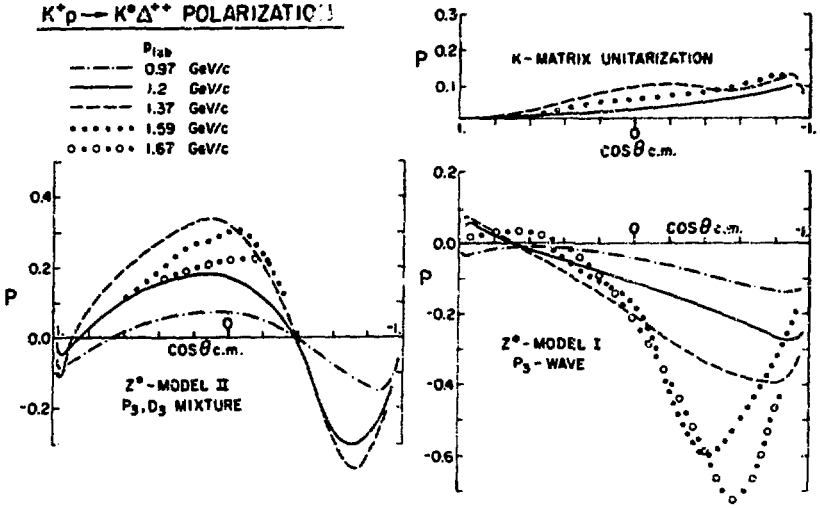

Figure 8. Estimated polarizations from Ref. 25 in $K^+p \to K^0\Delta^{++}$ integrated over all Δ^{++} decays. Shown are both resonant Z^* models and a nonresonant model --the latter is marked "K-matrix unitarization."

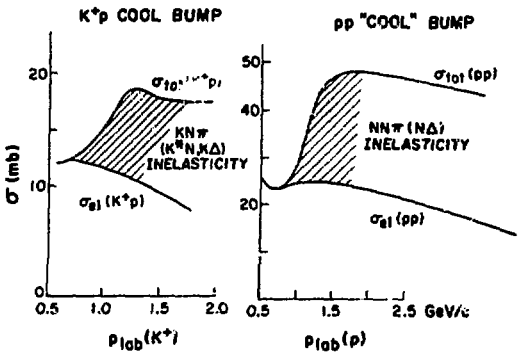

Figure 9. Comparison of K^+p and pp total cross sections from Ref. 25 showing the rapid rise in both cases near the first inelastic thresholds.

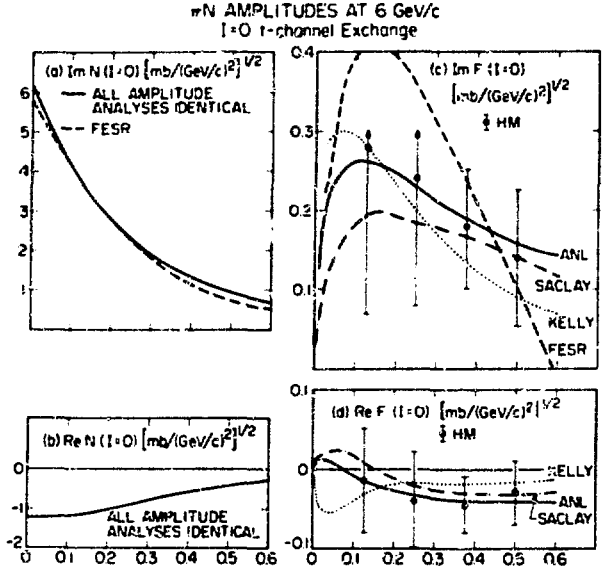

Figure 10. Summary, taken from Ref. 16, of πN elastic amplitude analyses at 6 GeV/c in the t-channel I = 0 state. Shown are real and imaginary part of nonflip N and spinflip F amplitudes. Marked are four analyses--marked HM (Halzen and Michael), KELLY (R.L. Kelly), ANL (Argonne polarization group) and SACLAY (Saclay polarization group) which are cited and compared in Ref. 16. Also drawn is a simple finite energy sum prediction (marked FESR).

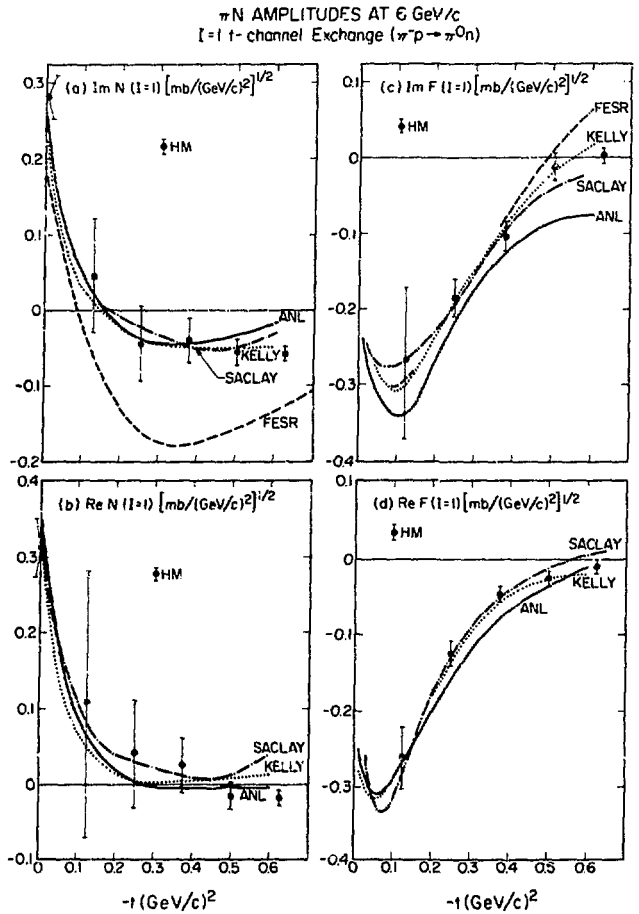

Figure 11. This is the same as Figure 10 except the graphs now refer to the I = 1 t-channel (i.e., $\pi^- p \to \pi^0 n$) amplitudes.

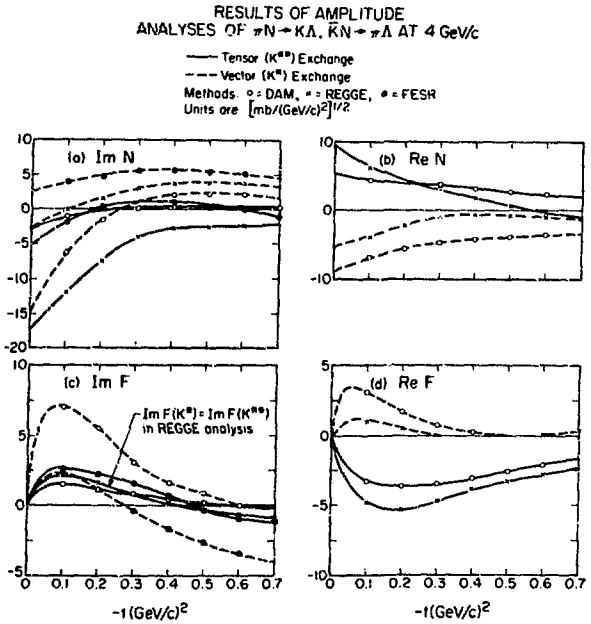

Figure 12. Comparison, taken from Ref. 16, of three amplitude analyses of $\pi N \to K\Lambda$ and $\bar{K}N \to \pi\Lambda$ at 4 GeV/c. Shown are dual absorptive (DAM), pure Regge in spinflip (REGGE) and FESR innocent analyses. The vast differences between the analyses and unwarranted violations of exchange degeneracy and SU(3) (not obvious from this figure) show danger of supplementing incomplete data with innocent theoretical assumptions.

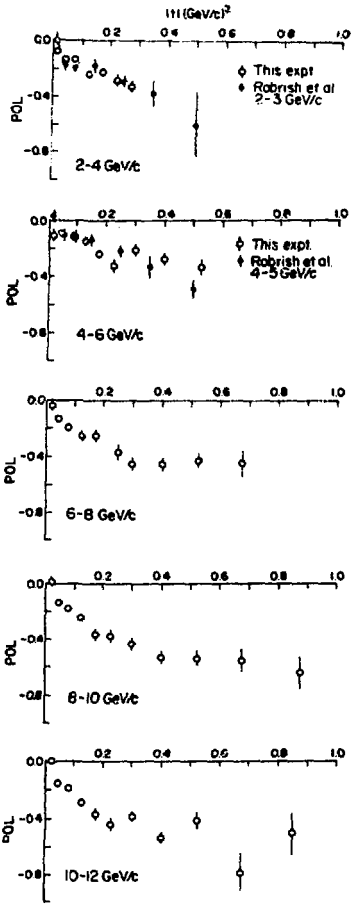

Figure 13. Polarization in np CEX from references 34 and 35.

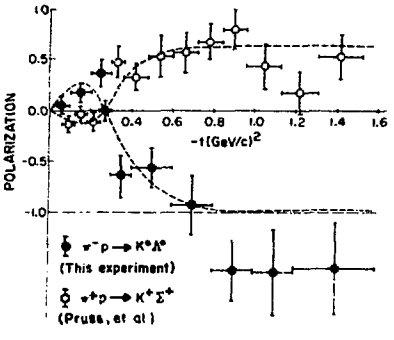

Figure 14. Polarization from Ref. 37 in $\pi^- p \to K^0\Lambda^0$ and $\pi^+ p \to K^+\Sigma^+$ at 5 GeV/c.

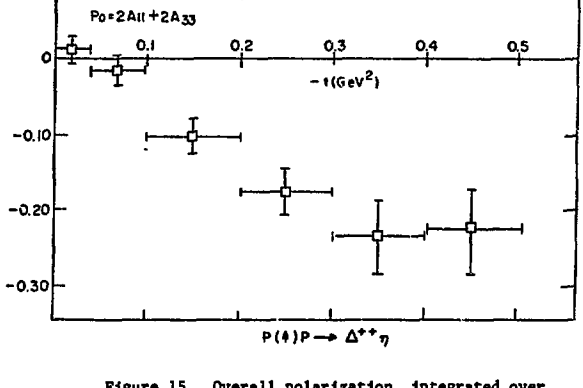

Figure 15. Overall polarization, integrated over all Δ^{++} decays, in $p(\uparrow)p \to \Delta^{++}n$ at 6 GeV/c from Ref. 38.

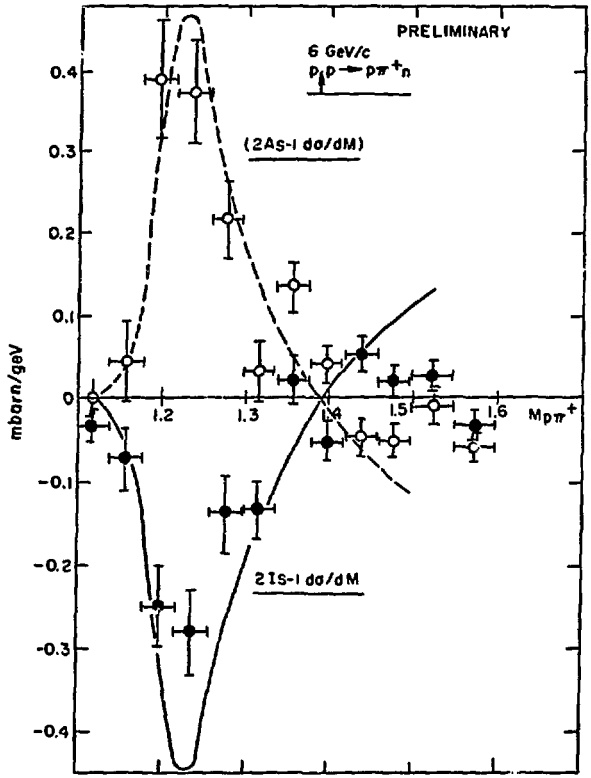

Figure 16. Two moments, in $p(\uparrow)p \to (\pi^+p)n$ at 6 GeV/c, of the π^+p decay angles that correspond to interference between $J^P = 3/2^+$ Δ^{++} and $J^P = 1/2^-$ π^+p waves. The solid and dashed curves are predictions of naive one pion exchange while data comes from Ref. 38 again.

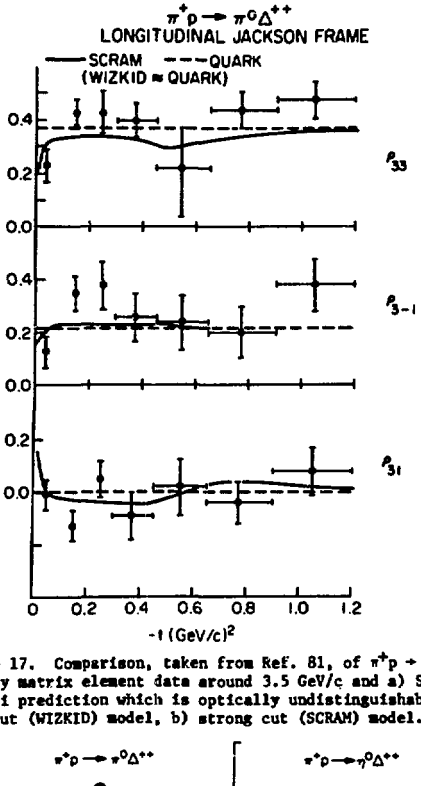

Figure 17. Comparison, taken from Ref. 81, of $\pi^+ p \rightarrow \pi^0 \Delta^{++}$ density matrix element data around 3.5 GeV/c and a) Stodolsky Sakurai prediction which is optically undistinguishable from weak cut (WIZKID) model, b) strong cut (SCRAM) model.

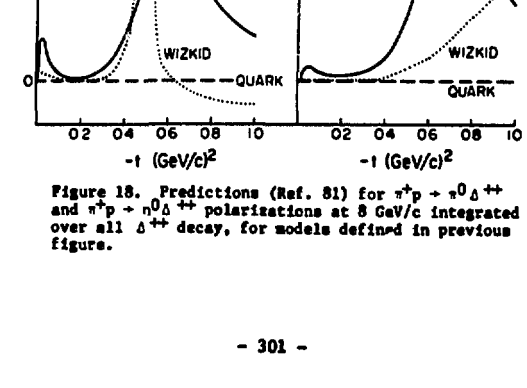

Figure 18. Predictions (Ref. 81) for $\pi^+ p \rightarrow \pi^0 \Delta^{++}$ and $\pi^+ p \rightarrow \eta^0 \Delta^{++}$ polarizations at 8 GeV/c integrated over all Δ^{++} decay, for models defined in previous figure.

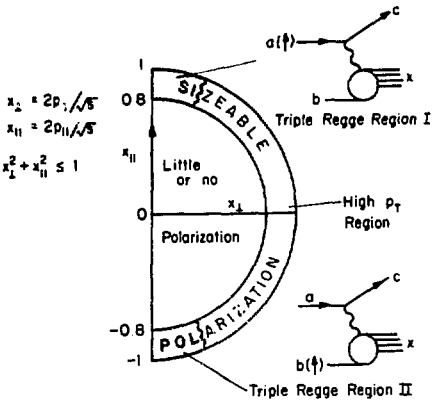

Figure 19. Kinematic regions as a function of $x_{||}$, $x_\perp$ for the inclusive process ab → cX.

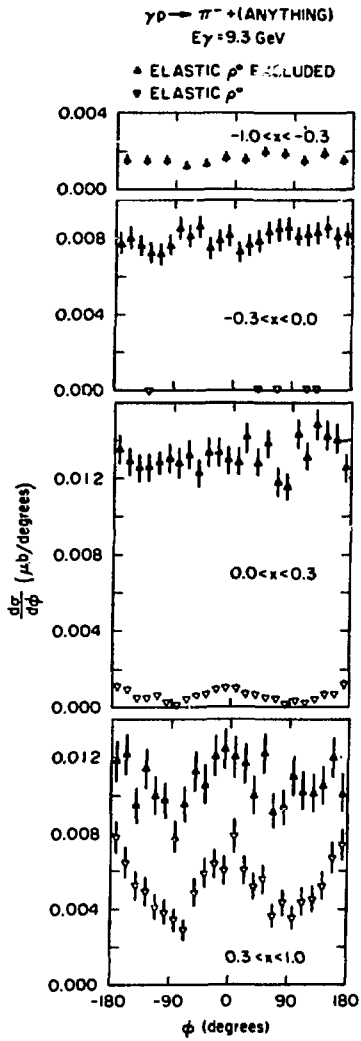

Figure 20. Photon polarization asymmetry discussed in text for $\gamma(\uparrow)p \to \pi^-$ plus anything at 9.3 GeV/c, (Ref. 44). The data is divided by various cuts in x for final π^- and the contribution from the strong exclusive process $\gamma(\uparrow)p \to \rho^0(\to \pi^-\pi^+)p$ is shown separately.

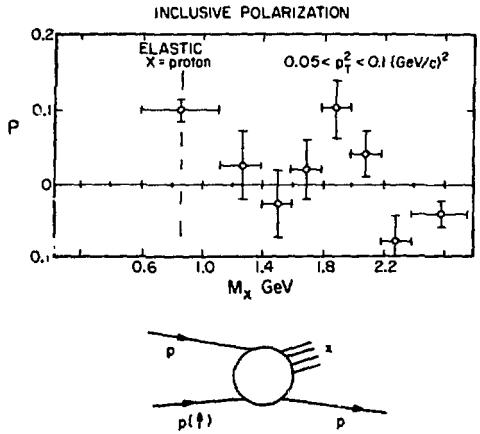

Figure 21. Inclusive polarization on p(↑)p → pX from Ref. 49 at 6 GeV/c. The full data is shown and discussed in greater detail by Field.[39]

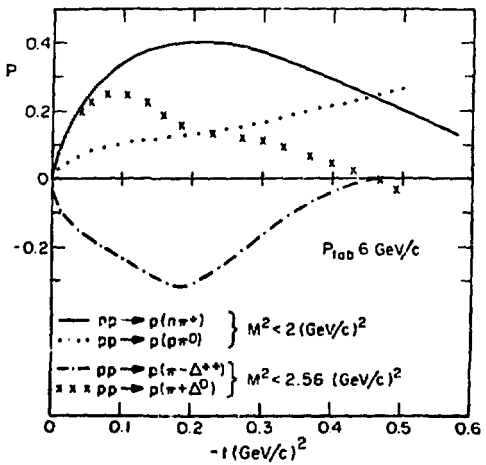

Figure 22. Predicted polarizations[50] from the π exchange Dack model for p(↑)p → p(nπ+,pπ0,π-Δ++ and π+Δ0) at 6 GeV/c and a low mass M cut for bracketed particles.

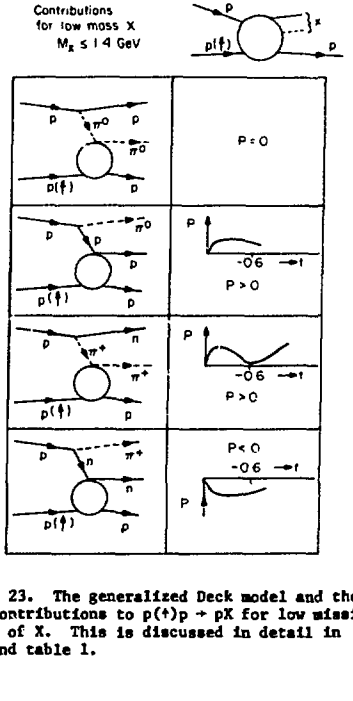

Figure 23. The generalized Deck model and the four contributions to p(↑)p → pX for low missing mass M of X. This is discussed in detail in text and table 1.

SECTION II

POLARIZED TARGET TECHNOLOGY AND NEW FACILITIES FOR POLARIZATION EXPERIMENTS

A HIGH POLARIZATION TARGET FOR INTENSE BEAMS*

Presented by W. Ash

Stanford Linear Accelerator Center
Stanford University, Stanford, California 94305

I would like to describe the polarized proton target which is being completed for an experiment in deep inelastic scattering of polarized electrons off polarized protons to be run at SLAC in the near future. The very interesting physics involved in this Yale-SLAC collaboration will be described by Vernon Hughes tomorrow morning.

As this conference seems more oriented to the use rather than the design of polarized targets, I shall give a quick summary of the device and concentrate on the aspects that are important to the use or novel to the design. Details that may be of interest can be handled in later discussions.[1]

The parameters of the target are given in Table I.

Table I SLAC-Yale polarized proton target

Temperature	1°K; Helium 4 system
Field	5 Tesla superconducting solenoid
Capacity	600 milliwatt; 25 cm^3
Material	1, butanol; porphyrexide doped
Polarization	$(\sim 70\%) \times \left(\frac{10 \text{ free protons}}{74 \text{ bound nucleons}}\right) \sim 10\%$
Microwaves	2 mm (140 GHz) backward wave oscillator
NMR	Constant voltage, parallel tank, 200 MHz
Special Features	Polarized parallel to beam $\pm 20^{\circ}$ exit aperture
	Daily target change due to radiation damage (electron beam)

The builders include myself and Dave Coward from the Spectrometer Group at SLAC; Steve St. Lorant from the Cryogenics Group at SLAC; Vernon Hughes, Asher Etkin, Peter Cooper, Satish Dhawan, John Wesley and Percy Yen from Yale. Strong technical support was received from both institutions.

The special feature of polarization parallel to the beam is a consequence of the experiment with longitudinally polarized electrons. This had substantial impact on the design of the magnet and cryostat. The electron beam, with its much higher damage per physics event, dictated more refrigeration,

*Work supported by the U. S. Atomic Energy Commission.

rapid and reproducible target changing, and mass production of target material. Our response to all this will be shown in subsequent figures.

Given the desire for high polarization we had an initial choice between a B/T of 5 Tesla/1° and 2.5 Tesla/.5° — each with special problems. We selected the first as indicated for a variety of reasons and so far are happy with that decision.

The magnet, of course, is superconducting and is essentially a solenoid with something better than ±100 ppm uniformity. Cooling is by a "conventional" helium 4 system with offline recovery and reliquefaction. We get about 600 mW of cooling in a 25 cc target volume at about 1.65°K.

This is not the first 5T/1K target but may be the first used in a high energy physics experiment—certainly at an electron machine.

The choice of material at this time is porphyrexide doped butanol. From CERN and DESY data plus preliminary results of our own, we expect a polarization of about 70% times the ratio of polarizable protons to total nucleons of 10/74 or about 10%. To the extent that scattering off neutrons is less than that off protons this ratio is increased. (A coincidence experiment that could distinguish between target protons and neutrons would increase this a factor of about 2.)

We expect to change targets daily and to anneal several times in between. This, among other things, means a lower average polarization.

The NMR system is a constant voltage type with a parallel tank running at about 200 MHz. The measured admittance is proportional to polarization.

Microwave power at 140 GHz is produced by a backward wave oscillator which delivers up to 400 mW to the target cavity.

Helium consumption is about 7 to 8 liquid liters of helium per hour including losses in cooling the magnet dewar.

The beam is expected to be 10^9 electrons per pulse at 180 pps scanning over a 6.5 cm^2 area or about 10^{14} e^-/cm^2h. This, with the expected damage time of something longer than 10^{15} e^-/cm^2h, gives our running schedule indicated above. In this regard the target is well matched to the maximum intensity expected from the polarized source. That the peak SLAC electron beam is some 100 times more intense gives a feeling for the mismatch between present targets and electron physics.

Figure 1 gives an idea of the physical layout of the target. Not shown is all the peripheral equipment such as 30 hp of pumps, power supplies for magnet and microwave source, etc. Note that the beam enters along the axis of the cryostat.

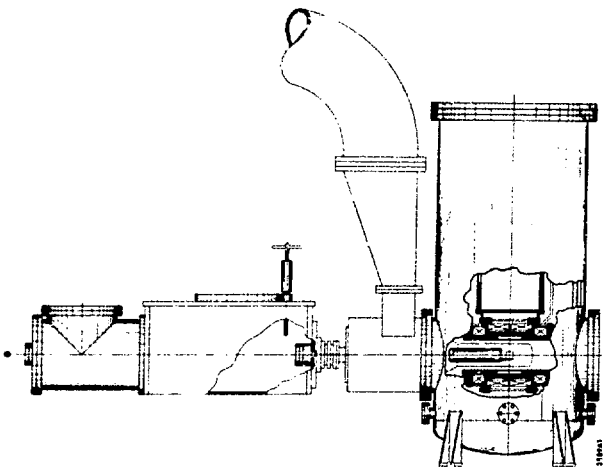

Figure 1.

The solenoidal superconducting magnet is shown in its 250 liter dewar which also serves as local reservoir for the running cryostat. Refilling during the daily run from an external dewar is still required however.

The extractor is partially described in this view as it allows withdrawal of the tube holding the target, per se, into a vacuum chamber.

The clear aperture can be a 20^{o} half cone angle although we are only using up to 10^{o} in a plane.

The various windows, target walls, NMR loops, cavity walls, which are required in any such target place nontrivial amounts of junk in the beam which makes life more difficult. The butanol comprises about 90% of the total collision length number of .04 and about 60% of the total radiation length number of .08.

In addition, of cource, one must face the problem of subtracting the large background from unpolarized nucleons. There are a variety of techniques including the use of 'diet butanol' (a mixture simulating C_4O instead of $C_4H_{10}O$) or using tabulated hydrogen cross sections.

The solenoidal field has some effects on the beam—slightly diverging the transmitted beam and slightly bending the scattered beam. Both effects are small compared to the respective apertures of beam monitor and spectrometer. This also requires us to shield several devices and to be

careful with ferromagnetic materials in construction. Not shown are the gas cooled leads for the magnet nor the transfer line details.

In Fig. 2 one gets a better idea of the target extractor. The target is now withdrawn into the vacuum chamber and the cryostat isolated. The insert containing the old material is removed; the new insert is substituted; and the target is returned to the cryostat.

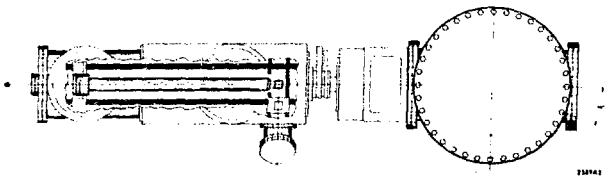

Figure 2.

The entire procedure should take minutes and be relatively free of contamination and anguish. The extractor has been tested warm, and also cold with the cryostat running.

The target assembly is not too clear in these drawings, but essentially we will have a copper wall box which holds helium and contains a single turn NMR loop. The target material is placed in a glass box which sits in this loop. This assembly then rides into a microwave cavity fixed in the cryostat.

Figure 3 gives more details of the cryostat per se. The second reservoir has been of little value. Isolation of the input helium line, even in the cryostat, has been important. The valve system is becoming straightforward with a precool valve for start up and a fine metering valve for running. Both derive liquid from the magnet dewar.

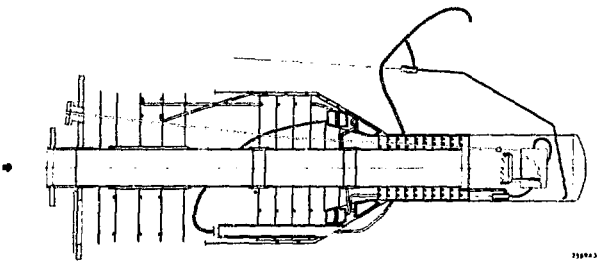

Figure 3.

Thorough cooling of the beads is most important to maintaining polarization in the presence of heating by beam and microwaves (typically 250-300 mW). Small diameter (less than 2 mm) beads have been a favored configuration for alcohol targets. In small quantities on infrequent occasions, producing the beads by dropping from a syringe onto liquid nitrogen works well. It tends to be a slow process because the drops must be made one at a time or in separated areas of the liquid or they coalesce before freezing. For daily changes, this is a problem.

In trying to find ways to speed up this process and to automate it some, I found a technique which kills two birds with one stone.

As shown on Fig. 4, we use a motorized syringe to feed liquid to a needle at a desired rate. If a potential is placed on this needle the electric field increases the volume force on the liquid thereby giving smaller drops for a given needle than gravity alone. The size of the drops is variable with the potential down to about 1 mm. Most importantly, however, the drops retain the charge and repel each other dramatically on an open surface. The prototype illustrated here allows a production rate of about 1 cc/min, and is easily paralleled.[2]

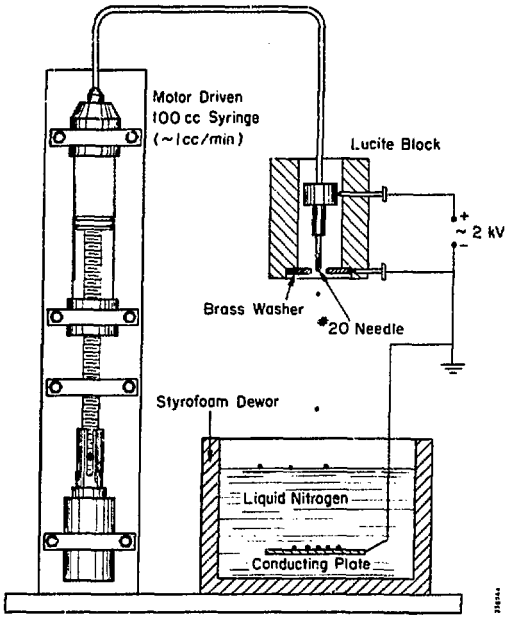

Figure 4.

In February, we polarized for the first time obtaining the rough data in Fig. 5. The enhancement, T_1, and T_2 are all consistent with data from other labs. We are hedging this statement because we did not have the NMR system completely debugged at the time; we were using a considerably smaller sample and the target assembly was quite different from the expected final design.[3]

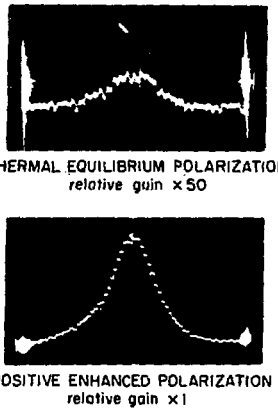

Figure 5.

We have a fair amount of confidence in the target at this point and a great deal of work ahead in converting it from a laboratory curiosity with a half dozen handmaidens to a remotely located working target on the floor of the SLAC end station.

REFERENCES

1. Details on the target design will be submitted for publication in the near future.
2. Although the charge repulsion feature is unique, this is the Nth reinvention of a device to produce small drops by electric fields. See, for example, Raghupathy and Sample, Rev. Sci. Instr. 41, 645 (1970) and references therein.
3. Since the above talk we have run again with a full sized target in final design obtaining polarizations of +66 ± 5% and -70 ± 5%.

EUROPEAN ORGANIZATION FOR NUCLEAR RESEARCH

POLARIZED DEUTERON TARGETS

M. Borghini
CERN, Geneva, Switzerland

Invited talk given at the
Brookhaven Study Meeting on Physics with Polarized Targets,
June 1974

Geneva - 28 February 1975

POLARIZED DEUTERON TARGETS

M. Borghini
CERN, Geneva, Switzerland

To our knowledge deuterons were first polarized in solid deuterium D_2, up to 1.5% at 1.5 K and 8.5 kG [1]. Then, they were polarized in lanthanum magnesium nitrate single crystals, doped with neodymium, up to ∿ 8-12% at 1.3 K and 17 kG and used as a target for thermal neutrons, to determine the neutron-deuteron scattering length[2].

Afterwards, deuterons have been polarized in organic substances and the polarization value has steadily increased during the last few years. (Table 1):

Table 1

Deuteron vector polarization in organic substances

P(D) a) (%)	Substance	Formula	Paramagnetic impurity	Temp. (K)	Field (kG)	Cryostat	Ref.
7	ethanol	C_2D_6O	porphyrexide	1.0	25	^{4}He	3
22	butanol	$C_4D_{10}O$	porphyrexide	0.5	25	^{3}He	4
26	butanol	$C_4D_{10}O$	porphyrexide	1.0	50	^{4}He	5
27	ethanediol	$(CD_2OH)_2$	Cr^V complexes	0.5	25	^{3}He	6
38	ethanediol	$(CD_2OH)_2$	Cr^V complexes	0.2 b)	25	dilution	7
44	propanediol	$C_3D_6(OH)_2$	Cr^V complexes	0.2 b)	25	dilution	8

a) P(D) = deuteron vector polarization $\equiv \langle I_z \rangle$.

b) The highest polarization required a dilution refrigerator[9]; the cooling temperature was 0.2 K and the sample temperature was estimated to be 0.37 K, the difference being due to surface resistance[10], which can be expressed as a resistance coefficient $R_K = 100\ A^{-1}T^{-3}$ K/cm^3/W, where A is the geometrical area of the sample.

A polarized target of 1-butanol, with 20% polarization was used in a test experiment, pd scattering at 1.21 GeV/c [11], at CERN. A polarized deuteron target of 1-butanol, with ∿ 20-22% polarization has been used in photoproduction experiments at Bonn[12]. A polarized deuteron target with

a dilution refrigerator, which is a copy of the one used in the CERN frozen spin target[11], is being built at CERN, to be used by a Saclay group for measuring the polarization in $K^+n \to K^0p$ charge exchange at 6 GeV/c.

The reason for using ethanediol and propanediol, where the hydroxyl groups (OH) are not deuterated, was the impossibility of producing the Cr^V complexes needed for dynamic polarization in fully deuterated compounds. A possible way of improving this situation is to mix propanediol-d6, prepared with an extra Cr^V-complex concentration with propanediol-d8: a deuteron polarization of 24% has thus been obtained in a mixture of 33% normal propanediol $C_3H_6(OH)_2$ and of 66% propanediol-d8, $C_3D_6(OD)_2$, at 0.5 K and 25 kG [14].

DEUTERON SPIN PARAMETERS

In dynamically polarized deuteron targets, placed as they are in a strong magnetic field directed along a direction Oz, the deuteron spin system is described by two parameters, for example

$$P(D) = \langle I_z \rangle \quad \text{and} \quad \langle 3I_z^2 - 2 \rangle$$

[$\langle I_x \rangle$ and $\langle I_y \rangle$, where Ox and Oy are two axes normal to Oz, are zero, while

$$\langle 3I_x^2 - 2 \rangle = \langle 3I_y^2 - 2 \rangle = -\tfrac{1}{2}A(D)\Big] .$$

These two parameters are related to the populations p^+, p^0 and p^- of the three magnetic sublevels $I_z = +1$, 0 and −1, by

$$P(D) = p^+ - p^- \quad \text{and} \quad A(D) = 1 - 3p^0 , \qquad \text{with } p^+ + p^0 + p^- = 1 .$$

In dynamically polarized organic compounds doped with porphyrexide or with Cr^V complexes, the populations happen to be related by

$$\frac{p^+}{p^0} = \frac{p^0}{p^-} ,$$

i.e. there exists a spin temperature[4,7]. This comes from the fact that the mechanisms of dynamic polarization acting in these substances establish a thermal contact between the nuclear spins and some electron spin-spin interaction reservoir; this reservoir is itself cooled by the action of the applied microwave field. This may not be the case of dynamic polarization by the "solid-state effect"[15], as in lanthanum magnesium nitrate (LMN)[2].

Then, there exists a relation between P(D) and A(D),

$$4A(D) - A(D)^2 = 3P(D)^2 \ .$$

For example, one would have

$$P(D) = 0.43 \ , \quad A(D) = 0.13 \ , \quad p^+ = 0.57 \ , \quad p^0 = 0.29 \ , \quad p^- = 0.14 \ .$$

For $P(D) = -0.43$, p^+ and p^- would simply be exchanged.

A way of varying A(D) independently of P(D) has been found at very low temperatures[16,17], but it is only of academic interest for the time being: because of solid-state complications, the average value of A(D) in the sample remains small, although A(D) may become as large as 0.6 for certain subsets of the deuteron spin system.

MEASUREMENT OF P(D) AND OF A(D)

i) P(D) and A(D) can be measured through usual nuclear magnetic resonance (NMR) techniques, with measurements of the deuteron thermal equilibrium signals, which are not very large. Such measurements have yielded a relative accuracy, $\Delta P/P$, of some 10%.

ii) When the polarization mechanisms establish a common nuclear spin temperature T_S, there is a definite relationship between the polarizations of protons and deuterons

$$P(H) = \tanh \left[\tfrac{1}{2} h\nu(H)/kT_S \right]$$

$$P(D) = \frac{4 \tanh \left[\tfrac{1}{2} h\nu(D)/kT_S \right]}{\left[3 + \tanh^2 \left(\tfrac{1}{2} h\nu(D)/kT_S \right) \right]} \ ,$$

where $\nu(H)$ and $\nu(D)$ are the Larmor frequencies of protons and deuterons, about 106 and 16 MHz in a field of 25 kG. Then, it is possible to measure the ratio of the enhanced NMR signals only, and to obtain a measurement of both P(H) and P(D) (Fig. 1)[7]. This method happens to be rather accurate for P(H), as one can get $\Delta P(H)/P(H) \simeq 1$-2% for an accuracy of 8% in the measurement of the ratio P(D)/P(H), at least for high values of P(H).

iii) Another way to measure P(D) is to measure the asymmetry in the deuteron magnetic resonance (DMR) line, which can be related to the ratio $x = p^+/p^0 = p^0/p^-$, as was done earlier for lanthanum in LMN [18]; again an accuracy of 10% can be reached by this method (Fig. 2). This value

can in turn be used for obtaining a precise determination of P(H) (Fig. 3). [Care should be taken since the phenomena which were observed at very low temperature[16,17] can change the DMR line shape, without changing the vector polarization, and impair the determination of the polarization by this method.]

* * *

REFERENCES

1) G.A. Rebka, Jr., and M. Wayne, Dynamic orientation of the nuclei of solid deuterium, Bull. Amer. Phys. Soc. 7, 588 (1962) and private communication.

2) V.P. Alfimenkov, V.I. Lushchikov, V.G. Nikolenko, Yu.V. Taran and F.L. Shapiro, Choice of the proper set of neutron-deuteron scattering lengths from experiments on transmission of polarized neutrons through a polarized deuteron target, Phys. Letters 24B, 151 (1967).

3) M. Borghini and K. Scheffler, Dynamic polarization of deuterons in frozen alcohol-water mixtures, Phys. Letters 31A, 535 (1970).

4) M. Borghini and K. Scheffler, A butanol polarized deuteron target, I : polarization at 25 kG, Nuclear Instrum. Methods 95, 93 (1971).

5) M. Borghini and A. Masaike, K. Scheffler and F. Udo, A polarized butanol deuteron target, II : polarization at 50 kG, Nuclear Instrum. Methods 97, 577 (1971).

6) W. de Boer, unpublished results (private communication).

7) W. de Boer, M. Borghini, K. Morimoto, T.O. Niinikoski and F. Udo, Dynamic polarization of protons, deuterons and carbon-13 nuclei: thermal contact between nuclear spins and an electron spin-spin interaction reservoir, J. Low Temp. Phys. 15, 249 (1974).

8) W. de Boer, Thesis (University of Leyden, 1974), and CERN 74-11 (1974).

9) T.O. Niinikoski, A horizontal dilution refrigerator with very high cooling power, Nuclear Instrum. Methods 97, 95 (1971).

10) W. de Boer and T.O. Niinikoski, Dynamic proton polarization in propanediol below 0.5 K, Nuclear Instrum. Methods 114, 495 (1974).

11) M.G. Albrow, M. Borghini, B. Bosnjakovic, F.C. Erné, Y. Kimura, J.P. Lagnaux, J.C. Sens and F. Udo, Asymmetry in the scattering of protons on polarized deuterons at 7.21 GeV/c, Phys. Letters 35B, 247 (1971).

12) K.H. Althoff, H. Beckschulze, H. Hennecke, H. Herr, E. Hilger, V. Kadansky, D. Menze and W. Meyer, Photoproduction of negative pions on a polarized neutron target in the resonance region, Bonn University report PIB 1-240 presented at the XVII Int. Conf. on High-Energy Physics, London, July 1974.

13) T.O. Niinikoski, A powerful dilution refigerator for polarized targets, to be published.

14) S.F.J. Cox, Research and developments for polarized targets (1973/74) Applied physics division report RL-74-147, Rutherford Laboratory, 1974, unpublished.

15) A. Abragam et W.G. Proctor, Une méthode nouvelle de polarisation dynamique des noyaux, CR Acad. Sci. 246, 2253 (1958).

16) W. de Boer, M. Borghini, K. Morimoto, T.O. Niinikoski and F. Udo, Sizeable pure tensor polarization of deuterons in a solid, Phys. Letters 46A, 143 (1973).

17) W. de Boer, Dynamic orientation of a deuteron spin system by RF irradiation of a polarized proton spin system, submitted to Phys. Rev. B, Jan. 1975.

18) A. Abragam et M. Chapellier, Détermination du signe d'un couplage quadrupolaire et mesure absolue de la température de spin d'un noyau polarisé dynamiquement, Phys. Letters 11, 207 (1964).

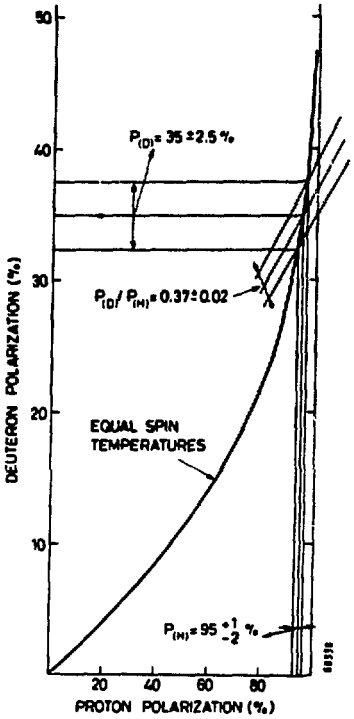

Figure 1. Measurement of the proton and deuteron polarizations P(H) and P(D) from the measured ratio P(D)/P(H). The solid curve corresponds to equal spin temperatures for protons and deuterons.

Figure 2. Nuclear magnetic resonance of deuterons in 1,2-ethanediol[7]; the asymmetry of the line shape is related to the deuteron polarization.

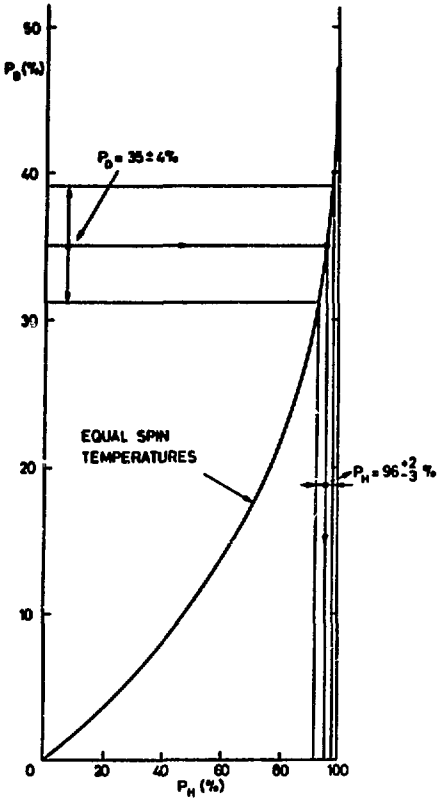

Figure 3. Measurement of the proton polarization from the value of the deuteron polarization deduced from the line-shape asymmetry and from the equality of proton and deuteron spin temperatures.

EUROPEAN ORGANIZATION FOR NUCLEAR RESEARCH

CERN FROZEN SPIN TARGET

M. Borghini
CERN, Geneva, Switzerland

Invited talk given at the
Brookhaven Study Meeting on Physics with Polarized Targets,
June 1974

Geneva - 28 February, 1975

CERN FROZEN SPIN TARGET

M. Borghini
CERN, Geneva, Switzerland

Preliminary studies on nuclear relaxation and dynamic polarization[1,2] in a small dilution refrigerator[3] having been successful, a frozen spin target has been constructed by a collaboration of the Low Temperature Laboratory of the Technological University of Helsinki and the CERN polarized target group[4]. It contains protons which are polarized up to 90% in a homogeneous magnetic field of 25 kG and can then be moved without loss of polarization into the more inhomogeneous magnetic field of a spectrometer, where they lose less than 1% polarization per day.

The spectrometer magnet used at present is the CERN-ETH magnet[5], with a useful magnetic volume of $0.6 \times 0.7 \times 1.7$ m^3, and a field value of 10 kG. The polarizing field is obtained by adding two tapered steel pole pieces, with a gap of 60 mm, at the entrance of the spectrometer, as was done in an earlier experiment to measure the polarization in $K^-p \to \bar{K}^0n$ charge exchange at 8 GeV/c [6,7], but in a corner of the magnet rather than in the middle of its entrance face (Fig. 1). The field homogeneity, over the target volume of 15 cm length and 16 mm diameter, is $\pm 2 \times 10^{-4}$ in the polarizing field, and about 1% in the holding field.

The target is made out of spheres (1 to 1.5 mm in diameter) of propanediol doped with Cr^V complexes*), contained in a thin (0.5 mm), leak tight, teflon cylinder, 17 cm long and 25 mm in diameter, which is the mixing chamber of a specially made dilution refrigerator[8] (Fig. 2). This refrigerator is horizontal, with a continuous flow of ^{4}He from 100 l dewars, and the incoming beam traverses it along its axis by going through a thin window. Two solid-state detectors are installed at low temperature, in front of the target, in a sealed box[9]. The microwave cavity, necessary for performing dynamic polarization, is a copper cylinder, 21 cm long, 36 mm in diameter, thermally attached to the refrigerator still, at a temperature between 0.6 and 0.8 K. The outside diameter of the cryostat nose, around the target, is 5 cm.

*) See Ref. 2 and references therein.

Dynamic polarization is started with microwave power, around 69.5 GHz, at a temperature of 0.5 K, where the refrigerator has a cooling power of 100 mW, with a ^{3}He flow rate of 25 mmole/sec. The initial rate of polarization is of 15 to 20%/min. After some time, reducing the microwave power allows one to reduce the temperature, and the polarization increases, although more slowly; it reaches 90% in about 2 h. This initial polarization value is then recorded.

Microwaves are then switched off completely, and the target cell is cooled down to a temperature below 50 mK in less than 10 min [8]. The cryostat is then moved aside and forward into a hole surrounded by anticoincidence counters, at the entrance of the spectrometer magnet. This motion takes about 2 min. The lowest value of the field experienced by the target during this move is 5 kG. The target is then used for experiment in the holding position for as long as one or two days. When going back into the 25 kG field, the polarization is remeasured, and is observed to differ from the initial value by less than 1% after 30 hours for positive polarization and by less than 10% for negative polarization [9].

The polarization measurement is made with three Q-meters, using coils wound around the mixing chamber; two are large coils used to measure the polarization at 25 kG; one is a smaller one and is used to monitor the polarization behaviour in the spectrometer magnet. Computer averaging is used to improve and to record the signals, and to watch the operation of the target [10].

This target is being used for measuring the three spin parameters in the reaction $\pi^- p \to K^0 \Lambda^0$ at 5 GeV/c [11]. When the target is placed in the holding position, the azimuthal access around it is about 300°, and the polar "ϕ" access is 360°.

REFERENCES

1) M. Borghini, T.O. Niinikoski, F. Udo and P. Weymuth, Dynamic polarization and relaxation of protons in 1.6-hexanediol and 1.8-octanediol: a feasibility study for a frozen spin polarized target, Nuclear Instrum. Methods 105, 215 (1972).

2) W. De Boer and T.O. Niinikoski, Dynamic proton polarization in propanediol below 0.5 K, Nuclear Instrum. Methods 114, 495 (1973).

3) T.O. Niinikoski, A horizontal refrigerator with very high cooling power, Nuclear Instrum. Methods 97, 95 (1971).

4) CERN polarized target group and Helsinki University of Technology, Proposal for a frozen spin target, November 1971 (unpublished).

5) P. Astbury, G. Finocchiaro, A. Michelini, D. Websdale, C.H. West, W. Beusch, B. Grobbi, M. Pepin, E. Polgar and M.A. Ponchon, Performance of a large magnet spark chamber, Nuclear Instrum. Methods 46, 6 (1967).

6) Ø. Runolfsson, A model of the 170 cm CERN-ETH-IC magnet modified for the use of a polarized target, CERN-NP Internal Report 69-26 (1969) (unpublished).

7) W. Beusch, M. Borghini, G. Misuri, E. Polgar, D. Websdale, F.X. Gentit, L. Fluri, K. Freundenreich, P. Mühlemann, J.S. Wilson, P. Astbury, J. Gallivan, J. Jafar and M. Letheren, P. Le Du and O. Guisan, Measurement of the polarization in $K^- p \to \bar{K}^0 n$ charge exchange at 8 GeV/c, Phys. Letters 46B, 477 (1973).

8) T.O. Niinikoski, A powerful dilution refrigerator for polarized targets, to be published.

9) T.O. Niinikoski and F. Udo, private communication.

10) F. Udo, Instrumentation for the CERN polarized targets, CERN-NP Internal Report, October 1974 (unpublished).

11) CERN-ETH Zürich-Techn. Univ. of Helsinki-Imperial Coll. London-Southampton Univ. Collaboration, Measurement of the helicity amplitude for associated production $\pi^- p \to K^0 \Lambda$, proposal PH. I/COM-73/16, March 1973 (unpublished).

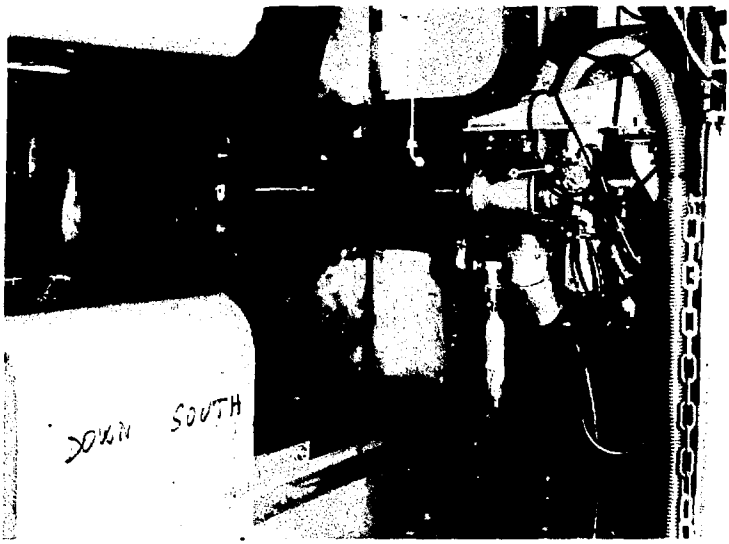

Figure 1. Photograph of the CERN frozen spin target. The spectrometer magnet is on the left. The cylindro-conical, horizontal, dilution cryostat containing the target is supported from a movable platform, on which stands a liquid ^{4}He dewar. Two flexible pumping lines are seen at the back, the pumping sets being on the far right of the picture. The beam comes from the right and goes through the cryostat along its axis. Two extra pole pieces, which make the polarizing field, are seen at the entrance of the magnet, and are located on the left of the beam path.

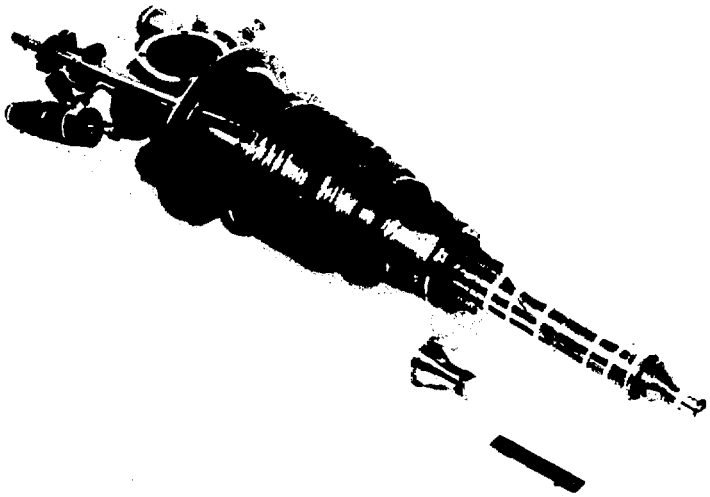

Figure 2. Photograph of the inner part of the dilution refrigerator[8] used in the CERN frozen spin target.

A He^3 COOLED POLARIZED PROTON TARGET

ASHER ETKIN
PHYSICS DEPARTMENT
YALE UNIVERSITY

TALK DELIVERED AT 1974 BNL WORKSHOP ON POLARIZED TARGETS

ABSTRACT

A DESCRIPTION IS GIVEN OF YALE UNIVERSITY E. P. I. GROUP'S POLARIZED PROTON TARGET, PRESENTLY IN USE AT BNL.

A He^3 COOLED POLARIZED PROTON TARGET

This target system which has been used in several experiments at Brookhaven National Laboratories is partially based upon a design developed at CERN. This target routinely gives a polarization of 60%. The principle components of the target are the 25 KG resistive magnet, the He^3-He^4 refrigerator, the 70 GHz source and the NMR system.

A 25 KG magnetic field is provided by a resistive C-frame iron magnet (shown in figure I) built with the help of the CERN magnet group[1] internal. This magnet provides a field homogenious to 1 part in 10^4 over the target volume 0.9" long, 0.8" wide, and 0.6" high, while permitting a large angular access, ±15 from the horizontal plane and ~270 in the horizontal plane (θ). In order to increase the available θ access the beam can be directed onto the target through a hole in the return yoke.

Power for the magnet is supplied by a modified P. P. A. power supply to which a ripple filter has been added and in which a high precision transductor[2] is used for current regulation. Current stability is of the order of a few parts in 10^5 long term at the nominal 600 amps 120 v output, and is probably limited by the control amplifier and comparison reference used and not by the transductor.

Since the magnet, power supply, and filter used a directly cooled conductor system a special cooling unit was built so as to permit the system to operate independent of the availability of a general low conductivity water recirculation system.

The He^3-He^4 cryostat used (fig. II) is a copy of the cryostat used at CERN[3] and is capable of operation at 0.55°k with a 12 mw microwave heat load. In operation Liquid He^4 is transferred directly into the separator, from the storage dewar, where any vapor is separated from the liquid.

Cold He^4 vapor is used to cool the radiation shields in the insulating vacuum space, and also cools the perforated discs that intercept heat flowing in from the room temperature end of the cryostat.

After expansion in a variable expansion valve the liquid He^4 is evaporated at low pressure in the evaporator. Resulting vapor is pumped away by a 2000 ft^3/min. pumping set. This cold vapor is also used to cool the perforated discs that in turn cool the incoming He^3 gas in the He^3 section.

A stainless steel tube separates the He^4 and the He^3 subsystems so that it is possible to remove and replace the He^3 insert without disturbing the He^4 section; this permits the He^3 insert to be cooled quickly after the target beads have been inserted in order to prevent melting the beads. This isolation also helps to prevent He^3 loss and allows the He^3 section to be changed without requiring modification of the He^4 section.(4)

The He^3 insert consists of a heat exchanger where the incoming He^3 gas is cooled by the counterflowing He^3 and He^4 vapor and by contact with the separator in the He^4 stage, a condenser cooled by the He^4 evaporator, where the He^3 is liquified, and the evaporator cavity where the target is cooled by the evaporating He^3 which has passed through a fixed expansion valve. The heat exchanger and condenser are coaxial with the He^3 pumping line and the wave guide which supports the evaporator cavity. Fig. III shows the cavity region of the cryostat, where one can see that there is very little material in the beam or outgoing particle path considering the requirements of the cryogenic system. The top of the cavity is easily removed and replaced to permit the beads to be quickly loaded into the cavity.

A special 300 m^3/hr roots type rotary pump with an internal motor and a specially sealed backing pump(5) are used to help prevent the loss of He^3. Exhaust He^3 gas is purified in a LN_2 cooled activated charcoal trap before

being recirculated.

A frequency sweept constant current Q-meter system is used to measure the Proton NMR signal of the target and thereby, the target polarization. In order to achieve high stability and ease of construction and maintanence, we have made extensive use of integrated and hybrid circuit technology throughout the system. A feedback loop is used to control the frequency of the oscillator to insure stability and sweep linearity. The audio output of the rf system is averaged by an Eductor[6] which is a multi-channel boxcar integrator, whose output is recorded on a chart recorder for subsequent analysis.

Calibration of the system is accomplished by measuring the N. M. R. signal (E_{TE}) when the target is in thermal equilibrium with the lattice and, therefore, the proton polarization is determined by:

$$P_e = \tanh\left[\frac{h\,\omega_{NMR}}{2k\,T_{BATH}}\right]$$

If the NMR signal (E_e) of the polarized target is measured, then the target polarization is given by:

$$P_n = \frac{\int E_e \; d\omega}{\int E_{TE} \; d\omega} \; P_e$$

Microwave power is supplied by a CO 40B carcinotron[7] that is frequency locked to a 200 MHz reference. Frequency stabilizing the carcinotron was very important in achieving the maximum polarization of the target stably.

This target has been used in two experiments at BNL that studied $K + P \rightarrow PK^+$ and $\pi^- P \rightarrow \pi^+ \pi^- n$ (at a $\pi\pi$ mases in the ρ region) (see figures IV + V). These experiments ran for over 1000 hours and the target operated satisfactorily with very little attention during the experiment.

1. CERN-N. P. Internal 69-5.
2. Both units were supplied by Transrex, Torrence, Calif.
3. Proceeding of the II International Conference on Polarized Targets - LBL-500, UC-34 Physics, TID-4500 (58 Th Ed).
4. At CERN a dilution refrigerator insert has been used in place of the He^3 insert.
5. MIV 350, Z 2030H Alcatel Vacuum Products, Hanover, Mass.
6. Made by Princeton Applied Research.
7. Supplied by Thomson-CSF. The system is described in more detail in "A Study of the Reactions $\bar{p}p \to \bar{p}p$ and $\bar{p}p \to \pi^- \pi^+$ Using a Polarized Proton Target" by A. Etkin, Yale University (unpublished).

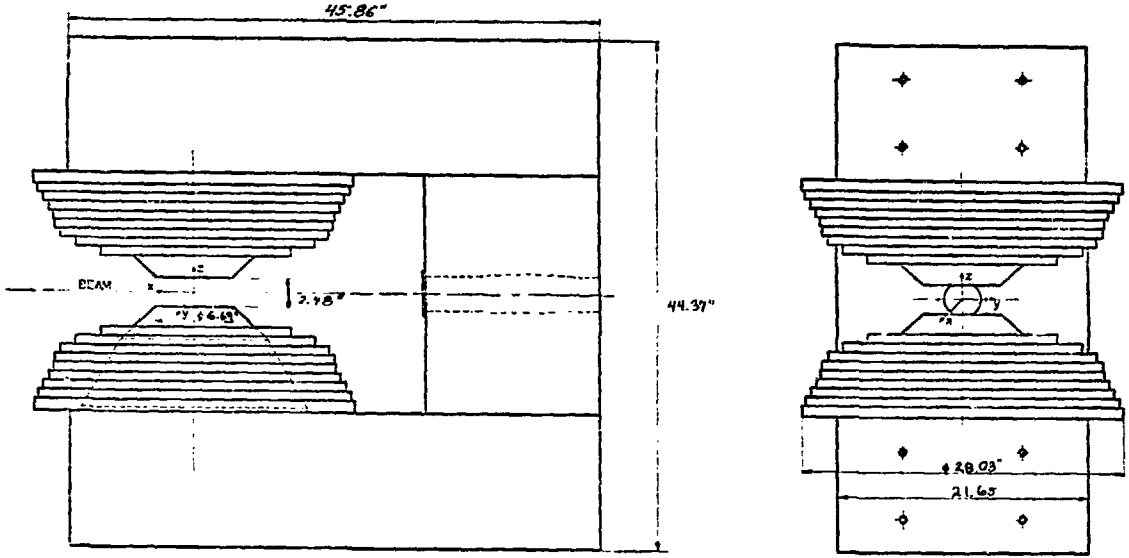

Figure 1.

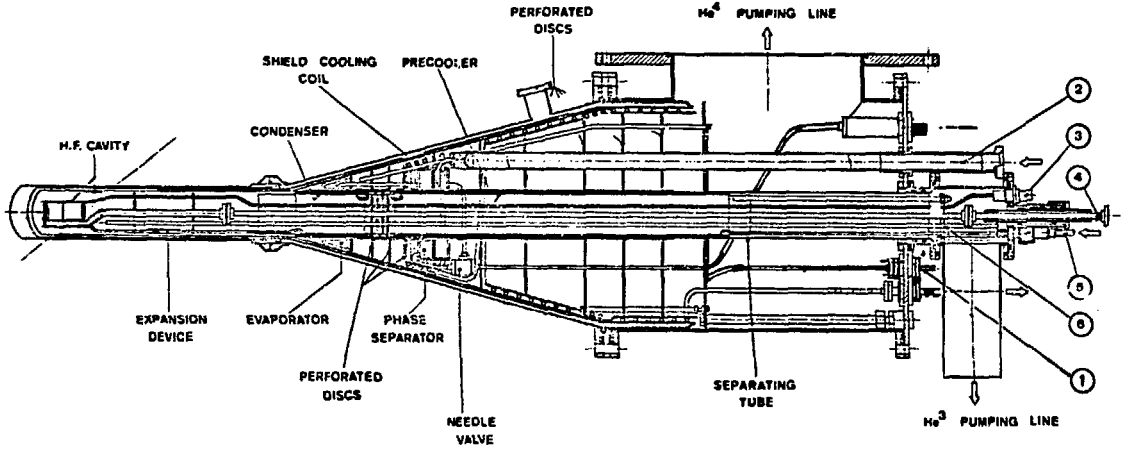

1 VAPOR PRESSURE He^4 EVAPORATOR
2 LIQUID He^4 TRANSFER LINE JACKET
3 TO NMR COIL
4 WAVE GUIDE
5 HP He^3 TO PRECOOLER AND CONDENSER
6 VAPOR PRESSURE He^3 CAVITY

Figure 2

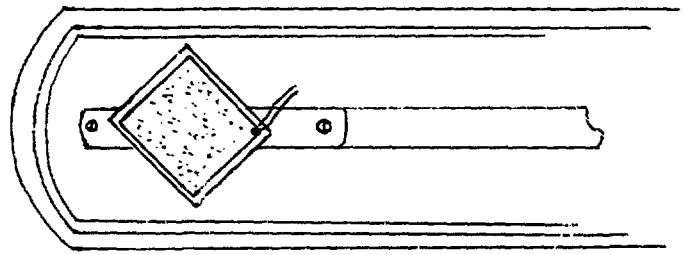

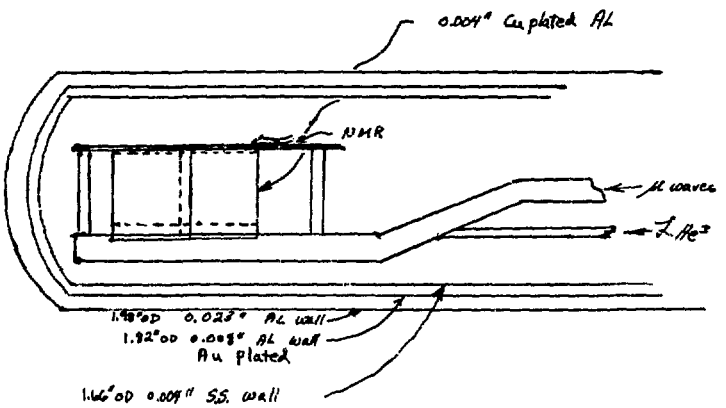

Target SIZE 0.900"L x 0.800" W x 0.500 h

Figure 3

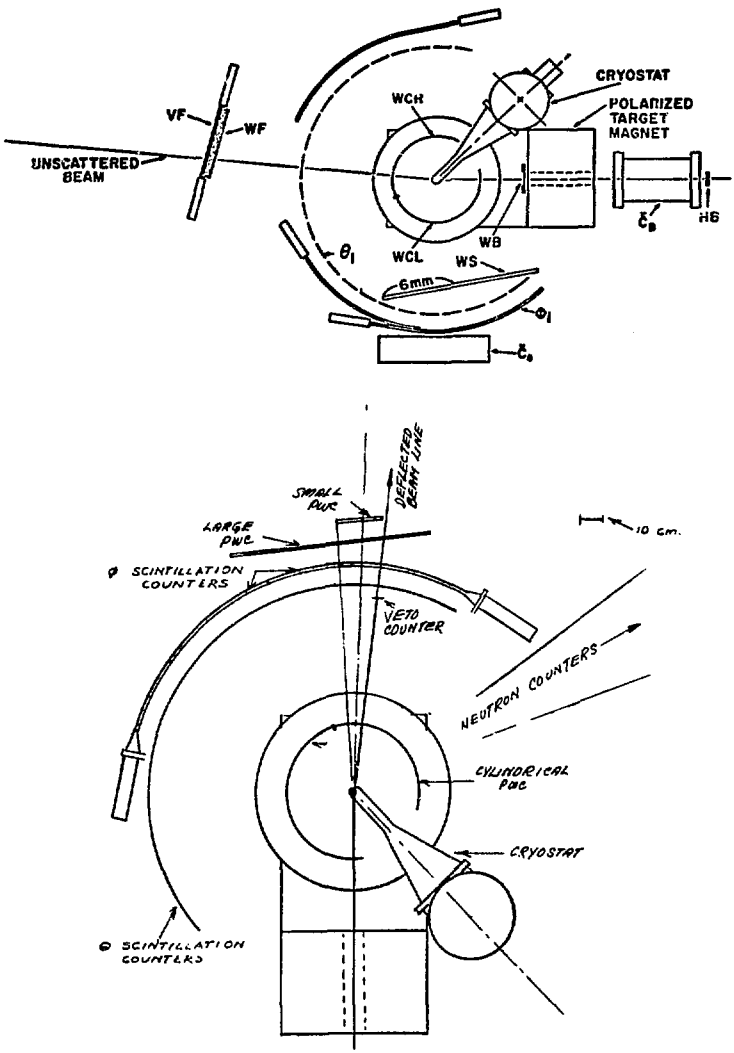
CRYOSTAT
POLARIZED TARGET MAGNET
WCH
VF
WF
UNSCATTERED BEAM
WB
WCL
WS
6mm
H6
SMALL PWC
DEFLECTED BEAM LINE
LARGE PWC
10 cm.
SCINTILLATION COUNTERS
VETO COUNTER
NEUTRON COUNTERS
CYLINDRICAL PWC
CRYOSTAT
SCINTILLATION COUNTERS

Figure 5.

LAMPF Polarized Target Program

C. Hwang

Los Alamos Scientific Laboratory

Los Alamos, New Mexico 87544

LAMPF Polarized Target Program

C. Hwang

At the present time, there are a total of six experiments approved for running time and two experiments in the deferred stage, all requiring polarized proton targets. A summary of these experiments is tabulated here below.

Measurements	Status	Beam Line	Kinetic Energy	Expected Flux
$\pi^{\pm}p$ Elastic R,A	Approved	High Energy Pions	100-600 MeV	$\leq 10^9$ for π^+ $\leq 10^8$ for π^-
$\pi^-p \rightarrow n\pi^0$	Approved	High Energy Pions	100-600 MeV	$\leq 10^8$ π^-
$\pi^-p \rightarrow n\gamma$	Approved	High Energy Pions	100-600 MeV	$\leq 10^8$ π^-
pp Elastic P	Approved	External Proton	300-800 MeV	$\leq 6 \times 10^{11}$ p
pp Elastic D,R,A	Approved	External Proton	300-800 MeV	$\leq 6 \times 10^{11}$ p
np Elastic P	Approved	External Neutron	280-780 MeV	$\leq 10^7 n/cm^2/sec$
pp Elastic Axx,Ayy,Azz	Deferred	External Proton	300-800 MeV	$\leq 3 \times 10^{11}$ p
np Elastic Axx,Ayy,Azz	Deferred	External Neutron	250-750 MeV	$\leq 10^5 n/cm^2/sec$

Since all these experiments require the polarized proton target to operate in rather high incident flux, we have designed our polarized target with this particular criterion in mind. We chose the 1-butanol doped with posphyrexide as target material for its known annealing property after radiation damage. The target will be about 10 cc in a 2.5 Tesla and 0.5°K environment. To avoid loss of He^3 (the refrigerant for achieving 0.5°K), the target will be immersed in a bath of He^4 which heat-exchanges with a 0.35°K He^3 bath. To facilitate target changes, we propose to flow in the 2-3mm diameter frozen butanol target material with

liquid nitrogen and remove them either by melting and draining or by flowing out the damaged target material in its frozen form as suggested by G. Shapiro and M. Zeller at this conference.

Our Roubeau cryostat, now under construction, is designed for 10-20 mW heat load and is pump-limited. With larger He^3 pumps, we expect 50-60 mW refrigeration capacity. The magnets to be used are a 6" ID x 10" OD x 10" long superconducting solenoid for longitudinal polarization and a Varian 22" "H" frame magnet with 2" gap for the transverse polarization targets. We have deliberately kept the helium 4 reservoirs for both our Roubeau cryostat and the superconducting solenoid small to facilitate the moving of target from one beam line to another and use continuous transfer from 500 liter Linde dewars for our helium supply. We hope to have this target in operation about the end of Calendar Year 1974.

CRYSTALLINE HD TARGETS*

E. H. Graf

SUNY at Stony Brook
Stony Brook, New York

ABSTRACT

Recent proton spin relaxation studies in HD are reviewed. The measurements were made under conditions of brute-force polarization of up to 40%. Proton relaxation times were determined as functions of temperature, applied magnetic field and H_2 and D_2 impurity concentration. Some practical considerations in building a usable target are discussed.

INTRODUCTION

In this communication we will outline recent nuclear magnetic resonance studies of solid HD and discuss the bearing they have on the problem of producing a practical polarized proton target by static methods. The work described is primarily the thesis research[1] of Dr. H. M. Bozler** and Mr. J. A. Brown.

Conceptually, the idea of static or "brute-force" polarization is extremely simple; one need only subject the protons to a large enough magnetic field H_o at a low enough absolute temperature T. The polarization P of an assembly of N protons with magnetic moment μ is then given by

$$P = (N_+ - N_-)/N = \tanh(\mu H_o/kT) \qquad (1)$$

where N_+ and N_- are the numbers of protons parallel and antiparallel to the field. As a rough rule of thumb, the polarization, for values of $P \lesssim 0.4$, is given approximately by $P \approx H_o/T$, if H_o is expressed in Teslas and T in mK. It is evident from this that a magnet in the 10-15 T range and a dilution refrigerator in the 10-30 mK range are necessary for static methods. Fortunately, both these requirements can be met by present technology.

Having decided that static polarization is feasible in principle, we must next determine material most suitable as a proton source. It is unfortunate that solid hydrogen, the most obvious choice, solidifies only in molecular (H_2) form and the antisymmetrization conditions imposed by quantum statistics require that odd molecular rotational states be associated with even nuclear spin states and vice-versa. Thus in ortho-H_2 the total nuclear spin is I=1 (protons parallel) and the molecular rotational state is restricted to values J=1,3,5,..., while for para-H_2, I=0 (protons antiparallel) and J=0,2,4,..... At temperatures low enough for appreciable polarization, the equilibrium state of hydrogen is the para state (the J=1 and J=0 rotational levels differ in energy by some 86 K), and since I=0 for that state, para-H_2 is not polarizable. On the other hand, non-equilibrium ortho-H_2 does exist for long periods of time at helium temperatures and converts but slowly to para-H_2 (at ~0.6%/hr.). Nevertheless, because of the heat released by the conversion process, it is not practical to cool ortho-H_2 to the mK region. For these reasons, H_2 is not a suitable material for static polarization.

The situation is quite different for solid HD, because the distinguishability of the nuclei removes the difficulties outlined above. As a target material, HD possesses a volume density of polarizable protons (2.7×10^{22} spins/cc) that compares favorably with other target materials and has the obvious advantage of containing relatively few extraneous nucleons. The factors that determine the practical utility of HD as a target material are the proton spin-lattice relaxation time T_1 and the thermal contact between the refri-

gerator and the sample. T_1 is affected by H_0, T and the impurity concentrations of H_2 and D_2. We will investigate the effects of each of these in the discussion to follow.

APPARATUS

The cryostat is shown schematically in Fig. 1. The dilution refrigerator is of a type described by Wheatley,[1a] but it has been modified to fit into the restricted geometry imposed by the 1" bore of the superconducting solenoid. This magnet, wound with niobium-tin ribbon and homogeneous to $\sim 10^{-4}$ over the sample volume, is capable of producing fields slightly over 10 T.

Fig. 2 shows the details of the mixing chamber of the dilution refrigerator. The HD sample is contained in a thin-walled stainless steel chamber which in turn is surrounded by the ^3He-^4He liquid mixture. Some heat exchange between the sample and the mixing chamber fluid is provided by sintered copper disks soldered to the inside and outside of the walls of the sample chamber. Temperature is determined by three separate thermometers, viz.: (1) a calibrated Speer carbon resistor (room temperature resistance of ~100 ohms), (2) a powdered copper NMR thermometer, and (3) the proton spins of the HD sample itself. The NMR thermometers are calibrated against ^3He vapor pressure at temperatures between 0.7 and 2.2 K. The resistance and copper thermometers are in direct contact with the mixing chamber liquid.

HD proton resonances are observed with the high-frequency constant-current Q-meter (Rollin) circuit shown in Fig. 3. The resonant circuit consists of a variable length of transmission line terminated at one end by the sample coil and at the other end by an open circuit. Directional couplers are used to drive the line and to measure its response. The driving frequency (which varies from 60 to 420 MHz depending on H_0) is tuned to a line resonance corresponding to a voltage standing wave maximum, as observed through the receiving directional coupler. Line resonances with a $Q \approx 40$ appear at regular intervals of ≈ 40 MHz in the driving frequency, corresponding to successive standing wave modes. These intervals conveniently cover the entire frequency range of interest. Intermediate resonant frequencies, when desired, are achieved by adjusting the length of the transmission line at the open end. Once a line resonance is tuned in, the nuclear resonance is observed by adjusting H_0 to the appropriate value and then modulating the driving frequency. Frequency rather than field modulation is used to eliminate eddy current heating and to allow the superconducting solenoid to be used in the persistent mode. The depth of modulation of the carrier as the protons are swept through resonance can be as much as 30% when the polarization is high, requiring corrections for non-linearity and admixture of the dispersive mode in the observed signal. These corrections are made by a computer simulation of the NMR circuit, using experimental parameters for the line impedance, line loss, circuit non-linearities, etc.

RESULTS

By observation of the proton resonance absorption, we have been able to determine that polarizations of >0.4 can be achieved with the apparatus described. The limiting factor seems to be temperature equilibrium between the dilution refrigerator and the sample, of which more will be said later.

The T_1 measurements are made by observing the regrowth of signal amplitude following saturation. The relaxation sometimes exhibits small deviations from exponential form, as has been observed by others,[2,3] probably due to non-uniform distribution of the impurity molecules, H_2 and D_2. Nevertheless, T_1 is taken as the time constant of the best least-squares exponential fit to our data. Relaxation time measurements range over $5 \text{ sec} < T_1 < 10^5$ sec with magnetic fields varying between 1.4 and 10.2 T.

It has been observed by ourselves[4] and others, in HD resonance work at higher temperatures,[2,3] that T_1 is strongly affected by the ortho-H_2 impurity concentration $c_{o\text{-}H_2}$. The intrinsic relaxation time of protons in HD directly to the lattice is exceedingly long at low temperatures and has never been measured below 10 K, where this time is of the order of 10^6 sec. The direct relaxation is due to self-diffusion, which weakens drastically as $T \to 0$.[5] At helium temperatures and below, relaxation of HD protons is thought to take place via an indirect process, in which the protons couple to impurity molecules in a $J=1$ state (these are present in the form of $o\text{-}H_2$ and $p\text{-}D_2$), and these molecules in turn relax rapidly to the lattice.[5,6]

Our HD samples contain 1-2% H_2 impurity and 0.5-1% D_2 impurity. The concentration of the ortho-H_2 and para-D_2 (i.e., $J=1$) impurities are varied by storing the HD samples at helium temperatures and allowing the $J=1$ impurities to convert to the $J=0$ ground state. The effect on T_1 of the storage time is shown in Fig. 4. By adding known amounts of H_2 to our samples, we have determined the ortho-para conversion rate for H_2 to be 0.57 ± 0.03 %/hr, in reasonable agreement with other experimental work.[3,7]

Figs. 5-9 are plots of our results. Fig. 5 shows the temperature dependence of T_1 for several values of H_0 and $o\text{-}H_2$ impurity concentration. In general, the data can be fitted to the form

$$T_1 = T_1^{\circ} e^{\alpha/T} \qquad (2)$$

where T_1° and α are constants. Values of α vary considerably with H_0, from $\alpha \sim 16$ mK at 1.4 T to ~ 54 mK at 9.9 T. The dependence of α on $c_{o\text{-}H_2}$, however, is seen to be much weaker.

The relative concentration of $o\text{-}H_2$ to $p\text{-}D_2$ also affects the temperature dependence of T_1. In Fig. 5, the ratio $c_{o\text{-}H_2}/c_{p\text{-}D_2}$ is

≈3. In Fig. 6, T_1 vs 1/T data are shown for varying ratios of J=1 impurity concentrations. We see qualitatively that the temperature dependence becomes weaker as the relative fraction of $p\text{-}D_2$ increases.

Fig. 7 shows the dependence of T_1 on $c_{o\text{-}H_2}$ for a number of values of H_o. The points follow a simple power law $T_1 \propto c_{o\text{-}H_2}^{-\beta}$ in the limit of low concentrations. In Fig. 7, the $o\text{-}H_2$ to $p\text{-}D_2$ concentration ratio is ≈3. In Fig. 8, similar curves (all taken at H_o=10 T) are shown, but the J=1 impurity concentration ratio is varied. It is seen that the power law dependence of T_1 on $c_{o\text{-}H_2}$ diminishes as the ratio $c_{o\text{-}H_2}/c_{p\text{-}D_2}$ diminishes.

A marked magnetic field dependence of T_1 is also evident from Fig. 7. We have measured this field dependence directly, holding the impurity concentrations constant. A plot of such data is shown in Fig. 9. The break in the linear portion of the curve corresponds to the deviation of T_1 from the simple power dependence on $c_{o\text{-}H_2}$.

COMPARISON WITH EXISTING THEORY

The problem of HD proton relaxation in the presence of small $o\text{-}H_2$ impurities has been treated theoretically by Sung.[6] He calculates the $o\text{-}H_2$ relaxation rate due to the intramolecular dipole-dipole interaction in the presence of a strong intermolecular electric quadrupole-quadrupole interaction[7] and a crystal field. The HD protons are in turn coupled to the $o\text{-}H_2$ by a rapid, energy-conserving cross-relaxation.[5] The calculated dependence of T_1 on $c_{o\text{-}H_2}$ and H_o describes our results in a qualitative way, but quantitative agreement is lacking. For example, Sung obtains $T_1 \propto c_{o\text{-}H_2}^{-2.25}$ as compared to our experiment in which the exponent ≈-3.75. The calculated field dependence is $T_1 \propto (aH_o+E_o)^{7/4}$, where a and E_o are constants, whereas experimentally T_1 is proportional to H_o at high fields. The theoretical temperature dependence of T_1 does not seem applicable to our system in the temperature and impurity concentartion regions covered. A more complete theory will have to include a temperature-dependent relaxation mechanism valid in the mK range, which, moreover becomes more strongly temperature dependent as H_o increases.

STATICALLY POLARIZED HD TARGETS

The experiments described here show that HD can be polarized to significant levels using existing technology. With no change in our apparatus except replacing the present superconducting solenoid with one that can produce a field of 14 T (which is readily available commercially), a polarization in excess of 0.60 is possible. Relaxation times are variable over a wide range; we have observed values of T_1 between ~20 sec to over one day.

As mentioned before, the limiting factor in our present apparatus is the temperature to which the sample can be lowered. Fig. 10 shows typical ratios of HD spin temperature to dilution refrigerator

bath temperature as a function of bath temperature. Curve 1 shows our results when the HD was condensed in the sample chamber by itself and curve 2 shows the temperature ratio when a small amount of heat-exchange liquid (pure ^{3}He or a ^{3}He-^{4}He mixture) was added to the sample after the latter had been condensed into the sample chamber. The ultimate attainable spin temperature has varied from run to run (probably due to variations in how the sample condensed, including grain size, adhesion to surfaces, etc.); in practice, we have found it difficult to reduce the spin temperature to less than 22 mK, even though the bath temperature is less than 18 mK. We believe this effect to be due to a sharp rise in the Kapitza boundary resistance at the lowest temperatures.

The samples used in the present experiment are ~0.3 cc in volume, too small to be of much use as a practical target. However, dilution refrigerators much larger than the one described here are in use[8] and could certainly be employed in large HD target work.

There are several approaches to the actual utilization of a polarized HD target. One is to maintain the polarization in situ during a beam experiment. The disadvatages here obviously are the presence of the large H_0 field and the possibility of beam heating. If we assume a heating rate of ~2 MeV/particle/cm, then a simple calculation shows that the heat load on a sample 10 cm long by 1 cm^2 in cross-section will be of the order of ~30 erg/sec if the beam flux is 10^6 particles/cm^2/sec. A dilution refrigerator operating in the 20 mK range will not tolerate heat loads much larger than this, so it would not be easy to maintain the sample temperature in fluxes larger than the one given above.

Of course, if T_1 were very long (say ≥ 3 days), the fact that the target warmed up to a higher temperature (e.g., 200 mK, where the refrigerator can handle much larger heat loads) would not be very significant because T_1 would still be $\gtrsim 1$ day at that temperature (see Figs. 5 and 6). We assume here that radiation damage would not cause a rapid relaxation of the proton spins, and indeed, recent radiation damage work[9] indicates that HD samples exposed to $\sim 10^{19}$ protons/cm^2 are not intolerably depolarized by the passage of these particles.

Much the same argument can be made for reducing the magnetic field, once polarization has been established, although here we have to be more careful because of the stronger dependence of T_1 on H_0. Reduction of H_0 by an order of magnitude would cause a similar reduction of T_1 (see Fig. 9). Thus in order to have a working T_1 of 1 day, it would be necessary to polarize the sample in a dilution refrigerator and wait until the J=1 to J=0 conversion causes T_1 to increase from a reasonable starting relaxation time of, say, 1 hr to a time of 10 days. Only then could the large field be reduced. This procedure would require some two weeks of continual-running dilution-refrigerator time.

The suggestion that long-T_1 HD targets be used under low-field, high-temperature conditions was first published by Honig[10] and he has proposed storing and using targets at helium temperature (4.2K). This scheme would require exceedingly long values of T_1 under high fields and low temperatures; reducing the field and raising the temperature to 4.2K would each lower T_1 by an order of magnitude (see Fig. 9 and Refs. 2 and 3, which give T_1 as a function of T for T > 1 K). Before the prepared target could be used, therefore, T_1 would have to be at least 100 days, requiring some three weeks to prepare the sample. It seems questionable whether the advantage of working at 4.2 K outweighs the longer production time and technical difficulties involved with transferring the target (particularly if it is made in stages in a small dilution refrigerator), as compared with the in situ methods discussed above. It would seem that a 4.2K target would find its best application when beam heating problems are extreme.

CONCLUSION

We may safely conclude that HD targets are, at this point, largely a matter of engineering; one or the other, if not all, of the outlined methods should work and the choice of which is to be pursued depends primarily on the user's application. The same is true of the larger question of whether the advantages of HD targets vis-a-vis other materials now used for targets justify the effort required to produce them.

REFERENCES AND FOOTNOTES

* Work supported by the National Science Foundation and the Office of Naval Research.

** Present address: Department of Physics, Cornell University, Ithaca, N. Y. 14850.

1. H. M. Bozler, Thesis, SUNY at Stony Brook (1972), unpublished.
1a. J. C. Wheatley, Am. J. Phys. 36, 181 (1968).
2. W. N. Hardy and J. R. Gaines, Phys. Rev. Lett. 17, 1278 (1966).
3. R. Rubins, A. Feldman and A. Honig, Phys. Rev. 169, 299 (1968).
4. H. M. Bozler and E. H. Graf, in Proc. II Int. Conf. on Polarized Targets, G. Shapiro, ed., Berkeley (1971), p. 103; and in Low Temp. Physics- LT 13, K. D. Timmerhaus et al., eds., Boulder, Colorado (1972), Vol. 2, p. 218.
5. M. Bloom, Physica 23, 767 (1957).
6. C. C. Sung, Phys. Rev. 177, 435 (1969).
7. T. Moriya and K. Motizuki, Prog.Theoret. Phys. 18, 183 (1957).
8. T. O. Niinikoski, in Proc. II Int. Conf. on Polarized Targets, G. Shapiro, ed., Berkeley (1971), p. 107.
9. H. Mano and A. Honig, to be published.
10. A. Honig, Phys. Rev. Lett. 19, 1009 (1967); and in Proc. II Int. Conf. on Polarized Targets, G. Shapiro, ed., Berkeley (1971), p. 99.

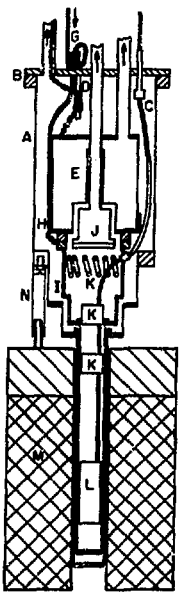

Figure 1. Simplified diagram of cryostat and superconducting solenoid. A. Exchange gas can; B. Lead O-ring flange; C. R.F. leads; D. Electrical leads and thermal grounding; E. ^{4}He pot; G. ^{3}He return line and precooler; H. ^{3}He condenser; I. 1 K heat shield; J. Still; K. Heat exchangers; L. Mixing chamber; M. Superconducting solenoid; N. Magnet support.

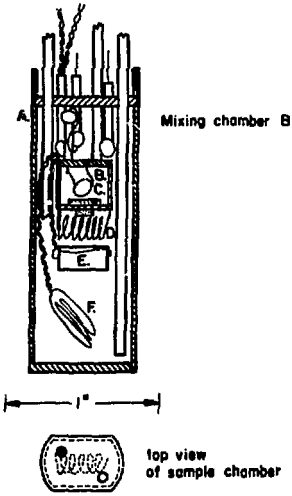

Figure 2. Detail of mixing and sample chambers. A. Stainless steel housing; B. Sample chamber; C. HD NMR coil; D. Copper NMR coil; E. Carbon resistor; F. Heater.

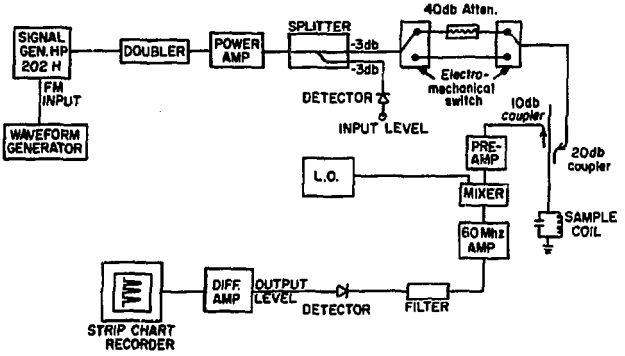

Figure 3. Block diagram of electronics for NMR at 250-420 MHz. The electronics for other frequency ranges are similar.

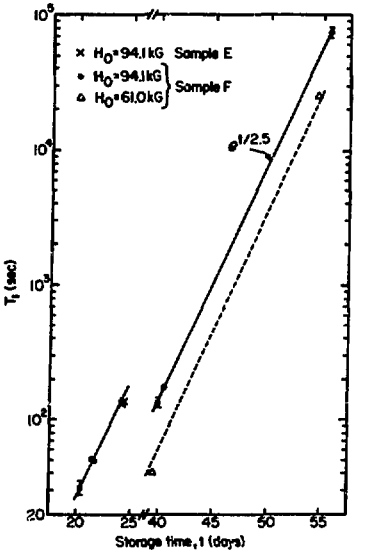

Figure 4. Proton relaxation time T_1 vs. storage time t. All data were taken at T=50 mK. The break in the slope of T_1 is due to the addition of fresh impurities.

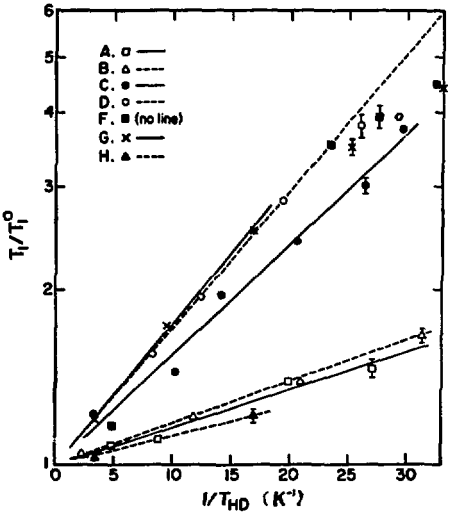

Figure 5. Temperature dependence of T_1. Values of T_1^o, α, H_o and $c_{o\text{-}H_2}$ are given below. See Eq. (2).

	A	B	C	D	F	G	H
T_1^o, sec	91.4	136	73.1	86.4	16.8	333	827
α, mK	15	16	44	54	51	57	10
H_o, kG	14.1	14.1	63.4	98.9	94.1	98.9	14.1
$c_{o\text{-}H_2} \times 10^4$	2.9	2.0	3.6	4.8	7.5	2.9	1.1

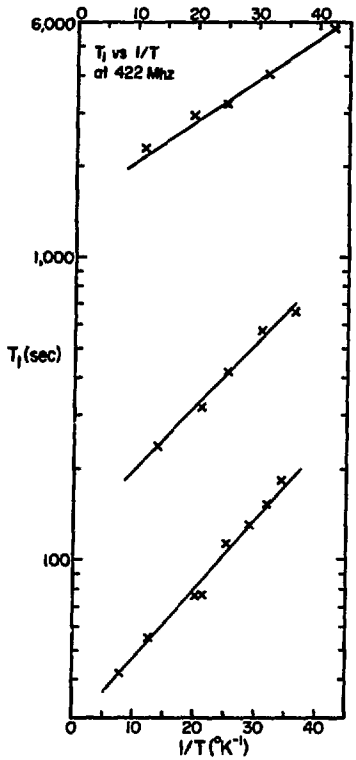

Figure 6. Temperature dependence of T_1. The ratio $c_{o\text{-}H_2}/c_{p\text{-}D_2}$ diminishes from ∿3 to ∿1 from bottom to top curves.

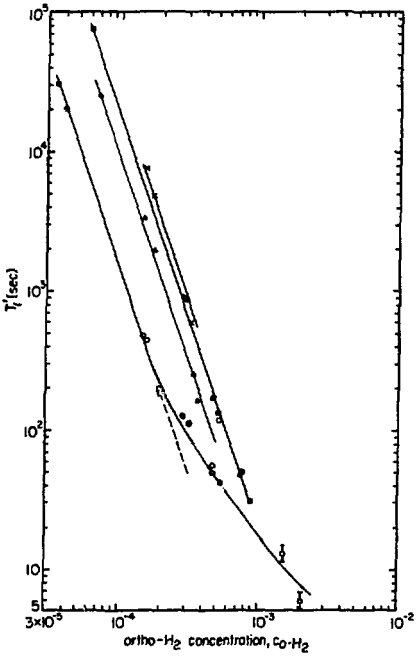

Figure 7. Dependence of T_1 on o-H_2 concentration for several values of H_o with T=50 mK. The curves, from bottom to top, were taken at H_o = 14.1, 63.4, 94.1 and 98.9 kG.

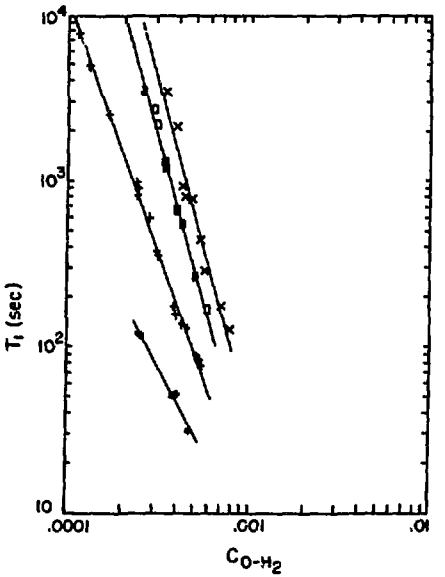

Figure 8. T_1 dependence on o-H_2 concentration with H_o = 100 kG and T=50 mK for several values of the ratio $c_{o\text{-}H_2}/c_{p\text{-}D_2}$. From bottom to top, the approximate ratios are 1, 2.6, 4.3 and 4.4. Corresponding exponents of the curves are -2, -3, -3.70 and -3.75.

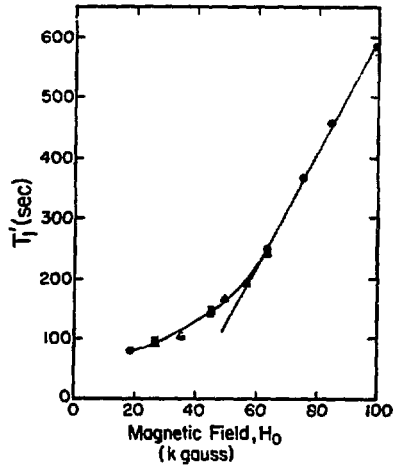

Figure 9. Magnetic field dependence of T_1. T=50 mK and $c_{o\text{-}H_2} = 3.3 \times 10^{-4}$ for circles; 46 mK and 3.3×10^{-4} for triangles.

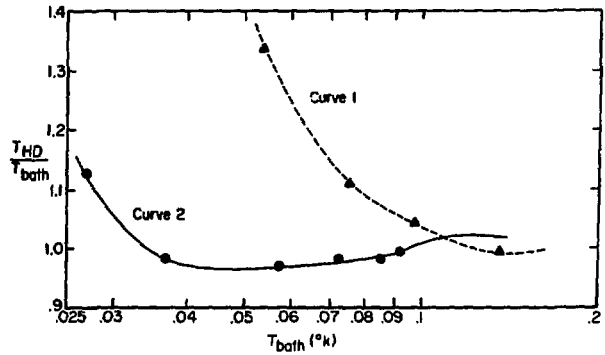

Figure 10. The ratio of the steady-state proton spin temperature of the HD sample T_{HD} to the mixing chamber temperature T_{bath}. Curve 1 represents a case where the o-H_2 concentration is 10^{-2} and no heat-exchange liquid is present. Curve 2 was taken with exchange liquid present and $c_{o\text{-}H_2} = 3 \times 10^{-4}$.

The BNL Multiparticle Spectrometer and Its Use with Polarized Targets*

Kenneth J. Foley

Brookhaven National Laboratory

Contribution to the Proceedings of

The BNL Workshop on Physics with Polarized Targets

June 3-8, 1974

* Work done under the auspices of the U.S. Atomic Energy Commission

A. Introduction

The Brookhaven Multi-Particle Spectrometer[1] is now in an advanced stage of construction. It is a very large solid angle, high resolution spectrometer employing digitized wire spark chambers in a magnetic field.

B. Magnet

The spectrometer is based on a large magnet built originally for a Heavy Liquid Bubble Chamber as part of the MURA project. The magnet has been modified at Brookhaven, using the coils and most of the steel. The new configuration is shown schematically in Fig. 1 and pictorially in Fig. 2. It is a "C" magnet, the only obstructions on the open side consisting of three 8" diameter stainless steel pillars. The size of the pole region is 4 ft. x 15 ft. and the gap is 4 ft. high. The central field in normal operation is $\approx$ 10K gauss. In order to use secondary beams from various external beams from the AGS, the magnet has been built to rotate by $\pm$ 15° about a vertical axis 18" downstream of the upstream edge of the lower pole -- this is achieved by a hydraulic bearing and piston system. The top pole is made up of 6" thick T-shaped plates with 5" gaps to permit the use of magnetostrictive readout; the chamber wires extend from the gap up above shielding slats on top of the magnet where the field is low enough to obviate the need for more shielding of the readout line.

The magnetic field has been mapped at three excitations corresponding to central field values of 10KG, 7.5KG and 5KG. The fitting of the field is proceeding and we expect to have fits which will permit field integrals to be evaluated with a precision of 1 part in 10^3.

C. Detectors

It is convenient to divide the spectrometer into three sections in order to describe the detectors:

1. The region downstream of (outside) the magnet;
2. The region in the magnet downstream of the target;
3. The region near the target.

(1) Region 1

Region 1 contains magnetostrictive readout chambers used previously in the MK1 spectrometer. These are described in detail elsewhere.[2] Two large modules (3 ft. x 10 ft. and 4 ft. x 13 ft. active area) will be used. This region will also contain a large scintillation counter hodoscope (120 elements each 2-1/2" x 84" x 3/4") and a Cerenkov counter hodoscope (20 elements each 2 ft. wide x 3 ft. high, $\gamma_{threshold} = 20$). A later addition (1976) will be a high pressure Cerenkov counter hodoscope with a threshold of $\gamma = 10$.

(2) Region 2

The downstream two-thirds of the magnet will be occupied by plane spark chamber modules to measure the angles and momenta of forward going particles. Two basic types of spark chamber modules are involved. One contains four gaps, two with vertical wires to measure the x projection and one each with wires at +15° or -15° from the vertical (MX

module). The other type contains two gaps with horizontal wires to measure the y projection (MY module).

Fig. 3 shows three MX modules hanging in a storage frame. The active area at the bottom is approximately 6 ft. wide by 4 ft. high, while the overall height of the modules is approximately 15 ft. The readout amplifiers can be seen at the top of the chambers. Fig. 4 shows several modules installed in the magnet during a recent test run.

Fig. 5 shows three MX modules plus two MY modules in the magnet. The active area of the MY modules is approximately 6 ft. wide x 4 ft. high and the wires are extended out beyond the region of field inversion to be read out in the region of low fringe field (≈ 100 gauss with no reversal in the sign of the vertical magnetic field). A typical experiment will run with 10 MX modules and 8 MY modules.

(3) Region 3

Unlike the other two regions, the arrangement in the target area is expected to vary considerably from one experiment to the next. Two totally different setups are under construction. One involves cylindrical chambers with the axis of the cylinders parallel to the incident beam. The wires are wound on mylar foils in the axial direction or to form a helix with a pitch angle of approximately 45° to give stereo information. Magnetostrictive readout will be used with the chamber wires extending to the low field region outside the magnet in front of the front shield plate. The diameter of the cylindrical chambers will vary from ≈ 12" to ≈ 47". With this setup the solid angle approaches 4π.

The other setup under construction is made up of plane chambers. A plan view is shown in Fig. 6. The main feature of this setup is a recoil proton detection system on the open side of the magnet. The

proportional wire chambers (PWC's) will be used to trigger on slow recoil protons. The other detectors are wire spark chambers with capacitive readout. The mass of the detectors has been minimized in order to get the best possible missing mass resolution. The other plane chambers shown help to detect decay products from the "forward going" set of particles. All of the spark chambers are the full height of the gap so a very large solid angle is achieved.

D. Resolution

We estimate the expected resolution of the various parts of the apparatus to be as follows: Forward direction, using only the chambers inside the magnet, $\Delta\theta \lesssim .15$ mrad; $\Delta p/p \lesssim 0.4\%$ at 10 GeV/c. With additional information for tracks that exit from the magnet and traverse the downstream chambers we expect $\Delta p/p \lesssim 0.2\%$. In the region near the target we expect $\Delta\theta \lesssim 1$ mrad, $\Delta p/p \lesssim 2\%$ for particles perpendicular to the field.

E. Beams

The beam currently available for use in the MPS is the Medium Energy Separated Beam (MESB) from the B target station. The momentum limit of the beam is $\lesssim 9$ GeV/c, but K,π separation is expected to be poor above 6 GeV/c. During 1975 we expect the completion of the High Energy Unseparated Beam (HEUB) from the A target station. This beam will be capable of transporting 30 GeV/c particles and should provide useful fluxes to $\gtrsim 25$ GeV/c. In each beam proportional chambers will be used to achieve an incident angle resolution of $\lesssim 0.25$ mrad with

$\Delta p/p$ of $\lesssim$ 0.2%. Cerenkov counters will be used to select the type of incident particle required for an experiment.

F. Trigger

Various trigger schemes will be used in experiments with the MPS -- scintillation counter hodoscopes of various sizes are being constructed as are proportional wire chambers of many shapes and sizes. Details of the schemes to be used can be found in the various approved and proposed experiments but they range from the selection of multiplicity in hodoscopes and PWC's (including Vee selection by a change in multiplicity following a decay space) to a fast digital trigger system using three PWC's to select missing mass and momentum transfer for slow recoil protons; a water Cerenkov counter will be used to identify protons. The various downstream Cerenkov counters can also be used in the triggers.

We encourage the use of very selective triggers - say $1/10^4$ beam particles - for low cross sections in order to achieve the very high sensitivity available with the MPS, 30,000 events per seen μb in 100 hours. This will also reduce the computer time required to analyze the data.

G. Approved Experiments

1. AGS experiment #557: A study of the ζ and R regions; University of Pennsylvania (W. Selove et al.), University of Massachusetts (J. Shafer et al.), Brandeis University (J. Bensinger et al.), and BNL collaboration. The objective is to do a high statistics experiment ($\sim$ 4000 events/μb) in selected regions of mass and momentum transfer for the reaction $\pi^- p \to X^- p$

with full detection of all the outgoing charged tracks. Emphasis will be given to a detailed study of the I = 1 boson resonances in the region of $\delta^-(970)$ and the $R^-(1600\text{-}1800)$. This experiment uses the target area assembly I (recoil proton detection) and trigger-selection will be made by a fast ($\approx$ 200 nsec) kinematical determination of the forward going missing mass and momentum transfer. A water filled threshold Cerenkov counter will identify the protons. A trigger-selection resolution for forward going missing mass of (ΔM) $\approx$ 50-100 MeV (FWHM) and a momentum transfer resolution (Δt) of .02 $(GeV/c)^2$ is expected (proportional wire chambers alone). Spark chambers interleaved with the proportional chambers will be used in the analysis to improve the resolution. The spark chamber systems on both sides of the target and downstream (all plane chambers) detect the charged decay products of the boson.

2. AGS experiment #594 (BNL/CCNY collaboration). A survey experiment with the BNL MPS; a systematic study of the production and decay of boson resonances and production of vee particles. In this experiment, forward going strange and non-strange boson spectra from $\pi^\pm p$, $K^\pm p$, pp and $\bar{p}p$ interactions will be studied in the $K\bar{K}$, $K\pi$ and $K\pi\pi$ decay channels. The emphasis will be on t and s dependencies of the production and measurements of the decay angular distributions. K^o and Λ production from $\pi^- p$, $K^- p$ and $\bar{p}p$ will also be studied with the aim of measuring the polarization of forward and recoil Λ^o's. The basic trigger selection is by counting the number of charged particles traversing proportional chambers and thus detecting the decay of a neutral vee. Typical reactions to be studied are:

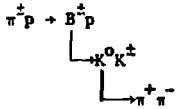

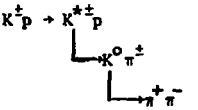

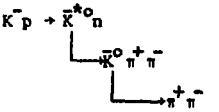

$$\pi^- p \to K^o Y^o$$

$$\pi^- p \to \Lambda \begin{pmatrix} K^o \\ K^{*o} \end{pmatrix}$$

$$\bar{p} + p \to K^o \bar{K}^o$$

$$\bar{p} + p \to \bar{\Lambda} \begin{pmatrix} Y^o \\ Y^{*o} \end{pmatrix}$$

3. AGS experiment #596: Tests of exchange models in two-body scattering including $\bar{p}p$ annihilations, exotic exchange, and other reactions from 4-10 GeV/c; Carnegie-Mellon University (R.M. Edelstein et al.) and Southeastern Massachusetts University (J.J. Russell et al.). In this experiment the object is to study several two-body and quasi-two-body scattering processes with a view toward making detailed tests of exchange models. Reactions included in this study are those characterized by allowed baryon exchange such as $\bar{p}p \to \pi^{\pm}\pi^{\mp}$, $\pi^{\pm}\rho^{\mp}$ etc.,

$\pi^- p \to p\pi^-$, $p\bar{p}^-$ etc., $\bar{p}p \to K^-K^+$, K^-K^{*+} etc. A study of reactions such as $K^- p \to pK^-$, $K^- p \to \pi^+\Sigma^-$, $K^- p \to K^+\Xi^-$, $\bar{p}p \to K^+K^-$, $\bar{p}p \to p\bar{p}$, $\pi^- p \to K^+\Sigma^-$, etc. is also proposed (the latter reactions are so-called first forbidden as exotic exchange processes). For this experiment the target will be located in front of the MPS and will be surrounded by a set of cylindrical spark chambers. A high pressure Cerenkov counter at the upstream end of the MPS will identify the forward going secondary.

4. AGS experiment #601: $\bar{p}p \to \bar{V}^o V^o$ + neutrals near 6 GeV/c; Brandeis University (L. Kirsch et al.), Syracuse University (M. Goldberg et al.), and University of Cincinnati (B. Meadows et al.). The cylindrical spark chamber arrangement will be used (inside the magnet). The final state of the reaction of interest is two neutral vee's decaying into two charged particles each plus neutrals, and the trigger selection will be made using a veto scintillation counter which surrounds the target and a cylindrical proportional chamber which detects the decay of neutral vees.

In addition to the above, a further 6 proposals or letters of intent have been submitted.

H. Comments on Use with Polarized Targets

The MPS is ideally suited for use with a polarized target. The large solid angle will give the highest possible data rates for a given target and, in addition will permit the selection of events with the target polarization either in or perpendicular to the plane of matter (plus any direction in between, of course) limited mainly by the cryostat and other equipment associated with the target. Thus, in addition

to the polarization parameter, P, one can envision measurements of the spin rotation parameters, R and D, particularly for those experiments involving Λ^o's whose polarization can be determined from decay distributions. This is of particular importance in the case where one is studying reactions of the type:

$$\pi + p \rightarrow (\text{strange boson}) + \Lambda^o$$

$$K + p \rightarrow (\text{non-strange boson}) + \Lambda^o$$

In this case the study of decay correlations, including joint correlations will permit complete determination of the scattering amplitudes.[3]

In those cases where the boson has spin zero, it is also necessary to study the reactions with a component of the polarization vector of the proton in the incident beam direction. Hence it is necessary either to bring in the incident beam at an angle to the horizontal plane or to rotate the MPS field in the region of the target -- or both. One can envision rotating the field with superconducting coils as a later development at the MPS.

There is one obvious restriction on the target to be used in the MPS. The detector system requires significant changes in order to run the spectrometer with the field reversed from the usual direction -- basically the necessary bias on the readout wires for the magnetostrictive readout would demand that the high voltage pulses be reversed if the field were reversed. Consequently it is highly desirable that the polarization be easily reversed without a change in the magnetic field.

At present, the most promising target suggested for use in the MPS is the frozen spin target.[4] This target would be polarized in a region of high, uniform field in the MPS produced by iron poles or field shaping coils and then moved into the main MPS field for experiments, the

polarization being retained by lowering the target temperature. Hence the solid angle would be limited only by the cryostat; careful design will give full azimuthal average. Polarizations approaching 90% can be expected with target materials with excellent fractions of free protons. Also, with this target the direction of polarization is determined by the frequency of the RF field and hence changes in the direction of the magnetic field are not necessary.

References:

1. The spectrometer is being built under the auspices of the Particle Detector Division of the Accelerator Department. The Lindenbaum/ Ozaki Group is responsible for construction of the spectrometer. Much assistance in the general program, plus actual construction of many parts of the system is being provided by various University users. I shall not attempt to list the people involved in each part of the project for fear of accidental omission of a few names!
2. K.J. Foley, W.A. Love, S. Ozaki, E.D. Platner, A.C. Saulys, E.H. Willen and S.J. Lindenbaum, Nuclear Instruments and Methods 108, 33 (1973).
3. R.D. Field, Polarization Effects in Inelastic Exclusive Processes, Part I, AEC Research and Development Report CALT-68-466, September 1974.
4. See, for example, Frozen Spins, CERN COURIER, Vol. 14, p. 293-4, September 1974; Private communication, M. Borghini.

MPS MAGNET

Weight	650 tons
Gap	6' wide x 4' high x 15' long
Central Field	10kG
Coils	14 pancakes, 11 turns ea.
Power	10,000 A @ 240V
Cooling Water	400 GPM @ 20°C rise
Downward Force at Midplane	550 tons (magnet powered)
Support	4 hydrostatic bearings, 30" dia. on steel plates
Rotation	± 15°, pivot 18" inside upstream end

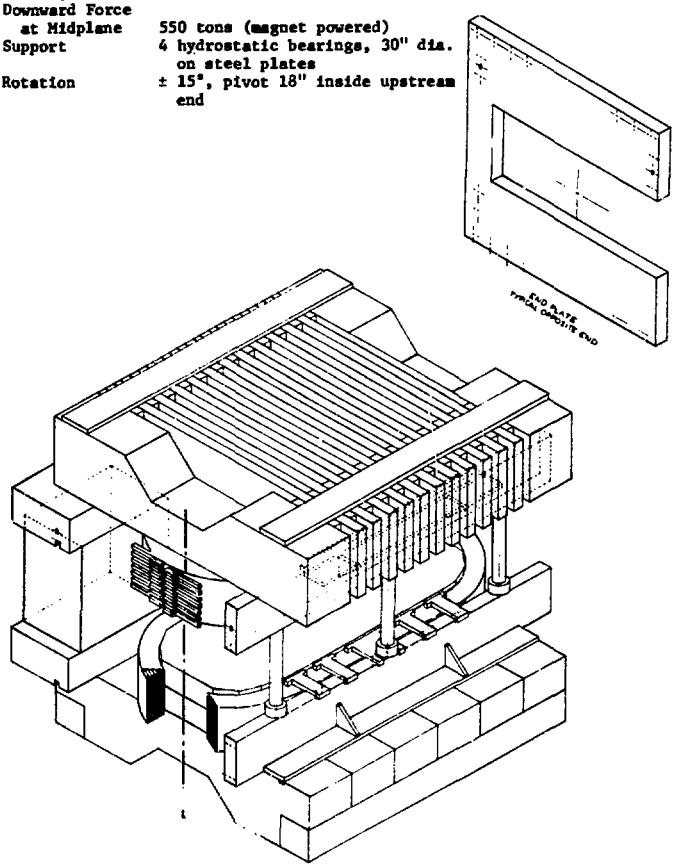

Figure 1.

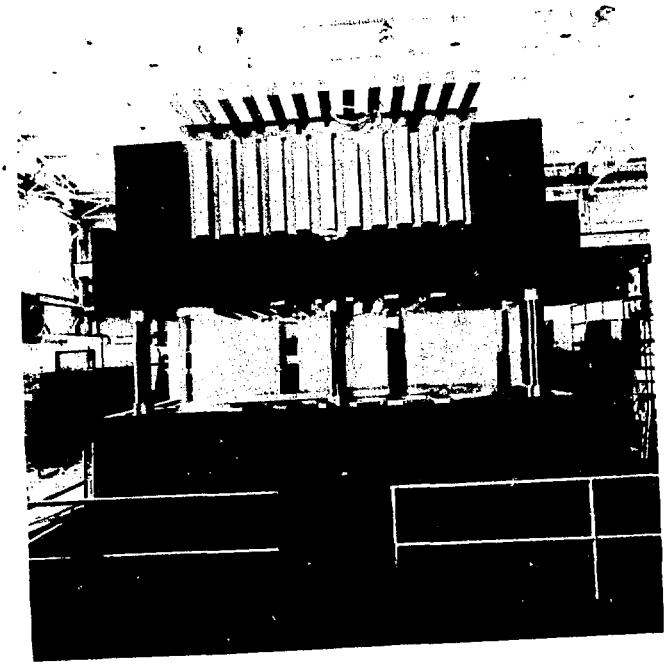

Figure 2.

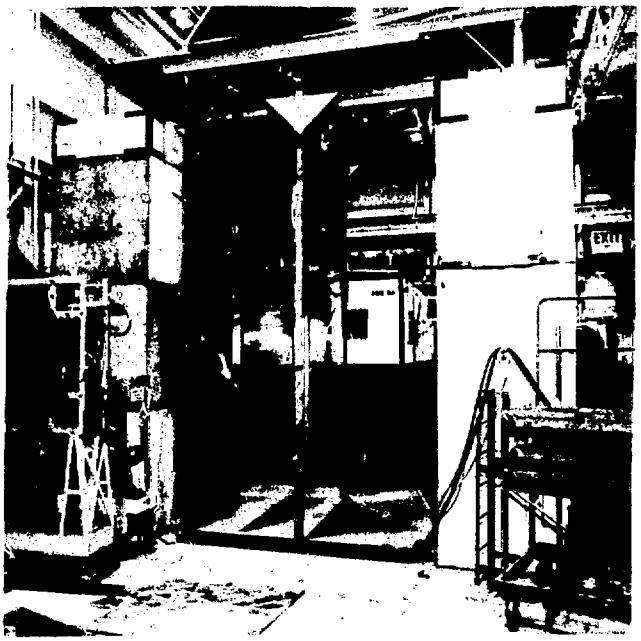

Figure 3.

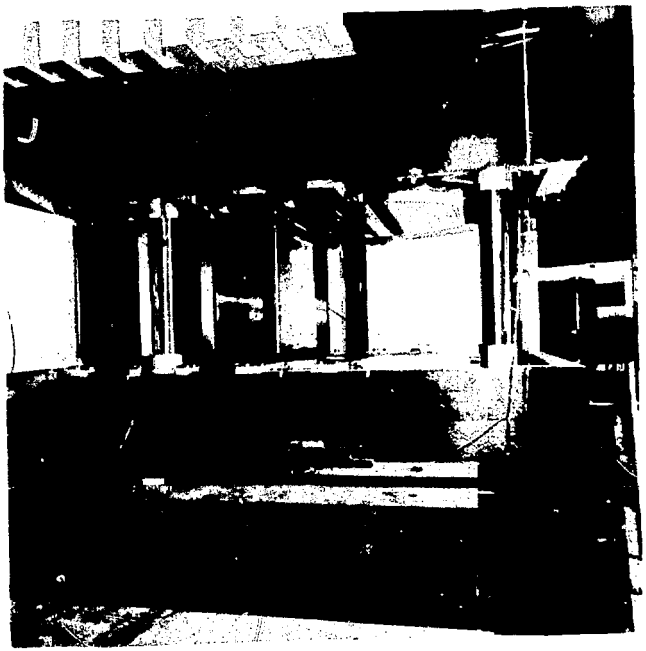

Figure 4.

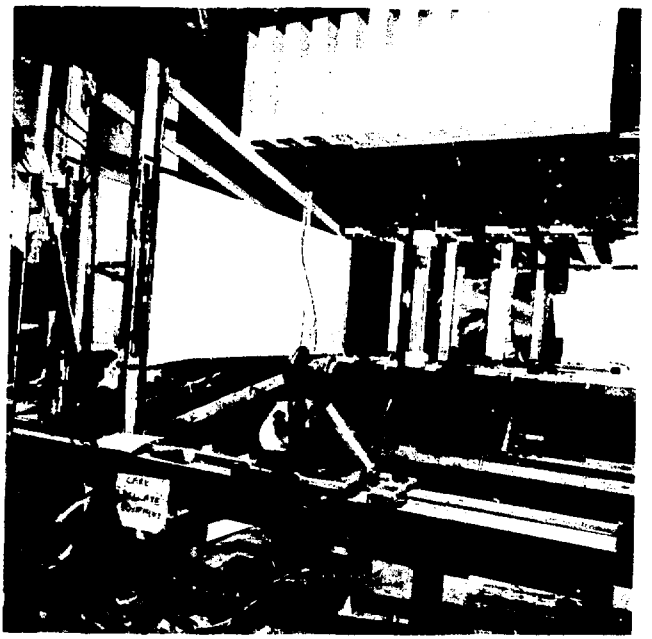

Figure 5.

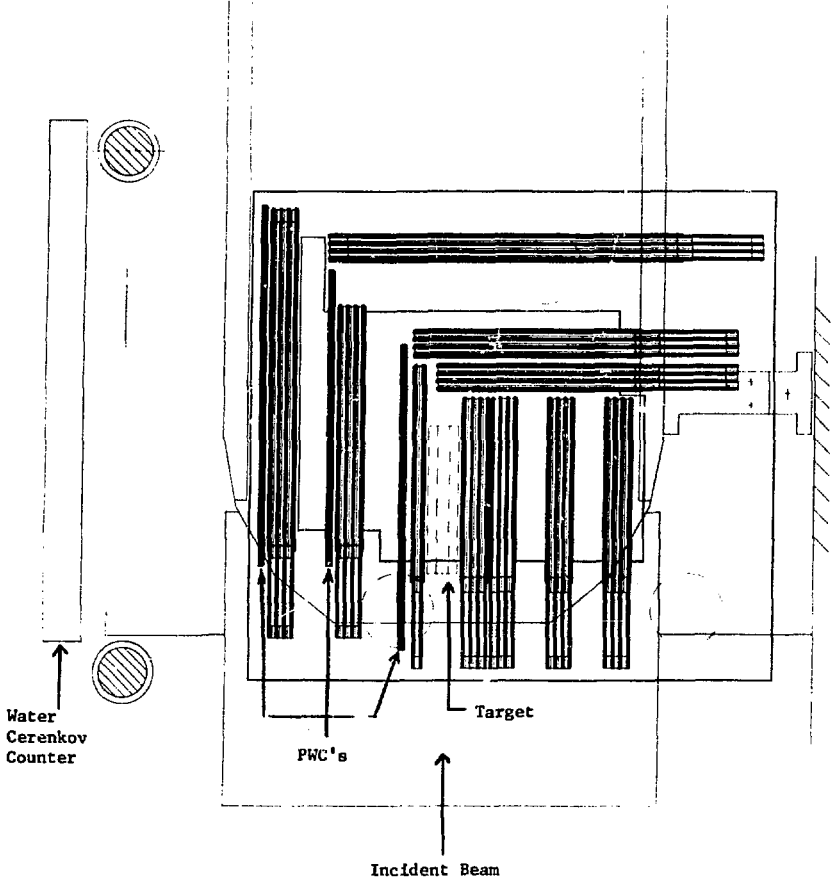

Figure 6.

BNL-19347

A POLARIZED PROTON TARGET FOR THE MPS

A. Etkin

City College of New York*

S.J. Lindenbaum

Brookhaven National Laboratory**

and

City College of New York*

S. Ozaki

Brookhaven National Laboratory**

Contribution to the Proceedings of

The BNL Workshop on Physics with Polarized Targets

June 3-8, 1974

* Work supported by the National Science Foundation

** Work supported by the U.S. Atomic Energy Commission

We propose building a polarized proton target which will allow the large acceptance of the MPS[1] to be utilized effectively.

This project has already interested a number of potential users. In particular we have been collaborating with Vernon Hughes and co-workers in the planning stages of this project. It is anticipated that a BNL/CCNY/Yale collaboration, which is informally in effect, could be expected to develop and provide such a target for the MPS, or alternatively serve as a nucleus for such a project.

It was very clear from our discussions during this summer study that particle, and particularly, resonance production and decay processes studied in the MPS would be much more readily and completely analyzed if polarized targets are employed.

We believe that if the large acceptance of the MPS, its inherent high statistics, high resolution capabilities, and its automatic data gathering and analysis capabilities were coupled with a polarized target facility, a large number of obvious experiments could be dramatically improved.

For example, in any t-channel production process if the produced particles or resonances have spin, much more information, which is often critical, can be obtained with a polarized target.

In polarized proton targets previously used in high energy physics experiments, the detector acceptance was severely restricted by the magnet required to continuously polarize the target. This condition, in general, is not very suitable for an investigation of multiparticle final states involved in the study of resonance production.

Therefore, in order to more fully utilize the large solid angle of the MPS, we propose to build a frozen spin target. In a frozen spin

target the target is polarized in one magnetic field configuration and used for scattering in another configuration (holding field). In order for this idea to be useful it is necessary that the proton polarization decay with a time constant (T_{1p}) of the order of at least 100 hours. Time constants of this order can be achieved in useful target materials (e.g. 1, 2 - propanediol containing Cr^{5+} complexes), if the polarized material is held in a magnetic field of 10KG and at a temperature of $\sim$100 m°K.

We plan to build a propanediol target system consisting of a polarizing magnet, dilution refrigerator, NMR polarization monitor, polarizing microwave source, and the MPS as the holding magnet. The target size is expected to be approximstely 10 cm long x 2 cm square. M. Borghini[2] and co-workers at CERN have successfully built and tested a propanediol frozen spin target, similar to the one we propose, that achieved a free proton polarization of 75 - 80%, which was constant to within errors for a period of approximately 30 hours. The little Ω magnet which was used for this system has a magnetic field similar in nature to that in the MPS (both have 10 KG fields and similar inhomogenuity). This target is presently being used to measure P, R and A for the reaction $\pi^- p \rightarrow K^o \Lambda$.[3]

Because we are using propanediol instead of pure hydrogen there is considerable background from the unpolarized bound nucleons (bound protons/free protons = 4.25 and bound nucleons/free protons = 8.5). If the momentum of all the outgoing particles are determined, then it is possible to reduce the background considerably by utilizing conservation of momentum and charge. Target nucleons that are bound have considerable fermi momentum so that if one looks at momentum balance with the assumption that the

target was free, one finds a peak (from free protons) with a broad background. We also plan to use partially deuterated propanediol to give a target with free deuteron polarization of greater than 30%. This material also has some polarized free protons (bound nucleons/free protons = 40 and bound nucleons/free deuterons = 5.67).

We expect to make a polarizing magnet by shimming a part of the MPS magnet and/or using booster coils that provide a 25 KG field homogenious to $\pm$ 1 part in 10^4 over the target volume. In addition to the polarizing magnet we plan to have the facilities to have a significant component of the target polarization along the beam direction to facilitate A measurements.

The frozen spin target requires a dilution refrigerator to cool the target material to ~0.5°K during polarizing and to less than 0.1°K during the holding operation. We plan to use the refrigerator design developed at CERN; this unit has a refrigeration capacity of 100 mW at 0.5°K required during polarization and can cool the sample to the holding temperature in a matter of minutes, thereby reducing the polarization loss due to relaxation. The refrigerator must be carefully mechanically isolated from the large pumping systems used with it in order to reduce heating caused by the cryostat vibrating in the magnetic field. In addition, the refrigerator must be mounted so that it can be moved smoothly from the polarizing magnet into the target position in the MPS while remaining in a magnetic field of several kilogauss at all times. The target material is contained in the mixing chamber which is surrounded by the cavity for the polarizing microwaves and the coils for the polarization monitoring NMR system. This refrigerator has a beam pipe for the incident beam coaxial with cryostat axis, thereby maximizing the detector solid angle.

Nuclear magnetic resonance will be used to monitor the polarization of the target during polarizing and holding in the MPS field. Because of the extremely long relaxation time in the holding field, data will be obtained very infrequently ($\sim$ once every 20 min.) although rapidly compared to T_{1p}. Since the NMR system will operate at two different frequencies, it will not be possible to calibrate the system in the conventional way. Instead, the 105 MHz section will be calibrated conventionally in the polarizing magnetic field by comparison of the signal when the target is polarized to that when the target is in thermal equilibrium at a known temperature. Calibration for the 42 MHz section is obtained by moving the polarized target from the polarizing field to the holding field, measuring the signal and then returning the target to the polarizing field and remeasuring the target polarization to allow correction for any depolarization during transport. It would be very difficult to calibrate the 42 MHz system directly due to the very inhomogenious magnetic field in the MPS. The entire system will be computer compatible to permit on-line data analysis.

A relatively conventional 70 GHz microwave source will be used to supply the microwave power required to polarize the target.

References:

1. See Kenneth J. Foley "The BNL Multiparticle Spectrometer and its Use with Polarized Targets", these Proceedings.
2. We are very grateful to M. Borghini for the invaluable advice and information he has given us.
3. See CERN Courier, No. 9, Vol. 14, pp. 293-4, September 1974; also, M. Borghini, these Proceedings.

EPAS 74-5

BNL 19153

BROOKHAVEN NATIONAL LABORATORY
Associated Universities, Inc.
Upton, New York

ACCELERATOR DEPARTMENT
Informal Report

AGS SECONDARY BEAMS AND PARAMETERS - FY75

D. Berley and C.L. Wang

June 25, 1974

ABSTRACT

A compilation is presented of the AGS secondary beam parameters and fluxes.

ACS SECONDARY BEAMS AND PARAMETERS - FY75

A compilation is presented of the ACS secondary beam parameters and particle fluxes. Fig. 1 shows the layout of the secondary beams at the ACS as of June 1974. Some details of the beams from the C10, A, B, B', C, C', and D target stations for 1974 and 1975 are given in Fig. 2 and 3 respectively.

Table I gives a summary of the secondary beams. Fig. 4, 5, and 6 indicate the π^+, K^+, and $\bar{p}$ fluxes obtained in various beams in typical running conditions of experiments.

References on beam properties are those available on hand, and no effort is made for completeness. The compilation will be revised when new beams and more information become available. We welcome comments and contributions from experimenters, especially with respect to measured beam fluxes.

Beam 4 - High Energy Separated Beam for 80-in. Bubble Chamber

Particles K^+, p^+, π^+, d

Momentum range	K, 3.5 to 15 GeV/c (flux limited below 3.5 GeV/c) $\bar{p}$, 3 to 15 GeV/c (flux limited above 15 GeV/c) π^+, to 24 GeV/c (focal strength limited above 24 GeV/c) π^-, to 25 GeV/c (unseparated) P, to 29 GeV/c (unseparated) d, 10 to 29 GeV/c (momentum separated)
Momentum bite	1%
Target location	External target near I 13
Target material	Be
Target size	0.2-in. wide, 0.15-in. wide, 10-in. long
Production angle	0°
Solid angle	0.0066 msr
Separator	Three deflectors
Length	119m
Purity	$\geq$ 90%

Beam 4 (continued)

Flux/burst (A)	Momentum (GeV/c)	particles/10^{12} incident protons (at 25 GeV/c) π^+	π^-	K^+	K^-	$\bar{p}$
	8	5000	2300	70	17	18
	10	4700	2000	85	16	10
	12	4000	1500	80	11	5
	15			60	4	2
(B)		particles/10^{12} incident protons (at 27 GeV/c)				
	4			30	20	200
	6			250	100	250

References: N.M.J. Woolsche, V.D. VanderBurg, T. Ferbel, and P. Yamin, in Summer Study on AGS Utilization (Ed. T.E. Toohig), BNL 14000 (1970).

N.M.J. Woolsche, private communication.

Beam 5A - Medium Energy Partially Separated Beam

Particles	K^+, $\bar{p}$
Momentum range	1.3 to 3.1 GeV/c
Momentum bite	± 2% (to ± 3%)
Target location	C10
Target material	Boron Carbide
Target size	.02-in. high, .04-in. wide, .64-in. long at 10° to the circulating beam.
Production angle	10°
Solid angle	0.47 msr
Length	1788-in.
Beam size	~ 0.8-in. diameter at experimenter's target
Separators	2 electrostatic separators
Purity	K^+/other ~ 0.5

Beam 5A (continued)

Flux/burst	Momentum	Particles/10^{12} circulating protons		
	(GeV/c)	K^+	K^-	$\bar{p}$
	1.3	3500		
	1.6	15000		8200
	1.8	28000	13000	17000
	2.0	50000	22000	29000
	2.2	68000	33000	42000
	2.4	85000		58000
	2.6	103000		70000

References: B. Barish and T.F. Kycia (preprint).
S. Mori, D. Lazarus, Y.Y. Lee, private communication.

Beam 5B - Medium Energy Partially Separated Beam

Particles	$K^{\pm}$, $\bar{p}$
Momentum range	1 to 2.5 GeV/c
Momentum bite	± 1 to ± 3%
Target location	G10
Target material	Boron Carbide
Target size	.02-in. high, .04-in. wide, .64-in. long at 10° to the circulating beam.
Production angle	10°
Solid angle	0.47 msr
Length	1522-in.
Separators	2 electrostatic separators
Purity	π^+/K^+ 1-4
	π^-/K^- 1-4
	$\pi^-/\bar{p}$ 1-15

Flux/burst	Momentum	Particles/10^{12} circulating protons		
	(GeV/c)	K^+	K^-	$\bar{p}$
	0.8			500
	1.0	950		1700
	1.5	11000	7500	12000
	2.0	30000	20000	25000
	2.4	5000	27000	40000

References: B. Barish and T.F. Kycia (preprint).
J.K. Yoh, et al., Phys. Rev. Letters 23, 506 (1969).
Y. Nagashima, private communication.

Beam 6A - G10 4.7° Neutral Beam

Particles	K_L^o
Momentum range	3 to 10 GeV/c
Target location	G10
Target material	Boron Carbide
Target size	.02-in. high, .04-in. wide, .64-in. long at 10° to the circulating beam.
Production angle	4.7°
Solid angle	3.09 μsr
Length	190-ft.

Flux/burst

Momentum (GeV/c)	K_L/sr/GeV/c/circulating proton at G10 target	$K_L/10^{12}$ circulating protons at detector
3	0.025	39000
4	0.026	48000
5	0.023	46000
6	0.020	42000
7	0.013	28000
8	0.008	18000
9	0.005	11000
10	0.003	7000
	Total	2.4×10^4 K_L

References: J.W. Cronin, in Possible Beams and Experiments for a High Intensity AGS (Ed. L.C.L. Yuan), BNL 7957 (1964), p. 44, also private communication.
E. Engels, private communication.

Beam 6B - Medium Energy Test Beam

Particles	π^+, p (unseparated)
Momentum range	2 to 17 GeV/c
Momentum bite	± 2%*

Beam 6B (continued)

Target location	G10
Target material	Boron Carbide
Target size	0.02-in. high, 0.04-in. wide, .64-in. long at 10° to the circulating beam.
Production angle	4.7°
Solid angle	9 μsr**
Beam size	3-4 in. horizontal, 2-3 in. vertical

Flux/burst

Momentum (GeV/c)	Particles/10^{12} circulating protons π^+	p
6	10^4	9×10^4
12	2.5×10^4	7×10^4
17	2×10^4	2×10^4

Remarks: *This is the maximum momentum beam transmitted. Under normal conditions the momentum defining aperture C_2 will be reduced so that the beam flux corresponds to the requirements of the Radiation Safety Committee.

**This is dependent upon the collimator C_1 at the input to quadrupole Q_1. The figure given here is for the collimator installed for Exp. 556 in the neutral beam. An acceptance of 150 μsr is attainable with no collimator.

References: T. Blair and D. Lazarus, EP&S Tech. Note 48 (1972).
D. Lazarus, private communication.

Beam 7A - G10 20° Neutral Beam

Particles	K_L^0
Momentum range	1 to 4 GeV/c
Target location	G10
Target material	Boron Carbide
Target size	0.02-in. high, 0.04-in. wide, .64-in. long at 10° to the circulating beam.
Production angle	20°
Solid angle	~ 0.0784 msr

Beam 7A (continued)

Flux	Momentum (GeV/c)	K_L^0/sr/100 MeV/c per 10^4 circulating protons
	1.0	0.63
	1.2	1.55
	1.4	2.12
	1.6	2.07
	2.0	1.55
	2.4	1.01
	2.8	0.63
	3.3	0.27
	3.8	0.14

Reference: D. Nygren, private communication.

Beam 7B - C10 18° Test Beam

Particles	$\pi^\pm$, $K^\pm$, $p^\pm$, D, T, H_e^3, H_e^4
Momentum range	0.8 to 3.3 GeV/c
Momentum bite	± 1%
Target location	C10
Target material	Boron Carbide
Target size	0.02-in. high, 0.04-in. wide, .64-in. long at 18° to the circulating beam
Production angle	18°
Solid angle	9.1×10^{-6} sr

Flux/burst

Momentum (GeV/c)	p	π^+	π^-	K^+	K^-
1.5	57000	54000	50000	8300	1700
2.5	22000	18000	14000	3600	1100
3.3	9000	6500	5000	1700	370

Particles/1.5 x 10^{12} circulating protons

(GeV/c)	p/π^+	$\bar{p}/\pi^-$	D/π^+	T/π	H_e^3/π^+	H_e^4/D
1.5	1.0	0.003	0.02	0.001	0.0002	0.02
2.5	1.2	0.006	0.03	0.001		0.003
3.3	1.5		0.04	0.0005		

References: A.S. Carroll, et al., Phys. Rev. Letters 20, 607 (1968).
C.L. Wang, Phys. Rev. Letters 22, 1011 (1969).

Beam: B1 - High Energy Charged Beam

Particles $\pi^{\pm}$, $K^{\pm}$, $p^{\pm}$

Momentum range 6 to 24 GeV/c

Momentum bite Variable (at the first focus, $\Delta p/p = \pm 1.2\%$ with ± 3/4" momentum slit)

Target location B station

Target material and size Be .2" x .2" x 6" .1" x .04" x 2" .05 diam x 6"

	Height	Width	Length	Angle
Cu (trapizoidal)	.04"	.1"	2"	6°
Heavymet (trapizoidal)	.04	.1	2	6
	.04	.1	4	6
	.04	.1	4	6 (w/heat sink)
	.04	.1	6	6

Production angle 0°

Solid angle ~ 0.3 mr

Length 3000-in.

Flux/burst (1) Based on preliminary data from Pennsylvania Group (Exp. 555, 635) ~ 2 x 10^6 particles at any momentum by varying the momentum slit

Approximate composition

Momentum	π^+	K^+	p	π^-	K^-	$\bar{p}$
10 GeV/c	.49	.01	.50	.98	.013	.005
20	.028	.003	97	.99	.006	.0002

(2) Based on Sanford-Wang curves (BNL 11299 and BNL 11479)

Momentum	π^-	K^-	$\bar{p}/10^{14}$ incident protons
6 GeV/c	1.3 x 10^7	2 x 10^6	1.9 x 10^6
12	1.1 x 10^7	2 x 10^5	8.7 x 10^4
18	3.1 x 10^6	1.8 x 10^4	6.0 x 10^3
24	2.8 x 10^5	2.7 x 10^3	70

Beam B2, B4 - Medium Energy Separated Beam

Particles	$K^{\pm}$, $\bar{p}$, $\pi^{\pm}$
Momentum range	K, 1.8 to 6.7 GeV/c $\bar{p}$, 0.5 to 9.6 GeV/c π, 0.8 to 10 GeV/c
Momentum bite	± 2.2 to ± 3%
Target location	B station

Target material and size

	Height	Width	Length
Be	.04"	.1"	4"
	.04	.1	2
Cu	.04	.1	2
W	.04	.1	2

Production angle	6° (phase 1) 3° (phase 2 - for this later phase, particle fluxes at higher momentum will be increased).
Solid angle	92 - 294 μsr
Separator	2 electrostatic separators
Beam size	~ 0.6-in. diameter at experimenter's target
Length	3182-in.

Flux/burst

Mode	3		combined			1
Momentum (GeV/c)	π^+	π^-	K^+	K^-	$\bar{p}$	$\pi^-/10^{12}$ interacting protons
2	6.7×10^{6}	5.2×10^{6}	1.7×10^{4}	5×10^{3}	2.5×10^{6}	3.4×10^{7}
3	9.2×10^{6}	7.0×10^{6}	1.4×10^{5}	4.8×10^{4}	4.3×10^{6}	4.6×10^{7}
4	9.2×10^{6}	6.6×10^{6}	3.7×10^{5}	1.3×10^{5}	4.8×10^{6}	4.1×10^{7}
5	7.6×10^{6}	5.5×10^{6}	2.3×10^{5}	8.6×10^{4}	4.2×10^{6}	3.3×10^{7}
6	5.6×10^{6}	4.0×10^{6}	1.4×10^{5}	4.3×10^{4}	3.1×10^{6}	2.5×10^{7}
8	2.7×10^{6}	1.7×10^{6}			1.5×10^{6}	9.1×10^{6}
10	1.0×10^{6}	7.0×10^{5}				

References: A.S. Carroll, in Summer Study on AGS Utilization (Ed. T.E. Toohig), BNL 16000.
J.D. Fox, EP&S Division Tech. Note No. 38 (1970).
J.D. Fox and C.T. Murphy, BNL 16916 (1972), BNL 18627 (1974).
C.T. Murphy, EP&S Division Tech. Note No. 59 (1973), No. 62 (1973).

Beam B5 - B Station Neutral Beam

Particles	K_L^o , K_S^o
Momentum range	3 to 10 GeV/c
Target location	B' station
Target material and size	Ir 0.1" diam. x 3"
Production angle	4°
Solid angle	360 μsr (K_L^o), 98 μsr (K_S^o)
Length	16-ft. (K_L^o) and 12.5 -ft. (K_S^o) from B' target to the beginning of decay volume. Length of decay volume 10-ft.

Flux/burst

Momentum (GeV/c)	K_L/sr/GeV/c/ incident proton	K_L/(1-3)x10^{11} incident proton at detector
3	.017	5.7 x 10^5
4	.017	6.0 x 10^5
5	.015	5.3 x 10^5
6	.013	4.7 x 10^5
7	.009	3.1 x 10^5
8	.005	1.7 x 10^5
9	.003	1.4 x 10^5
10	.002	0.7 x 10^5
	Total	2.9 x 10^6 K_L

Reference: Preliminary data from Princeton/U. of Mass. Group (Exp. 572), private communication.

Beam C1 Muon Beam

Particles	$\mu^{\pm}$
Mean momentum	5.8 and 7.3 GeV/c (momentum range 5-9.5 GeV/c) The beam is modified to extend the momentum up to 12 GeV/c.
Momentum bite	± 10%
Target location	C station
Target material	Cu
Target size	0.1-in. high, 0.2-in. wide, 1.5-in. long

Beam C1 Muon Beam (continued)

Horizontal spread (at target)	± 2.5 cm
Vertical spread (at target)	± 1.8 cm
Tagging efficiency	~ 60%
$\Delta p/p$ for tagged muons	1.5%
(r.m.s.)$\Delta\theta_x$=(r.m.s.)$\Delta\theta_y$ for tagged muons	10^{-3} radians
(r.m.s.)Δx = (r.m.s.)Δy for tagged muons	2.1 mm
Pion contamination	$< 5 \times 10^{-7}$
Beam/halo	2/1
Flux	$\sim 10^8/10^{12}$ protons on target

Reference: A. Entenberg et al., Univ. of Rochester Report, UR-469, COO-3065-68(1973).

Beam C2, C4 - Low Energy Separated Beam

Particles	$K^{\pm}$, $\bar{p}$, $\pi^{\pm}$
Maximum momentum	1.1 GeV/c
Momentum bite	± (1-2)%
Target location	Target station 'C'
Target material and size	Cu (0.1-in. high, 0.2-in. wide, 4.1-in. long) Ir (.2-in. diam. x 3-in.)
Production angle	10.5^{o}
Solid angle	2.64 msr
Separator	1 electrostatic separator
Length	580-in.
Beam size	2-in. wide, 1-in. high (FWHM) at 66-in. downstream of the last quadrupole

Beam C2, C4 (continued)

Flux and purity	Target	$\frac{\Delta p}{p}$	Momentum (GeV/c)	Flux Particles/10^{12} incident protons			Purity		
				K^+	K^-	$\bar{p}$	π^+/K^+	π^-/K^-	π^-/p^-
	Cu	±1%	.5		5.0×10^{2}	18		360	470
			.6	8.8×10^{3}	2.7×10^{3}	280	26	56	68
			.8	4.0×10^{4}	9.8×10^{3}	1300	7	13	17
			1.0	1.0×10^{5}	3.7×10^{4}	3400			16
			1.1			5000			
	Ir	±2%	.7		4.2×10^{4}				
			.75	2.5×10^{5}	8.0×10^{4}	15000	2.8	10	

References: J.D. Fox, EP&S Div. Tech. Note No. 7 (1967) and No. 20 (1968).
M. Zeller, L. Rosenson, and R.E. Lanou, Jr., in Summer Study on AGS Utilization (Ed. T.E. Toohig), BNL 16000 (1970).
A.S. Carroll et al., EP&S Div. Tech. Note No. 54 (1972), No. 64 (1973).
S. Smith, D. Cheng, private communication.

Beam C3 - Hyperon Beam

Particles	Σ^-, Ξ^-.
Momentum range	17 to 26 GeV/c
Momentum bite	± 0.5%
Target location	C' station
Target material	Be
Target size	0.1-in. high, 0.2-in. wide, 10-in. long
Production angle	0^o
Solid angle	22 μsr
Length	172-in.

Beam C3 (continued)

Flux detected/burst

Momentum (GeV/c)	Σ-trigger/10^{11} incident protons	$(\Sigma/\pi)_{trigger}$	$(\Xi/\Sigma)_{detected}$
19	12	7.4×10^{-5}	
20	28	2.5×10^{-4}	
20.5			2.85×10^{-2}
21	56	6.9×10^{-4}	
22	88	1.4×10^{-3}	
23	121	3.1×10^{-3}	
24	180	9.4×10^{-3}	
25	160	1.4×10^{-2}	
26	105	1.6×10^{-2}	

Yield

Σ^-/π^- production ratios and forward Σ^- production laboratory cross sections for protons on beryllium.

Secondary Momentum GeV/c	Σ^-/π^-	$d^3\sigma/dp\,d\Omega$ mb (sr GeV/c)$^{-2}$
	25.8 GeV/c Incident Protons	
17.75	0.329±0.042	14.41±1.8
18.75	0.465±0.048	13.3 ±1.4
19.75	0.669±0.067	12.0 ±1.2
20.75	1.08 ±0.077	11.7 ±0.8
21.75	2.41 ±0.14	14.9 ±0.9
22.75	2.85 ±0.14	9.4 ±0.5
23.75	21.91 ±1.4	4.0 ±0.2
	29.4 GeV/c Incident Protons	
17.0	0.185±0.011	25.3 ±1.5
19.0	0.263±0.016	19.0 ±1.2
20.0	0.374±0.022	19.0 ±1.1
20.5	0.380±0.021	16.3 ±1.0
21.0	0.463±0.028	16.3 ±1.0
22.0	0.648±0.037	15.3 ±0.9
23.45	1.19 ±0.07	15.0 ±0.9
25.0	1.72 ±0.16	10.1 ±0.9
26.0	2.62 ±0.16	6.0 ±0.4

Reference: V. Hungerbuehler et al, Phys. Rev. Lett. 24 1234 (1973), Nuclear Instr. and Methods 115 221 (1974).

Beam U Wide Bend Neutrino Beam

Particles ν, $\bar{\nu}$

Energy Peaked at ~ 1.5 GeV

Target location U station

Target material Sapphire

Target size Diameter 0.5 cm, length 45 cm

Length π, K decay region - 208-ft.
ν filter - 96-ft, iron
from target to bubble chamber - 336-ft.

Optics 3 magnetic fingers focusing pions and kaons toward the bubble chamber

Flux/burst

Energy (GeV)	Neutrinos/(interacting proton-meter^2·GeV) (averaged over 70 cm radius area)
.5	3.5×10^{-4}
1	9.5×10^{-4}
1.5	1.4×10^{-3}
2	1.1×10^{-3}
4	2.2×10^{-4}
6	3.7×10^{-5}
8	1.3×10^{-5}
10	6.8×10^{-6}
12	3.6×10^{-6}

Remark Recent estimate shows that approximately 1.5 times more flux than given above can be expected.

Reference: N.P. Samios, R.B. Palmer, W.B. Fowler, and R.I. Louttit;
AGS Proposal #A-427 (1967).
BNL neutrino beam group, private communication.

Distribution: B2

TABLE I

SUMMARY OF AGS SECONDARY BEAMS

Separated Beams	Production Angle(degree)	Solid Angle(msr)	Momentum Bite(%)	Momentum Range(GeV/c)	Flux
C2, C4	10.5	2.64	2 - 4	0 - 1.2	5.6×10^{5} K^- at 750 MeV/c
5	10	.47	2 - 6	1.3 - 3.2	2.2×10^{6} K^- at 2 GeV/c
B2, B4	6	.092-.294	4.4 - 6	1.5 - 9	4×10^{6} K^- at 5 GeV/c
Neutral Beams					
6A	4.7	.003	wide band	3 - 10	2.4×10^{5} K^0_L between 3-10 GeV/c
B5	4	.36	wide band	3 - 10	2.9×10^{6} K^0_L between 3-10 GeV/c
U			wide band	0.5 - 12	4×10^{5} ν at 1.5 GeV
Unseparated Beams					
B1	0	.3	2.4	6 - 24	$\sim10^{7}$ π^- at 12 GeV/c
A1					HEUB - mid 1975
Special Beams					
C1			20	5 - 9.5	10^{6} μ^+
C3	0	.022	1	19 - 26	300 Σ^- at 25 GeV/c

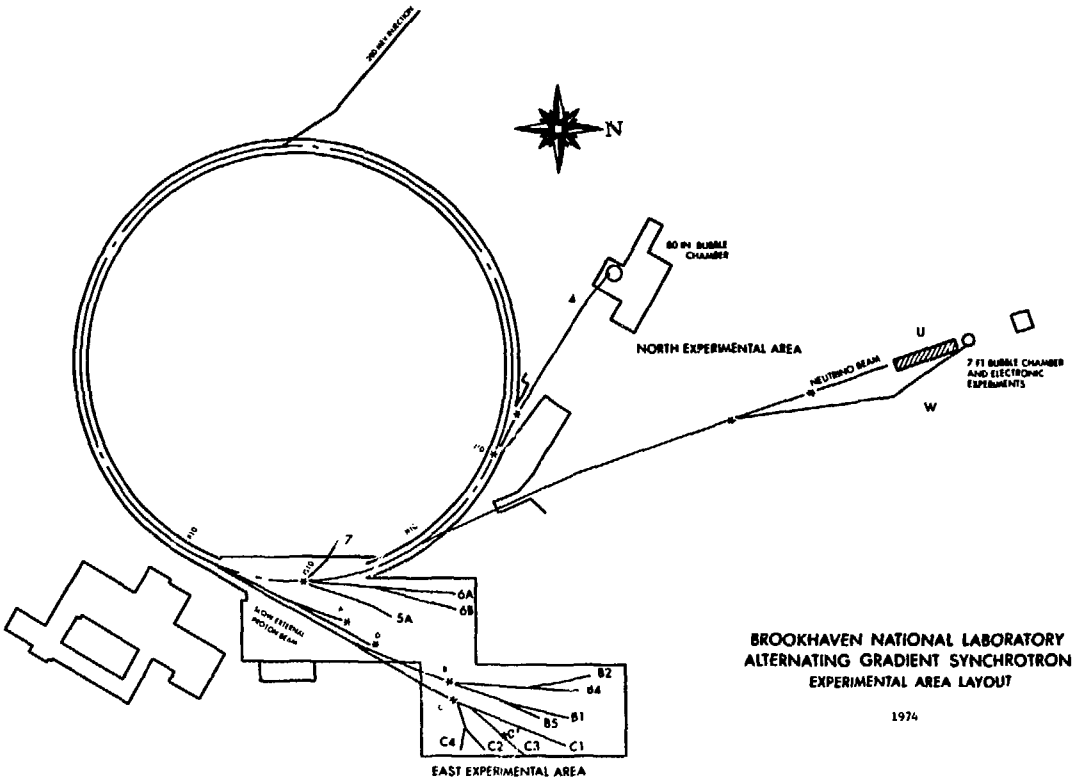
200 MEV INJECTOR
N
80 IN. BUBBLE CHAMBER
4
NORTH EXPERIMENTAL AREA
U
NEUTRINO BEAM
7 FT BUBBLE CHAMBER AND ELECTRONIC EXPERIMENTS
W
7
6A
6B
5A
SLOW EXTERNAL PROTON BEAM
B2
B4
B5
B1
C4
C2
C3
C1
EAST EXPERIMENTAL AREA
BROOKHAVEN NATIONAL LABORATORY
ALTERNATING GRADIENT SYNCHROTRON
EXPERIMENTAL AREA LAYOUT
1974

Figure 1

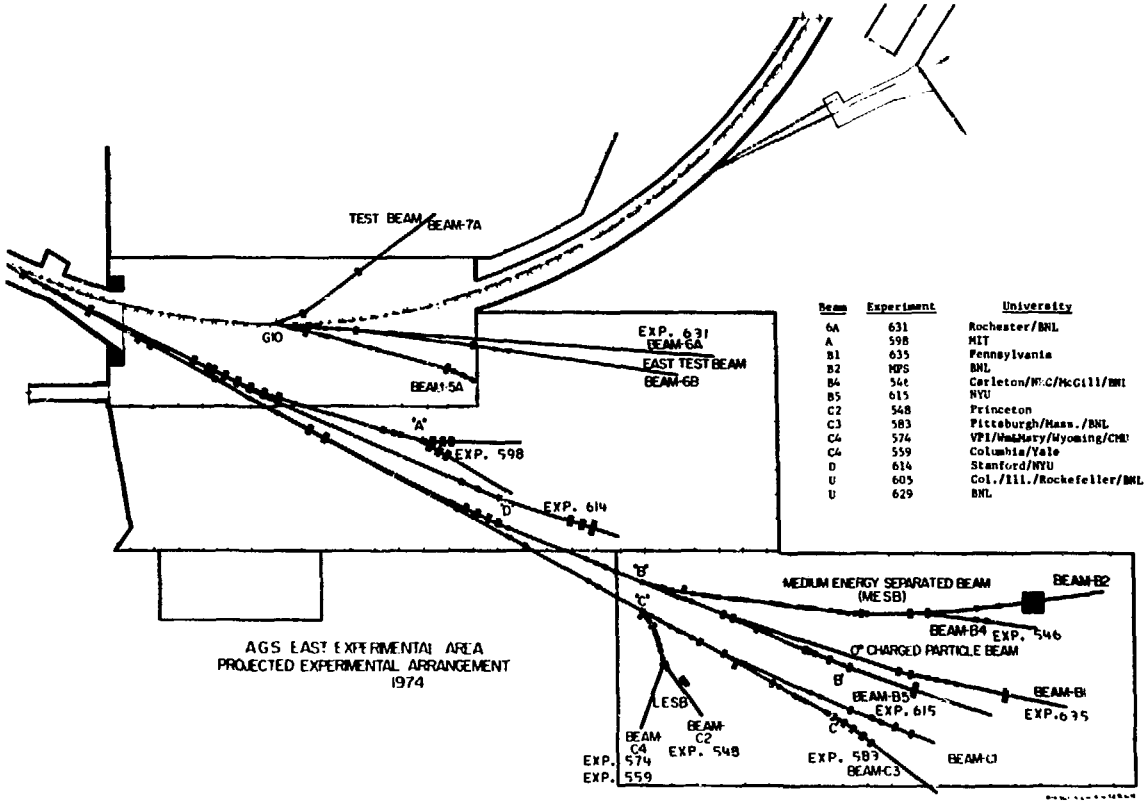

Beam	Experiment	Univeresity
6A	631	Rochester/BNL
A	598	MIT
B1	635	Pennsylvania
B2	MPS	BNL
B4	546	Carleton/MRC/McGill/BNL
B5	615	NYU
C2	548	Princeton
C3	583	Pittsburgh/Mass./BNL
C4	574	VPI/WmMary/Wyoming/CMU
C4	559	Columbia/Yale
D	614	Stanford/NYU
U	605	Col./Ill./Rockefeller/BNL
U	629	BNL

AGS EAST EXPERIMENTAL AREA
PROJECTED EXPERIMENTAL ARRANGEMENT
1974

Figure 2

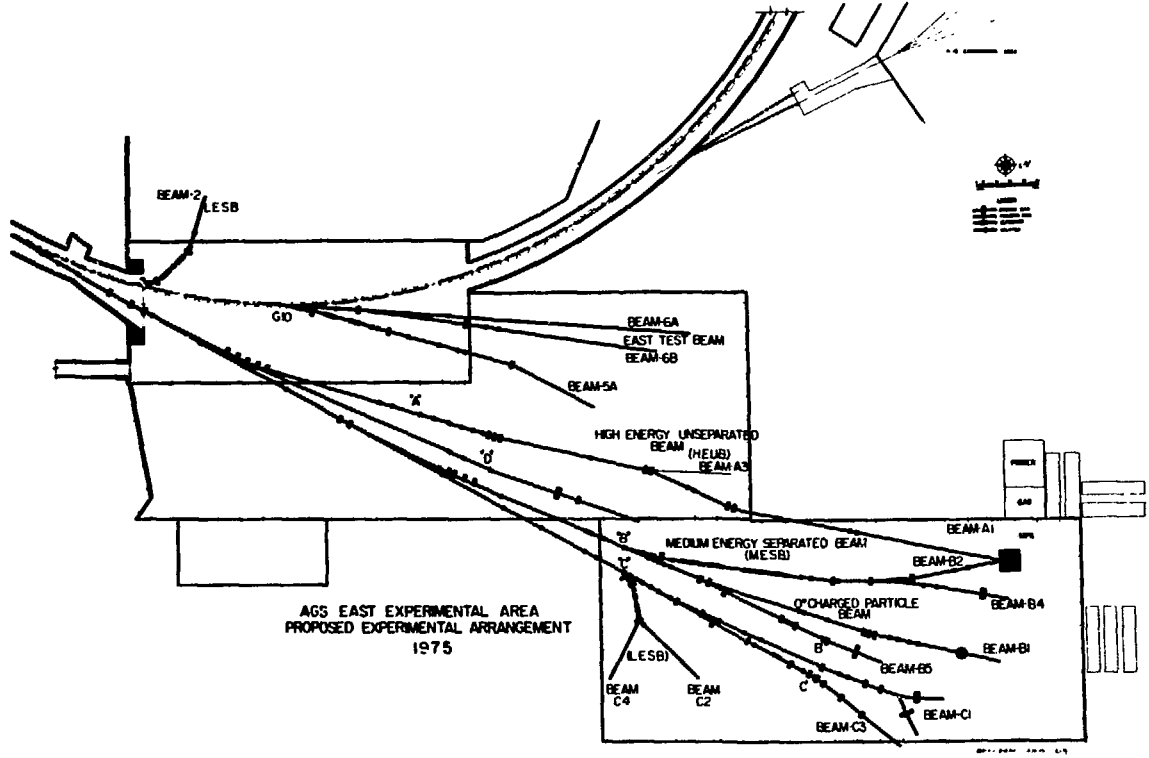
BEAM-2
LESB
GID
BEAM-6A
EAST TEST BEAM
BEAM-6B
BEAM-5A
'A'
'D'
HIGH ENERGY UNSEPARATED BEAM (HEUB)
BEAM-A3
BEAM-A1
'B'
'C'
MEDIUM ENERGY SEPARATED BEAM (MESB)
BEAM-B2
BEAM-B4
0° CHARGED PARTICLE BEAM
BEAM-B1
B
BEAM-B5
(LESB)
BEAM C4
BEAM C2
C
BEAM-C1
BEAM-C3
AGS EAST EXPERIMENTAL AREA
PROPOSED EXPERIMENTAL ARRANGEMENT
1975

Figure 3

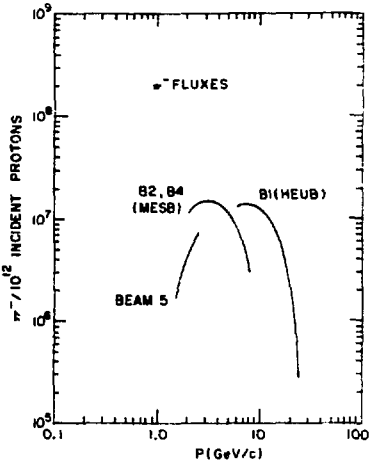
π^- FLUXES
$\pi^-/10^{12}$ INCIDENT PROTONS
82, 84
(MESB)
B1(HEUB)
BEAM 5
P(GeV/c)
0.1
1.0
10
100

Figure 5.

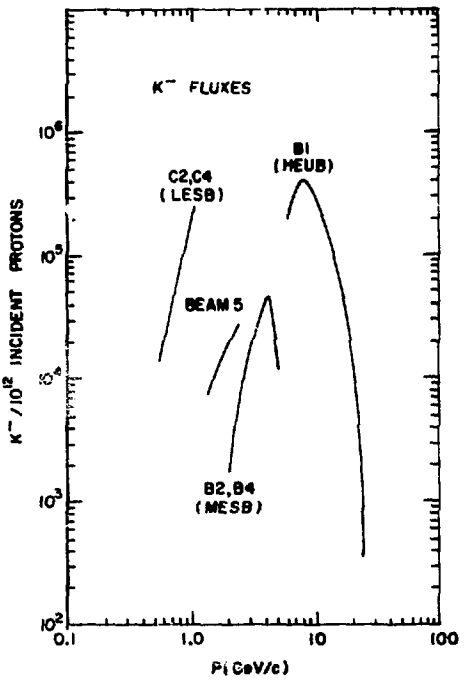
K⁻ FLUXES
B1
(MEUB)
C2,C4
(LESB)
BEAM 5
B2,B4
(MESB)
K⁻ / 10¹² INCIDENT PROTONS
10⁶
10⁵
10⁴
10³
10²
0.1
1.0
10
100
P(GeV/c)

Figure 5.

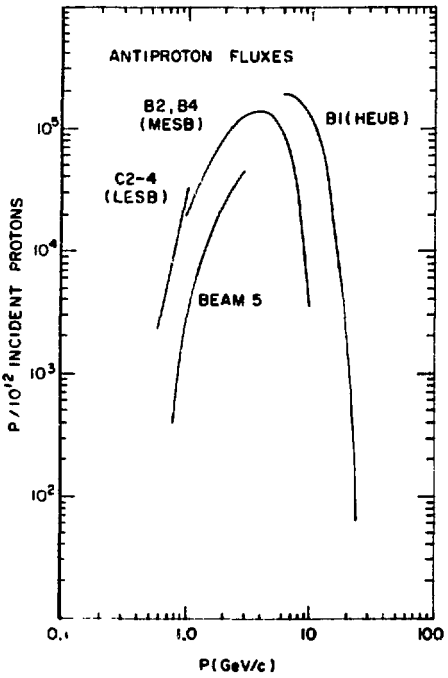
ANTIPROTON FLUXES
B2, B4
(MESB)
B1(HEUB)
C2-4
(LESB)
BEAM 5
P/10^12 INCIDENT PROTONS
10^5
10^4
10^3
10^2
0.1
1.0
10
100
P(GeV/c)

Figure 6.

NUCLEAR INSTRUMENTS AND METHODS 124 (1975) 1–10; © NORTH-HOLLAND PUBLISHING CO.

RESISTANCE OF SOLID HD POLARIZED-PROTON TARGETS TO DAMAGE FROM HIGH-ENERGY PROTON AND ELECTRON BEAMS*

H. MANO and A. HONIG

Syracuse University, Syracuse, New York 13210, U.S.A.

Received 6 November 1974

Solid HD samples, suitable for use as polarized proton targets by virtue of their low ortho-H_2 and para-D_2 impurity concentrations and consequently long proton spin-lattice relaxation times, T_1^H, were irradiated in the 10.4 GeV external beam of the Cornell electron synchrotron and in the 28 GeV extracted proton beam of the AGS synchrotron at Brookhaven National Laboratory. No *direct* beam-induced depolarization of the protons in HD was observed for integrated particle fluxes up to 10^{13} cm^{-2}. The proton beam exposure resulted in a spin-lattice relaxation rate, $(T_1^H)_{rad}^{-1}$, of 0.9×10^{-16} s^{-1} per unit integrated flux (i.e. per particle/cm^2), and the electron beam exposure led to a value about 30% higher, due mostly to the production of secondaries. The T_1^H recovers nearly to its original long value when the sample is melted and refrozen after irradiation, indicating that the *principal contribution* to $(T_1^H)_{rad}^{-1}$ *comes from* radicals such as atomic H or D and not from symmetry species conversion induced by the beams. After irradiation, annealing of the damage centers was observed at 4.2 K and 4.7 K by monitoring $(T_1^H)_{rad}^{-1}$ as a function of time. These experiments support the *proposed usage*, at temperatures between 1 and 4 K, of pure solid HD with long T_1^H as a metastably highly polarized proton target for high energy physics experiments at particle fluxes up to about 10^{13} particles/cm^2 s.

1. Introduction

A proposal to use solid HD as a novel type of polarized proton (and deuteron) target[1] was based largely on the spin-lattice relaxation properties[2,3] of solid HD containing small concentrations of H_2 and D_2 impurities. A detailed series of studies of proton spin-lattice relaxation times, T_1^H, as a function of ortho-H_2 concentration were carried out[4,5] at magnetic fields between 0–12 kOe and temperatures ranging from 0.4 to 10 K, and further measurements have been reported[6,7] at magnetic field strengths up to 100 kOe and temperatures down to 24 mK, where proton polarizations of ≈40% have been obtained. Because the ground rotational state of HD has zero angular momentum ($Jh=0$), T_1^H of the protons in pure HD is extremely long in the liquid helium temperature range, at least of the order of days, and the presence of a small H_2 concentration controls the HD proton relaxation rate. The protons in the symmetric nuclear spin state (ortho) variety of the H_2 impurity, for which $J=1$ in the lowest rotational state because of the Fermi-Dirac statistics obeyed by protons, relax efficiently through a bi-molecular quadrupole-quadrupole interaction coupled with a spin-rotation interaction[8]), and this relaxation is transferred to the protons in HD through the rapid proton spin-spin relaxation mechanism. A polarized proton target is obtained by utilizing a small ortho-H_2 impurity concentration to bring about equilibrium at a high magnetic field and very low temperature (e.g. 150 kOe and 0.012 K yields an equilibrium proton polarization of 85%), and waiting under the equilibrium conditions for sufficient ortho→para H_2 conversion to occur so as to eliminate the HD proton relaxation mechanism, thereby isolating the proton spin system from the lattice, even at 1 K or 4 K. Thus, experiments can be performed with metastably frozen-in polarized protons in the convenient 1–4 K temperature region, requiring only liquid helium coolant and a modest magnetic field of no special magnitude or homogeneity. The optimization of conditions for operating the target depends on the temperature and magnetic field dependence of T_1^H(o-H_2) as a function of the concentrations of ortho-H_2 (o-H_2) and para-D_2 (p-D_2: $J=1$ ground rotational state), which has previously been discussed[4,5]) and will be presented in a forthcoming paper in more detail.

The principal uncertainty as to the economical application of the method has been the rate of deterioration of the isolation of the metastably spin-polarized protons due to radiation damage caused by a high energy particle beam in the course of an experiment. Since considerable effort is expended in producing these samples (maintaining them at millidegree temperatures and high magnetic fields from one to two weeks), the feasibility of the target depends on how long it remains effective under bombardment by the experimental high energy particle beam. If it should be depolarized due

* Research supported in part by the National Science Foundation.

to radiation damage when exposed to a small integrated flux, the ratio of particle utilization to sample preparation time could be too small for profitable usage. In the experiments reported in this paper, the degradation of polarization for known high energy electron and proton exposures was measured, and the results in our opinion support the utility of solid HD polarized targets for high energy experiments derived from proton accelerators, and perhaps for some limited experiments derived from high energy electron accelerators. In addition, the relaxation mechanism induced by the particle beams was clarified and other factors related to use of HD as a polarized target were investigated.

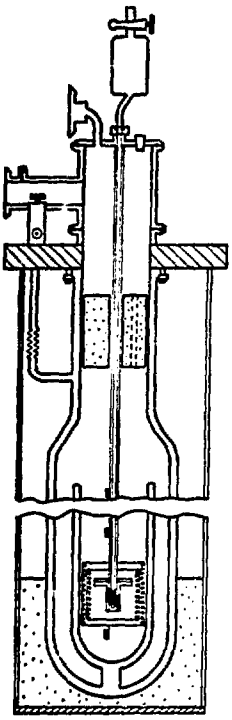

Fig. 1. Schematic drawing of the apparatus used for irradiation and NMR experiments on solid HD. Coils shown in inner (liquid ^{4}He filled) dewar are Nb-Ti superconducting windings, modulation coils and orthogonal NMR transmitter and receiver coils, from outside to center of dewar, respectively. Solid black rectangles close to axis of inner dewar are temperature sensing carbon resistors.

2. Experimental arrangements

Because measurements had to be made over an extensive time period both before and after the high energy particle beam irradiations, the apparatuses were made completely portable. Fig. 1 illustrates schematically one of three identical cryostats which were constructed. The multiplicity of cryostats allowed several samples differing in impurity content to be observed and irradiated during the same lengthy time period. The dewar used was a Superconductivity-Helium Electronics Corp (S.H.E.) vapor shielded model (VSD-850), which retained liquid helium without use of a liquid N_2 shield for approximately 18 h, with all the apparatus inserted. The long retention time was important for those experiments in which the samples had to be kept continuously at liquid helium temperatures, sometimes for more than a month prior to the irradiation. It was also desirable in principle to be able to make the trip to and from the accelerators without transferring liquid helium on the road, although we were equipped for this eventuality and made use of it in one instance. Despite the apparently fragile design with total support for the inner dewar at only a single joint at the bottom, approximately 5000 dewar-miles of transport were successfully undertaken with only one instance of breakage. Each apparatus had its own persistent current mode operating superconducting solenoid[9]), which was usually operated at between 1.5 and 3 kOe. An additional coil capable of providing peak to peak magnetic fields of several oersteds was used for magnetic field modulation at a modulation frequency of 850 Hz. Crossed coils orthogonal to each other but not to the axial magnetic field were wrapped about a cylindrical teflon form which enclosed the sample, and served as transmitter and receiver for the nuclear magnetic resonance (NMR) measurements. These components are readily discernible in fig. 1. The transmitter was driven by a General Radio type 1211-O unit oscillator which was frequency swept through the resonance with a motor drive. The receiver was tuned with an external capacitor and then decoupled from the external cable capacitance with a Tektronix P6045 FET probe with type 1121 amplifier. In this manner, resonance could be monitored remotely at distances of over 30 m, ample for monitoring resonance during particle beam irradiations. Upon

frequency sweeping the transmitter, the receiver output exhibited a broad resonance response associated with the tuned receiver coil circuit. The external capacitor was adjusted so that the much narrower proton resonance signal occurred at the peak of this broad instrumental resonance, and since the superconducting magnetic field in the persistent current mode drifted less than 0.05%/h, no adjustments had to be made for time periods of many hours. The magnetic field strength was monitored using the fluorine resonance signal from the teflon coil form. The background proton signal was very small, and varied from run to run. It was due to slight moisture condensation reaching the sample region during insertion of the HD sample into the cryostat. Characterized by a short T_1 ($\lesssim 1$ s), it could be readily subtracted from the HD proton signal. The sample was contained in a glass holder in the form of a $\frac{1}{4}$ l cylindrical bulb attached to a long stem of about 1 m length and 0.40 cm inside diameter, as seen in fig. 1. The samples were filled with HD to pressures, at room temperature, between 270 torr and 340 torr. Thus, at a typical sample pressure of 300 torr, the sample condensed at liquid helium temperatures to a vertical length of about 1.3 cm at the bottom of the glass stem. Condensation was produced by slowly lowering the sample tube through the sliding o-ring seal at the top of the cryostat, first producing liquid HD, and then solidification. Temperature indicating carbon resistors facilitated monitoring the condensation rates, which were "calibrated" by condensing the sample in a glass dewar set whose interior was visible. In this manner, a reproducible condensation procedure was formulated. This manner of sample handling kept air and water vapor out of the cryostat, allowed the sample to be annealed in the solid state, melted, or vaporized without removing it entirely from the cryostat, and permitted rapid transfer from one dewar to another; this latter feature was especially useful when a large external storage dewar was used for ortho to para H_2 conversion over long time periods.

The HD was prepared[10]) by reacting $LiAlH_4$ with D_2O and then double distilling[11]) the sample in a liquid H_2 cooled cryostat[12]) containing a Stedman packing. Middle fractions were used to minimize the H_2 and D_2 impurity concentrations. The fractions resulting from the first distillation were analyzed with a commercial mass spectrometer, capable of discriminating parts per thousand of H_2 and D_2 in HD. However, the resolution was no longer adequate for the second distillate, and the initial normal H_2 and D_2 ($n-H_2$ and $n-D_2$) concentrations were estimated respectively from the initial T_1^H value and the conversion time necessary for a change of slope of T_1^H with respect to conversion time[5]).

Four samples were used in the irradiation experiments. For reasons related to their histories, they are denoted by 1′, 3′, 1″, 3″. The samples denoted by a single prime superscript were irradiated at the Cornell electron synchrotron and those with double prime superscripts were irradiated at the AGS proton synchrotron at Brookhaven National Laboratory (BNL).

At the Cornell electron synchrotron, a 10.38 GeV external electron beam was defocussed to about a 2 cm high by 1.5 cm wide beam, consisting of about 10^9 particles per 0.1 ms pulse and 60 pulses per second. A fluorescent screen with cross-hairs denoting the position of the center of the HD sample was fixed to the dewar outer surface and monitored with a vidicon, enabling the beam to be aimed properly at the HD sample. In addition, a glass plate was positioned in the beam and the darkening due to formation of radiation induced centers was later monitored with an optical densitometer to obtain the beam profile. This result, together with a count of the total number of particles determined with a secondary emission counter which intercepted the entire beam, allowed the computation of the average integrated flux incident on the sample. At Brookhaven National Laboratory (BNL), a 28 GeV extracted proton beam about 2.2 cm high and 1.3 cm wide containing 2×10^{11} particles 0.7 s straggled pulse, and 1 pulse 2.5 s, traversed the sample. This was just under the beam intensity at which the Nb–Ti superconducting solenoid quenches. The beam was again aimed with the aid of a fluorescent screen monitored by a vidicon. The total particle flux was measured with a secondary emission chamber in hard vacuum, and the value was corroborated by measuring the activity of polyethylene foils placed in the beam. The values agreed well, and the latter also yielded the beam profile along vertical and horizontal axes through the center of the sample. This permitted computation of the average integrated flux incident on the sample.

Proton relaxation times in the HD samples, T_1^H, were determined by fitting the NMR signal amplitude after saturation to an exponential growth function. By maintaining the superconducting magnet in the persistent current mode, full amplitude NMR signals for specimens with long T_1^H values were obtained without difficulty. Unless otherwise specified, T_1^H values in this study are measured at 4.2 K. Because signal noise ratio was compromised in favor of necessary features of the apparatus, values of T_1^H are generally reliable only to $\pm 15\%$, which is, however, quite sufficient for the purposes of these experiments.

3. Experimental results

3.1. Electron beam irradiation experiments at Cornell synchrotron

An objective of these experiments was to measure for a known integrated beam flux the radiation induced proton relaxation rate, $(T_1^H)_{rad}^{-1}$, in two samples of HD: a pure one (sample 1'), and a pure sample doped with 1% n−D_2 (3'). The D_2 doped sample comparison was undertaken because it is possible that D_2 doping might be useful for producing an optimum target. It was also desired to establish that no spin-heating of the polarized protons of the HD occurred from direct (independent of the lattice) interaction with the high energy beam. Furthermore, we wished to determine whether the $(T_1^H)_{rad}^{-1}$ was the result of radical formation, such as atomic H and/or D, or the result of beam-induced conversion from p−H_2 to o−H_2 (or o−D_2 to p−D_2), a mechanism which had been suggested in connection with ^{60}Co irradiation of HD [2]. For this latter purpose, the sample after irradiation was to be melted and resolidified by raising it above the liquid helium level for approximately a minute and then reinserting it completely into the cryostat, a procedure we denote as *temperature cycling*. If $(T_1^H)_{rad}^{-1}$ results from para→ortho H_2 or ortho→para D_2 conversion, the $(T_1^H)_{rad}^{-1}$ would be expected to remain unchanged after temperature cycling, since temperature cycling completed in the order of minutes produces very little conversion among symmetry species. However, if radical or atomic species formation were responsible for $(T_1^H)_{rad}^{-1}$, the temperature cycling would "unfreeze" them, $(T_1^H)_{rad}^{-1}$ would be markedly decreased[13], and the observed T_1^H should return near to its value before irradiation.

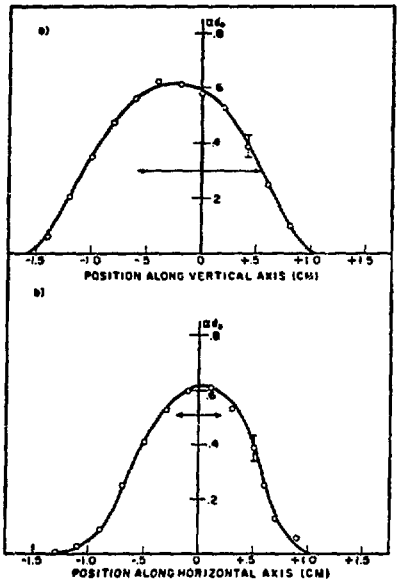

Fig. 2. Distribution of 10.38 GeV electron beam integrated flux with respect to center position of HD sample 1'. Ordinate is measured optical density of 0.91 mm thick glass plate which was in beam path. Arrows represent physical extent of the sample along each dimension.

The 10.38 GeV extracted electron beam from the Cornell synchrotron appeared on the vidicon to be approximately oval in shape and about 2 cm high by 1.5 cm wide. The integrated particle flux incident on the sample was determined by measuring the total number of particles in the beam using a secondary emission monitor, and determining the distribution of integrated particle flux over the sample from the subsequently measured optical density as a function of position on glass plates which were placed in the beam path. It was assumed that the optical density was linearly proportional to the incident particle density, and by repeating optical density measurements over a period of several days after the high energy electron beam exposure, it was ascertained that very little bleaching occurred after the exposure. In fig. 2 a typical pair of curves of the optical density $\alpha d_0[\alpha d_0 = \ln$ (fraction light transmission)] vs vertical and horizontal displacement with respect to the sample, are shown. The sample dimensional extent is indicated by the arrows. From these curves, we were able to determine the average integrated flux to which the sample was exposed by calculating the time averaged beam flux, $\langle \Phi_B(x,y) \rangle$, integrating it over the sample area, and multiplying by the exposure time. For sample 1', this was 8.5×10^{12} particles/cm^2, and for sample 3', it was 8.4×10^{12} particles/cm^2. Despite the few millimeters separation of the peak intensity position of the electron beam from the geometric center of the HD sample, the inhomogeneity in sample beam exposure was less than 50% from the mean value, and reasonably exponential spin-lattice relaxation processes were observed.

The history of sample 1' is illustrated in fig. 3. From the initial T_1^H value and small slope[4,5]) (0.14 ln units/

day) of the conversion curve prior to the electron irradiation for all but the first five days of conversion, the initial $o-H_2$ and $p-D_2$ concentrations are estimated as $\approx 5\times10^{-5}$ and $\approx 4\times10^{-5}$ respectively. *It is noteworthy that* at 4.2 K, a value of 1 d for T_1^H was easily reached for this sample, with no evidence of another relaxation mechanism entering the picture.

Immediately prior to the electron irradiation, the value of T_1^H was about 3×10^4 s, somewhat shorter than its maximum value because of some manipulations of samples among dewars. This value is actually more convenient than a longer one, because a full polarization could have been established within about a day if a cooling failure occurred before the scheduled irradiation time. After exposure to 8.5×10^{12}/cm^2 electrons, it is seen in fig. 3 that T_1^H drops to 930 s, yielding a $(T_1^H)_{rad}^{-1}$ of $(960)^{-1}$ s^{-1}, or a $(T_1^H)_{rad}^{-1}$ per unit electron integrated flux (i.e. per electron cm^2) of 1.22×10^{-16} s^{-1}. The sample was then temperature cycled, after which T_1^H rose to 1.15×10^6 s, more than a factor of ten larger than T_1^H immediately after the electron irradiation. From this, it can be concluded that at least 95% of the decrease in T_1^H after the electron irradiation is due to defect centers produced by the irradiation and not to para→ortho H_2 conversion induced by the electron beam.

For the first 10^{12}/cm^2 integrated flux incident on the sample, it was observed that no direct depolarization was produced by the electron beam. After that dosage, the nuclear resonance was saturated with rf power so that proton relaxation could be subsequently observed.

Sample 3', which consisted of a pure fraction of the distillate doped with 1% $n-D_2$ impurity, had an initial T_1^H of 30 s and showed a complicated T_1^H growth behavior with conversion time, a feature whose discussion will be deferred for a forthcoming publication since it is not of central concern here. This sample underwent H_2 and D_2 symmetry species conversion for a length of time which brought its T_1^H prior to irradiation to 1.5×10^4 s. After exposure to an electron integrated flux of 8.4×10^{12}/cm^2, T_1^H was measured to be 980 s, yielding $(T_1^H)_{rad}^{-1}$ of $(1050)^{-1}$ s^{-1}, and a $(T_1^H)_{rad}^{-1}$ per unit electron integrated flux of 1.13×10^{-16} s^{-1}, within experimental error of the value for sample 1'. From this, we conclude that very little ortho→para D_2 conversion is induced by the high energy electron beam, since sample 3' contained more than 100 times the $o-D_2$ concentration of sample 1'. Instead of temperature cycling this sample, $(T_1^H)_{rad}^{-1}$ was monitored while the sample remained at 4.2 K, with the results seen in fig. 4. $(T_1^H)_{rad}^{-1}$ was computed from the difference between the measured $(T_1^H)^{-1}$ and $(T_1^H)^{-1}$ extrapolated as if no irradiation had taken

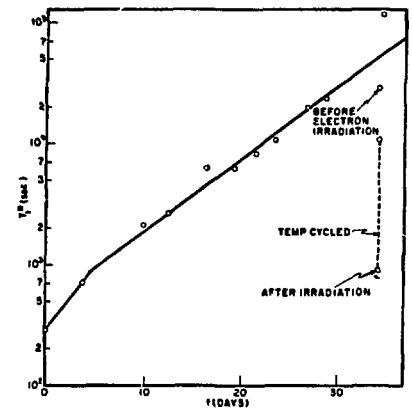

Fig. 3. History of HD sample 1'. Growth of T_1^H is due to conversion from $J=1$ symmetry species of H_2 and D_2 to $J=0$ species. Irradiation is by 10.38 GeV electrons, with integrated flux averaged over sample equal to 8.5×10^{12} electrons/cm^2. $T=4.2$ K, $H=2.8$ kOe.

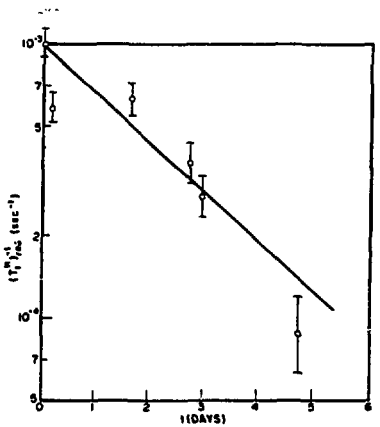

Fig. 4. Annealing at 4.2 K of radiation-induced centers in sample 3' after exposure to 10.38 GeV electron integrated flux, averaged over sample, of 8.4×10^{12} electrons/cm^2. $T=4.2$ K, $H=2.8$ kOe.

place. This procedure should lead to very little error for the first few days of the recovery period, and the slope for that period is 0.41 ln units day, which is a measure of the annealing rate for damage centers at 4.2 K.

3.2. Proton beam irradiation experiments at BNL–AGS synchrotron

The objectives of the experiments here were similar to those discussed previously in connection with the electron beam experiments. We also wished to determine whether additional relaxation or depolarizing processes particular to proton beams occurred, by comparing quantitatively the relaxation time results from minimum ionizing proton beams with those from the minimum ionizing electron beams. Usage of a greater integrated flux was planned in order to obtain a more accurate relationship between $(T_1^H)_{rad}^{-1}$ and the measured particle integrated flux. A further objective was to observe the annealing rate of the defect centers at two different temperatures, in order to determine whether at some temperature the annealing rate might be sufficiently faster than the spin-lattice relaxation rate so that the useful lifetime of a polarized target could be prolonged while in the particle beam by means of periodic short duration annealing episodes.

The 28 GeV extracted proton beam was defocussed and appeared visually on the vidicon to be approximately rectangular in shape and about 2.2 cm high by about 1.3 cm wide. The particle integrated flux was determined by measuring the total number of particles in the beam with a secondary emission counter which intercepted the entire beam, together with determining the beam profile along vertical and horizontal axes which intersected at the position corresponding to the center of the HD sample. This profile was measured by placing square polyethylene foils of about 50 mm² area and known weight on the two axes, and counting the disintegrations of the ^{11}C atoms which were produced by collisions of the high energy protons with the ^{12}C atoms in the polyethylene. In the computation[14], the value 25.9 mb was used for the ^{12}C activation cross-section under 28 GeV protons, 0.649 was taken as the counting efficiency, and 20.34 min was used as the half life of ^{11}C. The results for the beam exposure of sample 1* are presented in fig. 5. The continuous profile lines are constructed by taking into account the finite dimensions of the foils. The horizontal profile is seen to

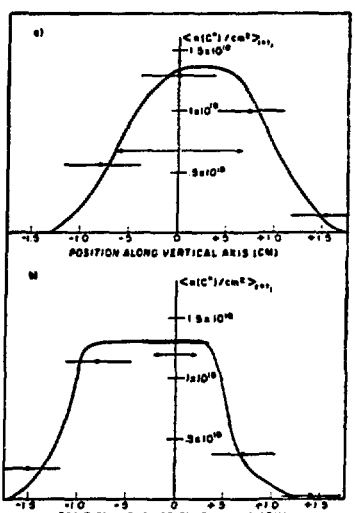

Fig. 5. Distribution of 28 GeV extracted proton beam integrated flux with respect to center position of HD sample 1*. Ordinate is average number of ^{11}C atoms per square cm of 4 mil. thick polyethylene foil, extrapolated back from time count was made to time at which irradiation terminated, t_1. Arrows represent physical extent of sample along each dimension.

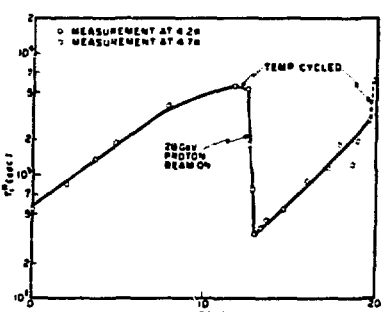

Fig. 6. History of HD sample 1*. After growth of T_1^H due to H_2 and D_2 symmetry species conversion, a temperature cycling is shown as a control. The irradiation consists of an integrated proton flux, averaged over the sample, equal to 3.0×10^{15} cm². The measurements during and after irradiation are shown in detail in figs. 7 and 8, respectively. $H = 2.8$ kOe.

be fairly constant over the region occupied by the sample, so that the average integrated flux incident on the sample is obtained from an average over the vertical profile. As with the electron beam exposures, the inhomogeneity of the exposure over the sample is less than 50% of the mean value, and observed relaxation processes were fairly exponential in form.

The history of sample 1" is shown in fig. 6. This was one of the purest fractions obtained, with initial $o-H_2$ and $p-D_2$ concentrations estimated as 4.5×10^{-7} and 3×10^{-5} respectively. Prior to the irradiation, a rapid temperature cycling was carried out to demonstrate that only a small change in T_1^p results from such an operation, as has been previously stated. The measurements during the irradiation, the subsequent increase of T_1^p, and a final temperature cycling which results in an increase in T_1^p, as with the electron beam experiments, are also illustrated. In fig. 7, $(T_1^p)_{ss}^{-1}$ is shown in detail for the portion of time in which the irradiation was actually in progress. For the first 500 s of irradiation during which about 10^{17} protons cm^2 were incident on the sample, the HD proton resonance signal corresponding to equilibrium polarization remained constant, insuring that the beam does not directly depolarize the protons. The resonance was then saturated and T_1^p was measured by monitoring the signal growth over a 3 min period. This procedure was repeated at 900 s after the commencement of the irradiation and at the end of the irradiation, with the results shown in fig. 7. The linearity of $(T_1^p)_{ss}^{-1}$ with proton exposure confirms that increased $o-H_2$ concentration resulting from a beam induced para→ortho H_2 reconversion process is not an applicable mechanism, since in such a case the $o-H_2$ concentration would be expected to be proportional to the exposure but $(T_1^p)^{-1}$ depends on a quadratic or higher power of the $o-H_2$ concentration[2,3]. The $(T_1^p)_{ss}^{-1}$ per unit proton integrated flux (i.e. per proton cm^2 exposure) is 0.8×10^{-18} s^{-1}, a value which must be increased by about 30% to yield the average value obtained under electron bombardment. Though at the limiting edge of the experimental error, the difference is probably real. A higher value of about 50% is indeed expected for electrons due to the generation of secondary electrons in the metal comprising the superconducting magnet and due to the differential relativistic rise of ionization loss for electrons compared with protons at the energies we employed.

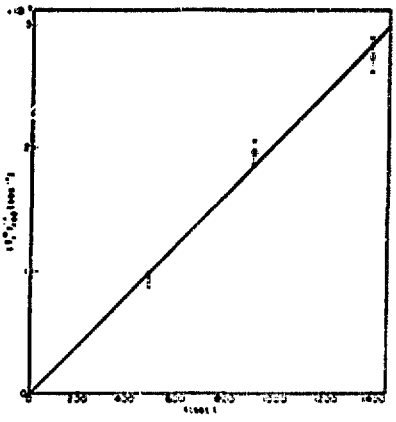

Fig. 7. Measurement of $(T_1^p)_{ss}^{-1}$ during irradiation with an approximately constant flux 29 GeV proton beam, up to an integrated flux of 3.0×10^{17} protons cm^2. $T = 4.2$ K, $H = 2.9$ kOe.

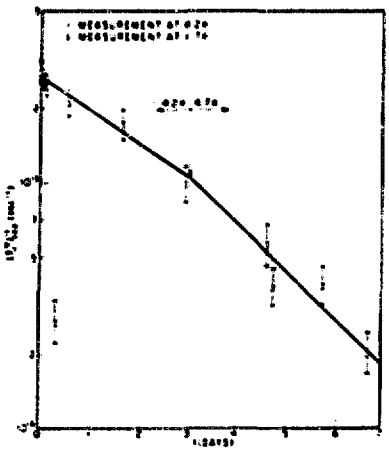

Fig. 8. Annealing of radiation induced centers in HD sample 1", after exposure to a 29 GeV proton integrated flux, averaged over the sample, of 3.0×10^{17} protons cm^2. The sample remained at 4.2 K for the first 3 d, and at 4.7 K beyond that time, as shown by the arrows. Relaxation measurements were made at 4.2 K, or 1.7 K, as indicated. $H = 2.9$ kOe.

After the irradiation, the decrease of $(T_1^H)_{rad}^{-1}$ was monitored as in the electron irradiation case, but this time at two different temperatures. The higher T value, 4.7 K, was maintained for a period of days by means of a pressure release valve set at 0.5 kg cm^2. When the annealing was carried out at 4.7 K, the T_1^H values were nevertheless *measured* at 4.2 K, as seen in fig. 8. A steeper anneal rate is indeed observed at 4.7 K, but the ratio of the 4.7 K rate to the 4.2 K rate does not exceed the ratio of the $(T_1^H)^{-1}$ values at the two temperatures, so that the extension of the lifetime of a polarized target by annealing at temperatures above 4.2 K does not seem practical. A single measurement right after the irradiation, at 1.7 K, is also shown in fig. 8, indicating that $(T_1^H)_{rad}^{-1}$ is an order of magnitude smaller at 1.7 K than at 4.2 K. A measurement at $H = 1.8$ kOe and $T = 4.2$ K was also taken soon after the irradiation, yielding a T_1^H value larger than that at 2.8 kOe and 4.2 K. This field dependence is opposite to that observed[3]) when the o–H_2 relaxation mechanism dominates, and again supports the damage center mechanism for $(T_1^H)_{rad}^{-1}$.

In figs. 9 and 10, results for sample 3" analogous to those in figs. 7 and 8 for sample 1" are presented. Sample 3" is slightly richer in initial o–H_2 concentration than sample 1" and also underwent very little conversion from its initial n–H_2 constitution (only 2 d at liquid helium temperature prior to irradiation). In addition it was subjected to a higher proton integrated flux than sample 1". The value obtained for $(T_1^H)_{rad}^{-1}$ per unit proton flux is 0.8×10^{-16} s^{-1}, in close agreement with the result in sample 1". The leveling off of T_1^H growth following the temperature cycling 10 d after irradiation is not understood, but possibly is due to paramagnetic centers formed in the glass sample container in this most strongly irradiated sample. The annealing behavior at 4.2 K and 4.7 K, as seen in fig. 10, is comparable to that of sample 1".

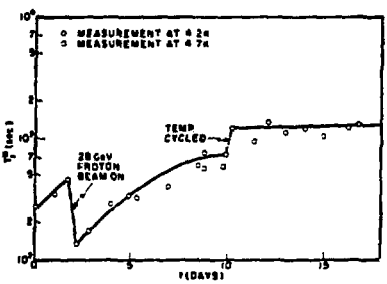

Fig. 9. History of HD sample 3". Integrated proton flux averaged over the sample equals 7.2×10^{15} protons/cm^2. The recovery after irradiation is shown in fig. 10. $H = 2.8$ kOe.

4. Discussion

The values of $(T_1^H)_{rad}^{-1}$ per unit particle integrated flux have been shown to be in reasonable agreement for electron and proton beams. It is of interest to compare the value obtained under proton bombardment for sample 1", 0.9×10^{-16} s^{-1}, with the result obtained by Hardy and Gaines from irradiation of solid HD with Co^{60} gamma rays[2]). They reported a $(T_1^H)_{rad}^{-1}$ value, for a radiation dose of 4×10^6 Rad, of 3.7×10^{-3} s^{-1}. Since a minimum ionizing particle integrated flux of 2.25×10^7 particles cm^2 produces a dosage of 1 Rad in HD, we see that the dosage from a minimum ionizing proton integrated flux of 9×10^{13} cm^2 is approximately equivalent to 4×10^6 Rad. Using this equality combined with the value of 0.9×10^{-16} s^{-1} for $(T_1^H)_{rad}^{-1}$ per unit proton integrated flux, one obtains 8.1×10^{-3} s^{-1} for $(T_1^H)_{rad}^{-1}$ corresponding to a 4×10^6 "Rad" proton beam dose, about a factor of two greater than the result for ^{60}Co

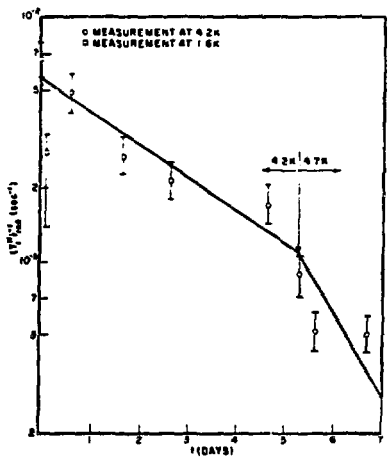

Fig. 10. Annealing of radiation-induced centers in HD sample 3", after exposure to a 28 GeV proton integrated flux, averaged over the sample, of 7.2×10^{15} protons/cm^2. 4.2 K and 4.7 K annealing regions are indicated by the arrows. $H = 2.8$ kOe.

irradiation. The details of the ^{60}Co experiments, such as the method of determing dose, were not given, so it is not clear if this difference has a physical significance.

The excess of the $(T_1^H)^{-1}$ value measured after temperature cycling over the $(T_1^H)^{-1}$ value measured prior to the irradiation amounted in sample 1' to 5.4×10^{-5} s^{-1} (see fig. 3), while for sample 1", the excess of the $(T_1^H)^{-1}$ value measured after temperature cycling over the $(T_1^H)^{-1}$ value extrapolated (according to the known T_1^H growth rate) from the time prior to irradiation to the time the temperature cycling was carried out, yielded 1.1×10^{-4} s^{-1} (refer to fig. 6). The ratio of these excess $(T_1^H)^{-1}$ values is about 0.50 compared with a ratio of 0.38 for the effective particle radiation doses applied to samples 1' and 1", respectively. In this case, the slightly sublinear dependence of the excess $(T_1^H)^{-1}$ on beam dose does not preclude as its cause the formation of $o-H_2$ and $p-D_2$, which can occur by recombination of atomic H or D, subsequent to the temperature cycling. The argument that the latter would lead to a quadratic or higher dependence on beam dose holds only if the generated $p-D_2$ and $o-H_2$ concentrations exceed the $p-D_2$ and $o-H_2$ concentrations present prior to the irradiation, which from the magnitudes of the excess $(T_1^H)^{-1}$ observed here, could not be the case. In fact, if the beam-generated $p-D_2$ concentration were only a small fraction of the existent $p-D_2$ concentration, experiments have indicated[5]) that at 4.2 K a sublinear dependence of $(T_1^H)^{-1}$ on added $o-H_2$ concentration would be expected. A rough estimate of the atomic H and D production under the irradiation is instructive at this point, and can be made from reference to the work of Sharnoff and Pound[15]). They deduce an effective energy per molecular dissociation in solid D_2 of $\sim 2 \times 10^2$ eV/molecule, or $\sim 10^2$ eV per atom formed. Using this same value for HD, the proton integrated flux of 3×10^{15}/cm^2 to which sample 1" was subjected should result in 6×10^{16} H and 6×10^{16} D atoms per cm^3 of solid HD. Assuming that $\frac{1}{2}$ of the recombination products will be H_2 (as opposed to D_2 or HD) and that $\frac{3}{4}$ of the H_2 formed will be of the ortho variety, we can expect about 1×10^{16} $o-H_2$ molecules to be so formed upon warm-up for each cm^3 of irradiated solid HD, yielding an additional $o-H_2$ concentration of 3×10^{-7}. The increment of $p-D_2$ mole fraction should be about three times smaller, indeed much less than $\sim 1 \times 10^{-5}$ $p-D_2$ concentration expected on the basis of the initial $p-D_2$ concentration estimate and the para→ortho D_2 conversion rate[5]) (0.048 d^{-1}) at 4.2 K in solid HD. The 3×10^{-7} added $o-H_2$ concentration for the essentially unchanged $p-D_2$ concentration is shown in ref. 5 to produce an excess $(T_1^H)^{-1}$ of $\approx 1 \times 10^{-4}$ s^{-1}, in agreement with the experimental observation. Thus, these experiments tend to support the estimate of Sharnoff and Pound for the energy required to dissociate D_2, which was subject to some controversy in that it is at least a factor of 5 lower than values deduced from other experiments. This discussion also serves to draw attention to the almost unique sensitivity of HD relaxation measurements for detecting very small amounts of $o-H_2$ or $p-D_2$. There may be other important applications for this property.

We now examine the results of the experiments in the context of employing solid HD as a polarized target for high energy particle experiments. Using 0.9×10^{-16} s^{-1} for $(T_1^H)_{rad}^{-1}$ per unit proton integrated flux, we calculate that under a typical particle flux of 10^6 cm^2 s, $(T_1^H)_{rad}^{-1}$ would be about $(1.3)^{-1}$ d^{-1} at the end of 1 d for an HD target maintained at $T = 4.2$ K, with self-annealing neglected. For this situation, the proton polarization would have degraded to about 70% of its original value in the 1 d period. If the sample were maintained at 1.7 K, however, the proton polarization would drop to 70% of its original value under these irradiation conditions only at the end of 3.0 d. Since $(T_1^H)_{rad}^{-1}$ has a stronger than linear T dependence near 1.7 K for dosages comparable to that received by sample 1", easily maintained temperatures down to 1.2 K should be considerably more favorable. HD samples can be directly produced, using double distillation, with very low $p-D_2$ and $o-H_2$ concentrations such that T_1^H at 1.2 K and 3 kOe is about 10^4 s. Under these circumstances, at 20 mK and 150 kOe, T_1^H should be in the neighborhood[6,7]) of 1 d. Depending on the $p-D_2$ concentration, in a period of 1–2 weeks, enough conversion should take place so that T_1^H at 1.2 K and 3 kOe exceeds several days[5]). The one week estimate holds in the limit of very low $p-D_2$ concentration, where the doubling time of T_1^H is ≈ 1.3 d at 1.2 K. The $o-H_2$ concentration for this typical sample is less than 10^{-4}, and the conversion heat should not strain a dilution refrigerator operating at about 20 mK. For lower temperatures and higher polarizations, less $o-H_2$ concentration must be used and the sample probably would have to be doped with $p-D_2$ to keep the relaxation time short enough at the millidegree temperatures and high magnetic fields for equilibrium polarization to be established within a 1–2 week period. For the same concentration, the $p-D_2$ conversion heat power is about a factor of seven smaller than that of $o-H_2$, but, of course, the waiting time at low T and high H would have to be extended in order to obtain a long enough T_1^H at 1.2 K, because of the longer T_1

doubling time at higher $p-D_2$ concentrations. It is hoped that these brief remarks suggest the flexibility in this system for optimizing samples for particular irradiation situations. Some additional experiments at very high magnetic fields and millidegree temperatures with accurately known $o-H_2$ and $p-D_2$ concentrations will be useful for more precise polarized target design.

In conclusion, we believe that it has been demonstrated that polarized solid HD targets are ready to be employed in high energy experiments, and that their great advantages more than make up for the preparation time and limited usage time between preparations. Preliminary results on deuteron relaxation in HD indicate that highly polarized deuterons are also readily achievable with the same methods. The technology of 4" and larger bore – 150 kOe superconducting magnets is already developed at probably bearable prices, and large ^3He-^4He dilution refrigerators capable of providing temperatures down to 12 mK without difficulty are currently in use. Although not completely necessary, techniques to transfer the sample from the dilution refrigerator to a simple thin-walled liquid helium-filled cryostat without warming the sample above 4.2 K are easily envisaged.

Enough is now known to put a polarized proton HD target into operation. Improvements such as increasing the rate of symmetry species conversion by means of an applied stress, or increasing the dependence of T_1^H on $o-H_2$ concentration with rare gas doping, for example, will almost certainly increase the economic efficiency of these targets in the near future.

Many people have our warm thanks for their aid in carrying out this work. At BNL, we are indebted to Dr D. Berley for encouraging the work and facilitating our adaptation at the AGS, to Dr W. Glenn at the AGS main control for his help and patience in all phases of the experiments there, and to Mr G. Tanguay for his efficient and friendly efforts in helping set up our experimental station. At Cornell, we are greatly appreciative of the help given us by Prof. J. DeWire, who made available time on the electron synchrotron and contributed to setting up the experiment. At Syracuse, we profited from several helpful discussions with members of the high energy experimental group. Special thanks are also due to Mr R. McCoy and Mr P. Vanier of our laboratory at Syracuse for generously taking time off from their own doctoral work when extra hands were needed in sample preparation, apparatus construction, and for the actual experiments at Cornell and BNL.

References

1) A. Honig, Phys. Rev. Letters 19 (1967) 1009.
2) W. N. Hardy and J. R. Gaines, Phys. Rev. Letters 17 (1966) 1278.
3) R. S. Rubins, A. Feldman and A. Honig, Phys. Rev. 169 (1968) 299.
4) A. Honig, 2nd Intern. Conf. on *Polarized targets*, Berkeley (Aug. 1971) p. 99.
5) R. Bernardi, Doctoral Dissertation (Syracuse University, June 1972).
6) H. M. Bozler and E. H. Graf, 13th Intern. Conf. on *Low temperature physics*, (1972).
7) H. M. Bozler, J. A. Brown and E. H. Graf, Bull. Am. Phys. Soc. Ser. II, 18 (1973) 545.
8) T. Moriya and K. Motizuki, Prog. Theor. Phys. (Kyoto) 18 (1957) 183; also, C. C. Sung, Phys. Rev. 177 (1969) 435, for application to relaxation in HD.
9) We are indebted to Dr W. Sampson of Brookhaven National Laboratories for constructing and loaning to us the three superconducting solenoids used in this work.
10) I. Wender, R. A. Friedel and M. Orchin, J. Am. Chem. Soc. 71 (1949) 1140; A. Farkson, P. Pomerantz and E. H. Rich, J. Res. Natl. Bur. Std. 47 (1951) 31.
11) A. Farkson, P. Pomerantz and S. J. Rothberg, J. Res. Natl. Bur. Std. 47 (1951) 449.
12) We wish to acknowledge the important contributions of Mr L. S. Honig to the design and construction of the HD purification still.
13) After temperature cycling, T_1^H may not return exactly to the value prior to irradiation for a number of reasons. Magnetic species produced in the glass stem may contribute to a small relaxation effect, temperature cycling even for a few minutes can produce a noticable change if T_1^H prior to irradiation is very long, and atomic H and D may be produced in sufficient quantity by the high energy beam to add a significant amount of $o-H_2$ and $p-D_2$ to the sample when allowed to recombine upon temperature cycling.
14) Dr Hudis of the Chemistry Department at BNL kindly helped us set up the polyethylene counting, and provided the values of the constants used for the beam calibration. The counting efficiency calculation is due to Dr J. Cummings, of BNL.
15) M. Shamoff and R. V. Pound, Phys. Rev. 132 (1963) 1003.